EPFL

Thèse n° 9674

AMP-activated Protein Kinase (AMPK): New molecular insights and novel downstream targets

Présentée le 9 décembre 2022

Faculté des sciences de la vie
Programme doctoral en approches moléculaires du vivant

pour l'obtention du grade de Docteur ès Sciences

par

Katyayanee NEOPANE

Acceptée sur proposition du jury

Prof. C. Brisken, présidente du jury
Dr P. Descombes, Prof. K. Schoonjans, directeurs de thèse
Prof. L. Bertrand, rapporteur
Prof. L. Fajas Coll, rapporteur
Dr B. Schneider, rapporteur

École
polytechnique
fédérale
de Lausanne

2022

What is not started
will never get finished.
— Johann Wolfgang von Goethe

ॐ श्री गणेशाय नमः

To my family…

Acknowledgements

This has been a unique experience and an incredible journey. As I am ready to grasp the end of this 4-year expedition, I would like to take some time to acknowledge the contributions of each individual without who I wouldn't have been able to reach this milestone creating many good memories.

Every Ph.D. is a roller coaster, with ups and downs, moments of frustration and uncertainties. But everything sorts out smoothly in the end when you have the proper guidance. I would immensely like to thank my supervisor **Prof. Dr. Kei Sakamoto**, first, for believing in me and giving me this excellent opportunity to do a Ph.D. thesis under his supervision; and second, for constantly guiding me from the beginning through the end and helping me succeed in this journey. In these four years, I have learned so much from you, from science to doing good/credible research and tackling various issues to developing organisational skills. You have always been a supportive and responsible supervisor, and I genuinely appreciate it.

I would also like to thank **Dr. Andreas Wiederkehr**, who supervised some parts of my thesis. Although unexpected circumstances did not allow us to finish my thesis together, I really enjoyed our discussions and learned a lot from your expertise and knowledge. Thank you for supporting and giving me good insights. Unlike most Ph.D. students, I was lucky enough to have three official supervisors and two co-supervisors during my 4-year Ph.D. period. I would like to thank **Dr. Patrick Descombes** who readily agreed to support me as my thesis director and helped me smoothly finish my thesis. I would also like to thank my co-supervisors **Prof. Dr. Etienne Meylan** and **Prof. Dr. Kristina Schoonjans** for their constructive feedback and support throughout.

Nestlé allowed me to meet so many brilliant scientists and wonderful people. I learned but also had so much fun during these four years. I started as a new Ph.D. student in the **"AMPK team"**, with fantastic team members – Matthew Sanders (AKA Matt), Caterina, Philipp, Maria, Eva, and Robin. A big THANK YOU to **Matt**, you taught me all about AMPK in the very beginning and helped me get ready for the adventure. I still remember our first few discussions on several AMPK papers (quite intense!!! :D But so helpful). My western blots during the first days were a mess; I am sure they had made you think, "WHAT ARE THESE??" but you encouraged me, and I hope I did better with time. Thank you so much also for supporting me advance my project, esp. the myristoylation part, and for motivating me when things were not working at the beginning of the project. You always have good feedback and scientific input, which I really

appreciate. I cannot forget to thank you for my first Lego (the Santa :D). I loved it! Also, I was happy that I could be a part of your team later and get support when needed. Your leadership is truly impressive, and I wish you all the best for future projects within the amazing NBS/BH team and also with your Legos. I hope you will collect more and more (3-4 caves) in the future!

Thanks also to **Robin**. We started at Nestlé on the same day, and we shared an office room for some time in the G building 2nd floor. I learned a lot from your expertise on AMPK. We had good times in the cell culture lab; although your hood would be a bit messy... and your bench (:D), you are a very hardworking and determined person, which always amazes me. By the way, it was not me who named you "Dirty Messy Spiller"; it was Matt and Philipp who exaggerated :D.

I can not miss **Maria (Deak)**, who was our cloning expert. Thank you so much for all your hard work and all the hundreds (or thousands) of constructs you made; very impressive, and made mine and others' lives so easy. You were also such a kind person and were always there to talk to about anything.

A big shout-out to the **Ph.D. community** at Nestlé, which has always made the work environment fun and lively. Thanks to the first generation Ph.Ds: Caterina, Philipp, Miriam, AK, Margherita, Angelique, Christopher, Sara, and Anna, who were there when I joined, and the second generation students Lucie, Minji, Shruthi, Alba, and NR students Robyn, Chrysanthi, and Selima, who joined after me. **Caterina** – We had only a few months overlap, but you were such a nice person. Thank you for your tips and tricks for experiments and for advising on my Italy trip (esp. Torino, where you suggested an amazing bakery :D). Your leadership in starting the FIR was amazing and has been a huge success. I hope we cross our paths sometime in the future :). **Philipp**- I don't think I have met anyone with as many smart/real-life ideas as you :D and witty jokes that would slam others' faces, really impressive! I always had fun listening to your conversations with Matt and Robin during lunchtime in the G building; I sometimes couldn't stop laughing, so thank you for creating a fun environment. And also, thank you for teaching me radioactivity assay (PhilIP) and showing me how to use a hair dryer to dry the p81 papers :D. **AK and Margherita** – I cannot even write your names separately. You guys were amazing, fun-filled, cheerful, and always making G building lively. AK- your voice is amazing, and your singing in the cell culture room is still in my head. Margie- I enjoyed playing badminton with you a lot; thanks heaps for that and for always being so kind and helpful. **Miriam** – You are a mitochondria master! It was always nice to have you around and chat with you; you brought good energy and good vibes to the G building. Your Christmas celebration idea was amazing! Everybody had so much fun, although there might have been several BBSes :D but thank you so much for your effort and creating an exciting environment. **Angelique** – And you are the master of pancreatic beta cells, very hardworking and dedicated. You are the sweetest person and very generous. Thank you so much for motivating me during the last stretch of my thesis and for always being there to talk to :) **Sara and Ana**, you guys are super hard working too. It was always nice to chat with you in the lab, corridor, or cafeteria. We are finishing almost simultaneously, so it gives me some relief that it's not just me on edge :D. I wish both of you all the best for the final stretch and for the future. **Christopher (AKA Chris)** – the battery man, the moustache man :D I'm glad we ended up in the same team. I

have many fun memories from our open office in H – the WALL of gloves to mark the territory was classic. It felt so empty when you left!! We also shared lab space for some time; I remember your messy bench :P (comparable to Robin's). It felt so clean after you left :D I also remember your thesis days; you were crazy sometimes- drinking cold soup every day for lunch and dinner, but you managed so well in the end. I miss our lunches together, dinners, and TAX RETURN... (LOL)! Speaking of which **Lucie**- what can I say? I have so many fun memories from the past year with you. The Nepali dinner, then the Indonesian dinner, followed by a Tax return with Chris, were amazing! I will miss doing sports together; you motivated me to go Spinning (GODD, it was insane, but I loved it!). Also, the sports at Nestlé were fun. But more importantly, what I will miss the most is our side-job at Nestlé (you know what I mean ;D). I have always admired how you enjoy your life – engaging in many activities/sports. Always be like that and always be happy. Also, keep up the good work of being a source of new information in the institute :D I wish you all the best in Amsterdam and for the remaining of your Ph.D. I'm sure you will nail it! **Minji**, I think I can say you are the zebrafish master :D. It was always nice to talk to you during lunch or in the lab space. We had fun making Christopher's videos with Lucie (thanks to your high-quality iPhone camera :P). We also had a memorable Nestlé Ph.D. day with other Ph.Ds. **Selima, Robyn, and Chrysanthi**, it was nice to meet and know you guys. You well-organised the Ph.D. day. Sad that I cannot join the 2023 edition; I am sure it will be exciting. Then the newly intaken Ph.Ds, **Shruthi and Alba**, I am glad I could meet you both. You guys are fun. Still remember our food-hunting at the end of the Ph.D. day (I still can't stop laughing) and Lucie getting stuck in the basement entrance. Then all the jumping photoshoots. Hanging out by the lake amidst a heat wave. I will cherish all these memories. Thanks to all of you for these amazing moments, and I wish every one of you a big success in your Ph.Ds.

I would also like to thank **Carles**, a great scientist who always gives great feedback and input and cares for Ph.D. students. I am sure everyone, including me, benefitted from the Science seminars you organised. I would like to thank **Magali** for helping me with ordering things when I was part of Carles's team for some time. I also enjoyed being a part of the planning committee for Angelique's farewell :D. I would also thank all the other G-building residents (past and present) for creating a good environment **(Judith, Maria, Arianna, Omid, Brice, Marinne, Corinne, Albert, and Christian** (Thanks, Christian, for the beautiful Crassula plants and your help in the 35-S radioactivity experiments). I would not forget **Joanna**, who was at Nestlé for six months as a master's intern. Thank you for your company during lunchtime, sports sessions, and drinks. I wish you all the best for the start of your Ph.D.

Moving from G to H building was difficult for me. It was like moving out of my comfort zone. But it turned out H is cool too. First of all, thanks to **Denis Barron**, who motivated all his team members to move to the H building. It was actually a good idea. Also, thank you for being a great group leader and welcoming us to your team. Then thank you to all the team members of NBS– **Olivier, Yann, Benjamin, Guillaume, Martine, Ali, and Steve**, now the BH team led by Matt. Special thanks to **Steve** for being ever ready to help with anything related to lab, ordering, or other issues. You are very proactive and helpful. I did not have to worry about lab-related matters when you were there, so thank you. Also, it was nice to meet Speedo, a very cool Dog!!

Thanks to **Olivier and Ali** for being great office mates. By the way, I understood everything you communicated with each other (in French :D). Olivier, I hope you won't always feel like a potato (it's funny when you say it), but it was always good to have you guys in front of my desk and have funny conversations. **Yann**, you make the entire team laugh out loud with your funny jokes :D You are full of fun but also a good scientist. I hope I did not disappoint you by not writing my thesis ;D. **Guillaume**, I wish I had more imaging experiments for you (just to check your data-storage skill – I remember you lost some data at some point :D). Also, doing a few sports sessions last year with you was fun. You were a champion! **Benjamin**, you are an orchid specialist. I always envy your orchids. They are constantly flowering and beautiful, unlike mine. Also, your serious jokes are hilarious; I don't know how you do it :D **Martine**, it is always lovely to talk to you; thank you for helping with purchases and other admin stuff when needed. I hope you will be able to maintain gender equality in the team with one woman-power. It was such a nice time in the BH team, group meetings were fun (I was a very good listener) and we had great fun during the Cell Biology Closure meeting with the "Who wants to be a M/Billionnaire" presentation (music still in my head). Thanks all for that.

Thank you to the former **Cell Biology Department**, led by Philipp Gut. Thanks to **Philipp** for always encouraging and supporting Ph.D. students and being ready to help and give feedback when needed. Thanks to all the other department members, thanks **Sebastien** for the intense badminton sessions: I think I have improved some of my skills :D. I ended my Nestlé journey with the **Musculo-skeletal health department**, led by Jerome Feige. Thanks to **Jerome** for supporting Ph.D. students, encouraging them to showcase their projects in the form of pitches and posters, and helping to initiate the unique Ph.D. day where students could network with the rest of the institute. Also, thanks to all the members of the MS department for help and support when needed. Everybody works hard in the institute to help each other. There are important people without whose effort, working would be difficult. **Laurent (Dobler)** is an IT master. Thank you for always having solutions to every IT issue I encountered and for your friendly nature. **Dan** for helping with admin-related problems, and **Eduardo and the delivery team** for their constant effort to deliver packages in time. You all are an integral part of the Nestle community. I am not able to thank everyone individually, but I would acknowledge every person in the institute for their hard work and determination. Thank you to the entire NIHS and the NR community.

For the success of my project, I would like to thank all the incredible collaborators: **Sandra Galic** from SVI, Melbourne, **Jeppe and Atul** from Copenhagen, and **MRC-PPU staff** from Dundee for great teamwork and exchange of resources and of course thanks to Kei who created this innovative environment.

This Ph.D. would never have been possible had I not come to Switzerland in the first place, and coming to Switzerland was not something I imagined during my undergrad studies back in Nepal. This happened when I met the former president of EPFL, **Prof. Jean C. Badoux**, who visited Kathmandu University and offered me an opportunity to do an internship at EPFL. I cannot thank Prof. Badoux enough for his generosity, selfless act, love towards Nepalese students, and constant effort to help in their career growth. I haven't seen anyone so proactive and engaged even so many years after retirement. Thank you so much for everything you

did for the students. Then I would like to thank my mentor **Prof. Dr. Bruno Correia**, who I consider my mentor not just for the official Ph.D. program but for my life outside of Ph.D. He has supported me constantly since I came to Switzerland and joined his lab as a naïve intern. I learned research from his lab, and I especially thank **Che and Fabian** for teaching me how to work in a lab. My motivation for doing a Ph.D. was induced when I worked as a master's thesis student and then as an intern in **Prof. Dr. Oliver Hantshcel**'s lab at EPFL, where I learned so many valuable skills. I especially thank **Nadine** for being so enthusiastic and encouraging and helping me find my way. Then I would like to thank the EPFL EDMS community, especially **Tatiana Dubi**, for always helping with EPFL admin procedures and being cheerful every time and also thanks to all the fellow Ph.Ds at EPFL with whom I share memories in different events, tea-times, happy hours, courses and while doing TA.

Life outside of home country is never always easy. But everything becomes more manageable if you encounter people who make you feel at home and with family. I would like to express my deep gratitude to the **Wyssa family** (Claude/Claudine, René, Christian/Sara, Michael/Cheyenne, Stephan/Joe, and Thomas, Remi, Justin, Leticia, Beatrice, and Joule) for their warmth and support which made my stay in Switzerland very smooth and fun. I was fortunate to meet you and stay at Chemin du Cèdre for more than two years :) and share many dinners and interesting talks (about Swiss/Nepali culture, politics, etc.). Thank you so much for always supporting us in everything and making us a part of the family. I will always be grateful for that.

I would also like to thank the **Nepali community** in Switzerland for helping and making my life here easy. First, thank you Saroj/Samjhana for supporting me during the first days of my arrival and for helping me get adapted to a foreign country. Then a big thank you to all the crazy and fun-loving people who I became close friends with during these 4 years in Switzerland and who are my means of fun and recreation outside Worklife :D. It's always cool to hang out with you guys and engage in fun activities, from BBQing to hiking to insane biking, sledging to just road-tripping, boating, or bachelor-partying :D or just chatting with good food and horror/stupid movies. So, thank you to **Lekhnath, Niran/Aditi, Sabnam, Saurav/Elina, Dinesh, Subash/Bandana, Bikram, Anil, Nitesh, Rupesh, Kusum, Aishwarya, Rakesh/Manisha and Prakash/Bishnu** for all these memories.

They say a man is nothing without a family. I am nothing without the love and support of my family. I am blessed with three extraordinary sisters to love me to eternity. What would I do without them? Thank you **Nani, Binu, Mune** for your unconditional love and support in every step of my life and for being responsible elder sisters :D I hope to meet all of you soon from four corners of the world, and we will make memories for life <3.

I can not thank enough **my parents (buwa, aama, mummy, and baba)**. They are my pillars and my source of motivation. They have always loved and supported me no matter what and always believed in me; I hope I can always be able to meet their expectations. Thank you so much for everything. My father is my role model. His discipline and determination have taught me a lot in life, and I hope I make him proud.

Last but not least, **Avip**. What can I say? I have no words. I would not be anything without your love and unconditional support. Thank you would be so small but still thank you so much

for always being there with me and making my Ph.D. adventure an easy one. Without your moral support and open and calm nature, and without you pissing me off with your silly jokes (with the aim to make me laugh), I would have struggled so hard, not just in the Ph.D. but in my life before and definitely after this. I feel blessed to have you as a partner in life, partner in crime, and partner in fun and adventure. We've been through a lot in the past ten years but have always dared to face everything together; we have made countless lifetime memories; many more to come, and I have no doubt we will conquer every challenge as we have and will continue making the best memories. Lots of love and hugs!

Once more, I would like to thank everyone who made me able to accomplish this great challenge; apologies if I miss any particular name. I hope we can keep in touch and cross our paths somewhere in this small world in the future.

Lausanne, 29 August, 2022 K.N.

Abstract

AMP-activated Protein Kinase (AMPK) is a central regulator of energy homeostasis and a promising drug target for metabolic disorders. It exists as complexes of three subunits, a catalytic α, and two regulatory β and γ subunits. The regulation of AMPK involves reversible phosphorylation and allosteric regulation by adenine nucleotides. It is activated by phosphorylation of Thr172 on the catalytic α subunit as a consequence of various energy-depleting conditions. Once activated, AMPK regulates a plethora of metabolic processes through the phosphorylation of target proteins to maintain energy homeostasis. The β subunit has a vital role as a structural scaffold stabilising the AMPK heterotrimeric complex. It is also known to regulate AMPK activity through different posttranslational modifications (i.e., phosphorylation and myristoylation). Although myristoylation of Glycine-2 (Gly2) of the β subunit has been shown to be required for sensing stress signals and achieving maximum AMPK activity *in vitro*, its physiological relevance at the cellular and organismal levels remains unknown. Critically, the underlying molecular mechanism by which β subunit myristoylation controls AMPK activity is elusive.

The primary aim of this thesis was to investigate the molecular basis of AMPK regulation by the β subunit myristoyl switch. I showed that mouse embryonic fibroblasts (MEFs) isolated from knock-in (KI) mice carrying Gly2 to Ala point mutation of β1 and β2 isoforms (β1/2 G2A double knock-in (DKI)) displayed increased activity and phosphorylation of Thr172 in the α subunit. Using proximity ligation assay, I found that the loss of β1 myristoylation impedes the interaction/proximity of the phosphatases PPM1A/B with AMPK in cells. *In vivo*, β1 G2A KI mice showed increased AMPK activity in the liver and were protected from high-fat diet-induced obesity, hepatic lipid accumulation, and insulin resistance.

The second aim of the thesis focused on the identification of novel AMPK substrates to expand our understanding of the AMPK system/signalling in the control of metabolic and also in non-metabolic processes. We performed an unbiased phosphoproteomics analysis which revealed that AMPK phosphorylates several proteins involved in regulating Golgi structure and function. I observed that pharmacological activation of AMPK induces Golgi fragmentation in wild-type but not in AMPK-deficient human U2OS cells and MEFs. We identified AMPK-dependent phosphorylation of three Golgi-related proteins and focused on the Oxysterol-binding protein like 9 (OSBPL9), a novel AMPK substrate phosphorylated on a threonine residue (Thr335).

Interestingly, knockdown of OSBPL9 in cells induced Golgi fragmentation, linking the AMPK-OSBPL9 pathway to Golgi regulation.
Collectively, this study expands our understanding of the regulation and novel biological roles of AMPK. This will advance future studies to elucidate the significance of AMPK in the treatment of metabolic as well as non-metabolic disorders.

Key words: AMP-activated protein kinase, energy homeostasis, myristoylation, β subunit, phosphorylation, substrates, oxysterol-binding protein like 9, Golgi fragmentation

Résumé

La protéine kinase activée par l'AMP (AMPK) est un régulateur central de l'homéostasie énergétique et une cible prometteuse pour des médicaments contre les troubles du métabolisme. Elle existe sous forme de complexes de trois sous-unités, une sous-unité α catalytique, et deux sous-unités β et γ régulatrices. La régulation de l'AMPK implique une phosphorylation réversible et une régulation allostérique par des adénine nucléotides. Elle est activée par la phosphorylation de la Thr172 sur la sous-unité α catalytique, à la suite de diverses conditions d'épuisement énergétique. Une fois activée, l'AMPK régule une pléthore de processus métaboliques par la phosphorylation de protéines cibles afin de maintenir l'homéostasie énergétique. La sous-unité β joue un rôle essentiel en tant qu'échafaudage structurel stabilisant le complexe hétérotrimérique de l'AMPK. Elle est également connue pour réguler l'activité de l'AMPK par le biais de différentes modifications post-traductionnelles (par exemple la phosphorylation et la myristoylation). Bien qu'il ait été démontré que la myristoylation de la glycine-2 (Gly2) de la sous-unité β est nécessaire pour détecter les signaux de stress et atteindre une activité maximale de l'AMPK in vitro, sa pertinence physiologique aux niveaux cellulaire et organique reste inconnue. En particulier, le mécanisme moléculaire sous-jacent par lequel la myristoylation de la sous-unité β contrôle l'activité de l'AMPK reste insaisissable.

L'objectif principal de cette thèse était d'étudier la base moléculaire de la régulation de l'AMPK par le myristoyl en tant que commutateur de la sous-unité β. J'ai montré que des fibroblastes embryonnaires de souris (MEFs) isolés de souris knock-in (KI) portant une mutation ponctuelle de Gly 2 en Ala des isoformes β1 et β2 (β1/2 G2A double knock-in (DKI)) ont présenté une activité accrue d'AMPK et une phosphorylation de la Thr172 de sa sous-unité α . En utilisant le test de ligation par proximité, j'ai découvert que la perte de la myristoylation de la sous unité β1 entrave l'interaction/la proximité des phosphatases PPM1A/B avec l'AMPK dans les cellules. In vivo, les souris β1 G2A KI présentaient une activité AMPK accrue dans le foie et étaient protégées contre l'obésité, l'accumulation de lipides hépatiques et la résistance à l'insuline induites par un régime riche en graisses.

Le deuxième objectif de la thèse portait sur l'identification de nouveaux substrats de l'AMPK afin d'élargir notre compréhension du système de signalisation par l'AMPK dans le contrôle des processus métaboliques et non-métaboliques. Nous avons effectué une analyse phosphoprotéomique non biaisée qui a révélé que l'AMPK phosphoryle plusieurs protéines

impliquées dans la régulation de la structure et de la fonction du Golgi. J'ai observé que l'activation pharmacologique de l'AMPK induit une fragmentation du Golgi dans les cellules U2OS humaines et MEF de type sauvage, mais pas dans les cellules déficientes en AMPK. Nous avons identifié la phosphorylation dépendante de l'AMPK de trois protéines liées au Golgi et nous nous sommes concentrés sur la oxysterol-binding protein like 9 (OSBPL9), un nouveau substrat de l'AMPK phosphorylé sur un résidu thréonine (Thr335). Il est intéressant de noter que le knockdown de l'OSBPL9 dans les cellules a induit une fragmentation du Golgi, reliant la voie AMPK-OSBPL9 à la régulation du Golgi.
Globalement, cette étude accroît notre compréhension de la régulation et des nouveaux rôles biologiques de l'AMPK. Elle fera progresser les études futures visant à élucider l'importance de l'AMPK dans le traitement des troubles métaboliques et non métaboliques.

Mots clefs : protéine kinase activée par l'AMP, homéostasie énergétique, myristoylation, sous-unité β, phosphorylation, substrats, Oxysterol-binding protein like 9, fragmentation du Golgi

Contents

List of Figures

List of Tables

1 Introduction

1.1 General background

Energy homeostasis is a biological process maintaining the inflow and outflow of energy with coordinated regulation of different cellular pathways. An organism needs to sustain intracellular energy levels to function correctly and maintain homeostasis. Disturbances in this balance can cause changes in metabolism, thereby leading to metabolic disorders such as excess body weight gain (i.e., obesity), a significant condition globally. Strategies have been adopted to combat obesity as it is a major risk factor for cardiovascular diseases, type 2 diabetes, and other metabolic disorders. Since energy balance is crucial in every aspect of cellular processes, there is a coordinated sequence of events at the cellular level that maintains this equilibrium. There has been growing interest and research on mechanisms and regulators of this crucial process. Of these, the AMP-activated Protein Kinase (AMPK), a central energy sensor and metabolic master switch, has become an attractive drug target to combat obesity and metabolic disorders.

1.2 AMPK and its subunit isoforms

AMPK is a key energy sensor and metabolic regulator at the cellular and whole-body levels. It is a heterotrimeric complex made up of a catalytic α subunit and regulatory β and γ subunits, each existing as multiple isoforms (α1, α2; β1, β2; γ1, γ2, γ3) forming 12 different possible combinations of AMPK heterotrimeric complexes (Ross et al., 2016). AMPK is activated primarily by phosphorylation of Thr172, present in the kinase domain of catalytic α subunit. Activation is achieved under various energy-lowering/stress conditions, e.g., starvation, contractions, hypoxia, or ischemia (Mu et al., 2001; Rousset et al., 2015). All these conditions lower intracellular adenosine triphosphate (ATP) levels while increasing adenosine monophosphate (AMP) or adenosine diphosphate (ADP) concentrations. Increased AMP:ATP or ADP:ATP triggers AMPK activation leading to inhibition of anabolic or ATP-consuming processes (e.g., lipogenesis, protein synthesis) and stimulation of catabolic or ATP-generating

processes (e.g., fatty acid oxidation, glycolysis, glucose uptake) (Gowans and Hardie, 2014). In this way, AMPK plays a key role in cell survival and adaptation to energetic stress in different cell types/tissues, including liver, adipose, heart, and skeletal muscle.

AMPK subunit isoforms have differential tissue expression profiles. α1 is ubiquitously expressed across tissues, while α2 is highly predominant in skeletal muscle and abundant in the heart and liver (Quentin et al., 2011). β1 is ubiquitously expressed, while β2 is abundant in skeletal muscle and less expressed in the heart (Thornton et al., 1998). The distribution of AMPK subunit isoforms can also vary between species. For example, in the liver of rodents, β1 is the predominantly expressed isoform, whereas the β2 isoform is highly expressed in humans (Wu et al., 2013). γ1 is ubiquitously expressed. γ2 is also present in many tissues; however, its importance in the heart is of particular interest given its gain-of-function mutation linked to cardiomyopathy called Wolff-Parkinson syndrome (Yavari et al., 2017). While γ3 has been reported to be exclusively present in the glycolytic muscle fibres of skeletal muscle (Mahlapuu et al., 2004), modest expression of this isoform in brown adipocytes has been detected (Rhein et al., 2021).

As represented by the domain structure of AMPK in **Fig 1.1**, the α subunit consists of a kinase domain at its N-terminus region, where the phosphorylation site Thr172 is present in the conserved activation loop (Hawley et al., 1996). It also consists of an Auto-Inhibitory Domain (AID) responsible for kinase inhibition. Additionally, two regulatory subunit interacting motifs (α-RIM1 and 2) and a C-Terminal Domain (CTD) are present that mediate interaction with the γ and the β subunits, respectively (Crute et al., 1998). The regulatory β subunit stabilises the AMPK heterotrimer through its Sequence Interacting Domain (SID) by interacting with the α-CTD and the N-terminus of the γ subunit and maintains kinase activity (Iseli et al., 2005). The β subunit also consists of a Carbohydrate Binding Module (CBM) which forms an Allosteric Drug and Metabolite (ADaM) binding site by interacting with the α subunit (Xiao et al., 2013). This will be discussed in detail in **section 1.4**. The second regulatory γ subunit consists of four tandem repeats of Cystathionine Beta Synthase (CBS) domains. The interface between the two CBS domains generates two nucleotide-binding regions, making four potential nucleotide-binding sites, although only three are occupied (Cheung et al., 2000). Overall, AMPK activity increases more than 100-fold when phosphorylated at αThr172. Binding of AMP or ADP causes conformational changes that promote net Thr172 phosphorylation by (i) promoting phosphorylation by upstream kinases (e.g., Liver kinase B1 (LKB1) or calcium/calmodulin-dependent protein kinase kinase 2 (CaMKK2), detailed in **section 1.5.1**) (ii) preventing dephosphorylation by protein phosphatases (iii) additionally, binding of AMP (and not ADP) further stimulates AMPK activity up to 10-fold by allosteric activation (Gowans et al., 2013).

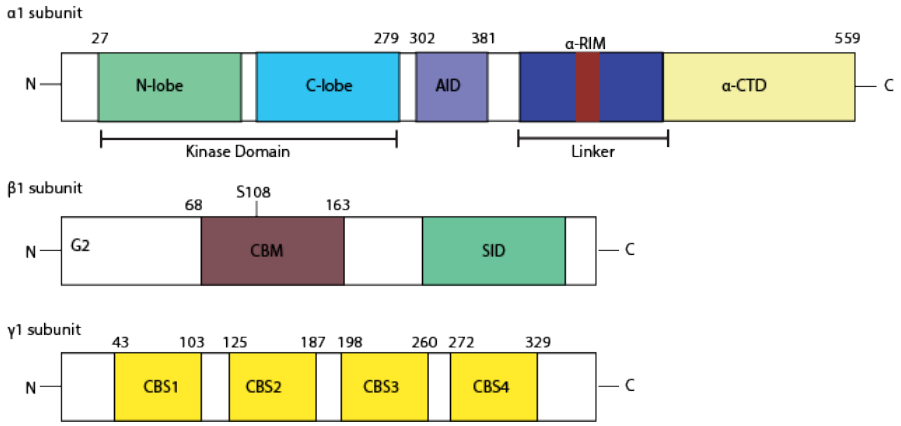

Figure 1.1: **Domain structure of AMPK subunits** Representation of human catalytic $\alpha 1$ (Uniprot ID Q13131), and regulatory $\beta 1$ (Uniprot ID Q9Y478) and $\gamma 1$ (Uniprot ID P54619) subunits and their respective domains. Auto-Inhibitory Domain (AID); C-Terminal Domain (CTD); Carbohydrate Binding Module (CBM); Sequence Interacting Domain (SID); Cystathionine Beta Synthase (CBS). Residue numbering is based on human sequences, according to Uniprot.

1.3 AMPK agonists and antagonists

Given the importance of AMPK in metabolic health, several modulators (activators and inhibitors) have been identified and characterised. **Fig 1.2** gives an overview of AMPK modulators which are briefly discussed below:

1.3.1 Activators

AMPK is activated under different cellular stress conditions such as glucose deprivation, hypoxia, ischemia or physiological conditions such as physical exercise/muscle contractions, which lower intracellular energy levels. In addition, hormones/cytokines (e.g., leptin, ghrelin, adiponectin) have also been shown to modulate AMPK activity. Several mechanisms have been proposed to elucidate the role of leptin and ghrelin in regulating appetite and modulating AMPK activity in the hypothalamus (Andersson et al., 2004; Kola, 2008), and of adiponectin in activating AMPK in the liver and muscle to promote fatty acid oxidation (Yamauchi et al., 2010); however, the exact mechanism of hormone-mediated AMPK regulation is not well understood.

There has been a significant advancement in discovering compounds that activate AMPK indirectly or directly. The first series of activators are those that elevate intracellular AMP/ATP or ADP/ATP ratio and indirectly activate AMPK. Examples of such compounds include metformin (the most widely used anti-diabetic drug globally), oligomycin (ATP synthase inhibitor) and many natural compounds (J. Kim et al., 2016). However, these compounds also modulate several other proteins and cellular processes (e.g., inhibition of mitochondrial

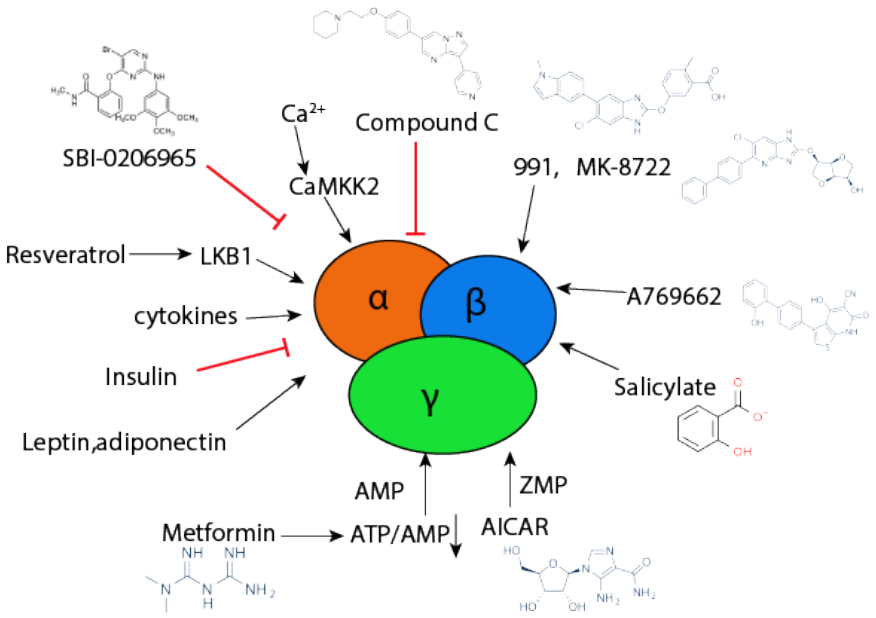

Figure 1.2: **AMPK modulators** Graphical representation of several direct and indirect modulators of AMPK activity that act through specific subunits of AMPK. Black arrows represent activators, and red bars represent inhibitors.

respiration, thereby altering cellular energy levels) and are not specific to AMPK. The second category of activators includes AMP mimetics, such as prodrug 5-Aminoimidazole-4-carboxamide ribonucleotide (AICAR), which gets metabolised inside the cells into ZMP (AMP analogue), and activates AMPK. AICAR/ZMP is also known to modulate other AMP-sensitive enzymes (Višnjić et al., 2021). The third category of AMPK activators includes the ADaM-site binding drugs, which activate AMPK through allosteric activation and protection of αThr172 dephosphorylation from phosphatases. These compounds bind the ADaM site (formed at the interface of α and β subunits) and are potent and specific activators of AMPK. However, these compounds have preferential β subunit isoform specificity. A thienopyridine compound, A769662 (developed by Abbott Laboratories), is the first member in this category which has been shown to selectively activate β1-containing complexes (Treebak et al., 2009). **Fig 1.3** shows crystal structure of human AMPK α2β1γ1 heterotrimer resolved with A769662 bound in the ADaM site (Garcia and Shaw, 2017). Abbott, however, has been reported to have poor oral availability and cause several off-target effects in cells and tissues when used at high concentrations. Next, a cyclic benzimidazole 991, developed by Merck, is 5-10-fold more potent than A769662 and has been shown to stimulate both β1- and β2- containing complexes (Bultot et al., 2016). It has no reported off-target effects to date. However, 991 has poor bioavailability. The two other benzimidazole derivatives of 991 (MK-8722 and PF739, developed by Merck and Pfizer, respectively) have also been identified as highly specific AMPK activators with improved bioavailability that can activate all 12 AMPK complexes. They have been shown to stimulate insulin-independent glucose uptake in

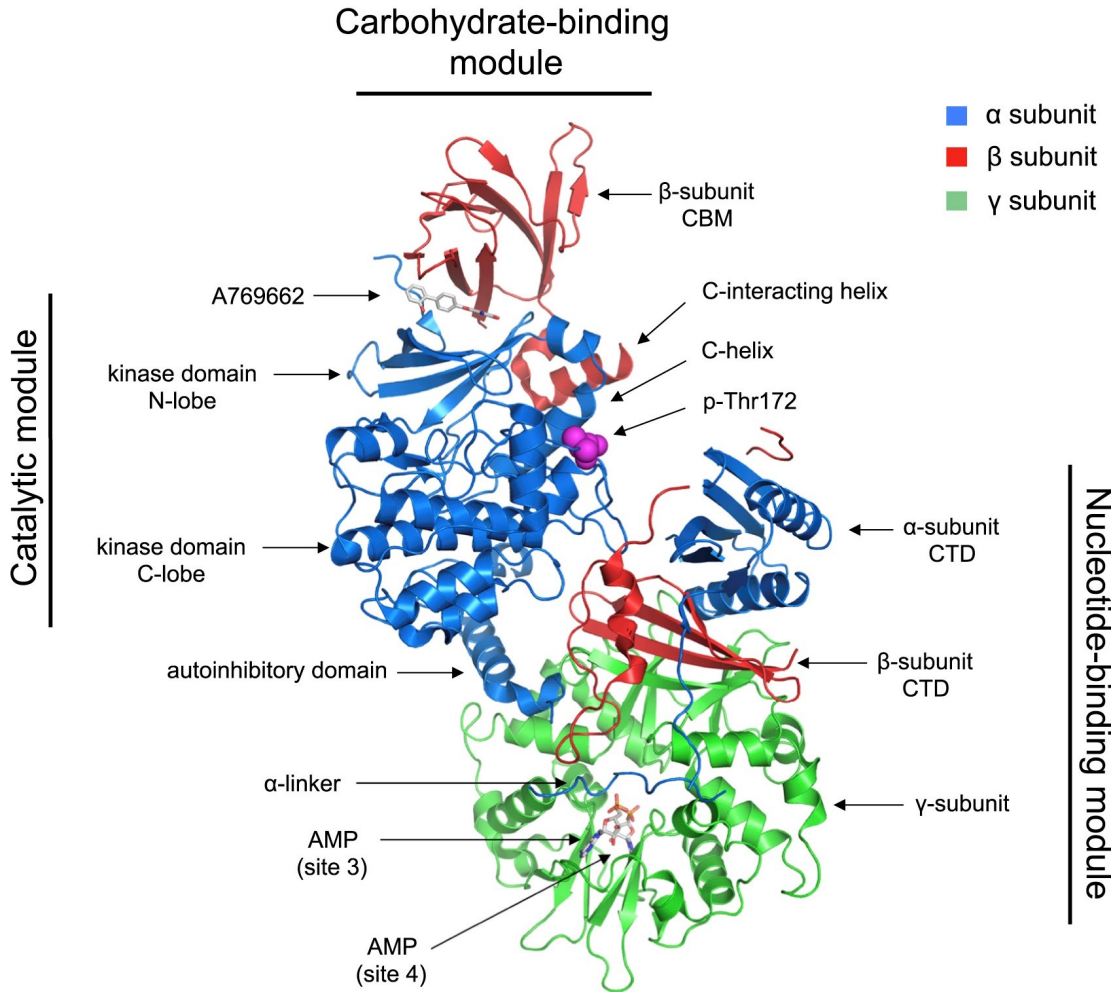

Figure 1.3: **AMPK heterotrimeric complex** Crystal structure of AMPK ($\alpha 2\beta 1\gamma 1$) in complex with the activator A769662 shown in stick representation which binds at the interface of the α kinase domain and the β-CBM. Key elements include the Thr172 phosphorylation site in the catalytic module of the α subunit, the carbohydrate-binding module of the β subunit and two molecules of AMP-bound in the nucleotide-binding module of the γ subunit. PDB: 4CFF (Garcia and Shaw, 2017).

skeletal muscle with resultant improvements in glycemia in rodents and monkeys *in vivo* (Aledavood et al., 2021; Feng et al., 2018). Identifying these compounds and demonstrating their effects on AMPK activation have represented a promising approach for treating various metabolic abnormalities.

1.3.2 Inhibitors

AMPK activation has been proven beneficial for restoring cellular energy demands. AMPK inhibition has also been considered advantageous under certain pathophysiological contexts

(Russell and Hardie, 2020). Therefore, specific AMPK inhibitors would be an important research tool to study the role and function of AMPK in different physiological and pathological states. However, the availability of small-molecule AMPK inhibitors is limited. The most widely used inhibitor is the pyrazolopyrimidine derivative Compound C (or Dorsomorphin) (Zhou et al., 2001). It is an ATP-competitive inhibitor which binds to the highly conserved active site of the α subunit catalytic domain. In the cell-free assay, Compound C has been shown to inhibit several other kinases with similar or even much greater potency than AMPK, producing AMPK-independent cellular effects (Liu et al., 2014; Vucicevic et al., 2011).

Another recently characterised inhibitor is a 2-aminopyrimidine derivative, SBI-020696531 (SBI). It was first identified from a library screen as an ATP-competitive inhibitor of autophagy initiator kinase ULK1, which could inhibit ULK1 signalling in glioblastoma cells (Egan et al., 2015). However, in a cell-free screen against a selected panel of human protein kinases, it was reported that SBI could inhibit AMPK more potently (80%) compared to ULK1 (63%) and was more potent and selective compared to Compound C (Dite et al., 2018). In a recent study, the effect of SBI on AMPK signalling was extensively characterised. It was shown that SBI could dose-dependently attenuate 991-mediated ACC Ser79 phosphorylation and lipogenesis inhibition in primary mouse hepatocytes and modestly inhibit AMPK signalling in C2C12 myotubes and adipocytes (Ahwazi et al., 2021). In addition, it could potently inhibit basal and insulin-stimulated glucose uptake. Using an expanded protein kinase screen, it was discovered that SBI could strongly inhibit other AMPK-related kinases, including NUAK1 and SIK2. Importantly, an *in silico* molecular docking analysis has revealed a gatekeeper methionine residue near the ATP binding cleft of a panel of kinases which is crucial for binding SBI. Mutation of this methionine to a threonine in AMPK rendered resistance to SBI both *in vitro* and in cells. This study provides new insights into the identification of a more potent and specific AMPK inhibitor and the design of an inhibitor-resistant mutant form of AMPK, which can be utilised as a valuable research tool in the field of AMPK.

1.4 AMPKβ subunit

The β subunit is known to have a vital role in AMPK trimeric complex stabilisation. However, apart from such a role, molecular mechanisms by which it impacts AMPK activity relative to the α, and the γ subunits remain elusive. The β subunit exists as two isoforms: β1 and β2 (Thornton et al., 1998). Sequence analyses have shown that in humans, they are >75% identical, with the predominant variation in the N-terminal region **(Fig 1.4)**. The functional significance/consequence of this variation is unknown. The β subunit is needed for assembly of AMPK heterotrimer and is crucial for AMPK activity (Iseli et al., 2005). In support of this, whole-body deletion of both β1 and β2 results in embryonic lethality (Quinn et al., 2010), providing genetic evidence that at least one of the β isoforms is required for development and survival. Muscle-specific deletion of both β1 and β2 isoforms resulted in impaired exercise-stimulated glucose uptake and mitochondrial integrity/biogenesis, demonstrating an obligatory role for the β subunit in skeletal muscle energy homeostasis (O'Neill et al., 2011).

Whole body β1 KO mice displayed no distinguishable general phenotype compared to the WT. On a low-fat or an obesity-inducing high-fat diet, β1 KO mice had reduced food intake, reduced adiposity, and reduced total body mass. At molecular levels, β1 deficiency resulted in tissue-specific defects in AMPKα Thr172 phosphorylation and activity. The most pronounced effect was observed in the liver, but not in the heart and skeletal muscle, where α1 and α2 levels were significantly reduced and AMPK activity profoundly impaired (Dzamko et al., 2010). In contrast, whole-body β2 KO mice showed impaired glucose homeostasis, which was associated with poor AMPK activity in muscle, but not in the liver (Steinberg et al., 2010). These observations suggest an isoform-specific role for the β subunit in different tissues. However, it is unclear if such isoform-specific functions are attributed to their distinct subcellular localisation or substrate specificity and recognition. A key point, as mentioned in **section 1.2**, is that β subunit isoforms are differentially expressed in humans and rodents. While β1 is the predominant isoform in the liver in rodents, in humans, it is β2 that is mainly expressed. This should be an essential consideration while developing β subunit isoform-specific AMPK activators.

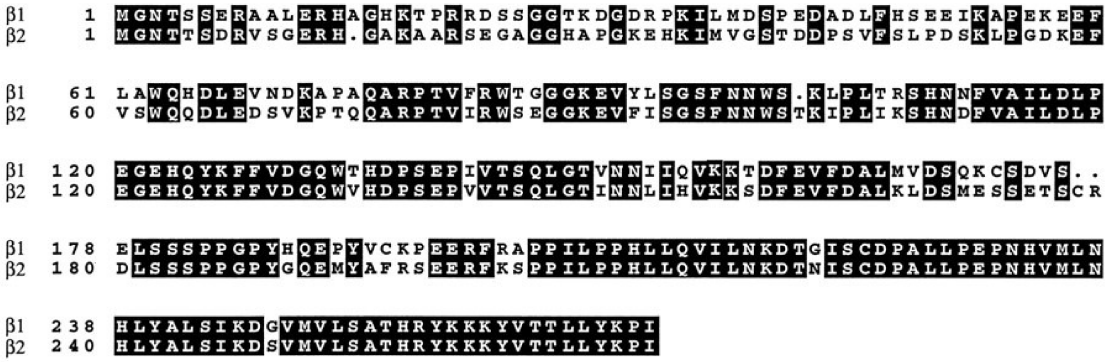

Figure 1.4: **AMPKβ subunit isoforms** Sequence alignment of human β isoforms (Thornton et al., 1998) (Uniprot ID: Q9Y478-AAKB1 and O43741-AAKB2). The black regions indicate identical residues.

The β subunit has a crucial regulatory role, and this is attributed mainly to the presence of a specific domain (i.e., CBM) or different posttranslational modifications (e.g., phosphorylation, myristoylation). These characteristic features have made the β subunit an exciting topic of study with possible physiological significance. Below is a short description of CBM, phosphorylation sites and myristoylation site of the β subunit, the latter being one of the main topics of my thesis.

1.4.1 Carbohydrate Binding Module (CBM)

The β subunit consists of a CBM, which is similar to the starch-binding domains of many glycosyl hydrolase families of enzymes (Polekhina et al., 2003). As its name implies, this domain is responsible for binding carbohydrate molecules, particularly glycogen. Specific mutations in CBM have been shown to prevent glycogen binding in cell-free (Polekhina et

al., 2005) and in cellular assays (Bendayan et al., 2009). AMPK has been shown to regulate glycogen synthesis by a dual mechanism which involves phosphorylation and inhibition of glycogen synthase, thus inhibiting glycogen synthesis in skeletal muscle following AICAR treatment (L. Miyamoto et al., 2007). However, this inhibition is overridden by an increase in glucose uptake as a result of AMPK activation that increases the level of glucose-6-phosphate, which allosterically activates glycogen synthase (Hunter et al., 2011). Furthermore, α2 KO or β2 KO mice show lower levels of glycogen in basal conditions in skeletal muscle, which implies the positive role of AMPK in glycogen synthesis (Jørgensen et al., 2005). There are still many unanswered questions relating AMPK and glycogen and how they regulate each other. In a more recent *in vivo* study, glycogen binding was disrupted in mice via whole-body knock-in (KI) mutation of a key glycogen binding residue in either β1 (W100A) or β2 (W98A) CBM (Hoffman et al., 2015). β2 W98A KI mice had impaired glucose handling and exercise capacity owing to an impaired AMPK activity compared to the WT animals, indicating that glycogen binding is critical for AMPK activity *in vivo*. In addition to glycogen binding, CBM of AMPK has also been shown to be an important region for binding small molecule activators by forming an ADaM binding site as mentioned in **section 1.3.1**. It has been shown that phosphorylation of Ser108 in the CBM stabilises the binding pocket in the ADaM site, thereby forming an interface for binding. The precise physiological role of Ser108 phosphorylation in the CBM is not fully understood. However, a mutation in Ser108 (S108A) has been shown to affect drug binding in the ADaM site and thus reducing its effect on AMPK activity. Complete removal of the CBM has been shown to reduce catalytic activity of AMPK and fully abolish AMPK activation by small-molecule activators (e.g., A769662) (Xiao et al., 2013), demonstrating critical roles of CBM and Ser108 in direct AMPK activation by these compounds. These findings have led to an interesting hypothesis that there could be a possible involvement of a physiological metabolite, (e.g., Long-chain fatty acyl-CoA esters (Pinkosky et al., 2020)), in the regulation of AMPK, making the β subunit an important therapeutic target.

1.4.2 Phosphorylation

Phosphorylation is one of the most common and critical mechanisms for regulating the activity/function of enzymes and proteins and is arguably the most prevalent form of posttranslational modification. Although Thr172 in the α subunit of AMPK is the major phosphorylation site that regulates its activity (Hawley et al., 1996), several additional phosphorylation sites have been identified with possible physiological significance. In addition to Thr172, Thr258 and Ser485 were identified to be phosphorylated by AMPK kinase in the α subunit using bacterially expressed AMPK complex and mass spectrometry (Woods, Vertommen, et al., 2003). *In vivo*, these sites were confirmed to be autophosphorylated but did not show a direct effect on AMPK activation *in vitro* and in cells. However, in another study, cAMP-mediated inhibition of AMPK activity was associated with reduced phosphorylation of αThr172 and enhanced phosphorylation of Ser458, indicating a possible involvement of multisite phosphorylation of the α subunit in AMPK activity regulation (Hurley et al., 2006).

While a few phosphorylation sites have been identified in the γ subunit (Puustinen et al., 2020), several phosphorylation sites have been reported in the β subunit isoforms (Tuerk et al., 2009). One of the most characterised autophosphorylation sites is Ser108 in both β isoforms, which has already been discussed in **section 1.4.1**. In the β1 isoform, Ser24/25, Ser96, Ser101, Thr148 and Ser182 have been additionally reported, while in the β2-isoform, Thr148 and Ser182 have been identified (Sanz et al., 2013). Among these sites, Ser24/25, Ser108 and Thr148 are autophosphorylated by the catalytic activity of the α subunit. Kinase(s) responsible for the phosphorylation of these residues (apart from Ser108 phosphorylation by ULK1 (Dite et al., 2017)) are still unknown. The precise roles of these sites have not been established; however, some of these sites are reported to have effects on subcellular localisation and kinase activity of AMPK. Mutagenesis studies have shown that Ser24/25 and Ser182 affect β1 localisation with alanine mutants mediating nuclear translocation of β1 but do not affect AMPK activity. In contrast, Ser108 affects kinase activity but not its localisation (Warden et al., 2001). Meanwhile, Thr148 is implicated in glycogen binding (Polekhina et al., 2005). It has been shown that Thr148 phosphorylation in the β subunit isoforms abolishes glycogen binding, affecting glycogen turnover and that this phosphorylation is associated with increased AMPK activity (Oligschlaeger et al., 2015). This could be an important mechanism as it will dissociate AMPK from glycogen, thereby changing its subcellular localisation. The exact physiological roles of Thr148 or other phosphorylation sites in the β subunit are still not completely clear, but they could have subtle effects on AMPK regulation. Collectively, a deeper understanding of these phosphorylation sites would be interesting to uncover precise cellular functions of AMPK.

1.4.3 Myristoylation

Myristoylation is a co/posttranslational modification of a protein that involves adding a 14-carbon saturated fatty acid, myristic acid, to the N-terminal glycine within a consensus motif of MGNXXS/T (Martin et al., 2011). This requires prior removal of the initial methionine residue by methionyl peptidase. The process of myristoylation is catalysed by the N-myristoyltransferase (NMT) enzyme (**Fig1.5A**). There are two isoforms of NMT: NMT1 and NMT2, and both isoforms have been extensively studied and validated as drug targets in human cancers or in infectious diseases (Ducker et al., 2005). Myristoylation has been shown to promote the binding of the proteins to cell membranes or change their subcellular localisation for various biological functions. It may also influence protein-protein interaction or regulate enzymatic activity. For instance, the activity of Src kinase, an oncogenic protein, is proposed to be regulated by myristoylation as a knockdown of NMT1 to block myristoylation downregulated its activity (S. Kim et al., 2017).

The β subunit of AMPK contains a myristoylation site at its N-terminal region (Gly2). Myristoylation occurs in both β1 and β2 isoforms. Like other myristoylated proteins, this modification has been shown to regulate the physical association of AMPK with intracellular membranes in response to stress signals (Ali et al., 2016). It has been proposed that AMPK can

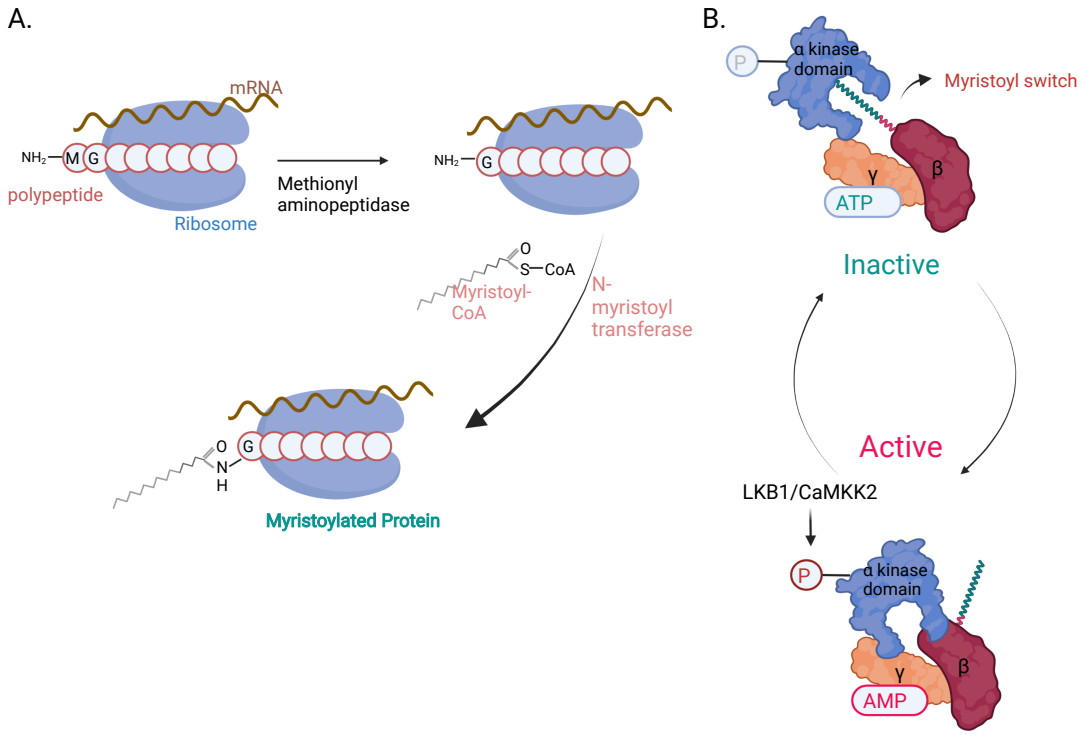

Figure 1.5: **Myristoylation of AMPK β subunit and proposed myristoyl switch hypothesis** (A) Schematic representation of the synthesis of a myristoylated protein. During protein synthesis, the initiator methionine is cleaved by methionyl peptidase, and a myristoyl-CoA is attached to the exposed glycine residue by N-myristoyl transferase generating a myristoylated protein. (B) Under physiological conditions or lower intracellular AMP:ATP, the myristoyl group interacts with the kinase domain (OFF), suppressing the phosphorylation of αThr172 and conferring AMPK at an inactive state. When AMP:ATP rises, binding of AMP releases the myristoyl group (ON) thereby facilitating phosphorylation and activation of AMPK by upstream kinases. Modified from Fig 5 of Oakhill et al., 2010. *Created using BioRender.*

undergo ligand-induced "myristoyl switch" between membrane-bound and cytoplasmic forms (Mitchelhill et al., 1997). This allows AMPK to sense energy stress signals and mediate proximity to its upstream regulators and downstream effectors. The myristoyl switch model has not yet been explicitly validated; however, the importance of myristoylation has been highlighted in several studies. Myristoylation appears to be required for maintaining AMPK at inactive state at physiological condition (Oakhill et al., 2010). Using bacterially expressed AMPK complexes, it has been shown that the myristoyl group binds near the interface of the DFG motif and the catalytic loop of the kinase domain, conferring an autoinhibitory effect (Ali et al., 2016). Under conditions that lower intracellular ATP levels and promote binding of AMP, the myristoyl switch is triggered that facilitates membrane association and AMPK activation. Illustration of "myristoyl switch" in response to AMP is depicted in **Fig1.5B**. Since myristoylation allows AMPK to sense stress signals, it is required for AMP-mediated Thr172

phosphorylation and is required to achieve maximum kinase activity *in vitro*. The importance of myristoylation has also been addressed in AMPK association with lysosomal (Wen et al., 2019) and mitochondrial membranes (Liang et al., 2015). Myristoylation targets AMPK to the damaged mitochondria for selective mitophagy, and loss of myristoylation impairs this association leading to mitochondrial defects. In Rheumatoid Arthritis (RA) T-cells, expression of NMT1, but not NMT2, has been shown to be significantly reduced, consequently reducing global as well as AMPK myristoylation. This indicated NMT1 to be possibly responsible for AMPK myristoylation. Lack of AMPK myristoylation in these cells prevented AMPK association with lysosomes, impairing LKB1-mediated AMPK activation and mTORC1 inhibition. This consequently resulted in hyperactive mTORC1 signalling leading to inflammation (Wen et al., 2019).

These interesting studies have highlighted the critical roles of myristoylation in AMPK activity. However, it will be essential to know the physiological relevance of this modification in cells and at the organism level to uncover a layer of AMPK regulation by the β subunit isoforms.

1.5 AMPK upstream regulators

AMPK activity is primarily regulated by adenine nucleotides allosterically or by reversible phosphorylation of αThr172 as discussed in previous sections (**Fig1.6**). In addition, there are secondary regulatory sites whose phosphorylation have also been shown to influence AMPK activity (as discussed in **section 1.4.2**). In this section, I will briefly discuss known/proposed kinases and phosphatases responsible for phosphorylation/dephosphorylation of key residues in AMPK which directly impact many AMPK-mediated signalling pathways.

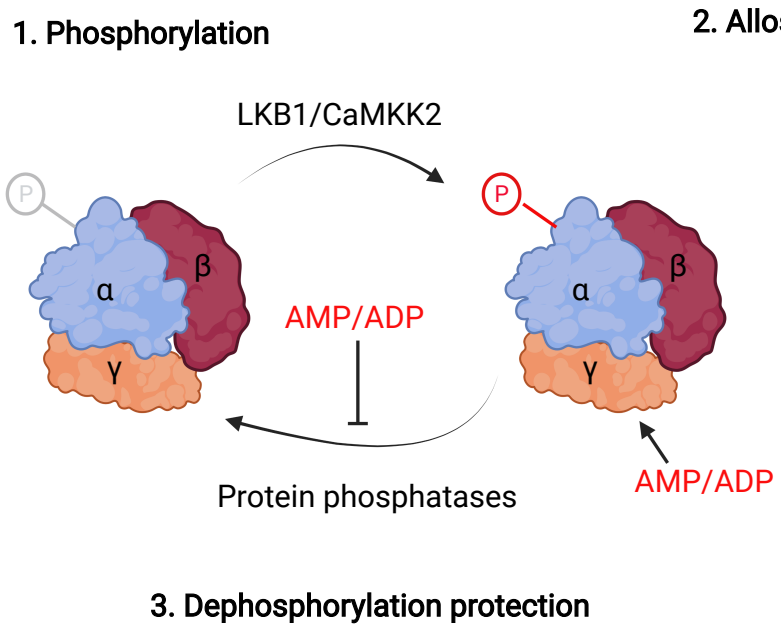

Figure 1.6: **Regulation of AMPK**: Schematic representation of AMPK regulation by adenine nucleotides (AMP, ADP) via three mechanisms (i) enhancing phosphorylation of αThr172 by upstream kinases (ii) allosteric activation (by AMP) (iii) protecting from dephosphorylation by phosphatases. *Created using BioRender.*

1.5.1 Kinases

Previous works from several groups have shown that LKB1 and CaMKK2 are the major upstream kinases that phosphorylate and activate AMPK. LKB1 is a tumour suppressor which forms a trimeric complex with the two accessory subunits STE-20 related adaptor protein (STRAD) and MO25 (Hawley et al., 2003). Loss-of-function mutations in *lkb1* gene have been associated with different forms of tumors (Jenne et al., 1998). LKB1 is a master regulator of members of AMPK-related kinase family, including the α1 and α2 subunit isoforms of the

AMPK (Woods, Johnstone, et al., 2003). It has been shown that LKB1 activity is not sensitive to changes in energy levels and is constitutively active (Sakamoto et al., 2004). As for AMP-mediated AMPK activation, this is achieved via allosteric activation and protection from dephosphorylation by phosphatases increasing net αThr172 phosphorylation (Hunter et al., 2011). *In vitro*, purified LKB1 complex directly phosphorylates AMPK on αThr172. In cells lacking LKB1 (e.g., HeLa cells), AMPK activation in response to stimuli that increase AMP/ATP ratio is abolished (Hawley et al., 2003), indicating LKB1 is necessary for AMP-mediated AMPK activation. Moreover, LKB1 deletion in skeletal muscle is shown to almost completely abolish α2 activity in response to contraction or AICAR (Sakamoto et al., 2005) and deletion of LKB1 in adult liver has been shown to strongly reduce total AMPK activity (Shaw et al., 2005). These studies indicate that LKB1 is the predominant upstream kinase required for AMPK activation in different tissues.

Although LKB1 was found to be primarily responsible for activation of AMPK in a number of cell types/tissues, significant activity of AMPK was detected in some LKB1-deficient cells, suggesting the possible existence of alternative AMPK kinase(s). Different studies have reported that CaMKK2 can phosphorylate AMPK. *In vitro*, CaMKK2 efficiently phosphorylates AMPKα Thr172 (Hawley et al., 1995). In cells, CaMKK2 activates AMPK in response to elevated intracellular Ca^{2+} levels, for instance, thrombin- and T-cell antigen receptor-mediated activation of AMPK in endothelial cells and T cells respectively stimulated by an increase in Ca^{2+} (Stahmann et al., 2006; Tamás et al., 2006).

In addition to adenine nucleotides and Ca^{2+}, more recent studies have identified other kinases to directly phosphorylate AMPK on key regulatory residues upon different stimuli. For instance, upon stimulation with insulin, Akt (also known as Protein Kinase B) phosphorylates Ser485/Ser491 in the ST loop of the α1/α2 isoforms, subsequently attenuating LKB1-mediated αThr172 phosphorylation in the ischemic heart in rodents (Horman et al., 2006). Agents that elevate cellular cAMP (e.g., Forskolin) also inhibited CaMKK2-mediated AMPK activation by enhancing phosphorylation on Ser485/Ser491 of the α isoforms by cAMP-dependent protein kinase (Hurley et al., 2006). Moreover, in the hypothalamus, p70S6 kinase has been shown to phosphorylate α2 subunit on Ser491, inhibiting AMPK activity in response to leptin (Dagon et al., 2012). Interestingly, a more recent study has demonstrated that mTORC1 reciprocally suppresses AMPK activation and signalling through directly phosphorylating α1 at Ser347 and α2 at Ser345 (Ling et al., 2020).

1.5.2 Phosphatases

AMPK activation is essential for activating ATP-generating signalling pathways during energy-deficit conditions. Inhibition of AMPK is equally necessary for its regulation and energy homeostasis. In energy-replete situations (i.e., high ATP/AMP or ATP/ADP), phosphatases can access Thr172 of the α subunit and keep AMPK inactive. When AMP/ATP or ADP/ATP becomes higher, the binding of nucleotides to the γ subunit prevents phosphatases from accessing the α

subunit, thereby increasing AMPK phosphorylation. Several studies have attempted to identify phosphatases responsible for regulating AMPK; however, these studies have discrepancies and inconsistencies. The lack of robust experimental approaches and specific pharmacological modulators has made it challenging to elucidate specific AMPK phosphatase(s). To the best of my knowledge, there is no consensus or validated AMPK phosphatase(s) (e.g., using genetic models) at tissue or organismal levels.

The Ser/Thr protein phosphatases (PP) have been divided into two families: 1. The PPP family includes the subfamilies PP1, PP2A and PP2B; 2. The metal-dependent PPM family includes the PP2C subfamily and consists of highly conserved protein phosphatases with 17 distinct genes in the human genome (Pang Ching et al., 1997). In humans, monomeric PP2C exists in two isoforms (α and β), while in mice, the β isoform further has five variants (β1-β5). PP2A exists as heterotrimers with two regulatory subunits, A and B, and one catalytic subunit, C. Early studies showed that AMP-mediated AMPK phosphorylation was inhibited in cell-free assays in the presence of PP1, PP2A or PP2C (Carling et al., 1987; Davies et al., 1995). Furthermore, chronic calcium release in C2C12 cells or muscle tissues inhibited AMPK activity via activation of PP2A, suggesting calcium-mediated AMPK regulation by PP2A (Park et al., 2013). In rat aortic smooth muscle cells, inhibition of PP2A activity was correlated to an increase in AMPK activity. In the aorta of high fat-fed mice, PP2A formed a complex with AMPK inhibiting its activity suggesting regulation of AMPK by PP2A in diseases associated with cholesterol dysregulation (Joseph et al., 2015). However, in intact hepatocytes, it was shown that PP2C is mainly responsible for AMPK dephosphorylation, as AMPK activity was unchanged in the presence of okadaic acid (a potent inhibitor of PP1 and PP2A), to which PP2C is insensitive (Moore et al., 1991). Biochemical characterisation of recombinant human PP2Cα showed that AMPK and other phosphopeptides containing identical sequences around the regulatory phosphorylation site are excellent substrates of PP2Cα (Marley et al., 1996). In another study using lentiviral-mediated gene silencing in HEK293 cells, PPM1E and PPM1F, but not PPM1A/PP2Cα, were shown to contribute to AMPK dephosphorylation (Voss et al., 2011). Meanwhile, another study by Chida et al. showed that in addition to PPM1E and PPM1A/PP2Cα, PPM1B/PP2Cβ also contributes to AMPK dephosphorylation. Interestingly, they have described that similar to the AMPKβ subunit, ectopically-expressed PPM1A and PPM1B are N-myristoylated and that they require this modification to be able to dephosphorylate their substrates (Chida et al., 2013). This implicates an additional regulatory mechanism of AMPK by phosphatases; however, the authors did not provide evidence of endogenous PPM1A and PPM1B to be myristoylated and co-localised with their substrates in cells.

1.6 AMPK downstream effectors – Phosphoproteomics approaches

AMPK controls numerous cellular functions through the regulation of target proteins by phosphorylation. Initially, AMPK was identified to phosphorylate the two crucial enzymes in lipid metabolism, acetyl-CoA carboxylase (ACC) and 3-hydroxy-3-methylglutaryl coenzyme A (HMG-CoA) reductase at Ser79 and Ser871 respectively, both in cells and *in vivo* (Moore et al., 1991). Phosphorylation of these proteins by AMPK inactivates their activities, thereby inhibiting lipid synthetic pathways. After that, many efforts have been made to identify proteins phosphorylated by AMPK directly influencing several downstream processes.

Several groups have used different techniques and methods to identify AMPK substrates in cells/tissue models confirming AMPK to have both metabolic and non-metabolic roles. Using a chemical genetics screen, AMPKα2 was shown to phosphorylate proteins involved in mitosis, cytokinesis and cytoskeletal organisation (Banko et al., 2011), particularly protein phosphatase one regulatory subunit 12C (PPP1R12C) and p21-activated protein kinase (PAK2), for mitotic progression when cells were serum-starved or stimulated with 2-deoxyglucose. This approach allowed the labelling of direct substrates of AMPK in HEK293 cells by replacing a gatekeeper residue in the ATP-binding pocket of the kinase with a smaller amino acid, generating an analogue-specific (AS) kinase. The AS kinase, but not a WT kinase, can use a modified bulky ATP-analogue N6 (phenethyl) ATPγS as a substrate. The transferred thiophosphate is then alkylated and recognised by a third antibody. Using the same approach and mode of AMPK activation in U2OS cells coupled with peptide capture and tandem mass spectrometry (MS), direct phosphorylation sites of substrates of both AMPKα1 and α2 were identified. These were proteins involved in cell motility, adhesion and invasion, with a particular focus on RHOA guanine nucleotide exchange factor NET1A, which, when phosphorylated by AMPK, inhibits extracellular matrix degradation (Schaffer et al., 2015).

To identify tissue-specific AMPK substrates, a chemical genetics screen approach was applied to the 991-treated mouse primary hepatocytes. This resulted in identifying proteins involved in cellular processes, such as vesicle trafficking, lipid/glucose metabolism or cytoskeletal organisation. This included GTPase-activating protein and VPS9 domain-containing protein 1 (Gapvd1), and starch-binding domain 1 (STBD1) (Ducommun et al., 2019). In another study, using the affinity proteomics strategy, more than 50 proteins were found to be uniquely enriched in the activator-treated mouse primary hepatocytes (AICAR+A769662), including mitochondrial fission factor (MFF), indicating the role of AMPK in mitochondrial dynamics (Ducommun et al., 2015). This study has made use of an antibody to isolate and identify proteins from hepatocytes that contain an AMPK substrate recognition motif **(Fig1.7)**, further highlighting the critical role of AMPK in the liver.

AMPK is widely known to regulate exercise response in muscles. Two studies were conducted to identify conserved pathways during exercise using three different exercise models – cycling in human subjects, trade-mill running in mice and *in situ* contraction in rats. Global phosphoproteomics analysis in these studies involving phosphopeptide enrichment and

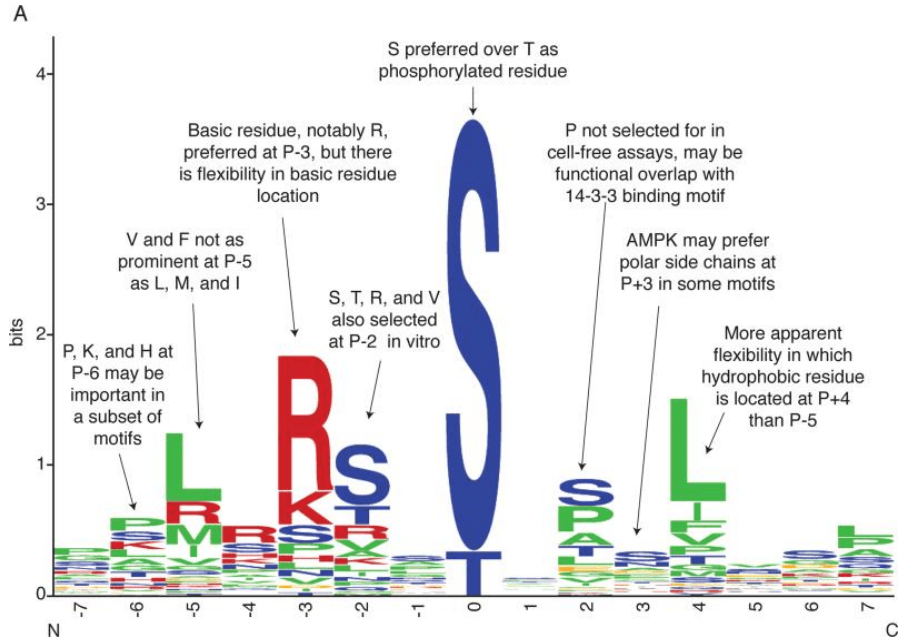

Figure 1.7: **AMPK phosphorylation motif** The logo motif of 64 known AMPK phosphorylation sites from P-7 to P+7 and points of interest in the AMPK recognition motif (Hardie et al., 2016).

sequential elution from immobilised metal ion affinity chromatography (SIMAC) revealed more than 22,000 phosphosites which were common in mice, rats and humans, with AMPK-Ca^{2+} being the most highly enriched signalling pathway across all three exercise models (Nelson et al., 2019). This study revealed that AMPK phosphorylates stromal interaction molecule 1 (STIM1) and negatively regulates store-operated calcium entry (SOCE) which is required during exercise.

Continued interests in identifying novel AMPK substrates are growing, mainly because AMPK is a primary target for various chronic diseases, and an in-depth understanding of the consequences of AMPK activation/inhibition is required. Some techniques used in previous studies were not sensitive enough to capture even highly expressed known AMPK substrates. Some methods were less efficient due to background phosphopeptides. Therefore, a more robust system and a thorough investigation of phosphoproteins are invaluable to further understanding AMPK-mediated or AMPK-dependent pathways.

1.7 AMPK and Golgi

The second part of this thesis focuses on identifying novel substrates and biological roles of AMPK by unbiased phosphoproteomics. As described in previous sections, the role of AMPK in classic metabolic signalling pathways is well known. It has been well validated, for example, as an essential regulator of lipid and glucose/carbohydrate metabolism. Additionally, there has been growing interest in AMPK regulation of pathways not conventionally classified as metabolic, such as autophagy, cell growth, and cell migration. Interestingly, our current phosphoproteomics screen identified several novel targets of AMPK, which are linked to regulation of Golgi structure and function. This section will briefly discuss the Golgi apparatus, its structure and role in different cellular processes and the current understanding of AMPK-Golgi biology.

1.7.1 Golgi Structure and function

The Golgi complex is a central organelle in the secretory pathway which receives proteins synthesised in the Endoplasmic Reticulum (ER), sorts, modifies, and packages them into vesicles for transport to the destination: the plasma membrane, the endosomal/lysosomal membrane or extracellular domain (Boncompain and Weigel, 2018). The organisation of the Golgi structure differs among organisms. In mammals, they exist as Golgi ribbons made of flat cisternae arranged into stacks and connected by tubular membrane bridges (Lowe, 2011). The cisternae are highly polarised with the -cis face receiving cargo that is synthesised in the ER and the -trans face or the Trans Golgi Network (TGN) sorting cargo for post-Golgi transport (Gonatas, 1997). The major function of the Golgi apparatus is the correct cargo receiving and processing, which is important for an organism's normal development and physiology. This involves modifying proteins by adding carbohydrates (producing glycoproteins and proteoglycans) by glycosylation or adding phosphate by phosphorylation (Boncompain and Weigel, 2018). Early glycosylation events are mediated by enzymes residing at the -cis membrane, while late and terminal glycosylation enzymes are located in the -trans membrane (Novikoff et al., 1971). Golgi apparatus has also been shown to function as a Ca^{2+} store as several proteins responsible for Ca^{2+} regulation (Ca^{2+} pumps, Ca^{2+} channels, and Ca^{2+} binding proteins) reside in the Golgi apparatus (Pizzo et al., 2011; Rabouille et al., 1995). More recently, the Golgi ribbon has been shown to be a site for localisation and activation of mammalian target of rapamycin (mTOR) (independent of lysosomal pools of mTOR), highlighting the role of Golgi stacks in pathways important in cellular homeostasis (Gosavi et al., 2017).

1.7.2 Regulation of Golgi morphology

Golgi's highly dynamic structure allows rapid changes, disassembly, and reassembly under different physiological conditions. For instance, a dramatic change in its structure is observed during cell division (Jackson, 2018) **(Fig1.8)**. The Golgi apparatus appears as a stacked compact

ribbon localised in the juxtanuclear position near the Microtubule Organising Centre (MTOC) during interphase and undergoes extensive fragmentation during mitosis, which is required for the G2/M transition of the cells (Tang and Wang, 2013). This is mediated by the small GTPase Arf1, activated by a Guanine nucleotide exchange factor (GEF) named Golgi-specific Brefeldin A-resistance factor 1 (GBF1). Arf1 has a dynamic association/disassociation with the Golgi membrane and is regulated by GTP binding and hydrolysis. In the event of mitosis, the level of active GTP-bound Arf1 decreases. This is partly because GBF1 undergoes inhibitory phosphorylation events during mitosis, dissociating it from the Golgi membrane, thereby making it incapable of activating Arf1 (Walton et al., 2020). This inactivation of Arf1 prevents the recruitment of cytosolic effectors to the Golgi membrane and leads to Golgi disassembly (Altan-Bonnet et al., 2004).

Golgi structure has also been shown to be regulated by microtubules (MT). They play an important role in the organisation of the Golgi complex (Thyberg and Moskalewski, 1999). An intact MT network is required for the integrity of the Golgi apparatus by localising it in the perinuclear position. Furthermore, the Golgi complex can also directly induce nucleation of a subset of MT (A. A. W. M. Sanders and Kaverina, 2015). This has been shown both *in vitro* and *in vivo* (Chabin-Brion et al., 2001), indicating Golgi complex to be a microtubule-organising organelle. Consistent with the MT-Golgi relationship, microtubule depolymerising agents (e.g., Nocodazole) dramatically alter Golgi structure and integrity. The cisternal stacks are separated and dispersed along the stable MTs after depolymerising the most labile MT subpopulation (Chabin-Brion et al., 2001). Removal of nocodazole, however, allows reassembly of MTs and translocation of the Golgi elements along the newly polymerised microtubules, finally reassembled as intact Golgi complex (Guizzunti and Seemann, 2016). All these studies indicate a strong functional relationship between the structure and organisation of the Golgi complex and microtubules.

1.7.3 Oxysterol-binding protein and Oxysterol-binding protein-related proteins

The structure of the Golgi apparatus is also regulated by different lipid modifying/transfer proteins. The Golgi apparatus generates vesicles to transport lipid and protein cargo within a cell. There is a constant flux of lipid molecules like ceramide, cholesterol, phosphoinositides (PI) in the Golgi, which is maintained by several lipid modifying or binding proteins (Emr et al., 2009). Some of the examples are Nir2, Ceramide Transfer Protein (CERT) and Oxysterol-Binding Protein (OSBP) or oxysterol-binding protein-related proteins (ORPs). These proteins localise in the ER-Golgi Membrane Contact Site (MCS) where they transfer lipids (glucosylceramide, ceramide or sterols) from the ER to the trans-Golgi (Walton et al., 2020). OSBP is a cytosolic protein that was first discovered as a protein with oxysterol-binding activity (Taylor and Kandutsch, 1985). Oxysterols are the 27-carbon products of cholesterol oxidation and suppressors of HMG-CoA reductase activity and of cholesterol biosynthesis in cultured cells (Kandutsch and Chen, 1973). OSBP translocates from cytosol to the Golgi membranes upon stimulation with 25-hydroxycholesterol (25-OHC) (Ridgway et al., 1992). A

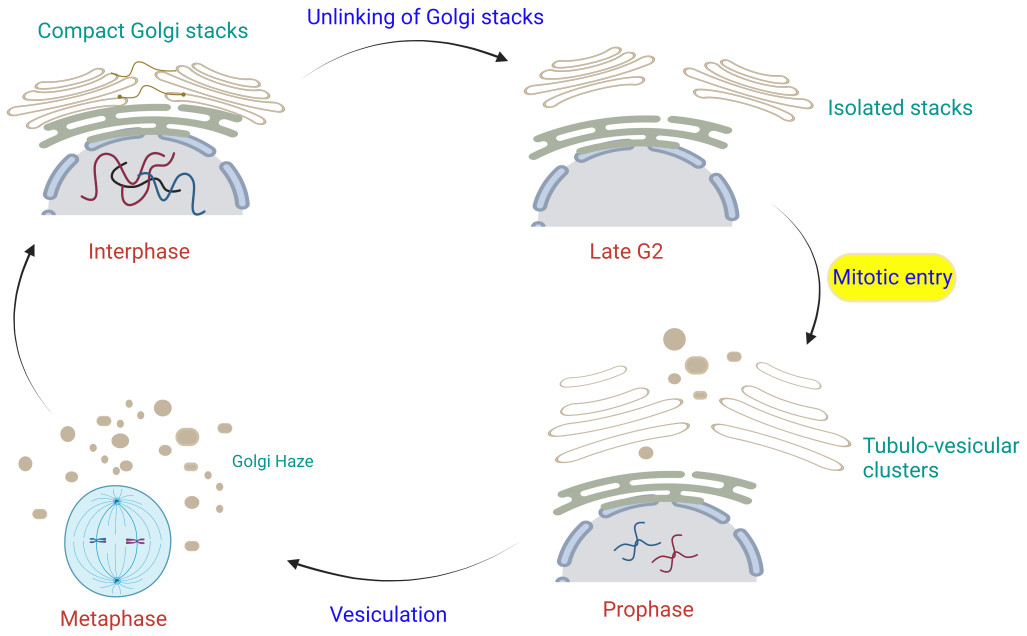

Figure 1.8: **Golgi during mitosis** Graphical representation of different phases of mitosis and associated structural changes in the Golgi apparatus. Adapted from Persico et al., 2009. *Created using BioRender.*

distinct domain mediates sterol binding in the carboxy-terminus of OSBP, namely, the oxysterol binding domain and the Golgi targeting is mediated by the pleckstrin homology (PH) domain in the amino-terminus (Lehto and Olkkonen, 2003). 25-OHC binding to the sterol-binding domain induces a conformational change that exposes the PH domain, thus translocating OSBP to the Golgi. The role of OSBP on cellular cholesterol metabolism has been addressed in several studies (Lehto and Olkkonen, 2003; Ridgway et al., 1998; Storey et al., 1998). Recent studies have highlighted the importance of posttranslational modification of OSBP, particularly phosphorylation, for its subcellular localisation. For instance, OSBP is phosphorylated by protein kinase D (PKD), a Golgi-localised Ser/Thr kinase, inhibiting 25-OHC-mediated Golgi localisation of OSBP, thereby, inducing Golgi fragmentation (Nhek et al., 2010). Therefore, OSBP plays a significant role in Golgi regulation and cellular lipid homeostasis.

Identification of homologues of OSBP has provided new insights into the control of lipid metabolism. These are a family of lipid transfer proteins that are greatly conserved in all higher eukaryotes. These proteins are known as oxysterol-binding protein-related proteins (ORPs) or Oxysterol-binding protein like proteins (OSBPLs). In yeasts, there are seven members in this family; in humans, 12 members have been identified. One common feature of the

ORP family members is the lipid-binding domain or the oxysterol-binding protein-related domain (ORD) which binds lipid ligands, oxysterols being the first ligand to be identified. Several studies have shown that ORD can also bind to other lipid molecules like cholesterol, phosphoinositides, phosphatidylserine (PS) or phosphatidylcholine (PC). The 12 members have been grouped into six classes based on sequence homology and domain structure and organisation **(Fig1.9)**. Most of these proteins have partial cytoplasmic localisation, but mostly they possess distinct localisation patterns (e.g., between organelles, in the nucleus, in the MTs etc.). Different groups of ORPs, their reported subcellular localisation and intracellular functions are summarised in the **Appendix Table A.1** (Pietrangelo and Ridgway, 2018).

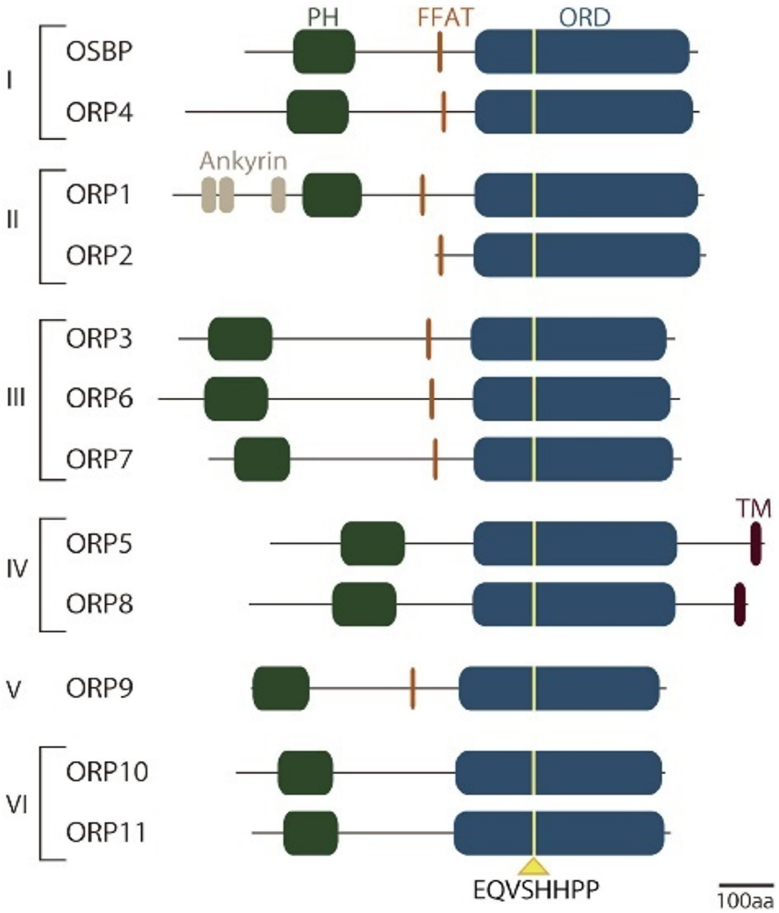

Figure 1.9: **OSBP and related proteins** Domain structure of Oxysterol binding protein (OSBP) and different isoforms of Oxysterol binding protein-related proteins (ORPs or OSBPLs). Key elements include the phosphatidylinositol-binding PH domain, the FFAT motif and the oxysterol-binding domain (ORD) (Nakatsu and Kawasaki, 2021).

OSBP and OSBPL9/ORP9 (Wu et al., 2013) are present at the ER-Golgi MCS where they interact with the ER via two phenylalanines (FF) in an acidic tract (FFAT) motif and Vesicle-Associated Membrane Protein-Associated Protein A (VAP-A) binding (Peretti et al., 2008). When cells are packed with cholesterol (e.g. by stimulation with exogenous oxysterols) or depleted of cholesterol to induce *de novo* synthesis, OSBP and OSBPL9 associate at the

ER-Golgi contact sites and transport the ER-derived cholesterol to the Golgi and in turn, Golgi-derived phosphatidylinositol 4-phosphate (PI(4)P) to the ER (Mesmin et al., 2013). At the ER, PI(4)P is degraded by PI(4)P phosphatase Sac1. Golgi then has enriched cholesterol, which mediates recruitment of phosphatidylinositol-4-kinase (PI4K)IIα inducing an increase in the level of PI(4)P. Increase in PI(4)P then recruits CERT to the MCS via the PH domain, thereby transporting ceramide from the ER to the Golgi, which is used as a substrate for sphingomyelin synthesis (Banerji et al., 2010). In this way, lipid transfer proteins at ER-Golgi MCS, such as OSBP or OSBPL9, are required to maintain cholesterol and sphingolipid-enriched membranes, which subsequently are required for efficient cargo secretion. Furthermore, silencing OSBPL9 in cells has shown to result in Golgi fragmentation, indicating this protein's important role in maintaining Golgi integrity. Loss of Golgi structure by silencing OSBPL9 further resulted in defective cargo trafficking from the ER to the Golgi as demonstrated by vesicular stomatitis virus G (VSVG) transport assay (Ngo and Ridgway, 2009). Although the exact molecular mechanism of how these proteins are regulated intracellularly is incompletely understood, these studies demonstrate the importance of lipid transport/sensing proteins in cholesterol homeostasis and maintenance of integrity and positioning of organelles to which they are associated.

1.7.4 AMPK in Golgi signalling

AMPK has differential localisation dynamics; for instance, it shuttles between the nucleus and cytoplasm in response to specific physiological stimuli. AMPK has also been shown to localise in particular cell compartments, including endomembrane structures (Mitchelhill et al., 1997). Such compartmentalisation could allow AMPK to regulate several substrates that localise at distinct locations. A recent study from Miyamoto *et al.* developed a genetically encoded FRET-based AMPK biosensor that can selectively monitor AMPK dynamics at individual subcellular components (T. Miyamoto et al., 2015). This fluorescent biosensor revealed AMPK activity at specific compartments, including lysosomes, ER, Golgi apparatus and mitochondria and revealed that AMPK activity is higher in these endomembrane structures than in the cytosol. AMPK's role in mitochondrial function has been well studied, and it has been shown that it phosphorylates MFF to promote mitochondrial fission and regulate mitophagy and biogenesis (Herzig and Shaw, 2018). Furthermore, mitochondria-localised AMPK has been shown to regulate exercise-induced mitophagy (Drake et al., 2021). Similarly, the lysosome is a well-known signalling hub for AMPK and mTORC1 pathways regulating autophagy and lysosomal biogenesis (Zhang et al., 2014). Although a few reports indicate the protective function of AMPK against ER stress (Dong et al., 2010; H. Kim et al., 2015), studies linking AMPK and Golgi are minimal, with limited knowledge on AMPK regulation of Golgi-specific substrates.

As discussed in **section 1.7.2**, the Golgi apparatus undergoes extensive fragmentation during mitosis to allow a smooth transition of cell cycle and prevent cell cycle arrest. These cellular activities require a balance of nutrients such as glucose and amino acids. AMPK, being an energy sensor, has been shown to regulate several of these cellular processes, e.g., cell polarity,

cytokinesis, and mitotic progression through phosphorylation of proteins associated with these events (Nakano and Takashima, 2012; Vazquez-Martin et al., 2009). Under glucose-depleted conditions, AMPK has been shown to phosphorylate GBF1 at Thr1337 (T. Miyamoto et al., 2008). Additionally, 2-deoxyglucose, Carbonyl cyanide-p-trifluoromethoxyphenylhydrazone (FCCP), and AICAR also induced GBF1 phosphorylation in cells, indicating metabolic stress-mediated regulation of GBF1. Phosphorylation at Thr1337 has been shown to dissociate GBF1 from the Golgi membrane, thereby inhibiting its GEF activity to Arf1 resulting in Golgi disassembly or fragmentation (T. Miyamoto et al., 2008). Therefore, the importance of GBF1 and its phosphorylation during mitosis has been described. It has also been shown that AMPK activity is enhanced during mitotic progression by measuring pThr172 AMPKα and pSer79 ACC signals in mitotic HEK293 cells and that activated AMPK interacts with GBF1 by co-immunoprecipitating endogenous AMPK from GBF1-overexpressed HEK293 cells (Mao et al., 2013). Compound C treatment abolished the interaction and phosphorylation of GBF1, thereby resulting in cell cycle arrest (G2/M), indicating AMPK-mediated GBF1 phosphorylation. Although these studies claim GBF1 phosphorylation to be dependent on AMPK during mitosis or energy-depleted conditions, compounds utilised to activate/inhibit AMPK are not specific and could have off-target effects. Therefore, appropriate controls are required to elucidate the AMPK-Golgi relationship.

In another study, AMPK's involvement in the mitotic entry in cells was further explored by investigating α subunit isoform-specific roles in mitosis. The authors showed that α2, and not α1 is responsible for cell cycle progression. Knockdown of α1 did not alter cell cycle whereas α2 knockdown resulted in cell cycle arrest, effects similar to Compound C treatment (Lee et al., 2015). Furthermore, α2 depletion delayed mitotic Golgi fragmentation in synchronised HeLa cells. They also observed AMPK activation and pThr172α signals localisation at Golgi during mitosis, indicating AMPK contribution to Golgi fragmentation and G2/M transition. In addition, the authors showed that CaMKK2 is responsible for AMPK activation during mitosis and the late G2 phase. Treatment with CaMKK-inhibitor STO-609 abolished pThr172 AMPKα signals from Golgi and delayed mitotic Golgi fragmentation and G2/M transition. This study presented the CaMKK2-AMPKα2 axis as a regulator of mitotic Golgi fragmentation and cell cycle progression; however, it is still unknown what specific Golgi-associated substrates of α2 could be involved in this process. GBF1 is one of the substrates to be phosphorylated by AMPK during mitosis and energy depletion. Nevertheless, Golgi is a complex organelle regulated by multiple proteins during different physiological conditions. This would suggest that numerous Golgi-related substrates of AMPK could be involved in regulating the structure and function of Golgi, irrespective of cell cycle states, which are not yet investigated.

2 Results

2.1 Regulation of AMPK by the β subunit myristoylation

2.1.1 Background and aim of the study

The β subunit of AMPK is a crucial component of the heterotrimeric complex because it functions as a scaffold to stabilise the trimer and forms a binding pocket for small molecule allosteric ligands. Notably, the β subunit is also posttranslationally modified by reversible phosphorylation and N-terminal myristoylation. The β subunit isoforms (β1 and β2) undergo the myristoylation at Gly2. This modification has been proposed to play a role in energy sensing of AMPK, possibly through association with subcellular compartments such as lysosomes, in response to increased levels of AMP or stress signals (e.g., glucose starvation) (Liang et al., 2015; Oakhill et al., 2010). However, how this modification mechanistically influences AMPK activity is still a question to address, and this could present a significant challenge in understanding the overall regulation of AMPK function. This study aimed to investigate the molecular basis of AMPK regulation by the β subunit myristoyl switch and physiological/metabolic consequences of myristoylation deficiency in mice *in vivo*.

Using robust cell and animal models, we investigated the importance of β subunit myristoylation. Using the Flp-In-mediated recombination system in the β1/2 double knockout (DKO) human U-2 Osteosarcoma (U2OS) cells, I generated stable isogenic cell lines that express either wild-type (WT) or myristoylation-deficient Gly2Ala mutant (G2A) β1 or β2 isoforms. We collaborated with the group of Drs. Sandra Galic and Bruce Kemp (St. Vincent's Institute, Melbourne) who generated mouse models with whole-body knock-in (KI) mutations of the myristoylation site (Gly2) of the β subunit isoforms to alanine (β1 G2A KI or β1/2 G2A double KI (DKI)). We studied the role of myristoylation in whole-body energy metabolism and focused on metabolic regulation, specifically in the liver, using the β1 G2A KI mice. Using mouse embryonic fibroblasts (MEFs) derived from the KI mice and the stable U2OS cell lines, I studied the effects of loss of myristoylation on cellular AMPK activity and localisation.

Results obtained using MEFs and β1 G2A KI mice make up a large part of this work and are

available in the Appendix section as a manuscript which is under revision in Cell Reports.

Katyayanee Neopane, Natalie Kozlov, Lisa Murray-Segal, Florentina Negoita, Ashfaqul Hoque, Luke M. McAloon, Dingyi Yu, Naomi X.Y. Ling, Matthew J. Sanders, Jonathan S. Oakhill, John W. Scott, Kim Loh, Bruce E. Kemp, Kei Sakamoto, and Sandra Galic (2022) **Loss of β1 subunit myristoylation enhances AMPK activity with beneficial effects on metabolic health *in vivo***
Under revision (Cell Reports)

2.1.2 Study of AMPKβ subunit myristoylation using human U2-Osteosarcoma cell lines

2.1.2.1 Characterisation and validation of genetically modified cell models

To study the role and regulation of AMPK by the β subunit myristoylation, robust cellular and genetic model systems are necessary. Our group has generated β1 knock-out (KO) and β1/2 double knock-out (DKO) U2OS cell lines using CRISPR-Cas9 genome editing technology in collaboration with Horizon Discovery (Cambridge, UK) (M. J. Sanders et al., 2022). The KO cell lines were generated using the U2OS parental wild type (WT) cell line that expresses functional AMPK with the Flp-In TREX system integrated (generous gift from Prof. John Rouse, University of Dundee). This allows for Flp recombinase-mediated DNA integration at Flp recombination target (FRT) site to generate isogenic stable cell lines expressing the gene of interest **(Fig 2.1)**. The β1/2 DKO Flp-In TREX cells allow for a single copy and stable reintroduction of the WT and mutant forms of the β subunit.

To characterise and validate the β subunit KO cell lines, I initially performed a quantitative immunoblot analysis (**Fig 2.2A**). Complete deletion of β1 protein in the β1 KO cells and β1/β2 in the DKO cells was validated using a β1-specific antibody which recognises the N-terminal region of β1 isoform or pan-β1/2 antibody which recognises the conserved C-terminal region of both isoforms. The expression of each isoform was quantified which revealed that the expression of total α subunit in β1 KO cells was reduced by ~ 50% compared to WT, while in the DKO cells, total α was undetectable (**Fig 2.2B**). Consistent with prior studies, this confirms the important role of the β subunit in stabilising the AMPK trimeric complex. A modest reduction (~ 20%) in the expression of the γ1 subunit was observed in β1 KO, while in the DKO cells, γ1 expression was reduced by ~ 50%. Collectively, these data validated the respective knockouts and confirmed critical roles for the β subunit forming stable trimeric AMPKαβγ complexes in human U2OS cells.

Next, I assessed AMPK activity in the KO cells following treatment with A769662 and 991. I chose saturating/maximal concentrations of these compounds (10μM 991, 100μM A769662) based on our previous studies (Göransson et al., 2007, Bultot et al., 2016) and the dose-response analysis performed in our group (data not shown). As described in **section 1.3.1**, A769662 selectively activates β1-containing complexes while 991 activates both β1- and β2-containing complexes. Both 991 and A769662 robustly activated AMPK in WT cells, assessed

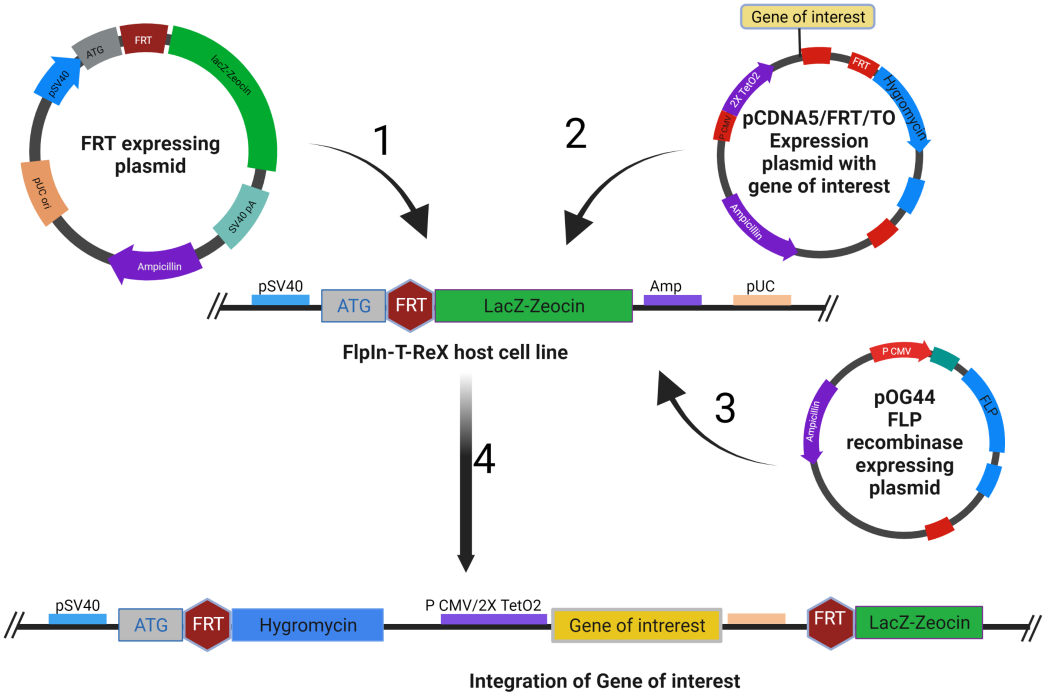

Figure 2.1: **Flp-In recombination system** Schematic representation of the Flp-In system of gene integration to generate isogenic stable cell lines expressing the gene of interest. An Flp-recognition site (FRT) is introduced into the genome of a cell line of choice using an FRT expressing plasmid (1) and an expression vector containing a Hygromycin resistance gene, and the gene of interest is integrated into the genome (2) via the Flp recombinase-mediated DNA recombination which is expressed by the pOG44 plasmid (3), giving a Flp-In cell line expressing the integrated gene of interest and conferring hygromycin resistance for selection. Adapted from Invitrogen. *Created using BioRender.*

by phosphorylation of AMPKα Thr172, ACC Ser79, and Raptor Ser792 (**Fig 2.2 C and D**). As anticipated, 991, but not A769662, elicited a robust effect on AMPK in β1 KO cells. Neither 991 nor A769662 activated AMPK in β1/2 DKO cells (**Fig 2.2 E and F**).

I also validated AMPK activation in U2OS cells by measuring ACC phosphorylation using a Homogenous Time-Resolved Fluorescence (HTRF) assay to monitor dose-response in a comprehensive way (**Appendix Fig A.1A**). HTRF is a sensitive and higher throughput assay (compared to immunoblotting) combining Fluorescence Resonance Energy Transfer (FRET) with TR measurement. TR-FRET generates a signal through fluorescence energy transfer between the donor and the acceptor only when they are in proximity. Using the HTRF assay, fold changes in phospho-ACC in the presence or absence of the activators were obtained for the respective cell lines. As expected, WT cell lines showed a dose-dependent ACC phosphorylation in response to both 991 and A769662, an effect abolished in the DKO cells (**Appendix Fig A.1B**). β1 KO cells were responsive only to 991, confirming the selectivity of

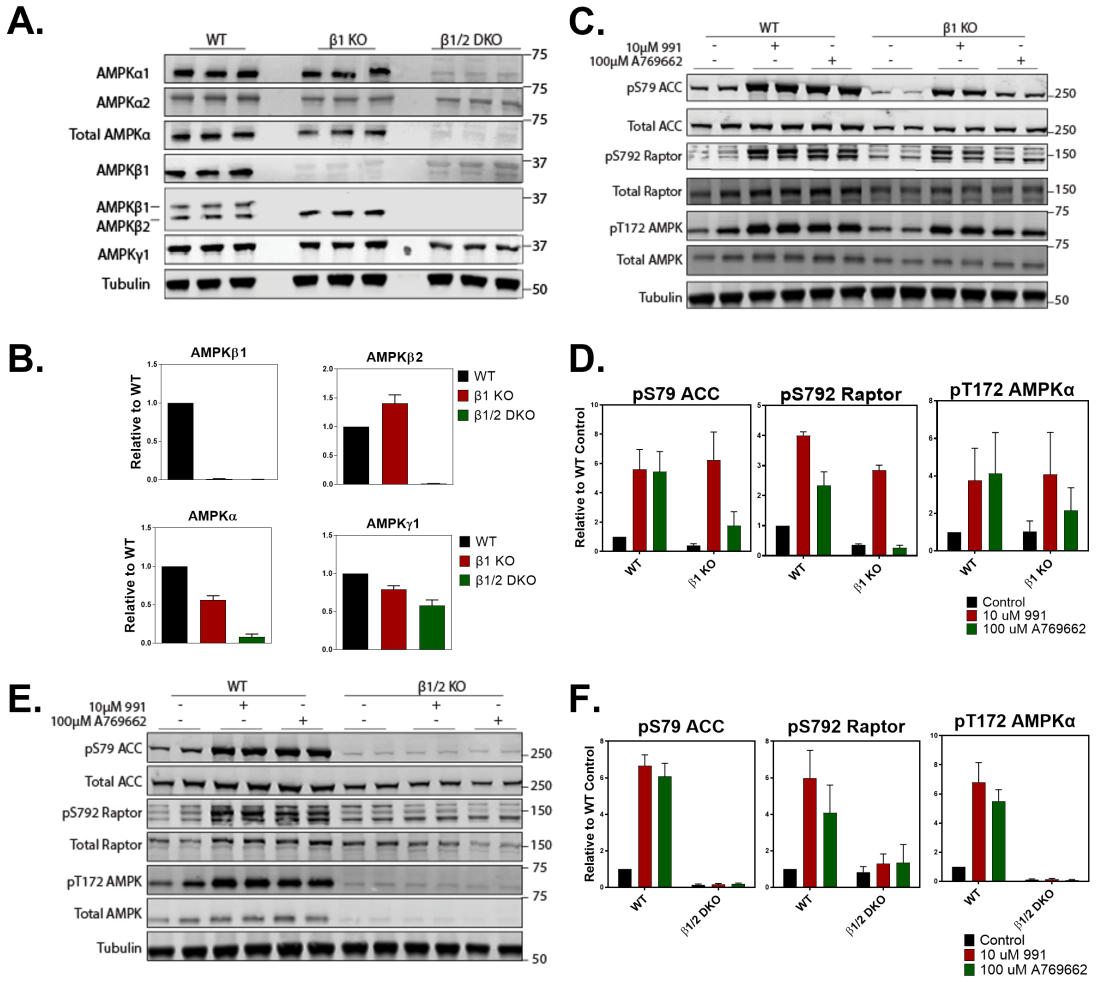

Figure 2.2: **Characterisation of AMPKβ-deficient U2OS cell lines** (A) Immunoblot analysis of AMPK subunit/isoform expression in U2OS WT, β1 KO and β1/2 DKO cells and (B) corresponding quantification normalised to tubulin and shown as relative to WT. (C) Immunoblot analysis and (D) quantification of phosphorylation of AMPKα and its substrates ACC and Raptor in U2OS WT and β1 KO or in (E, F) WT and β1/2 DKO cells after treatment with 10μM 991 or 100μM A769662 for 30 min. Phosphorylation levels were normalised to respective total protein and shown as relative to WT untreated (control). Figures are representative of three independent experiments. Error bars represent mean ± s.e.m.

A769662 towards β1 and the effect of 991 on the β2 isoform. These results further verify the KO cell lines and the dose-dependent effects of AMPK activators on respective β subunit isoforms. To benchmark the HTRF assay, I performed immunoblot analysis and assessed ACC phosphorylation in parallel and confirmed that both assays provide similar data (**Appendix Fig A.1C**). Therefore, the HTRF is a useful assay to monitor cellular AMPK activity in a high-throughput manner.

2.1.2.2 Generation of isogenic stable cell lines and study of the effect of epitope tag location in the β subunit on AMPK

To study the functional role of β subunit isoforms, I reintroduced either β1 or β2 in the β subunit KO cell lines using the Flp-In recombination strategy (**Fig 2.1**). Initially, I used a mammalian expression vector with an N-terminal FLAG tag (N-FLAG-β1 WT or N-FLAG-β2 WT). As shown in **Fig 2.3**, expression of AMPKα total, β1, and γ1 was restored upon reintroduction of β1 WT in the β1/2 DKO cells. I further characterised the stable cell lines by assessing AMPK activity in response to two different AMPK activators, 991 and AMP-mimetic AICAR. Immunoblot analysis showed that phosphorylation of AMPK substrates (ACC and Raptor) was higher in the absence of activators in the N-FLAG-β1 WT expressing cells, and no further increase was observed after treatment with either of the activators (**Fig 2.3B**). HTRF assay further clarified higher basal AMPK activity in the N-FLAG-β1 WT expressing cells and a blunted dose-response effect of 991 (**Fig 2.3C**). A similar result was observed when N-FLAG-β1 WT was expressed in β1 KO cells; however, a modest increase in ACC and Raptor phosphorylation was observed when treated with 991, possibly via stimulation of β2 complexes (**Appendix Fig A.2A and B**).

I reasoned that this impaired substrate phosphorylation in response to the activators in the N-FLAG-β1 WT expressing cells could be due to blockage of N-myristoylation (Gly2) in the β subunit by the N-terminal epitope tag (FLAG). Based on this, I generated stable cell lines expressing C-terminally FLAG-tagged β1 WT in the β1/2 DKO cells. As illustrated in **Fig 2.3D**, stable cell lines expressing either N- or C-FLAG β1 WT had a similar level of AMPK subunit expression. Analysis of AMPK activity and substrate phosphorylation revealed that the cell lines expressing C-FLAG β1 WT had lower basal AMPK activity (comparable to the parental WT cells), which increased upon treatment with 991 or A769662 (**Fig 2.3E**). Similar effect was observed in stable cell lines expressing β2 isoform (**Appendix Fig A.2C**). These results were further confirmed using the HTRF assay, which showed a dose-dependent increase in ACC phosphorylation in the C-FLAG β1 WT in response to 991 (**Fig 2.3F**).

In summary, the tag's location in the β subunit does not affect restoration of the AMPK subunits in the β subunit KO cells. AMPK activity and substrate phosphorylation, however, could be restored by C-terminal, but not N-terminal tagged β subunit, suggesting that the position of the epitope tag in the β subunit could affect the overall cellular activity and responsiveness of AMPK to its activators.

2.1.2.3 Loss of β subunit myristoylation results in enhanced AMPK activation in U2OS cells

To test our hypothesis that N-terminal tagging in the β subunit could interfere with the myristoylation (Gly2), I generated stable cell lines expressing C-terminally FLAG-tagged β1 G2A mutant. I compared expression levels of AMPK subunits by immunoblot analysis, which confirmed that all the subunits were rescued at a comparable level in both β1 WT and β1 G2A-expressing cell lines (**Fig 2.4A**). Immunoprecipitation with a FLAG antibody further confirmed

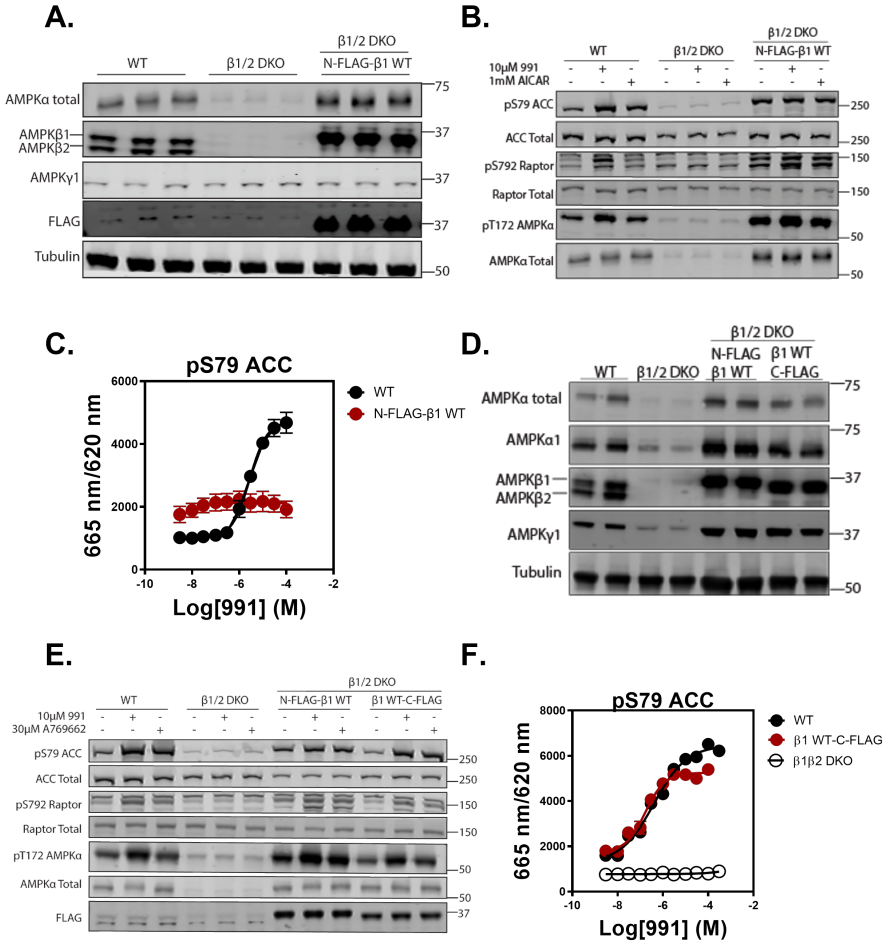

Figure 2.3: **Generation and characterisation of isogenic stable U2OS cell lines** (A) Immunoblot analysis of AMPK subunit/isoforms expression in U2OS WT, β1/2 DKO cells and stable cell lines expressing N-FLAG β1 WT. (B) Immunoblot analysis of phosphorylation of AMPKα and its substrates ACC and Raptor in the respective cell lines after treatment with 10μM 991 or 1mM AICAR for 30 min. (C) Dose-response curves of ACC phosphorylation in the respective cell lines were measured by the HTRF assay after treatment with 991 for 30 min at increasing concentrations. (D) Immunoblot analysis of AMPK subunit/isoforms expression or (E) phosphorylation of AMPKα and its substrates in U2OS WT, β1/2 DKO cells and stable cell lines expressing either N- or C-FLAG β1 WT after treatment with 10μM 991 or 30μM A769662 for 30 min. (F) Dose-response curves of ACC phosphorylation in the respective cell lines were measured by the HTRF assay after treatment with 991 for 30 min at increasing concentrations. Figures are representative of three independent experiments. Error bars represent mean ± s.e.m.

that the binding of β1 to α and γ1 subunits is not affected by the G2A mutation (**Fig 2.4B**).

Next, I assessed cellular AMPK activity in β1 G2A-expressing cell lines by monitoring AMPK substrate phosphorylation upon 991 treatment (**Fig 2.4 C and D**). I left β1 WT or β1 G2A

cells untreated or treated with increasing doses of 991 for 30 min. 991 robustly increased phosphorylation of AMPKα Thr172 and its substrates, ACC, Raptor, and ULK1 in β1 WT cells. In contrast, phosphorylation of AMPKα and its substrates was markedly higher in untreated β1G2A cells, with only modest increases observed upon treatment with 991. Enhanced basal AMPK activity in G2A-expressing cells was further confirmed by the HTRF assay (**Appendix Fig A.3**), where I observed only a modest increase in ACC phosphorylation in response to 991, A769662, or AICAR. I also generated stable cell lines expressing C-terminally FLAG-tagged β2 G2A mutant (**Appendix Fig A.4A**). Consistent with the findings obtained using β1G2A cells, β2G2A cells also had increased basal phosphorylation of AMPK substrates with a very modest change in phosphorylation with 991 or AICAR treatment (**Appendix Fig A.4B**). Both immunoblotting as well as HTRF assay confirmed this observation (**Appendix Fig A.4C**).

Collectively, these results show that loss of myristoylation in the β subunit, irrespective of isoforms, is associated with enhanced activity of AMPK in cells.

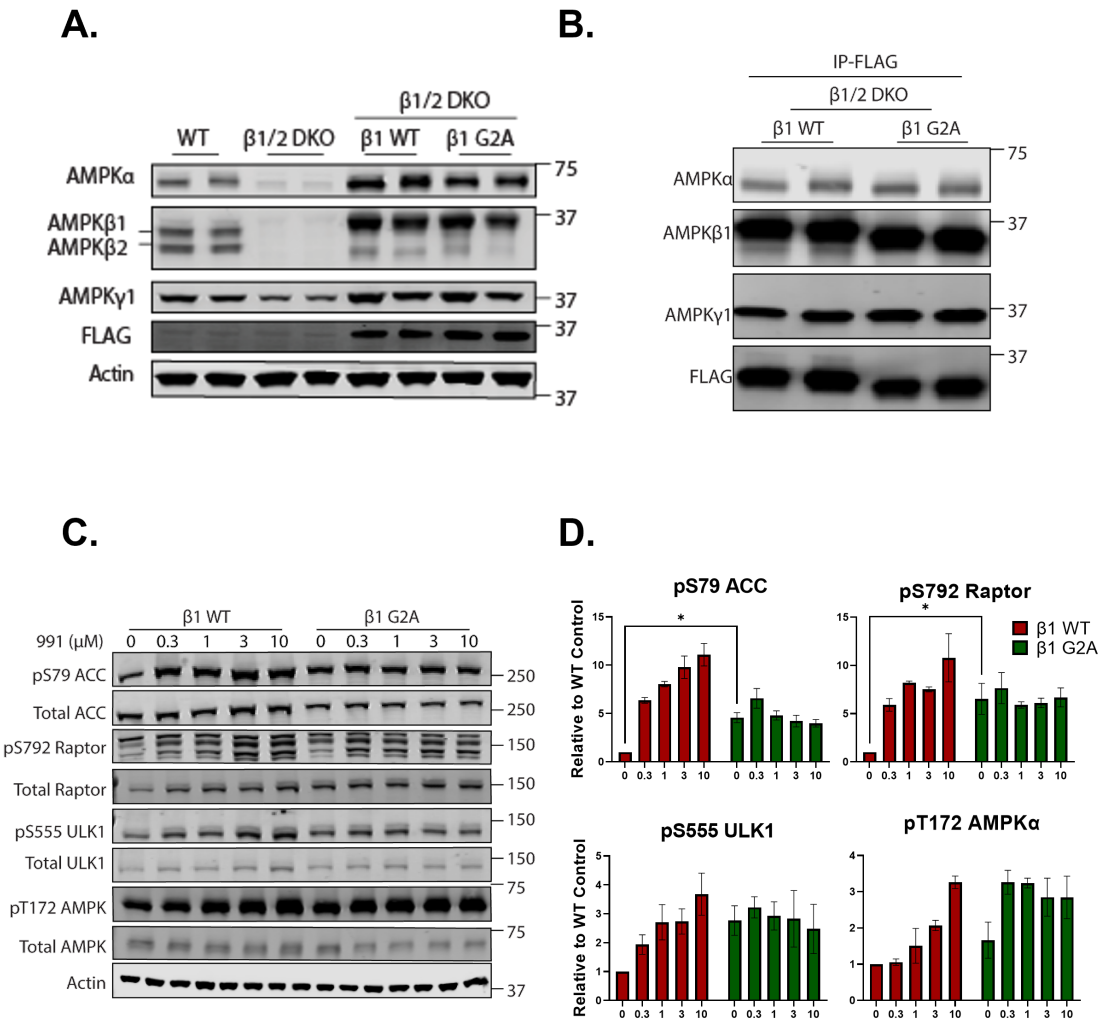

Figure 2.4: **Loss of β-subunit myristoylation (G2A) results in enhanced AMPK activation in U2OS cells** (A) Immunoblot analysis of AMPK subunit expression in U2OS WT, β1/2 DKO cells and stable cell lines expressing C-FLAG β1 WT or β1 G2A in the β1/2 DKO background. (B) Immunoprecipitation of β1 WT or β1 G2A using a FLAG antibody and immunoblot analysis of subunit interaction. (C) Dose-dependent changes in phosphorylation of AMPK substrates in β1 WT or β1 G2A cells with increasing 991 concentrations and (D) corresponding quantification. Phosphorylation levels were normalised to respective total protein and shown as relative to WT untreated (control). Figures are representative of three independent experiments. *P<0.05 represents genotype difference as analysed by two-way ANOVA and Šídák's post-hoc test. Error bars represent mean ± s.e.m.

2.1.3 Study of β subunit myristoylation using Mouse Embryonic Fibroblasts (MEFs)

2.1.3.1 Characterisation of myristoylation-deficient β subunit G2A knock-in MEFs

Mouse Embryonic Fibroblasts (MEFs) serve as a valuable tool for biological research and, when immortalised, can be easily cultured, and utilised to study specific proteins and pathways at the endogenous level. Mouse models carrying whole-body knock-in (KI) of the β subunit isoform-specific G2A point mutation (β1G2A KI and β2 G2A KI) were generated by the group of Drs. Bruce Kemp and Sandra Galic (SVI, Melbourne) using CRISPR/Cas9 gene editing method. The two strains were then inter-crossed to generate β1/2 G2A DKI mice that completely lack myristoylation of the β subunit in tissues. Respective MEFs were isolated from each strain and immortalised by transfection with an SV40 large T-antigen expression construct by the Kemp/Galic group and shipped to us for my studies.

I initially performed quantitative immunoblot analysis to characterise and validate MEFs obtained from WT and β1/2 G2A DKI mice. I used β1 KO and β2 KO MEFs as control, which showed complete loss of β1 and β2 proteins, respectively (**Fig 2.5A**). I observed that expression of β subunit isoforms was profoundly reduced (~70% reduction of β1 and ~80% of β2) in the β1/2 G2A DKI compared to the WT MEFs. Since the β subunit is crucial to stabilise the heterotrimeric AMPK complex, a reduction in its expression was associated with reduced expression of total AMPKα (~50%) and γ1 (~50%) subunits (**Fig 2.5B**). To investigate if the stoichiometry of heterotrimeric complex formation was compromised as a result of reduced expression of the β subunit, I immunoprecipitated β1 from WT or β1/2 G2A DKI MEFs and immunoblotted total AMPKα and γ1 subunits. Despite reduced expression, the relative interaction of β1 with α and γ1 subunits was comparable between WT and G2A mutant, which indicates that loss of myristoylation (G2A mutation) does not affect trimeric complex formation (**Fig 2.5 C and D**).

2.1.3.2 Enhanced AMPK activation in myristoylation-deficient (β1/2 G2A DKI) MEFs

Next, I assessed AMPK activity and substrate phosphorylation in myristoylation-deficient β1/2 G2A DKI MEFs upon 991 treatment. I treated WT and β1/2 G2A DKI MEFs with increasing concentrations of 991 for 30 min (**Fig 2.6**) or with 10μM 991 for up to 60 min (**Appendix Fig A.5**) and assessed phosphorylation of AMPK substrates. I observed that the DKI MEFs have higher basal phosphorylation of AMPKα and its substrates, which is consistent with what I observed in U2OS cells. 991 treatment did not result in a further increase in ACC and ULK1 phosphorylation in G2A DKI MEFs, while there was a modest increase in AMPKα Thr172 phosphorylation and a 2-fold increase in Raptor phosphorylation (**Fig 2.6 A and B**). This differential effect on substrate phosphorylation by 991 in G2A DKI MEFs could be due to changes in the localisation of AMPK as a consequence of myristoylation-deficiency/β G2A mutation. Enhanced basal phosphorylation of ACC and AMPKα in G2A DKI MEFs was also observed using the HTRF assay (**Fig 2.6C**). The increase in ACC phosphorylation was

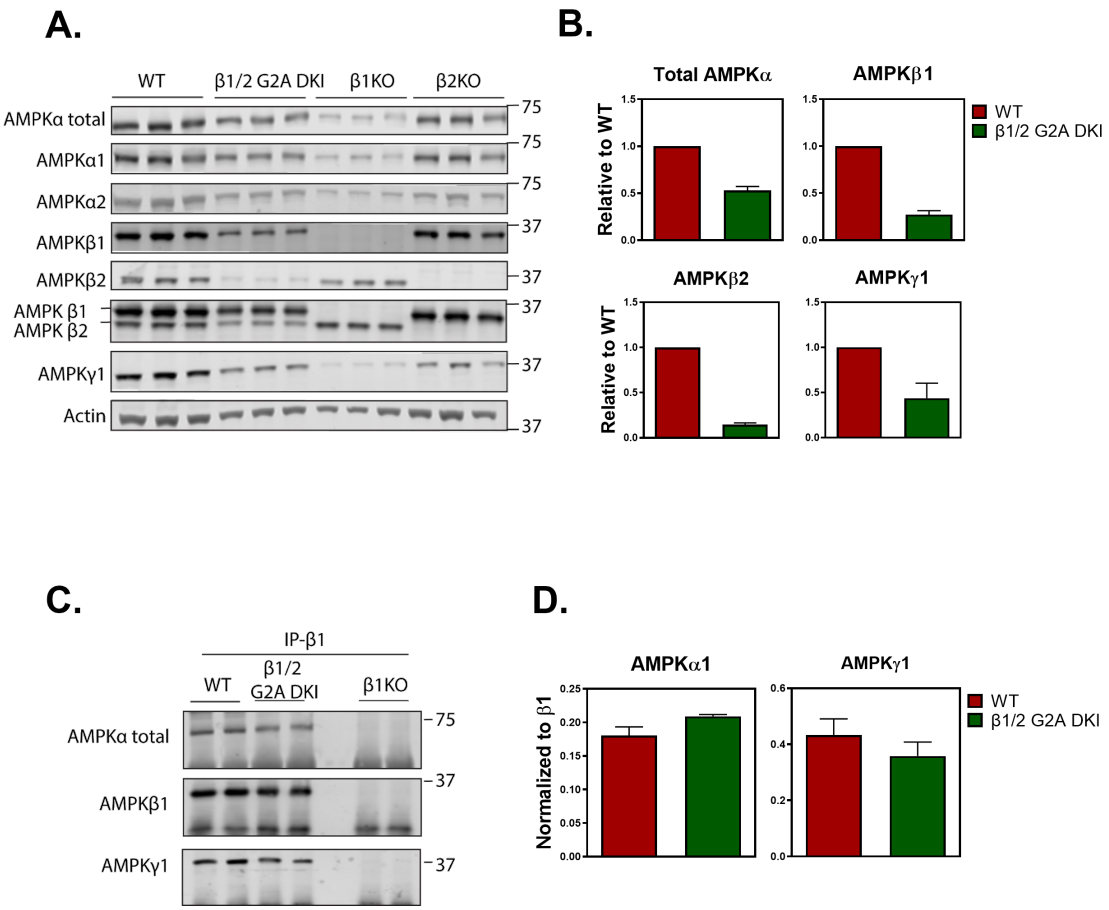

Figure 2.5: **Characterisation of β G2A KI MEFs**(A) Immunoblot analysis of AMPK subunit expression in WT, β1/2 G2A DKI, β1 KO, or β2 KO MEFs. (B) Quantification of expression in WT or β1/2 G2A DKI normalised to actin and expressed as relative to WT. (C) Immunoprecipitation of WT, β1/2 G2A DKI, or β1 KO MEFs using a β1-specific antibody and immunoblot analysis of subunits interaction. (D) Quantification of α1 and γ1 normalised to total β1 immunoprecipitated. All data are mean ± s.e.m. from three independent experiments.

marginal with 991, A769662 or AICAR (**Fig 2.6D** and **Appendix Fig A.6**). Consistent with these observations, the enzymatic activity of AMPKα1 was significantly higher (~3-fold) in β1/2 G2A DKI compared to WT MEFs (**Fig 2.6E**).

I also analysed MEFs from β1 G2A and β2 G2A single KI mice. I observed that each single KI MEFs have a reduction in the expression of the corresponding β isoform. While β1 KI MEFs showed markedly lower β1 expression but no effect on β2 level, β2 KI MEFs had a substantial reduction in the β2 expression with no effect on β1 expression compared to the WT MEFs (**Appendix Fig A.7A**), suggesting that myristoylation has a protective effect on β subunit stability. I observed enhanced basal phosphorylation of ACC and ULK1 in β1 KI MEFs, a phenotype similar to the DKI MEFs, while this effect was not observed in β2 KI MEFs (**Appendix Fig A.7B**). In MEFs, β1 is the predominant β subunit isoform; thus, the effect caused

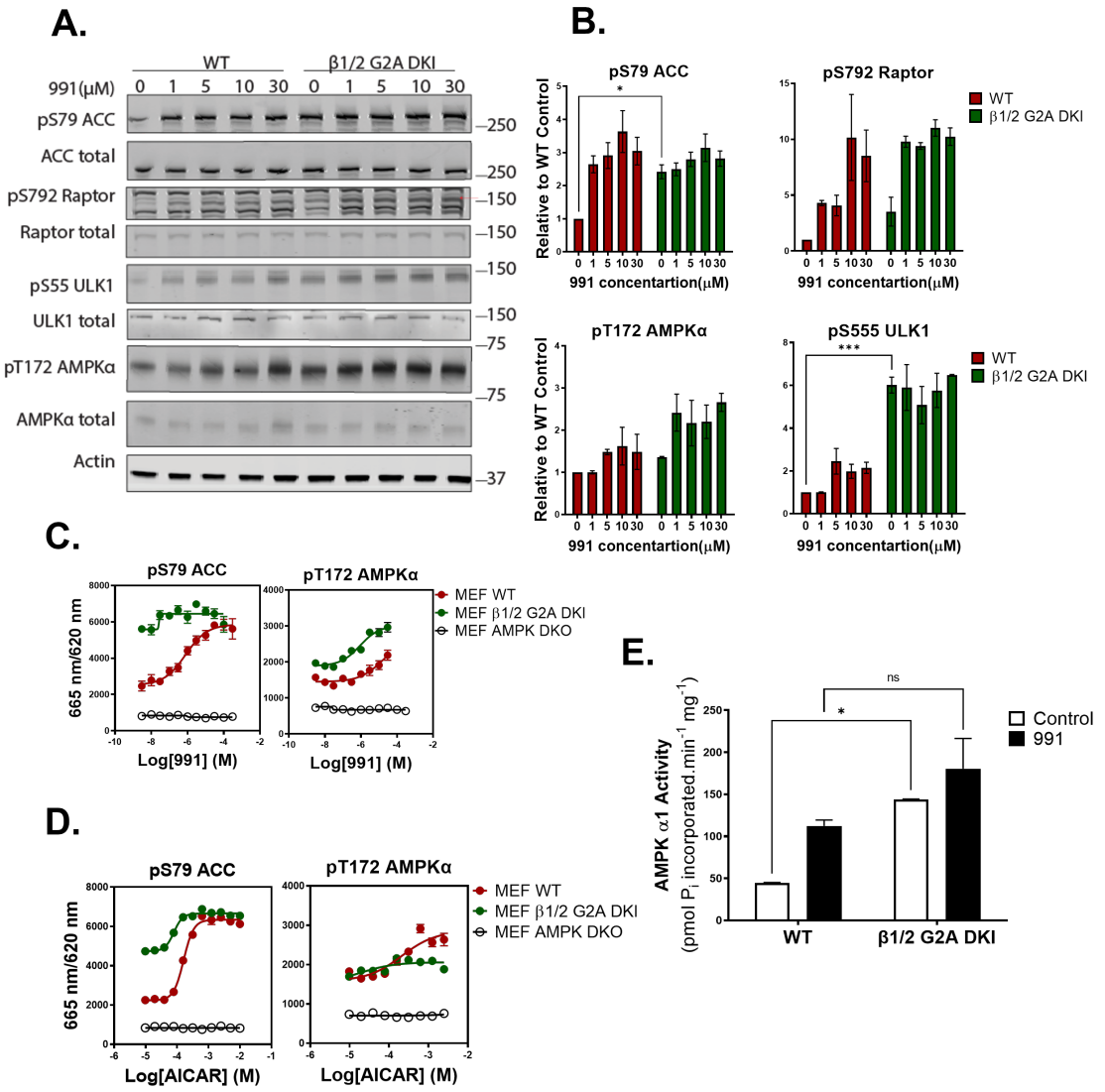

Figure 2.6: **Myristoylation-deficient (β1/2 G2A DKI) MEFs have an enhanced AMPK activity** (A) Immunoblot analysis and (B) respective quantification of phosphorylation of AMPK substrates in WT or β1/2 G2A DKI MEFs after treatment with increasing concentrations of 991 for 30 min. Phosphorylation levels were normalised to respective total protein and shown as relative to WT untreated (control). (C) Dose-response curves of pSer79 ACC and pThr172 AMPKα in the respective MEFs measured by the HTRF assay after treatment with 991 or (D) AICAR for 30 min at increasing concentrations. (E) AMPKα1 was immunoprecipitated from vehicle (0.1% DMSO)- or 991 (10 μM)-treated WT or β1/2 G2A DKI MEFs, and an *in vitro* AMPK activity assay was performed. * P<0.05, ** P<0.005, *** P<0.0005 as analysed by two-way ANOVA and Šídák's post-hoc test. All data are mean ± s.e.m. from three independent experiments.

by non-myristoylated β2 (β2 G2A KI) is expected to be modest, if any, and can be compensated by the myristoylated β1 isoform.

Collectively, these results show that loss of β subunit myristoylation results in enhanced activity of endogenous AMPK and increased substrate phosphorylation in cells.

2.1.3.3 Effect of myristoylation deficiency (G2A) on subcellular localisation of the β subunit

The myristoylation of a protein plays a role in its subcellular localisation and/or protein-protein interaction. Therefore, I next explored whether enhanced AMPK activity and phosphorylation of substrates in G2A cells were due to a change in localisation of the β subunit. I performed immunofluorescence analysis of β1 localisation in MEFs using a mouse monoclonal β1-specific antibody. I first confirmed specificity of the antibody using β1 KO MEFs as control in both immunoblot (**Appendix Fig A.8A**) and immunofluorescence assays (**Appendix Fig A.8B**). As an additional control, I transfected β1 KO MEFs with a plasmid expressing β1 WT-FLAG, stained the cells with an anti-FLAG antibody, and co-stained them with the β1-specific antibody (**Appendix Fig A.8C**)). I observed co-localisation of the β1/FLAG signal, further confirming the specificity of the β1 antibody.

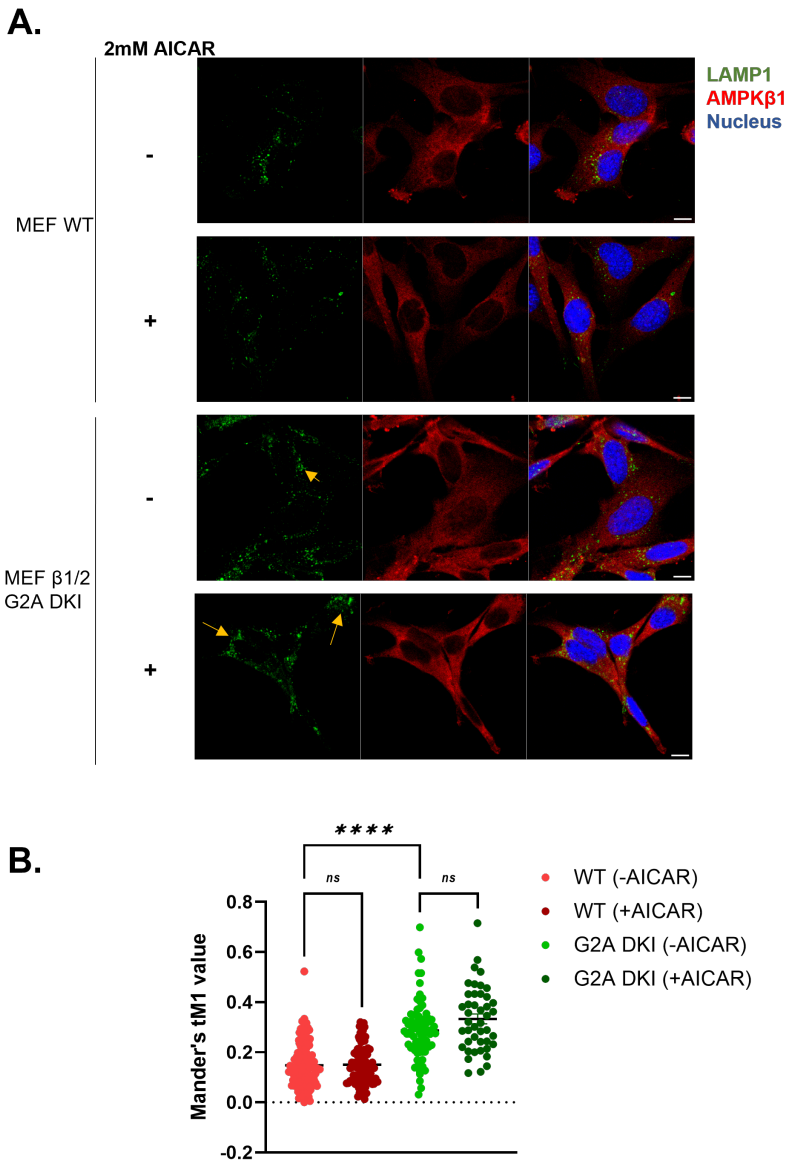

Figure 2.7: **Analysis of β1 co-localisation with lysosomes by immunofluorescence** (A) Confocal images of WT or β1/2 G2A DKI MEFs left untreated or treated with 2mM AICAR for 1 hour and stained with antibodies against LAMP1 (Green) and AMPKβ1 (Red). (B) Quantification of Mander's co-localisation coefficient (tM1, t=thresholded) per cell using macro in ImageJ. Images are representative of two independent experiments. Scale bar =10μm. **** P<0.0001 represents the genotype effect as determined by ordinary one-way ANOVA and Šídák's post-hoc test.

I then used the validated antibody to visualise the localisation of endogenous β1 in WT and β1/2 G2A DKI MEFs. Consistent with a previous study, β1 was found to be widely distributed across the cytosol, and no apparent differences in subcellular distribution were observed between β1 WT and G2A DKI MEFs at basal or when treated with the allosteric AMPK activators 991 or MK-8722 (**Appendix Fig A.9**). A previous study reported that the myristoyl group facilitates the association of AMPK with cellular membranes when β1 was ectopically-expressed in HEK293 cells (Mitchelhill et al., 1997). Using liposomes, it was shown that AMP increases membrane association of purified β1 WT by 2-fold, while loss of myristoylation significantly reduces this association (Oakhill et al., 2010). Furthermore, myristoylation was shown to be required for targeting AMPK to lysosomes upon glucose starvation (Zhang et al., 2017). I used confocal microscopy imaging to determine the co-localisation of endogenous β1 with the lysosome, a signalling hub for AMPK activation by LKB1, in WT and β1/2 G2A DKI MEFs in the presence or absence of AICAR (**Fig 2.7A**). As expected, the β1 antibody broadly stained the entire cell, and co-localisation with LAMP1 (a lysosomal marker) was challenging to assess visually. To obtain unbiased and quantitative results, I used a macro in ImageJ, which detects nuclei and measures co-localisation parameters between the two channels, such as Mander's coefficients M1 and M2, per cell. M1 is a measure of pixels of channel 1 (LAMP1) that overlap with the pixels of channel 2 (AMPKβ1) and M2 vice versa. Since β1 staining is distributed across the entire cell, I took into account tM1 (thresholded M1 values), which shows the incidence of LAMP1 colocalised with β1. I observed that treatment with AICAR has no discernible effects on LAMP1-AMPKβ1 co-localisation. However, a significantly increased co-localisation was observed in β1/2 G2A DKI compared to WT MEFs (**Fig 2.7B**). I also noticed that G2A DKI cells had a higher number of lysosomal speckles than WT, and they mostly existed in clusters which might have resulted in a biased quantification.

To quantify co-localisation exclusively in the lysosomal compartments, I took advantage of proximity ligation assay (PLA), which is a well-established method to visualise and quantify endogenous protein-protein interaction/co-localisation *in situ* (**Fig 2.8**) (Alam, 2018). Using primary antibodies recognising LAMP1 and β1, I quantified the number and mean intensity of PLA dots (representing positive interaction between the proteins assessed) per cell. Consistent with the immunofluorescence analysis, PLA showed no effect of AICAR in co-localisation while LAMP1/β1 interaction was substantially higher in the G2A DKI MEFs (**Fig 2.9**). To date, there is little information on how post-translational modifications of AMPK regulate its subcellular localisation. These findings suggest that loss of myristoylation in the β subunit might increase the lysosomal localisation of AMPK, thereby facilitating its activation via LKB1. However, this increased localisation could result from increased lysosomes in the G2A DKI cells. Therefore, clarifying the effects of loss of myristoylation on lysosomal morphology is critical to assess quantification from these microscopic analyses.

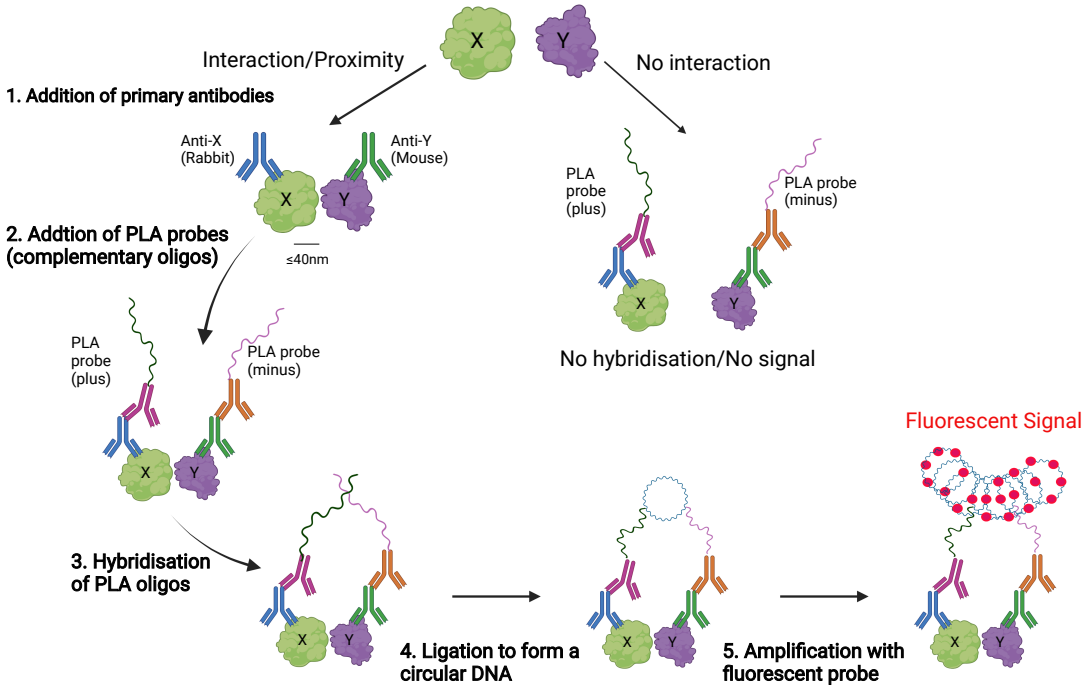

Figure 2.8: **Proximity Ligation Assay (PLA)** A schematic representation of Proximity Ligation Assay adapted from Sigma. *Created using BioRender.*

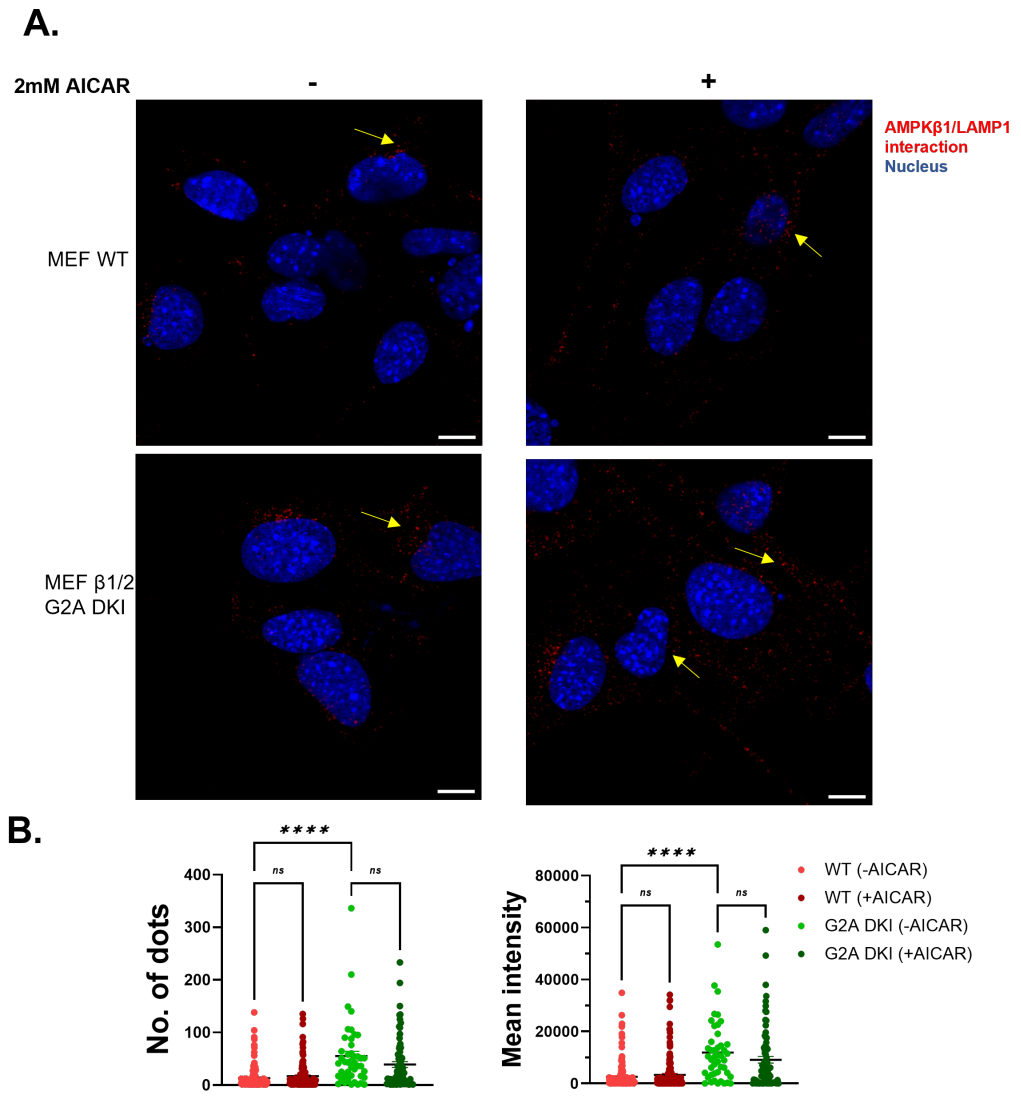

Figure 2.9: **Analysis of β1 co-localisation with lysosomes by Proximity Ligation Assay (PLA)** (A) Co-localisation of β1 and LAMP1 was visualised using PLA in WT and β1/2 G2A DKI MEFs untreated or treated with 2mM AICAR. Images are representative of two independent experiments. (B) Signal was quantified as number or mean fluorescence intensity of red dots per cell using ImageJ plugins. Scale bar = 10μm. ****P<0.0001 as determined by one-way ANOVA and Šídák's post-hoc test.

2.1.3.4 Loss of β subunit myristoylation (G2A) disrupts proximity with phosphatases

Previous studies have shown that phosphatases PPM1A/PP2Cα, PPM1B/PP2Cβ, and PPM1E are involved in AMPK dephosphorylation. Ectopically-expressed PPM1A and PPM1B have been reported to be myristoylated in HeLa cells (Chida et al., 2013). We sought to test if G2A mutation in the β subunit would disrupt its proximity to these phosphatases resulting in an

enhanced AMPK activity. Initially, to confirm myristoylation of the β subunit and the phosphatases, I used the click chemistry technique (**Fig 2.10A**). Briefly, cells were labelled with azido-myristic acid that gets incorporated into nascent myristoylated proteins. Immunoprecipitating the target protein of interest (e.g., AMPKβ1) from the labelled lysates results in the isolation of myristoylated and non-myristoylated β1. The use of alkyne-biotin to form azido-alkyne complex enables the visualisation of myristoylated β1 by immunoblotting with streptavidin. I first tested different concentrations of azido-myristic acid (0-50μM) and varying incubation times (0-24 hours) and established a robust labeling condition (25μM for 24 hours) (**Fig 2.10B**). I confirmed that β1 is myristoylated in WT MEFs as shown by the streptavidin signal, which was absent in the β1/2 G2A DKI MEFs validating the lack of myristoylation (**Fig 2.10C**). The green channel shows total β1 pulled down, confirming that β1 was equally immunoprecipitated from both WT and β1/2 G2A DKI MEFs.

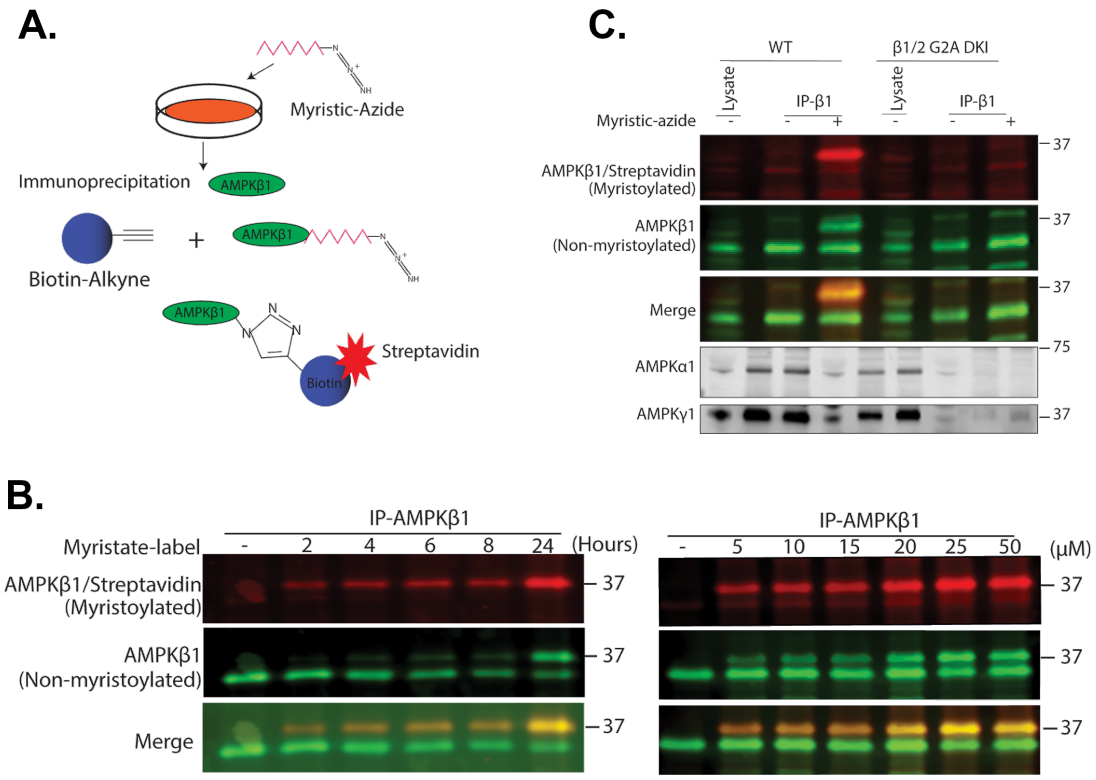

Figure 2.10: **Evidence of β1 myristoylation in MEFs by click chemistry** (A) Schematic representation of click chemistry approach. Cells are labelled with myristic-azide followed by β1 immunoprecipitation and reaction with biotin-alkyne to detect myristoylated β1 by streptavidin. (B) Immunoblot showing myristoylated β1 (red channel) and total β1 (green channel) from WT MEFs after click chemistry following labelling with 25μM myristic azide for 0-24 hours or at a concentration of 0-50μM for 24 hours. (C) Immunoblot showing myristoylated β1 (red channel) and total β1 (green channel) from WT, β1/2 G2A DKI, or β1 KO MEFs following labelling with 25μM myristic azide overnight and click chemistry. Figures are representative of 2-3 independent experiments.

Next, I confirmed specificity of myristoylation of the phosphatases PPM1A (**Fig 2.11A**) and PPM1B (**Fig 2.11B**) by siRNA-mediated knockdown followed by click chemistry. I used the same approach to test a non-myristoylated phosphatase PPP2C as a control. I observed an absence of streptavidin signal, confirming the specificity of the method (**Appendix Fig A.10A**). I also confirmed specificities of the PPM1A/1B/PPP2C antibodies by siRNA knockdown followed by immunoblot analysis (**Appendix Fig A.10B and C**).

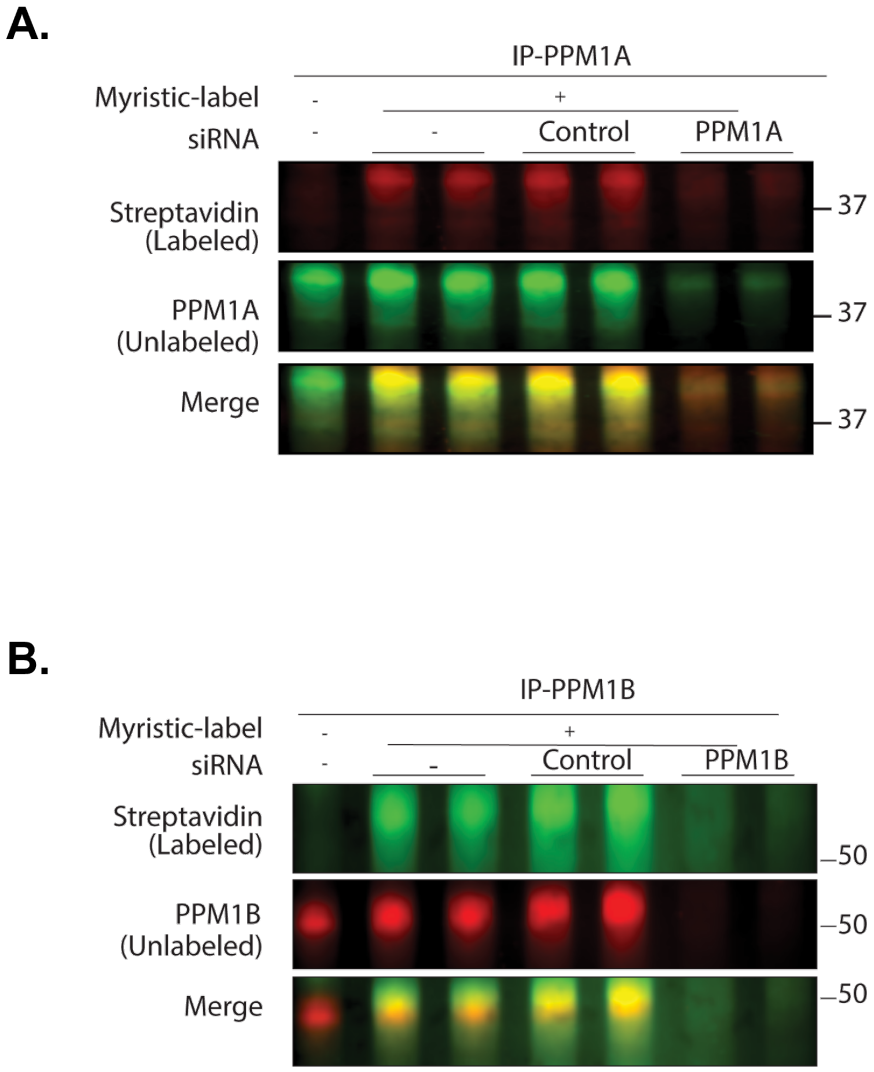

Figure 2.11: **Evidence of myristoylation of PPM1A and PPM1B by click chemistry** (A) Immunoblot showing myristoylated PPM1A (red channel) and total PPM1A (green channel) from WT MEFs after click chemistry following overnight labelling with 25μM myristic azide. (C) Immunoblot showing myristoylated PPM1B (green channel) and total PPM1B (red channel) from WT MEFs after click chemistry following overnight labelling with 25μM myristic azide. Figures are representative of two independent experiments.

Next, I investigated whether β1 localises in close proximity with PPM1A/PPM1B using PLA. As shown in **Fig 2.12**, PLA revealed a cluster of signals (red dots) in WT MEFs indicating the proximity of β1 with PPM1A (**Fig 2.12A**) and PPM1B (**Fig 2.12B**). In contrast, the number of dots and the mean fluorescent intensity were significantly reduced in the β1/2 G2A DKI and completely absent in the β1 KO MEFs indicating that G2A mutation in the β subunit disrupts interaction/proximity between β1 and phosphatases. I verified the specificity of the observed signal by siRNA-mediated knockdown of PPM1B (**Appendix Fig A.11A**) in WT MEFs which resulted in a loss of PLA signal (**Appendix Fig A.11B**). Furthermore, the interaction between AMPKβ1 and PPP2C was not observed using PLA (**Appendix Fig A.11C**), indicating the interaction of β1 is specific to PPM1A and PPM1B. These results are consistent with the study by Chida et al., 2013, where they showed that ectopic expression of non-myristoylated forms of PPM1A and PPM1B resulted in a blunted dephosphorylation of AMPKα Thr172 in HeLa cells.

Collectively, these results indicate that the AMPKβ subunit localises in proximity with PPM1A and PPM1B and that loss of myristoylation (G2A) disrupts this proximity resulting in an enhanced AMPK activity.

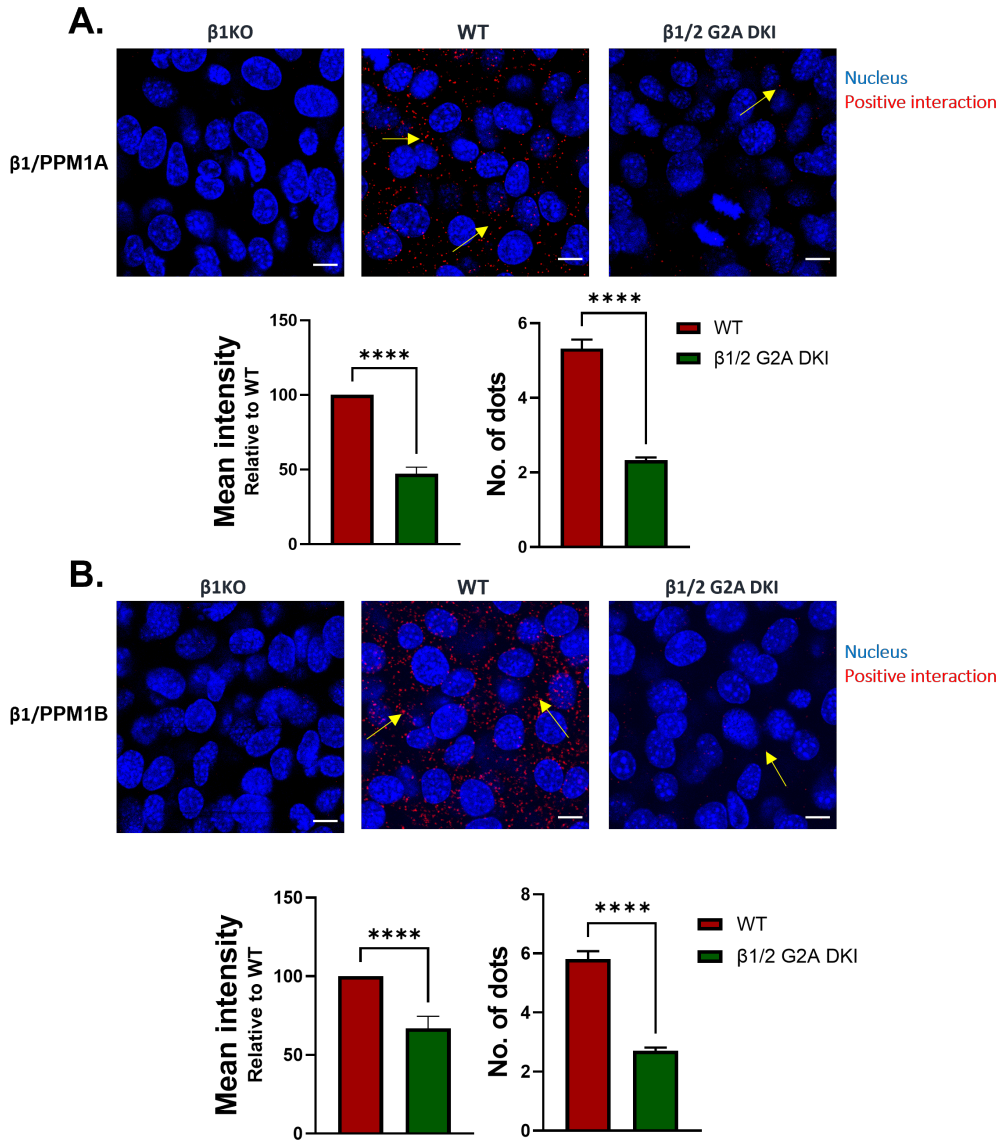

Figure 2.12: **G2A mutation disrupts the proximity of β1 and phosphatases in MEFs** Interaction/proximity of (A) β1 and PPM1A and (B) β1 and PPM1B were visualised using proximity ligation assay in β1 KO, WT and β1/2 G2A DKI MEFs. Signal was quantified as mean fluorescence intensity (relative to WT) or number of red dots per cell using ImageJ plugins. Scale bar = 10μm. ****P<0.0001 as determined by unpaired t-test. All data are mean ± s.e.m. from three independent experiments.

I applied the same approach in U2OS cells to ensure that the loss of PLA signal in β1/2 G2A DKI MEFs is not a result of lower β1 expression. I have shown that U2OS stable cell lines expressing either β1 WT or G2A have similar levels of expression of all the AMPK subunits (**Fig 2.4 A and B**). I first verified myristoylation in the β1 WT expressing cells by myristic azido labelling and FLAG immunoprecipitation followed by click chemistry (**Fig 2.13A**). β1 WT cells had a strong streptavidin signal indicating myristoylated β1, while the signal was completely absent in the β1 G2A cells confirming the absence of myristoylation (**Fig 2.13B**). PLA showed consistent observation indicating an interaction between β1 and PPM1A (**Fig 2.14A**) and β1 and PPM1B (**Fig 2.14B**) in β1 WT cells, while a significant reduction in PLA signal (number of dots or mean intensity) was observed in β1 G2A cells, indicating that the interaction/proximity is lost in myristoylation-deficient β1-expressing U2OS cells.

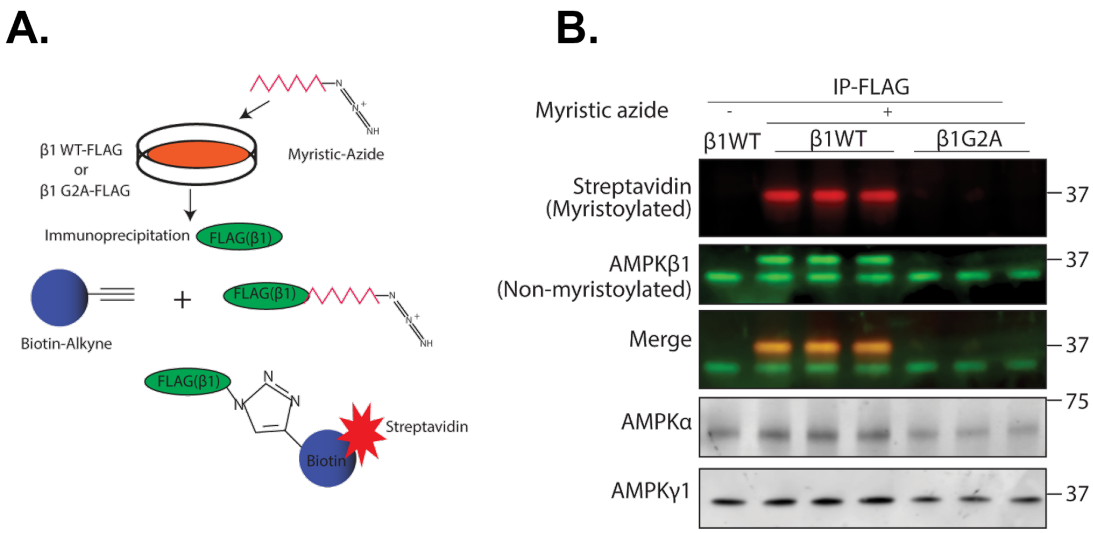

Figure 2.13: **Evidence of β1 myristoylation in U2OS cells by click chemistry** (A) Schematic illustration of click chemistry approach in U2OS stable cell lines. (B) Immunoblot showing myristoylated β1 (red channel) and total β1 (green channel) in U2OS stable cells expressing β1 WT or β1 G2A after click chemistry following overnight labelling with myristic azide and FLAG immunoprecipitation. Figures are representative of two independent experiments.

Taken together, I showed that the loss of β subunit myristoylation results in disruption of proximity between β1 and PPM1A/1B and an enhanced AMPK activity and substrate phosphorylation in two different cell types.

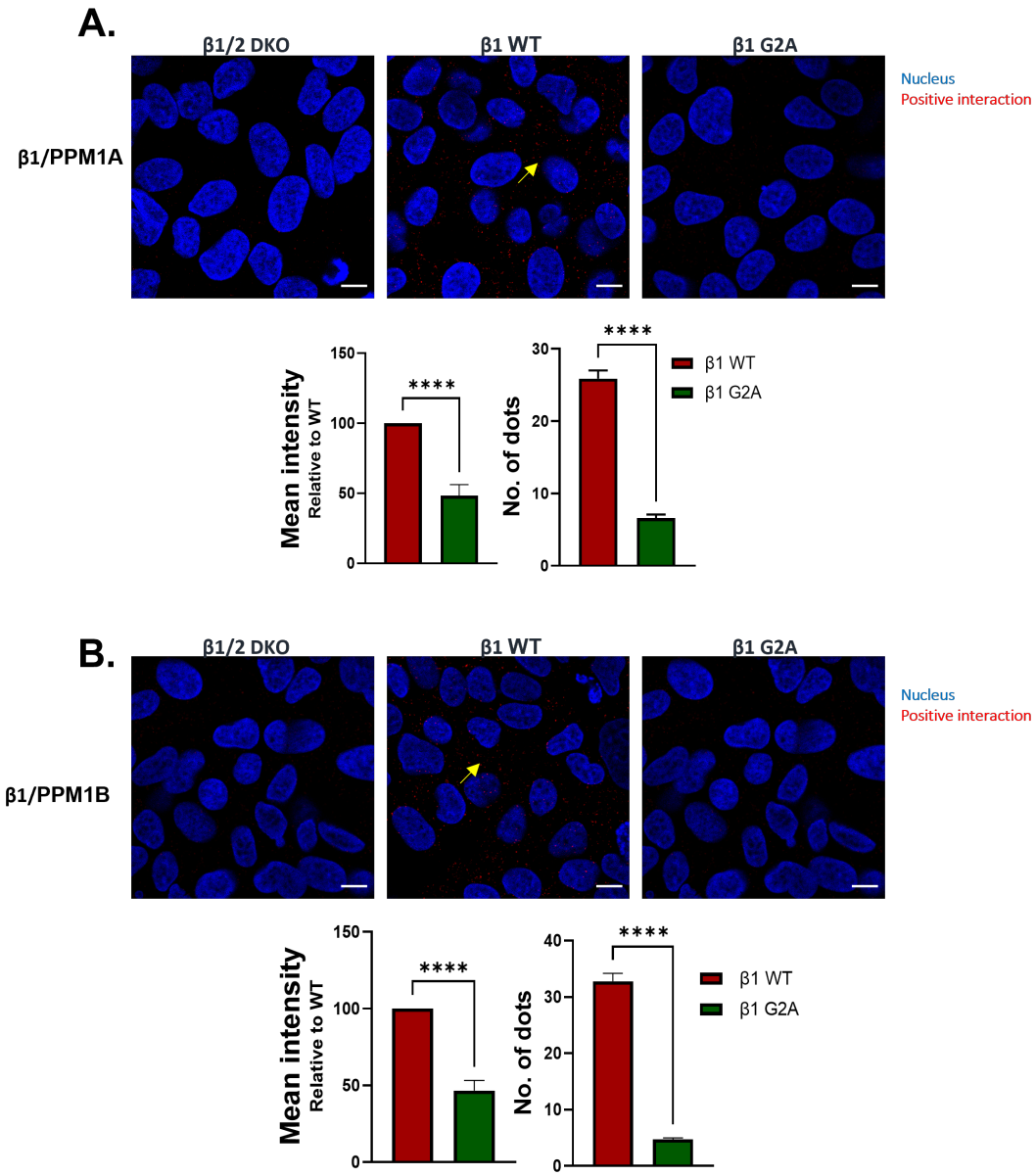

Figure 2.14: **G2A mutation disrupts the proximity of β1 and phosphatases in U2OS cells** Interaction/proximity of (A) β1 and PPM1A and (B) β1 and PPM1B were visualised using proximity ligation assay in U2OS β1/2 DKO cells or U2OS stable cell lines expressing β1 WT or β1 G2A. Signal was quantified as mean fluorescence intensity (relative to WT) or number of red dots per cell using ImageJ plugins. Scale bar = 10μm. ****P<0.0001 as determined by unpaired t-test. All data are mean ± s.e.m. from two independent experiments.

2.1.3.5 Physiological consequences of the loss of β1 myristoylation

To investigate the physiological consequences of the genetic loss of β1 myristoylation on peripheral and whole-body metabolism, as well as AMPK signalling, CRISPR-Cas9-generated AMPKβ1 (Glycine2-to-Alanine (G2A)) (β1 G2A KI) mice were analysed. I would like to acknowledge Natalie Kozlov and Dr. Sandra Galic from the St. Vincent Institute, Melbourne, for performing the *in vivo* experiments and analyses described in this section.

Initially, the expression of AMPK subunits was investigated in multiple tissues isolated from either WT or β1 G2A KI mice that were either *ad-libitum* fed or fasted for 16 hours. In rodents, the β1 isoform is predominantly expressed in the liver. Consistent with my results using the MEFs, the absence of β1 myristoylation resulted in ~50% reduction in the expression of β1 subunit in the liver and consequently ~40% reduction in α and ~70% reduction in the γ1 subunits (**Fig 2.15A**) in both fed and fasted states. The decline in β1 isoform was, however, accompanied by a 2-fold increase in β2 expression, which is possibly due to an upregulation of *Prkab2* gene expression as shown by qPCR analyses (**Appendix Fig A.12A**). Meanwhile, there were no changes in the mRNA expression of α or β1, indicating that the reduction of expression of these subunits is independent of changes in gene expression and is possibly a result of an increased posttranslational turnover. In skeletal muscle, β1 expression is negligible and consistent with this; loss of myristoylation in β1 had no substantial effect on AMPKα or β expression in this tissue (**Appendix Fig A.12B**).

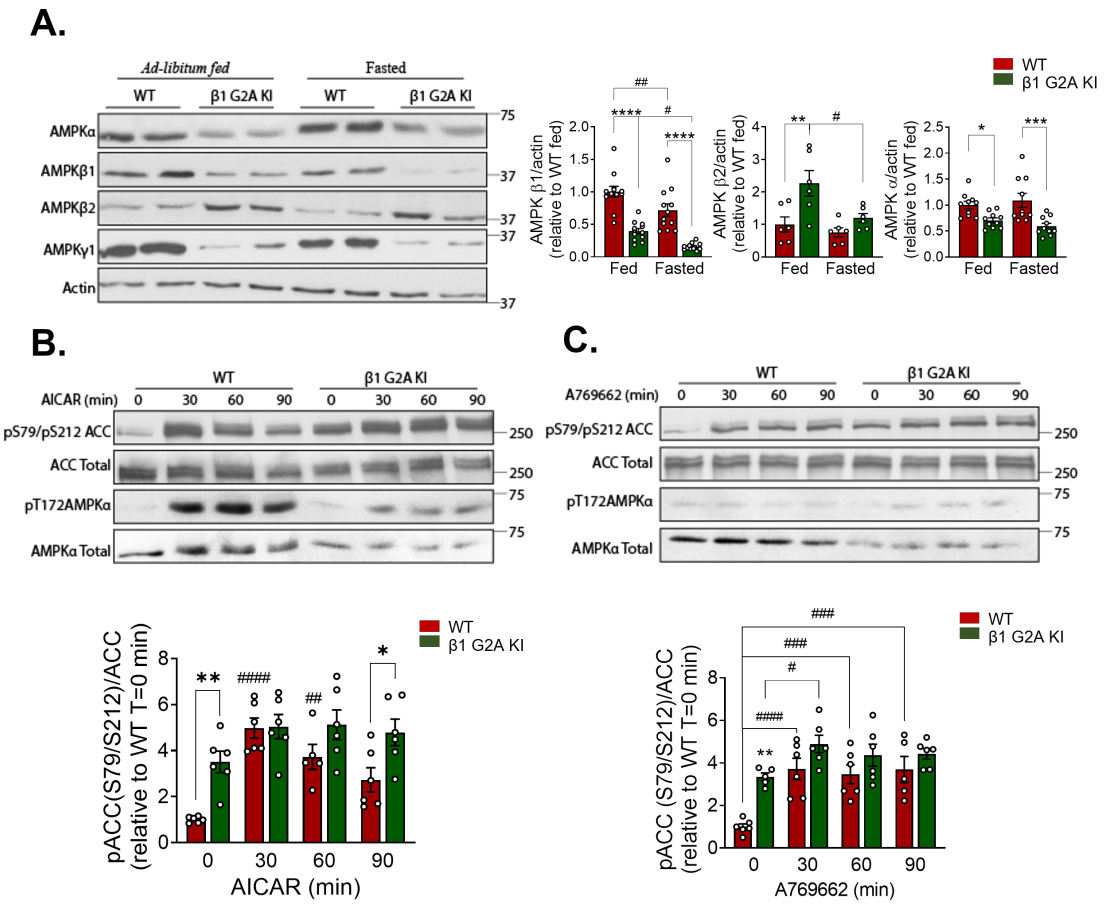

Figure 2.15: **Effect of loss of β1 myristoylation in hepatic AMPK signalling** (A) Immunoblot analysis of expression of AMPK subunits and respective quantification in primary hepatocytes isolated from *ad-libitum* fed and fasted WT or β1 G2A KI mice. Expression was normalised to actin and expressed as relative to WT. (B) Immunoblot analysis of phosphorylation of AMPKα Thr172 and Ser79/Ser212 ACC in primary hepatocytes isolated from WT or β1 G2A KI mice and treated with 0.25mM AICAR or (C) 10μM A769662 for up to 90 min. Phosphorylation levels were normalised to respective total protein and shown as relative to WT at 0 min (control). * P<0.05, ** P<0.01, *** P<0.001, **** P<0.0001 represent genotype differences. # P<0.05, ## P<0.01, ### P<0.001, #### P<0.0001 represent treatment effects as determined by two-way ANOVA and Šídák's post-hoc test. All data are mean ± s.e.m.

It has been shown that myristoylation of the β subunit is required for AMP-mediated AMPKα Thr172 phosphorylation. To investigate the effects of loss of β1 myristoylation on AMPK signalling in the liver in response to changes in intracellular AMP levels, primary hepatocytes were isolated from either WT or β1 G2A KI mice and were treated with AICAR. A significantly higher basal ACC Ser79/Ser212 phosphorylation was observed in the β1 G2A KI hepatocytes (**Fig 2.15B**). Prolonged stimulation with AICAR tended to negatively regulate ACC phosphorylation in the WT hepatocytes, possibly resulting from undesirable off-target effects. However, ACC phosphorylation was maintained for a more extended period in the β1 G2A KI

hepatocytes. Treatment with the β1-selective AMPK activator A769662 also showed elevated basal ACC phosphorylation and only a modest increase following treatment in the β1 G2A KI hepatocytes compared to the WT (**Fig 2.15C**). Taken together, these results are consistent with the findings obtained from U2OS and MEF cell models in that the absence of β1 myristoylation results in an enhanced AMPK activity and substrate phosphorylation, indicating a crucial role of β subunit myristoylation in regulating AMPK activity.

Next, to examine the consequences of enhanced hepatic AMPK activity and increased ACC phosphorylation in the β1 G2A KI mice, fat content was analysed in the liver of WT and KI mice fed with a chow diet or an obesity-inducing high-fat diet (HFD). No apparent morphological differences were observed in Hematoxylin/Eosin (H/E) staining of livers from chow-fed WT or KI mice, and the staining of Oil Red O (ORO) was consistent (**Fig 2.16A**). However, following a high-fat diet, livers from the β1 G2A KI mice had significantly smaller lipid droplets (**Fig 2.16B**). Moreover, liver triglyceride content was considerably lower in the chow- or HFD-fed KI mice under both fed and fasted conditions compared to the WT (**Fig 2.16 C and D**). It was also observed that primary hepatocytes isolated from the KI mice had reduced *de novo* triglyceride synthesis at basal or when induced with insulin (**Fig 2.16E**). This decreased lipogenesis was likely due to an increased ACC phosphorylation in the liver of KI mice which consequently resulted in the suppression of its activity. A769662, however, had a similar lipid-lowering effect in both genotypes, which is consistent with the previous observation that AMPK allosteric activators result in only modest increases in ACC phosphorylation in the β1 G2A cells.

Collectively, these results suggest an essential role of AMPKβ1 myristoylation in AMPK signalling because the loss of β1 myristoylation maintains liver AMPK in an active state, thereby preventing HFD-induced hepatic lipid accumulation by suppressing ACC activity.

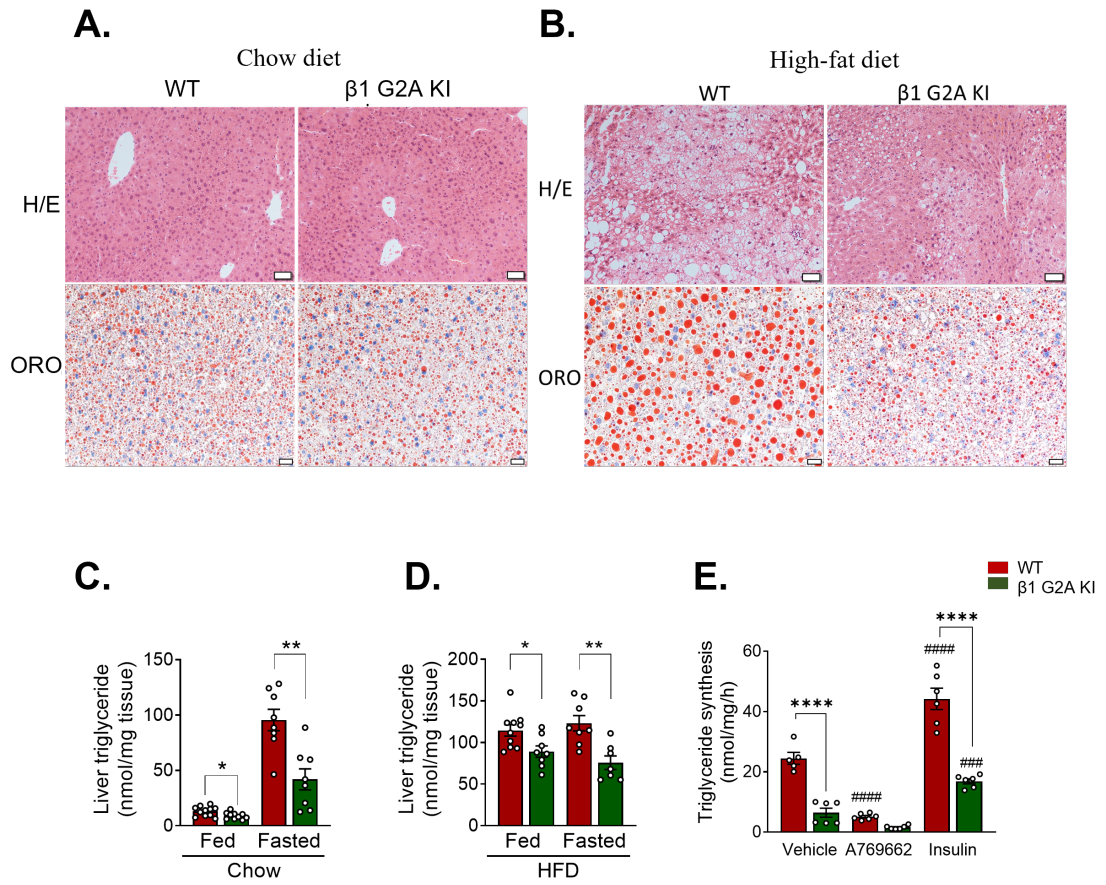

Figure 2.16: **Effect of Loss of AMPKβ1 myristoylation in hepatic lipid metabolism** (A) Haematoxylin and Eosin (H/E, top panel) and Oil Red O (ORO, bottom panel) staining of *ad libitum* fed β1 G2A mice and WT littermate controls on chow-diet or (B) on a high-fat diet (HFD). Shown are representative images from n = 6 mice per condition. Scale bar =50 μm for H/E and 20 μm for ORO. (C) Triglyceride content in the liver from *ad libitum* fed and 16 hour fasted β1 G2A and WT mice on chow diet (n = 8-11) and (D) HFD (n = 7-10). (E) Triglyceride synthesis (n = 6) in β1 G2A and WT primary hepatocytes in response to the respective treatments. * P<0.05, ** P<0.01, *** P<0.001, **** P<0.0001 represent genotype differences. # P<0.05, ## P<0.01, ### P<0.001, #### P<0.0001 represent treatment effects as determined by two-way ANOVA and Šídák's post-hoc test. All data are mean ± s.e.m.

2.1.3.6 Effect of loss of β1 myristoylation on global downstream signalling of AMPK

I demonstrated elevated cellular AMPK activity in U2OS β1 G2A- or β2 G2A-expressing cell lines and β1/2 G2A DKI MEFs by monitoring phosphorylation of known AMPK substrates (ACC, Raptor, and ULK1). However, whether this increased AMPK activity affects the phosphorylation of its substrates globally or only a subset of limited/selected substrates is unknown. To address this, we performed an unbiased phosphoproteomics analysis utilising MEFs (WT, β1/2 G2A DKI, as well as AMPKα1/2 DKO) to investigate the global effect of G2A mutation on AMPK-mediated substrate phosphorylation profile (**Fig 2.17A**). I would like to acknowledge Jeppe K. Larsen and Atul Deshmukh from the University of Copenhagen for phosphopeptide enrichment, mass spectrometry and bioinformatics analyses.

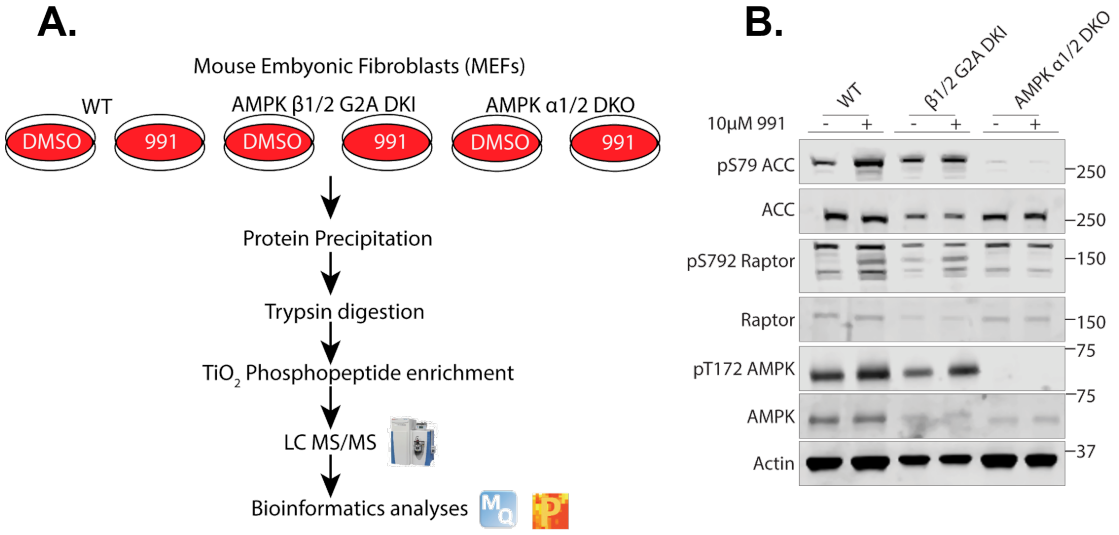

Figure 2.17: **Phosphoproteomics analysis to identify novel AMPK substrates** (A) A summary of the phosphoproteomics workflow. (B) Validation of AMPK activation following treatment with vehicle (DMSO (-)) or 10μM 991 (+) for 30 min by immunoblotting.

Efficacy of AMPK activation with 991 in cells was validated by immunoblot analysis (**2.17B**). We observed that more than 200 phosphopeptides were robustly upregulated with 991 in WT (**Fig 2.18A**), which was lacking in the AMPKα1/2 DKO MEFs, indicating phosphorylation of these proteins to be AMPK-specific/dependent (**Fig 2.18B**). We observed that in the WT MEFs, the majority of enriched peptides contained an AMPK substrate motif (LXRXXS*/T*) (**Fig 2.18C**). Interestingly, we observed more than 1000 phosphopeptides uniquely enriched in the β1/2 G2A DKI MEFs at basal conditions compared to the WT cells (**Fig 2.18D**). However, the majority of enriched peptides did not contain the AMPK substrate motif, and thus, an in-depth bioinformatics analysis would be needed to identify uniquely enriched peptides and associated cellular pathways and functions. In the meantime, we identified novel substrates of AMPK (from 991-treated WT MEFs) and, therefore, focused on detailed characterisation of these proteins and associated biological processes to investigate new roles of AMPK.

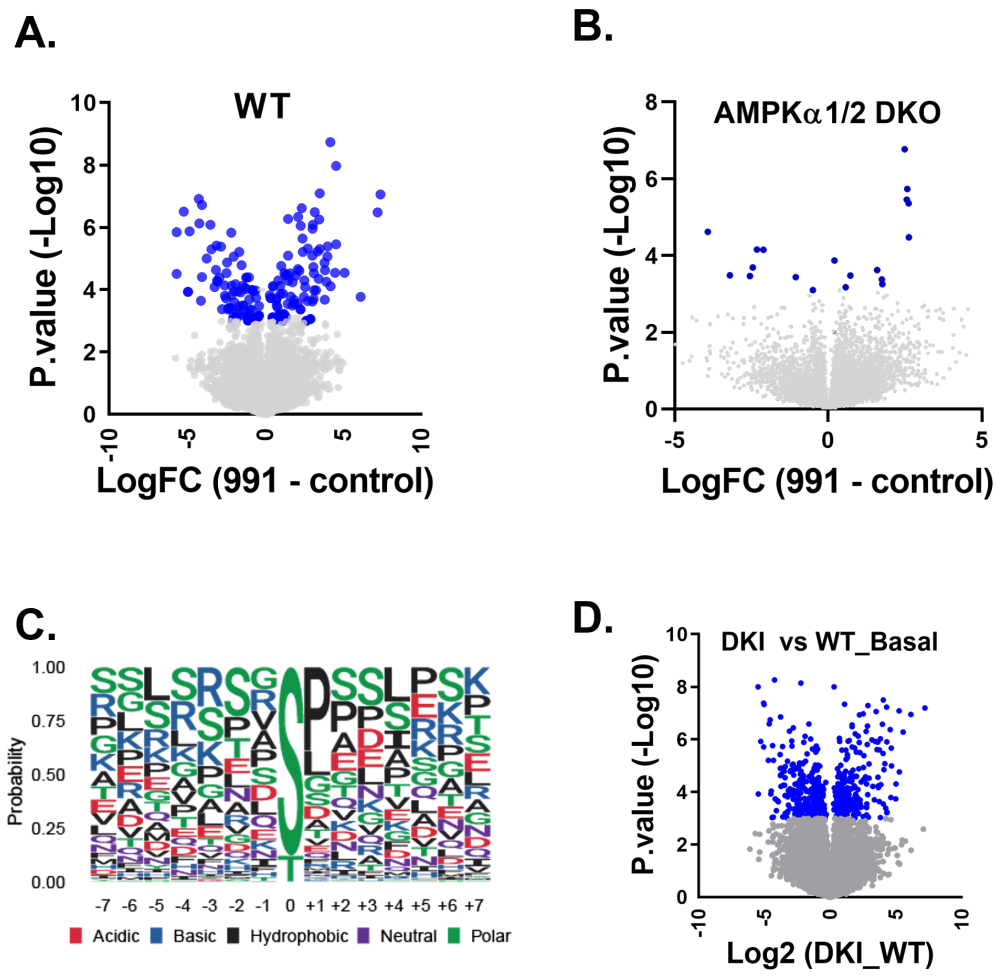

Figure 2.18: **Phosphoproteomics analysis**. (A) Volcano plots showing phosphosites upregulated (right) or downregulated (left) with 991 in WT or (B) AMPK DKO MEFs. (C) Sequence logo for phosphosites upregulated with 991 in WT MEFs. (D) Volcano plot showing phosphosites in β1/2 G2A DKI MEFs at basal (DMSO-treated) condition compared to WT MEFs. Volcano plots are depicted with the fold change of each phosphosite and the BH-adjusted p value was calculated by performing a student's t-test and a permutation test.

2.2 Investigation of novel substrates and biological roles of AMPK

2.2.1 Background and aim of the study

Protein phosphorylation is an important modulator of different cellular processes. Therefore, kinases have emerged as potential therapeutic targets for several diseases. As discussed in **section 1.6**, AMPK has been shown to regulate a plethora of metabolic processes by phosphorylation of key targets involved. The role of AMPK in classic metabolic processes is very well known, and it has been well validated as an essential regulator of lipid and glucose metabolism. However, there are growing interests in AMPK-controlled pathways that are not conventionally classified as metabolic, for instance, autophagy, cell growth, and cell migration, which link AMPK to many pathological conditions, e.g., cancer or neurological disorders. Current studies come with limitations and inadequate screening; meanwhile, AMPK can have diverse new roles in different biological mechanisms that remain unaddressed.

We aimed to identify novel substrates of AMPK that control different cellular processes. This will provide insights on previously unknown biological functions of AMPK, which would be necessary to broaden its therapeutic potential and off-target effects. We performed an unbiased Mass Spectrometry (MS)-based phosphoproteomics profiling using MEFs. For activation of AMPK, I treated cells with 10μM 991 for 30 min. This was followed by protein precipitation, protease digestion, TiO_2 phosphopeptide enrichment, Liquid Chromatography (LC)-MS-based detection of phosphopeptides, and bioinformatics analyses. Following phosphopeptide identification, I then biochemically validated proteins corresponding to the identified peptides that were significantly phosphorylated in 991-treated WT MEFs, as AMPK substrates. Using this approach, I discovered novel targets of AMPK that control different cellular processes, including Endoplasmic Reticulum (ER)/Golgi function and/or protein trafficking mechanisms.

2.2.2 Global phosphoproteomics profiling of novel AMPK substrates

We observed more than 400 phosphopeptides significantly regulated by 991 (205 sites upregulated and 212 sites downregulated) in WT MEFs. In contrast, only 34 sites were regulated in the AMPKα1/α2 DKO MEFs (10 downregulated and 24 upregulated) (**Fig 2.18**). A total number of 11,615 unique phosphosites (localisation probability ≥ 0.75) and 3179 proteins were quantified (**Fig 2.19A**). A majority of phosphosites predicted were serine (88.5%), followed by threonine (11.4%) and tyrosine (0.2%), which is consistent with a previous study indicating that AMPK mostly prefers serine residue for phosphorylation (Hardie et al., 2016). Kinase perturbation plot of scores calculated from the coordinated change of substrates shows AMPK to be the most regulated kinase in the 991- compared to vehicle-treated WT cells providing additional support for the specificity of 991 towards AMPK (**Fig 2.19B**). Next, using a machine learning approach that takes into account the

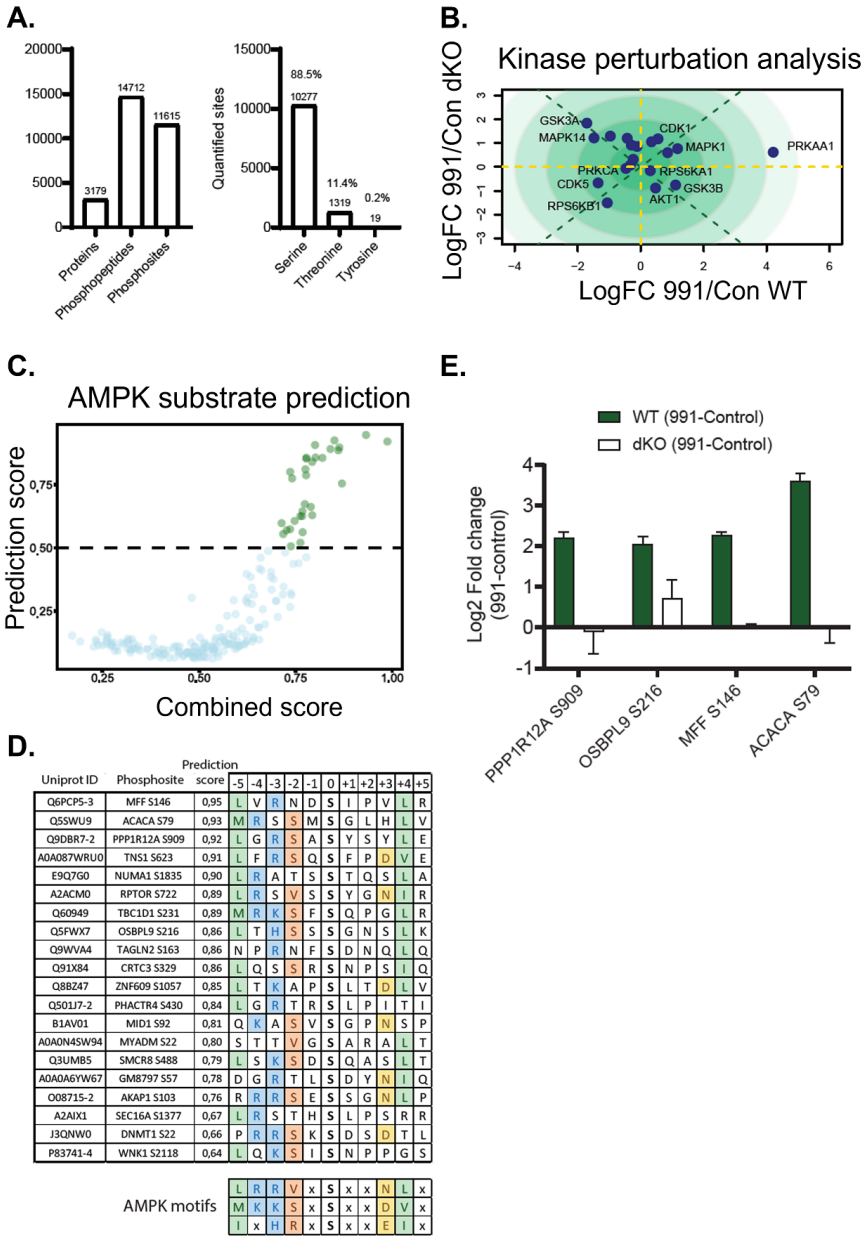

Uniprot ID	Phosphosite	Prediction score	-5	-4	-3	-2	-1	0	+1	+2	+3	+4	+5
Q6PCP5-3	MFF S146	0,95	L	V	R	N	D	S	I	P	V	L	R
Q5SWU9	ACACA S79	0,93	M	R	S	S	M	S	G	L	H	L	V
Q9DBR7-2	PPP1R12A S909	0,92	L	G	R	S	A	S	Y	S	Y	L	E
A0A087WRU0	TNS1 S623	0,91	L	F	R	S	Q	S	F	P	D	V	E
E9Q7G0	NUMA1 S1835	0,90	L	R	A	T	S	S	T	Q	S	L	A
A2ACM0	RPTOR S722	0,89	L	R	S	V	S	S	Y	G	N	I	R
Q60949	TBC1D1 S231	0,89	M	R	K	S	F	S	Q	P	G	L	R
Q5FWX7	OSBPL9 S216	0,86	L	T	H	S	S	S	G	N	S	L	K
Q9WVA4	TAGLN2 S163	0,86	N	P	R	N	F	S	D	N	Q	L	Q
Q91X84	CRTC3 S329	0,86	L	Q	S	S	R	S	N	P	S	I	Q
Q8BZ47	ZNF609 S1057	0,85	L	T	K	A	P	S	L	T	D	L	V
Q501J7-2	PHACTR4 S430	0,84	L	G	R	T	R	S	L	P	I	T	I
B1AV01	MID1 S92	0,81	Q	K	A	S	V	S	G	P	N	S	P
A0A0N4SW94	MYADM S22	0,80	S	T	T	V	G	S	A	R	A	L	T
Q3UMB5	SMCR8 S488	0,79	L	S	K	S	D	S	Q	A	S	L	T
A0A0A6YW67	GM8797 S57	0,78	D	G	R	T	L	S	D	Y	N	I	Q
O08715-2	AKAP1 S103	0,76	R	R	R	S	E	S	S	G	N	L	P
A2AIX1	SEC16A S1377	0,67	L	R	S	T	H	S	L	P	S	R	R
J3QNW0	DNMT1 S22	0,66	P	R	R	S	K	S	D	S	D	T	L
P83741-4	WNK1 S2118	0,64	L	Q	K	S	I	S	N	P	P	G	S
AMPK motifs			L	R	R	V	x	S	x	x	N	L	x
			M	K	K	S	x	S	x	x	D	V	x
			I	x	H	R	x	S	x	x	E	I	x

Figure 2.19: **Prediction of AMPK substrates** (A) Quantification of the total number of proteins, phosphopeptides and phosphosites identified (left), and a total number of phosphorylated residues (serine, threonine or tyrosine) quantified (right). (B) Kinase perturbation analysis to identify the most regulated kinase by 991. (C) Machine learning to predict AMPK substrates based on dynamic profile and motif sequence. (D) Residues surrounding the top 10 predicted AMPK substrates. (E) Bar graph of phosphorylation levels of known and novel sites regulated by 991 in WT and AMPK DKO MEFs.

kinase-substrate motif score and phosphoproteomics dynamics (**Fig 2.19C**), we identified phosphosites directly phosphorylated by AMPK that were ranked based on the prediction

score (**Fig 2.19D**). An exhaustive list of predicted substrates and their scores is listed in the **Appendix A.4**. We identified several previously validated AMPK substrates, including ACC, Raptor, MFF, and TBC1D1, as high-scoring substrates showing the robustness of our method. In addition, we identified several novel AMPK substrate candidates, e.g., PPP12R1A, OSBPL9, and CRTC3 significantly phosphorylated with 991 in WT while the effect of 991 on these proteins in the AMPK DKO cells was insignificant (**Fig 2.19E**). PPP12R1A or MYPT1, a myosin phosphatase, has been shown to regulate cell adhesion through phosphorylation by a member of AMPK-related kinases, NUAK1 (Zagorska et al., 2010). CRTC3 has been shown to be phosphorylated by another member of AMPK-related kinases, salt-inducible kinases (SIKs) and is known to regulate inflammatory pathways and metabolic processes (Darling and Cohen, 2021, Clark et al., 2012). I investigated whether these proteins are phosphorylated by AMPK by immunoblotting with phospho-specific (site-specific) antibodies. However, my results were not of sufficient quality (i.e., sensitivity) to validate these proteins as promising AMPK substrates (**Appendix Fig A.16**). Oxysterol-binding protein like 9 (OSBPL9), on the other hand, has been identified in a previous phosphoproteomics study from our group using primary hepatocytes (Ducommun et al., 2015), which triggered our interest in pursuing this protein in more detail. OSBPL9 has been reported to be localised in the ER/Golgi compartments and to regulate cholesterol trafficking between these organelles (Ngo and Ridgway, 2009). Collectively, our unbiased phosphoproteomics screen has identified potential substrates of AMPK that are involved in various biological processes such as regulation of cell migration and adhesion, gene transcription, and cholesterol trafficking, expanding the realm of the AMPK pathway.

2.2.3 OSBPL9 is a novel AMPK substrate phosphorylated at Thr335

OSBPL9 was identified in our phosphoproteomics screen as one of the high-scoring substrates of AMPK (**Fig 2.19D**). To further validate AMPK-mediated phosphorylation of endogenous OSBPL9, I initially undertook a biochemical method using a commercial AMPK substrate phospho-motif antibody raised against a degenerate peptide library containing fixed leucine and arginine residues at the -5 and -3 positions N-terminal to the phospho-acceptor (Ser/Thr) residue. By immunoprecipitating vehicle- or 991-treated cell lysates using this antibody and immunoblotting OSBPL9, I confirmed that OSBPL9 is indeed phosphorylated in an AMPK-dependent manner at an endogenous level in both MEFs (**Fig 2.20A**) and U2OS cells (**Fig 2.20B**). Next, I transiently expressed FLAG-tagged OSBPL9 in U2OS WT and AMPK DKO cells, followed by immunoprecipitation using a FLAG antibody. Immunoblotting of the immunoprecipitates with the AMPK substrate phospho-motif antibody showed that 991 robustly phosphorylates OSBPL9 in WT but not in the AMPK DKO cells (**Fig 2.20C**).

To investigate the regulation of OSBPL9 by AMPK, I explored potential site(s) in OSBPL9 catalysed by AMPK. I initially utilised a web-based bioinformatics tool called SCANSITE, which analyses short protein sequence motifs recognised by signalling proteins or phosphorylated by kinases using *in silico* prediction (Obenauer et al., 2003). Scansite at a medium stringency

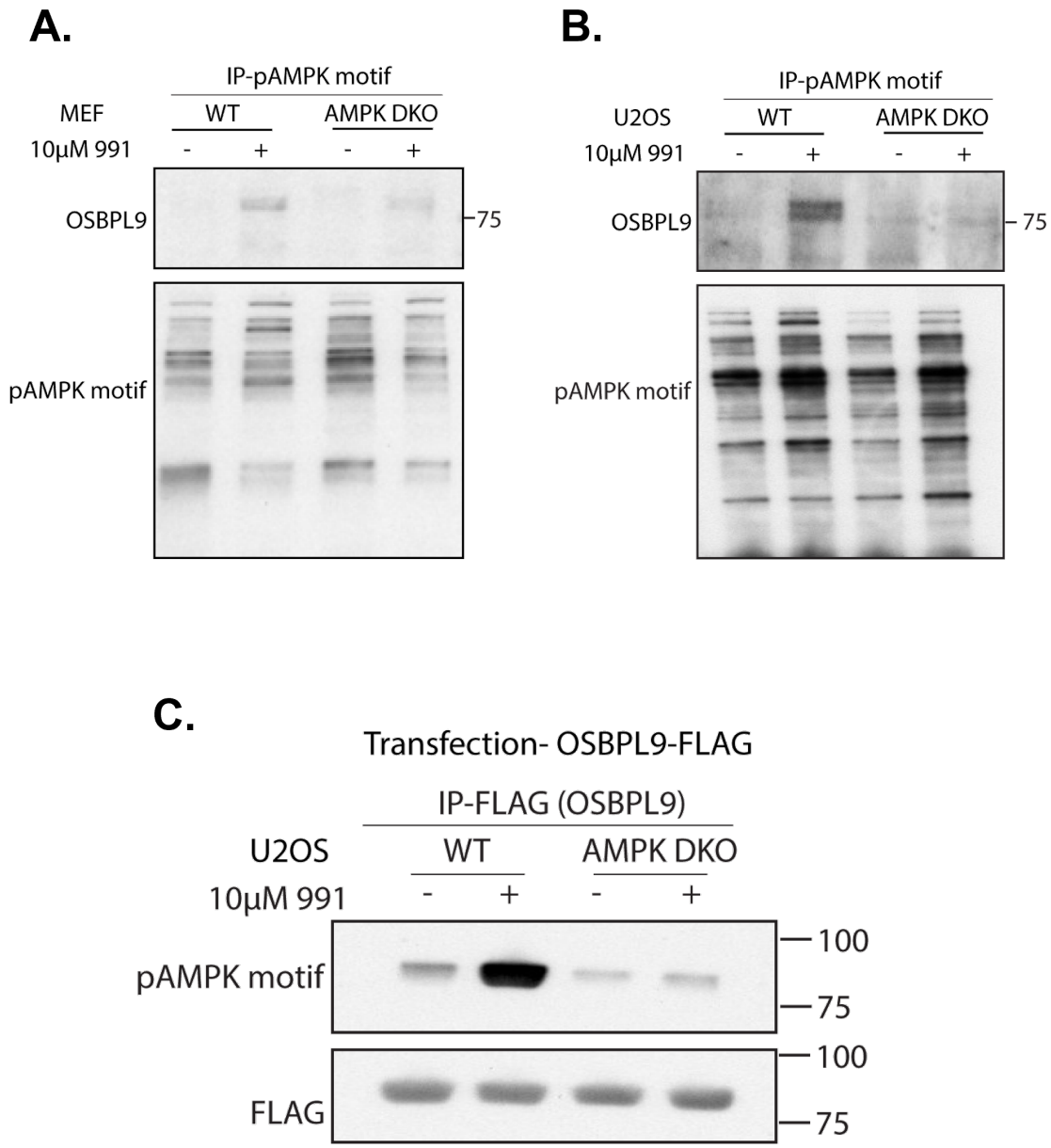

Figure 2.20: **Validation of OSBPL9 as an AMPK substrate** WT or AMPK DKO (A) MEFs or (B) U2OS cells treated with vehicle (DMSO (-)) or 10μM 991 (+) for 30 min were lysed and immunoprecipitated using a FLAG antibody and subjected to immunoblotting. (C) U2OS cells (WT or AMPK DKO) transiently transfected with FLAG-OSBPL9 were treated with vehicle (DMSO (-)) or 10μM 991 (+) and lysates immunoprecipitated using AMPK substrate phospho-motif antibody and subjected to immunoblotting. Figures are representative of two independent experiments.

scanning predicted three residues (Ser326, Thr335, and Ser348) in human OSBPL9 to be potential AMPK phosphorylation sites. We generated FLAG-tagged single and multiple alanine mutants of these residues and transiently expressed the mutants and WT OSBPL9 in U2OS

cells. Following treatment with vehicle or 991, lysates were subjected to immunoprecipitation with a FLAG antibody followed by immunoblotting with the AMPK substrate phospho-motif antibody. As shown in **Fig 2.21A**, I observed that mutations of either of the serine residues (Ser326 or Ser348) to alanine had no difference in OSBPL9 phosphorylation signal compared to WT. In contrast, mutation of Thr335 abolished 991- or MK-8722-stimulated phosphorylation of OSBPL9, an effect which was absent in the AMPK DKO cells (**Appendix Fig A.17A**). This suggests that Thr335 on OSBPL9 is a newly identified AMPK-regulated residue. I performed an alignment of OSBPL9 protein sequences from different organisms and found that Thr335 is conserved among multiple species (**Fig 2.21B**).

Next, we custom-generated a site-specific phospho Thr335 OSBPL9 antibody. The specificity of the antibody was assessed by transient expression of FLAG-tagged OSBPL9 WT or T335A in U2OS cells, followed by immunoprecipitation/immunoblotting analysis. WT OSBPL9-expressing cells showed a strong pThr335 OSBPL9 signal with 991 treatment, while the signal was abolished in the T335A expressing cells confirming the specificity of the antibody (**Fig 2.21C**). Additionally, $\alpha 1\beta 1\gamma 1$ complex (activated with 991) phosphorylated purified human OSBPL9 WT (expressed in bacteria) but not T335A mutant (**Appendix Fig A.17B**). To determine if the antibody recognises phosphorylated OSBPL9 at endogenous levels, I treated MEFs (WT or AMPK DKO) with vehicle or 991 and immunoblotted the lysates with pThr335 OSBPL9 antibody. I observed that 991 promoted phosphorylation of endogenous OSBPL9 by ~4 fold in WT MEFs (**Fig 2.21D**) as well as in U2OS cells (**Appendix Fig A.17C**) while the effect was completely absent in the respective AMPK DKO cells, providing compelling evidence that OSBPL9 is a novel AMPK substrate phosphorylated at Thr335.

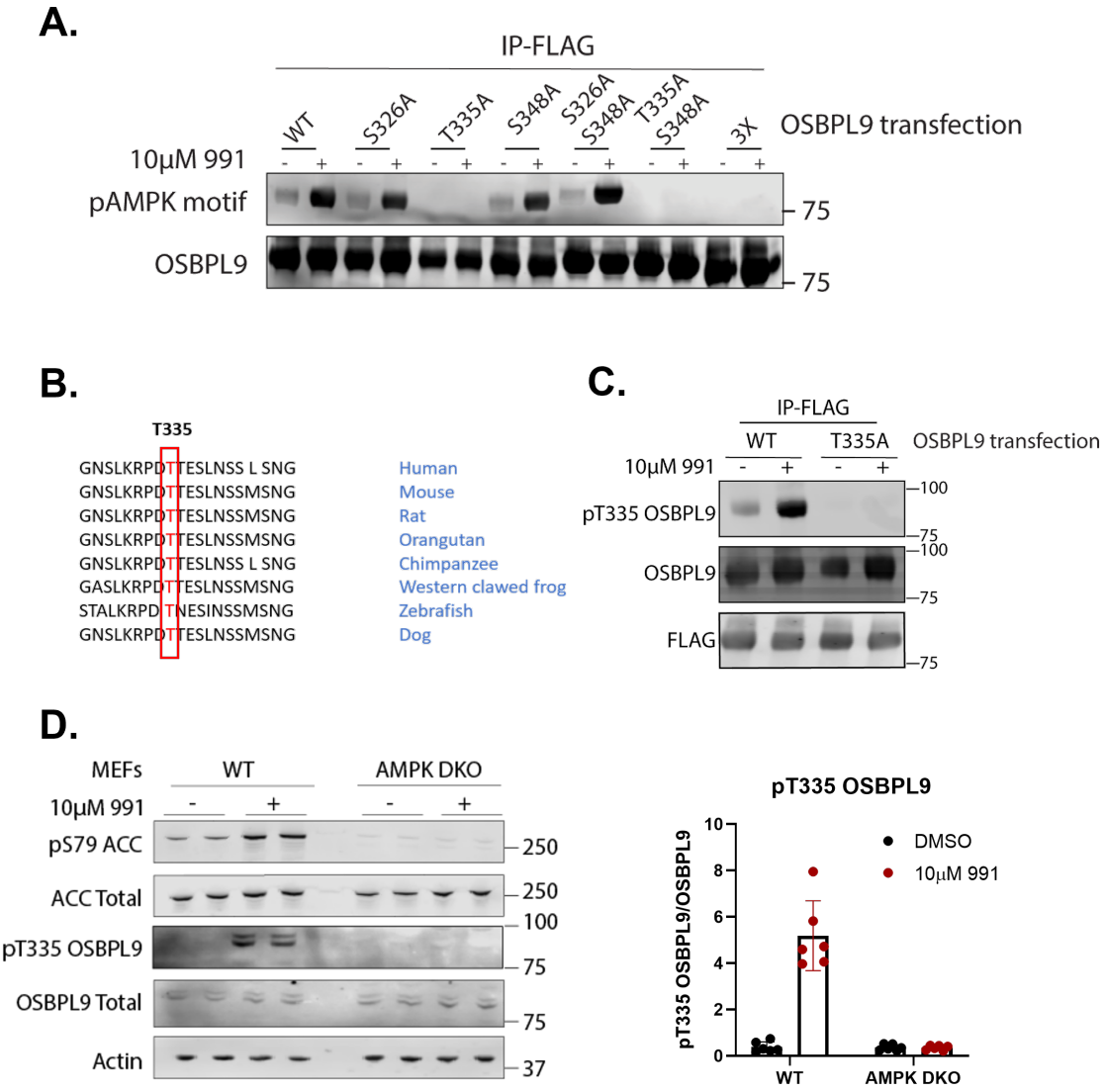

Figure 2.21: **AMPK phosphorylates OSBPL9 at Thr335** (A) U2OS WT cells transiently transfected with FLAG-OSBPL9 WT or respective mutants were treated with vehicle (DMSO (-)) or 10μM 991 (+) for 30 min and lysates immunoprecipitated using a FLAG antibody and subjected to immunoblotting. (B) OSBPL9 sequences from multiple organisms were aligned using Clustal Omega. The conserved Thr335 is highlighted in red. OSBPL9 UniProt ID for human: Q96SU4; mouse: A2A8Z1; rat: F1LRE5; orangutan: Q5R9W4; chimpanzee: A0A2R8ZJR9; western clawed frog: Q0IJ05; zebrafish: A0A2R8Q9E0; dog: A0A8C0N047. (C) U2OS WT cells transiently transfected with FLAG-OSBPL9 WT or FLAG-OSBPL9 T335A were treated with vehicle (DMSO (-)) or 10μM 991 (+) and lysates immunoprecipitated using a FLAG antibody and subjected to immunoblotting using phospho-specific pThr335 OSBPL9 antibody. (D) Phosphorylation of endogenous OSBPL9 (pThr335 OSBPL9) was assessed in MEFs (WT and AMPK DKO) treated with vehicle (DMSO) or 10μM 991 by immunoblot analysis and respective quantification. Data are mean ± s.e.m. from 2-3 independent experiments.

2.2.4 OSBPL9 knockdown results in Golgi dispersal/fragmentation in cells

I attempted to investigate the potential physiological relevance of OSBPL9 phosphorylation in cells. OSBPL9 has been reported to regulate Golgi structure and function (Ngo and Ridgway, 2009). Knockdown experiments in CHO cells resulted in Golgi fragmentation, inhibition of protein transport from the ER and accumulation of cholesterol in the lysosomal/endosomal compartments, indicating a role of OSBPL9 in maintaining Golgi integrity and early secretory pathway (Ngo and Ridgway, 2009). To follow up on these observations and replicate the findings in different cell types, I used U2OS cells and transfected them with either control siRNA oligos or oligos targeting OSBPL9 and stained Golgi apparatus with a Golgi marker Vicia Villosa (VVL), which recognises N-acetylgalactosamine of Golgi-resident proteins. Successful knockdown of OSBPL9 was confirmed by immunoblotting (**Fig 2.22A**). Confocal images showed that the Golgi apparatus appeared compact and perinuclear in cells transfected with control siRNA oligos. In contrast, the knockdown of OSBPL9 resulted in a dispersed or fragmented Golgi structure (**Fig 2.22B**). Quantification of the number of Golgi fragments per cell using ImageJ plugins further demonstrated a significant effect on Golgi structure upon silencing OSBPL9. These results confirm that OSBPL9 plays a role in maintaining Golgi integrity/structure.

2.2.5 AMPK activation results in Golgi dispersal/fragmentation in cells

Effect of OSBPL9 knockdown on Golgi structure and our finding of OSBPL9 as an AMPK substrate strongly suggests that AMPK may play a role in Golgi signalling/function. To explore this possibility, I first examined the effect of AMPK activation on Golgi morphology. I treated U2OS WT cells with 10μM 991 for multiple time points (up to 30 min) and stained them with the Golgi marker VVL. I observed that within 5 min of 991 treatment, a small proportion of cells appeared to have fragmented Golgi (**Fig 2.23A upper panel**), which is as early as the onset of other downstream AMPK signalling pathways such as ACC phosphorylation (**Fig 2.23A lower panel**). To demonstrate this as an AMPK-dependent effect, I utilised AMPKα1/2 DKO (AMPK DKO) cells. In WT U2OS cells, AMPK activation with 991 resulted in a fragmented Golgi phenotype, an effect which was abolished in the AMPK DKO cells (**Fig 2.23B**). Quantification of Golgi particles showed a significant effect of 991 on Golgi structure. I also assessed Golgi structure in MEFs, where I observed a similar effect of 991 on Golgi fragmentation in WT but not in the AMPK DKO cells (**Fig 2.23C**). In addition, 991-mediated Golgi fragmentation was observed in multiple cell lines such as HEPG2, HK-1 and primary rat cortical neurons (**Appendix Fig A.18**), suggesting that this is not a cell type-specific effect and that AMPK is involved in maintaining Golgi integrity and regulating Golgi signalling in different cell types.

Taken together, we showed from an unbiased phosphoproteomics screen using MEFs that AMPK regulates more than 400 phosphosites on several proteins and biochemically validated OSBPL9 as a novel AMPK substrate which plays a critical role in maintaining Golgi integrity. Proteins phosphorylated by AMPK from our screen are known to be involved in a variety of

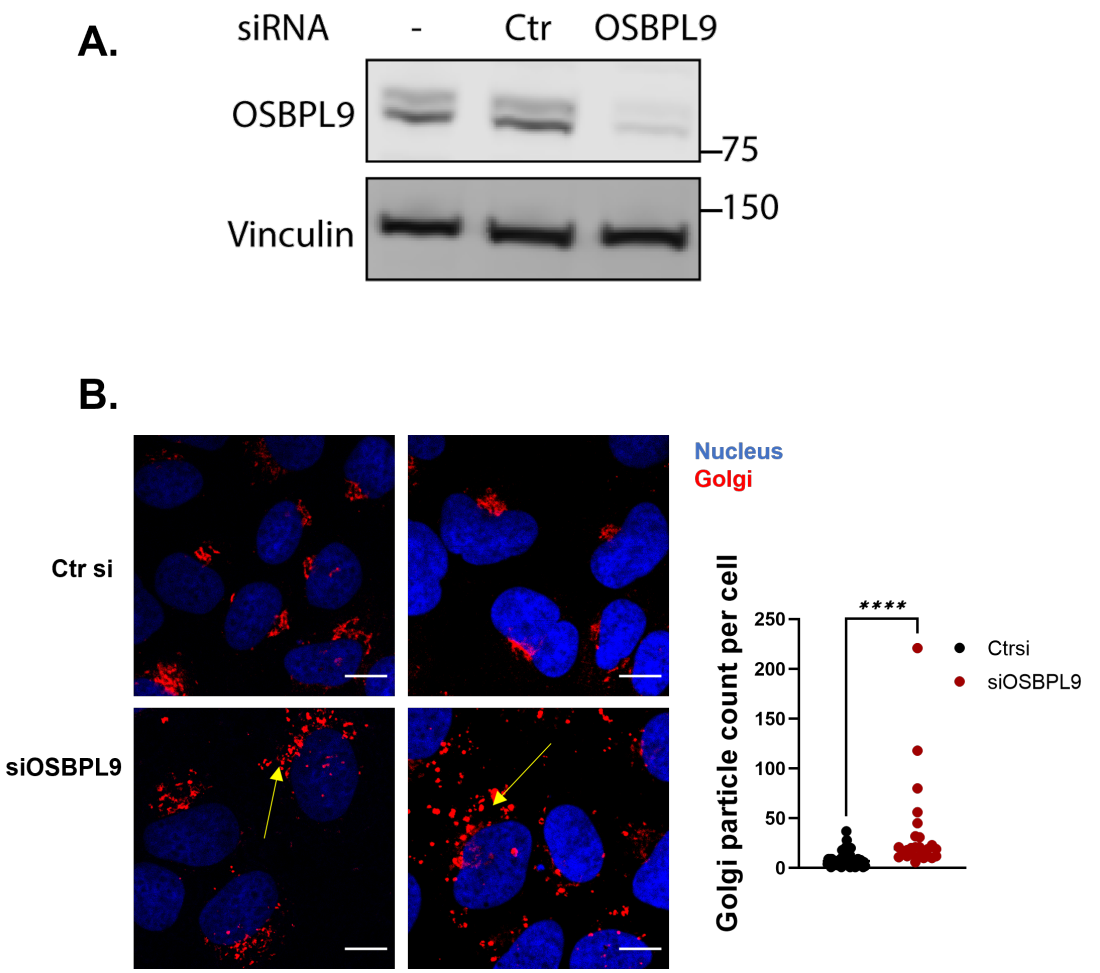

Figure 2.22: **OSBPL9 knockdown results in Golgi fragmentation** (A) U2OS WT cells were left untransfected or transfected with non-targeting siRNA oligos (Ctr) or siRNA oligos targeting OSBPL9 and lysates subjected to immunoblotting. (B) Confocal images of U2OS WT cells transfected with non-targeting siRNA oligos (Ctr) or siRNA oligos targeting OSBPL9 and stained with Golgi marker Vicia Villosa (Red) and nuclear marker Hoechst (Blue). The number of Golgi particles per cell was quantified using ImageJ plugins. ****p<0.0001, as represented by unpaired t-test. Scale bar = 10μm. Images are representative of 2-3 experiments.

cellular processes, such as cell migration, gene transcription, Golgi signalling and protein/cholesterol trafficking, which strongly indicates the involvement of AMPK in regulating these pathways and potential link to pathologies associated to these mechanisms.

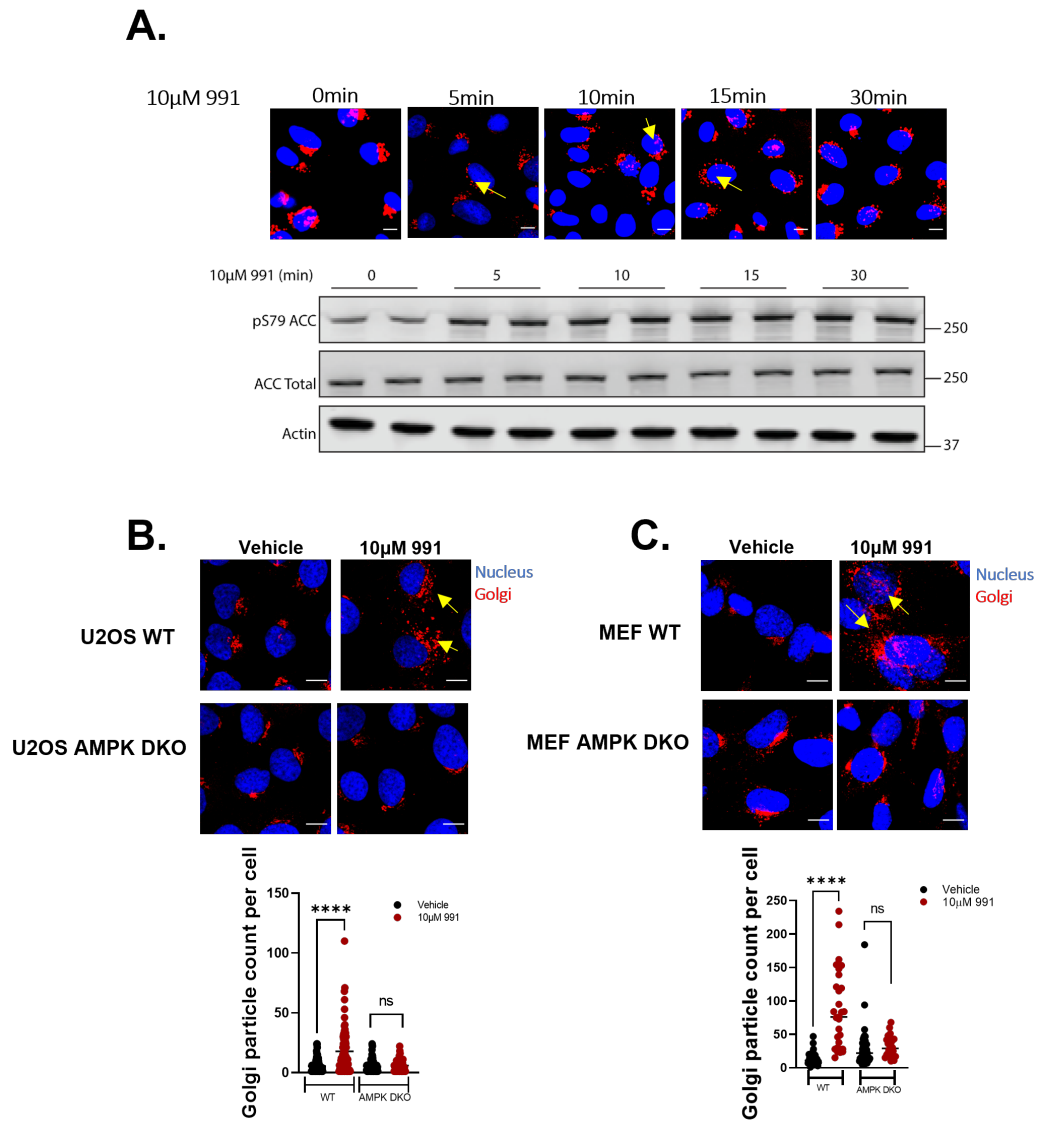

Figure 2.23: **AMPK activation results in Golgi fragmentation** (A) U2OS WT cells were treated with 10μM 991 for indicated time points and stained with Golgi marker Vicia Villosa (Red) and nuclear marker Hoechst (Blue). Immunoblot below confirms AMPK stimulation by 991. (B) U2OS cells (WT or AMPK DKO) or (C) MEFs (WT or AMPK DKO) were treated with vehicle (DMSO) or 10μM 991 for 30 min and stained as in A. The number of Golgi particles per cell was quantified using ImageJ plugins. **** p<0.0001, as represented by unpaired t-test. Scale bar = 10μm. Images are representative of 2-3 experiments.

2.2.6 SH3 domain-binding protein 4 (SH3BP4) is a novel AMPK substrate phosphorylated at Ser19

In addition to proteins regulating ER/Golgi function and structure, our analysis scored many targets as AMPK substrates known to have a wide range of biological functions. SH3BP4 was identified as a low-scoring target of AMPK in a previous study (Schaffer et al., 2015). Analysis of its sequence revealed it contained the consensus AMPK recognition motif. Although it has not been shown to be directly linked to Golgi structure, SH3BP4 is involved in endocytosis, indicating its role in membrane trafficking (Burckhardt et al., 2021). Furthermore, SH3BP4 has been shown to regulate mTORC1 signalling by binding to and negatively regulating Rag GTPases under amino acid starvation, indicating its role in metabolic signalling (Y.-M. Kim et al., 2012). Based on this knowledge, I wondered if AMPK phosphorylates SH3BP4, consequently regulating these processes.

Using similar approach to validate OSBPL9 as an AMPK substrate, I first confirmed in U2OS cells that endogenous SH3BP4 is phosphorylated by 991 using the AMPK substrate phospho-motif antibody (**Fig 2.24A**). AMPK-dependence was confirmed as evidenced by the loss of phosphorylation signal in the AMPK DKO cells. Based on the SCANSITE prediction, Ser19 is a potential AMPK-phosphorylated site on SH3BP4. We generated a plasmid expressing S19A mutant SH3BP4 and observed that phosphorylation was lost when cells were transfected with this mutant, confirming that AMPK phosphorylates SH3BP4 at Ser19 (**Fig 2.24B**). We generated an antibody specific to the phosphorylated Ser19 (pSer19 SH3BP4) for further validation. Following confirmation of the specificity of the antibody (**Fig 2.24C**), I analysed vehicle (DMSO)- or 991-treated MEFs and observed that SH3BP4 is phosphorylated by AMPK at Ser19 at an endogenous level (**Fig 2.24D**). Taken together, these results show that AMPK phosphorylates SH3BP4, a protein known to have a role in endocytosis and amino acid-mediated mTORC1 signalling, further widening the therapeutic potential of AMPK. However, AMPK-mediated regulation of these processes in relation to SH3BP4 needs further investigation.

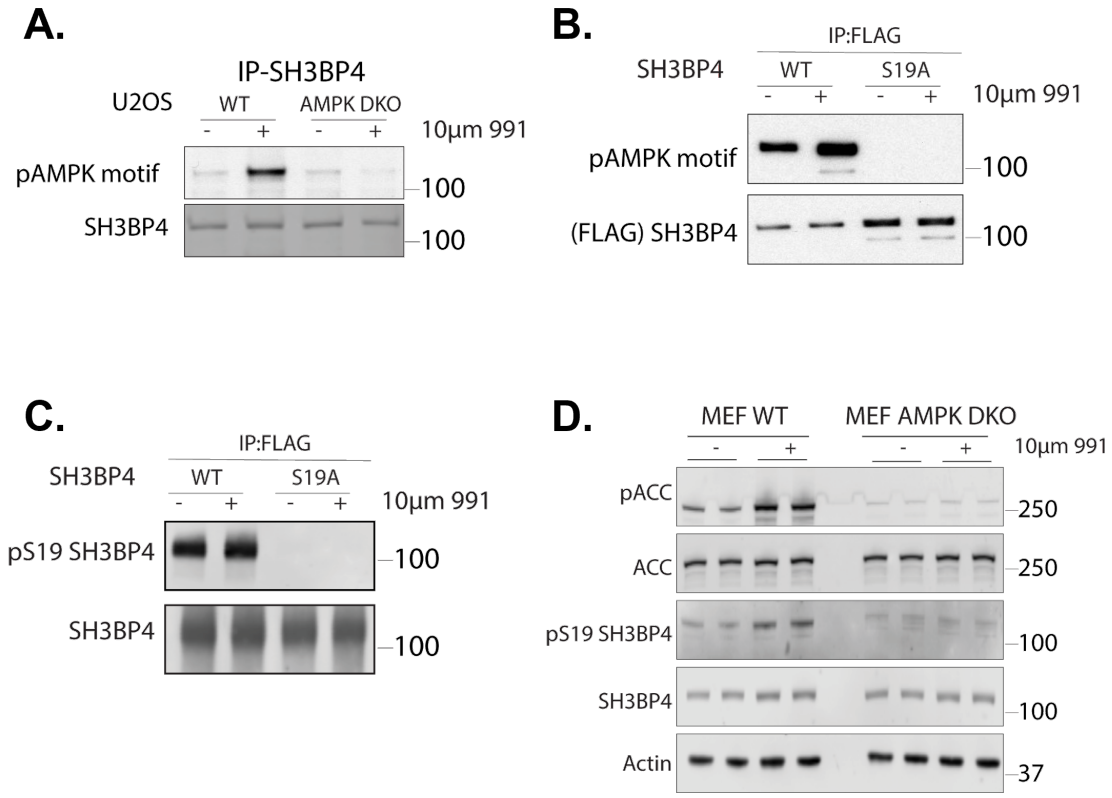

Figure 2.24: **SH3BP4 is a novel AMPK substrate phosphorylated at Ser19** (A) Endogenous SH3BP4 was immunoprecipitated from U2OS cells (WT or AMPK DKO) treated with vehicle (DMSO (-)) or 10µM 991 (+) and subjected to immunoblotting with AMPK substrate phospho-motif antibody. (B) U2OS WT cells transiently expressing FLAG-SH3BP4 WT or S19A were treated with vehicle (DMSO (-)) or 10µM 991 (+) for 30 min, and lysates immunoprecipitated using a FLAG antibody and subjected to immunoblotting. (C) The specificity of the pSer19 SH3BP4 antibody was confirmed in U2OS WT cells transiently transfected with FLAG-SH3BP4 WT or S19A and subjected to immunoprecipitation/immunoblotting. (D) Phosphorylation of endogenous SH3BP4 (pSer19 SH3BP4) was assessed in MEFs (WT and AMPK DKO), treated with vehicle (DMSO (-)) or 10µM 991 (+) by immunoblotting. Images are representative of two experiments.

3 Discussion

The therapeutic potential of AMPK has sparked interest in investigating and discovering novel mechanisms of AMPK regulation. Complexities in understanding AMPK function and signalling have increased with the identification of several posttranslational modifications in the α and β subunits (Ovens et al., 2021). The significant modification prevalent in AMPK subunits is reversible phosphorylation. Multisite phosphorylation, including the critical Thr172 phosphorylation, has been identified in the α subunit with possible physiological significance and involvement in regulating AMPK activity. In the β subunit, phosphorylation of Ser108 in the Carbohydrate Binding Module (CBM) has gained major attention regarding regulation by ADaM-site-specific allosteric activators, suggesting the presence of possible natural ligand(s) capable of activating AMPK via this site (Xiao et al., 2013, M. J. Sanders et al., 2022). The β subunit provides another level of AMPK regulation via a lipid modification in which a myristate is added to the N-terminus Gly2 (myristoylation). Previous studies have proposed that under metabolically stressed conditions (e.g., glucose starvation), myristoylation regulates AMPK association to intracellular membranes, facilitating AMPK proximity to upstream regulators, thereby suggesting its requirement for AMP-mediated phosphorylation of Thr172α (Oakhill et al., 2010). These observations led to a hypothesis for a possible "myristoyl switch" that allows AMPK to sense stress signals influencing its activation and signalling (Ali et al., 2016). Therefore, myristoylation is a crucial mechanism with a potentially important role in regulating AMPK activity and its downstream signalling. Efforts have been made to elucidate the mechanism of β subunit myristoylation-mediated AMPK regulation, for instance, on AMPK localisation and activity (Oakhill et al., 2010, Mitchelhill et al., 1997). However, previous studies have primarily relied on cellular overexpression or *in vitro* recombinant proteins which are less reliable in unlocking the significance of the myristoyl group at the endogenous level. In this study, we utilised two different genetic models to investigate the function of β subunit myristoylation. Using a complete genetic knockout model of human U2OS cells (β1/β2 DKO), I generated stable cell lines expressing either β1 WT or G2A. Complete knockout of the β subunit isoforms prevented any influence from endogenous proteins. In addition, we utilised a mouse model carrying CRISPR-Cas9-generated Gly2-Ala knock-in, enabling disruption of myristoylation of the

endogenous β subunit. MEFs isolated from these mice served as a powerful tool to study the functionality of β myristoylation at the endogenous level.

My findings using two genetic models: human U2OS and MEFs, showed that the loss of myristoylation of the AMPKβ subunit leads to enhanced basal AMPK activity and downstream substrate phosphorylation. In MEFs from the β1/2 G2A DKI and primary hepatocytes from the β1 G2A KI mice, expression of the β1 subunit was reduced by ~2 fold, correlated to a reduction of α and γ1 subunits. This reduction was independent of changes in gene expression as qPCR analysis showed no differences in mRNA levels (**Appendix Fig A.12A**). One hypothesis for a reduced expression is compromised stability due to loss of myristoylation. This is in line with a study where the loss of myristoylation of Cardiolipin and phosphatidic acid-binding protein (CLPAPB) was shown to be more unstable than the WT form of the protein (Maeda et al., 2018), indicating the importance of N-myristoylation in protein stability. Myristoylation of several other proteins has been shown to contribute to protein structural and thermostability (e.g., cAMP-dependent protein kinase (Zheng et al., 1993), and picornavirus capsid protein (VP4) (Chow et al., 1987). However, despite reduced expression, I have shown that the relative interaction of the β subunit with the α and γ1 subunits is not affected by the G2A mutation indicating that the heterotrimeric complex formation is intact. N-terminal glycine is recognised for proteasomal degradation by Cullin-RING E3 ligases, CUL2ZYG11B and CUL2ZER1, and this degradation is protected by N-myristoylation as loss of myristoyltransferases (NMT1/2) resulted in destabilisation of the protein (Timms et al., 2019). However, the presence of alanine in position 2 increased protein stability in that study, indicating that in the context of AMPK, other ubiquitin systems could have resulted in the β subunit degradation due to the loss of the myristoyl group. Specific ubiquitin ligases have been reported to mediate AMPK ubiquitination and subsequent degradation; e.g., Cidea has been shown to interact with the β subunit leading to AMPK degradation in brown adipose tissues (Qi et al., 2008). Also, cancer-specific MAGE-A3/6-TRIM28 ubiquitin ligase has been shown to ubiquitinate and degrade AMPKα1 in several tumour cell lines (Pineda et al., 2015).

Despite reduced expression of AMPK subunits in the β1/2 G2A DKI MEFs or primary hepatocytes from β1 G2A KI mice, AMPK activity was substantially enhanced at the basal condition as observed by phosphorylation of AMPKα Thr172 or substrates of AMPK. Higher basal AMPK activity was consistent in stable U2OS cell lines expressing β1 G2A. However, reduced subunit expression was not observed in this case as we selected clones with comparable expression levels of β1 (**Fig 2.4**). It has been previously reported using *in vitro* AMPK preparations that loss of β subunit myristoylation increases AMPK activity at basal conditions correlated with increased Thr172α phosphorylation suggesting that myristoylation plays an autoinhibitory role in AMPK regulation (Oakhill et al., 2010). However, maximal activation of AMPK by AMP or glucose deprivation in COS7 cells expressing β1 G2A could not be achieved, indicating a binary role of this modification and its requirement to initiate AMPK signalling in response to stress signals. Myristoyl group has been predicted to bind at the interface of the DFG motif and the catalytic loop suppressing Thr172α phosphorylation. Therefore, one possible explanation for an increased AMPK activity is that the absence of

myristoylation could mimic the conformation whereby the myristoyl group releases out of the pocket, relieving autoinhibition and activating AMPK. Treatment with ADaM-site activators (991 or A769662) or AMP-mimetic AICAR only modestly increased phosphorylation. This could be because the basal phosphorylation levels were close to saturating levels, and treatments with AMPK activators were ineffective in inducing a further increase. However, the hypothesis of "myristoyl switch" has not been explicitly validated, and therefore detailed structural studies that could resolve myristoylation are needed to examine the precise mechanism.

Another essential aspect of β subunit myristoylation is its role in regulating AMPK intra/subcellular localisation. Using fluorescently-tagged AMPKβ subunits, it has been shown that G2A mutant β1 attains a diffused localisation pattern in contrast to a particulate extranuclear distribution of the WT form (Mitchelhill et al., 1997). Furthermore, the importance of myristoylation has been depicted in the context of AMPK localisation to different subcellular compartments such as mitochondria and lysosomes to regulate mitophagy (Liang et al., 2015) and autophagy (Finlay, 2019), respectively. This indicates that myristoylation keeps AMPK membrane-bound and close to upstream regulators like kinases and phosphatases. Loss of myristoylation could change AMPK localisation, thereby releasing it from membrane-bound to cytosolic form. I attempted to investigate endogenous β1 localisation by imaging MEFs using a β1-specific antibody. I observed no visual differences in β1 distribution between WT or β1/2 G2A DKI MEFs under basal or allosteric activators-treated conditions using confocal microscopy (**Appendix Fig A.9**). Since lysosomes are proposed as the activation hub for AMPK, I investigated co-localisation between β1 and LAMP1 using two approaches (immunofluorescence and PLA), followed by quantitative analyses. I used AICAR to mimic an increase in intracellular AMP levels, which has been shown to facilitate AMPK membrane binding. I observed no apparent effect of AICAR on co-localisation, while G2A DKI cells showed a significantly higher co-localisation, as demonstrated by Mander's co-localisation coefficient and the number and mean intensity of PLA signal. It should be noted that G2A DKI cells seemed to have a higher number of lysosomes appearing mostly in clusters which could have biased our automatic quantification. Loss of β1 myristoylation may have direct effects on lysosomal morphology and regulation. These cells have enhanced cellular AMPK activity, which could have resulted in increased lysosomal biogenesis, thereby resulting in increased values of co-localisation parameters in our analyses. Detailed knowledge of the chronic effect of β1 subunit G2A mutation on lysosomes is needed to normalise the quantification and have a more precise interpretation of the lysosomal localisation of AMPK. Here, we only assessed AMPK localisation in lysosomes; however, future studies should utilise additional organelle-specific markers (e.g., ER, mitochondria) for assessing co-localisation using high-resolution microscopy techniques to explore AMPK subcellular localisation with time kinetics. Genetically encoded FRET-based AMPK biosensors have been developed recently to selectively monitor AMPK dynamics at individual subcellular components (T. Miyamoto et al., 2015). Such tools could potentially be used to distinguish localisation differences between AMPKβ1 WT and G2A mutant.

Our findings suggest that the myristoyl group regulates AMPK activity. Since the myristoyl group has been suggested to facilitate the localisation of AMPK, I attempted to investigate the effect of loss of myristoylation on AMPK localisation/interaction with its upstream regulators. Although the identity of primary AMPK-kinases (LKB1 and CaMKK2) has been well established, the identity of AMPK-phosphatase(s) remains elusive. In cell-free assays, recombinant preparations of PP1, PP2A and PPM1A were shown to dephosphorylate AMPKα Thr172 (Carling et al., 1987; Davies et al., 1995). In HeLa cells, RNAi-knockdown of PPM1A/B and 1E resulted in inhibition of AMPKα dephosphorylation (Chida et al., 2013), while in HEK293 cells, depletion of PPM1E, but not PPPM1A increased AMPKα Thr172 phosphorylation (Voss et al., 2011). Ectopically expressed PPM1A and PPM1B were shown to be myristoylated at Gly2, and overexpression of WT but not G2A PPM1A/B decreased AMPKα phosphorylation (Chida et al., 2013). To extend this observation, I showed that endogenous PPM1A and PPM1B are myristoylated. I also showed that phosphatases PPM1A and 1B remain in proximity with AMPKβ1 in WT cells (both MEFs and U2OS) and that this proximity is lost in the G2A cells. These results suggest that myristoylation of β1 and PPM1A/1B play a key role in maintaining proximity, contributing partly to lowering the AMPKα Thr172 phosphorylation level and keeping AMPK at a lower activity state. It should be noted that it is unlikely that AMPK dephosphorylation is entirely regulated by PPM1A or/and PPM1B, at least in MEFs and U2OS cells. I observed that knocking down either PPM1A or PPM1B or a combination of both did not result in any discernible changes in phosphorylation of AMPKα or its substrates in MEFs (**Appendix Fig A.13**) or in U2OS cells (data not shown), suggesting that other phosphatases might play a compensatory role in regulating AMPK in the absence of these phosphatases.

At the whole-body level, we observed a substantial effect on adiposity and liver lipid metabolism in β1 myristoylation-deficient mice. We found that β1 G2A KI mice had reduced HFD-induced obesity. Since β1 is the predominant isoform in the liver of rodents, we observed reduced fat accumulation in the liver of the β1 G2A KI mice. This was correlated to an increased ACC phosphorylation in primary hepatocytes, which leads to reduced lipid synthesis. These findings are consistent with previous mouse models where liver-specific AMPK activation protected them from diet-induced obesity and liver steatosis (Garcia et al., 2019).

An important consideration of the current study is the mutation of glycine residue to alanine. Even though stable cell lines expressing myristoylation-deficient β1G2A and mouse models carrying endogenous non-myristoylated (G2A) β1 are the best possible working models to study myristoylation, certain artefacts may be associated with alanine mutations. This has been reported in the context of some specific proteins, e.g., alanine mutation resulted in structural changes in deubiquitinating enzymes (Morrow et al., 2018) and collagen proteins (Roder, 2022). I tried to address this possibility by modulating N-myristoyltransferases (NMTs), either by knocking them down by the siRNA method or by chemically inhibiting their activities, as an alternative to G2A mutation. In MEFs, I could not detect NMT2 protein by immunoblotting (data not shown); therefore, I knocked down NMT1 and observed a modest

increase in ACC and Raptor phosphorylation which was correlated with an increase in Thr172 AMPKα phosphorylation (**Appendix Fig A.14A**). However, the increase in AMPK activity upon NMT1 knockdown was not as substantial as in β1 G2A mutant cells. This is possibly because the siRNA approach did not entirely abolish NMT1 expression or, although undetectable by immunoblot, NMT2 might have played a compensatory role as β1 myristoylation was only 50% reduced after NMT1 knockdown (**Appendix Fig A.14B**). In addition, I chemically inhibited NMTs with an NMT1/2 inhibitor (IMP-1088) (Kallemeijn et al., 2019), which abolished AMPKβ1 myristoylation at a concentration of 1μM (**Appendix Fig A.15A**). Treating WT MEFs with IMP-1088 resulted in a robust increase in ACC phosphorylation and a modest increase in Raptor phosphorylation which was again correlated to an increased Thr172 AMPKα phosphorylation (**Appendix Fig A.15B**). These results show that inhibiting or knocking down NMT1 and NMT2 reduces β1 myristoylation, which results in an enhanced AMPK activity in MEFs, indicating that the phenotype is not an artefact from the G2A mutation. However, inhibiting NMT1 and NMT2 is not an ideal approach because at least 0.5% of eukaryotic proteins are myristoylated (Hayashi and Titani, 2010), and their activities could be compromised as a result of global loss of myristoyltransferases.

To investigate the effect of β1 G2A mutation on global substrate phosphorylation, we performed an unbiased phosphoproteomics analysis using MEFs; however, most phosphoproteins in the G2A dataset did not contain an AMPK substrate consensus motif, and therefore an in-depth bioinformatics analysis is required. We intriguingly identified more than 400 phosphoproteins regulated in WT compared to AMPK DKO MEFs in the presence of 991. Out of 200 proteins upregulated (increased phosphorylation) by 991 in WT MEFs, I validated OSBPL9 as a new AMPK substrate using multiple methods. AMPK phospho-motif antibody has been previously used to identify and validate AMPK-mediated phosphorylation of substrates that have consensus AMPK substrate motif [L-X-R-X-X-*S/*T] (Ducommun et al., 2015). I used the same method to confirm the 991-mediated phosphorylation of OSBPL9 in both U2OS cells and MEFs. OSBPL9 is one of the top ten hits in our phosphoproteomics screen, including known targets, e.g., ACC and Raptor. OSBPL9 was also identified in a previous AMPK screen in hepatocytes by our group (Ducommun et al., 2015), but it has never been further validated as an AMPK-specific/-dependent substrate. Since a mechanistic understanding of signalling pathways requires analysis of phosphorylation sites of proteins involved, we were interested in identifying AMPK-dependent phosphosites on OSBPL9. Mass-spectrometry (MS) analysis revealed Ser216 as an enriched site; however, bioinformatics prediction by scansite suggested that using their algorithm, this residue does not fully meet the criteria for AMPK substrate consensus motif, while three other residues, Ser326, Thr335, and Ser348 were predicted to be phosphorylated by AMPK. Mutagenesis and cellular assays confirmed Thr335 to be phosphorylated by AMPK. This is an interesting finding because AMPK has been known to favour serine over threonine (Dale et al., 1995). To date, only a handful of substrates have been fully validated (e.g. using site-specific phospho-antibody) to be phosphorylated at a threonine residue by AMPK at the endogenous level, including Golgi-specific brefeldin A resistant guanine nucleotide exchange factor 1

(GBF1) (T. Miyamoto et al., 2008). Consistent with the previous study (Ngo and Ridgway, 2009), I confirmed using our cell model that OSBPL9 plays a role in maintaining Golgi structure as its knockdown in cells resulted in a significant loss of Golgi integrity. The physiological significance of OSBPL9 phosphorylation by AMPK is unknown. One of the consequences of this event could be the loss of Golgi structure as AMPK activation by 991 also resulted in significant dispersal of the Golgi apparatus in both U2OS cells and MEFs. In addition to OSBPL9, our screen revealed at least 24 proteins (991-upregulated) to be involved in ER/Golgi regulation (**Appendix table A.3**). This is based on published studies and predicted functions of the identified proteins. I wanted to examine whether AMPK regulates one or more of these proteins because the morphology of Golgi has also been shown to depend on different ER/Golgi-resident proteins. Based on the consensus AMPK substrate motif, I selected Conserved Oligomeric Golgi complex 3 (COG3) and Transport protein particle complex 10 (TRAPPC10). I analysed their phosphorylation following AMPK activation using immunoprecipitation/immunoblotting with the AMPK substrate phospho-motif antibody. COG and TRAPP proteins have been shown to have crucial importance in various stages of the secretory pathway and different cellular processes (Bailey Blackburn et al., 2016, Yamasaki et al., 2009, Zhao et al., 2017). In addition, I analysed phosphorylation of the General vesicular transport factor p115. Although it was not present in our list, p115 contains the consensus substrate motif for AMPK and has been extensively studied in Golgi morphology and signalling context. Additionally, it is regulated by phosphorylation at Ser942 in the C-terminal domain by a casein kinase II-like enzyme, which regulates its localisation and association with the Golgi membranes (Sohda et al. 1998). I found that P115 and COG3 were robustly phosphorylated in both MEFs and U2OS cells following 991 treatment (**Appendix FigA.20**). TRAPPC10 phosphorylation was evident in U2OS cells while it could not be observed in MEFs, possibly indicating a cell type-specific effect. In both cell types, I analysed GBF1, a known AMPK substrate involved in Golgi signalling (T. Miyamoto et al., 2008), and confirmed its phosphorylation using our method, which validates our approach. These results indicate that Golgi fragmentation by 991 could be a direct consequence of AMPK activation via phosphorylation of OSBPL9 and/or other proteins identified here.

Many studies have linked Golgi with the Endoplasmic Reticulum (ER) suggesting the two organelles are functionally related (Presley, 1997; Wang et al., 2020). ER-stress inducers such as thapsigargin have been shown to induce Golgi fragmentation (Ireland et al., 2020). To test whether 991 resulted in Golgi fragmentation via ER stress, I looked at the expression of BiP and phosphorylation of Eukaryotic Initiation Factor eIF2α, markers of ER stress, following 991 treatment in U2OS cells. 991 did not result in ER stress as evidenced by insignificant changes in BiP expression and eIF2α phosphorylation (**Appendix Fig A.19A**). This is in line with a previous study that showed AMPK attenuates, but not increases, hypoxia-induced ER stress in neonatal rat cardiomyocytes (Terai et al., 2005).

It is well known that the Golgi apparatus is a complex organelle whose structure is dynamic but tightly regulated. The Golgi morphology is maintained by the actin and tubulin cytoskeleton (Thyberg and Moskalewski, 1999). Microtubules are essential for the

characteristic juxtanuclear orientation of the Golgi apparatus and for maintaining the organisation of Golgi cisternae. Interestingly, our phosphoproteomics screen revealed several proteins that are phosphorylated upon 991 treatment to be involved in microtubule/cytoskeletal organisation (**Appendix table A.2**). I speculated if AMPK activation results in disruption or changes in microtubules leading to Golgi fragmentation. Nevertheless, treatment of U2OS cells with 991 did not result in any discernible changes in microtubule morphology, as evidenced by β-tubulin staining. At the same time, Nocodazole, a known tubulin-depolymerising agent (Gerlitz et al., 2013), caused complete depolymerisation of tubulin (**Appendix Fig A.19B**). These findings suggest that AMPK activation causes Golgi fragmentation independent of microtubule disorganisation. This is in line with a study that showed AMPK regulates microtubule polymerisation by phosphorylating CLIP-170 (Nakano et al., 2010). However, another study showed that AMPK activation phosphorylates MAP4 leading to microtubule destabilisation (Fassett et al., 2013). Further studies are needed to interpret the role of microtubules/tubulin in AMPK-mediated Golgi fragmentation, for instance, using microtubule modulators with different modes of action (e.g., taxol, colcemid, etc.), which have been shown to induce Golgi fragmentation (Thyberg and Moskalewski, 1999) or by investigating AMPK effects on tyrosination of tubulin as Golgi complex and tubulin tyrosination are functionally linked (Skoufias et al., 1990).

In addition to Golgi-linked proteins, I analysed an additional protein called SH3 domain-binding protein 4 (SH3BP4), which has been addressed in studies linking to a variety of biological mechanisms (**Fig 2.24**). SH3BP4 has been shown to negatively regulate amino acid-mediated mTORC1 activation by binding to the Rag GTPase complex during amino acid starvation (Y.-M. Kim et al., 2012). A recent study showed that SH3BP4 promotes endocytosis of neuropilin-1 and α5-integrin and modulates cell-matrix interactions. This process is shown to be regulated by Akt, which phosphorylates SH3BP4 at Ser246 and promotes binding to 14-3-3 adapter protein. This excludes it from clathrin-coated pits inhibiting endocytosis, thereby linking SH3BP4 at the interface of signalling and membrane trafficking (Burckhardt et al., 2021). It is unknown whether AMPK-mediated phosphorylation of SH3BP4 at Ser19 would impact these mechanisms; therefore, future studies are needed to clarify the role of AMPK in SH3BP4-regulated cellular processes.

4 Conclusion and future perspectives

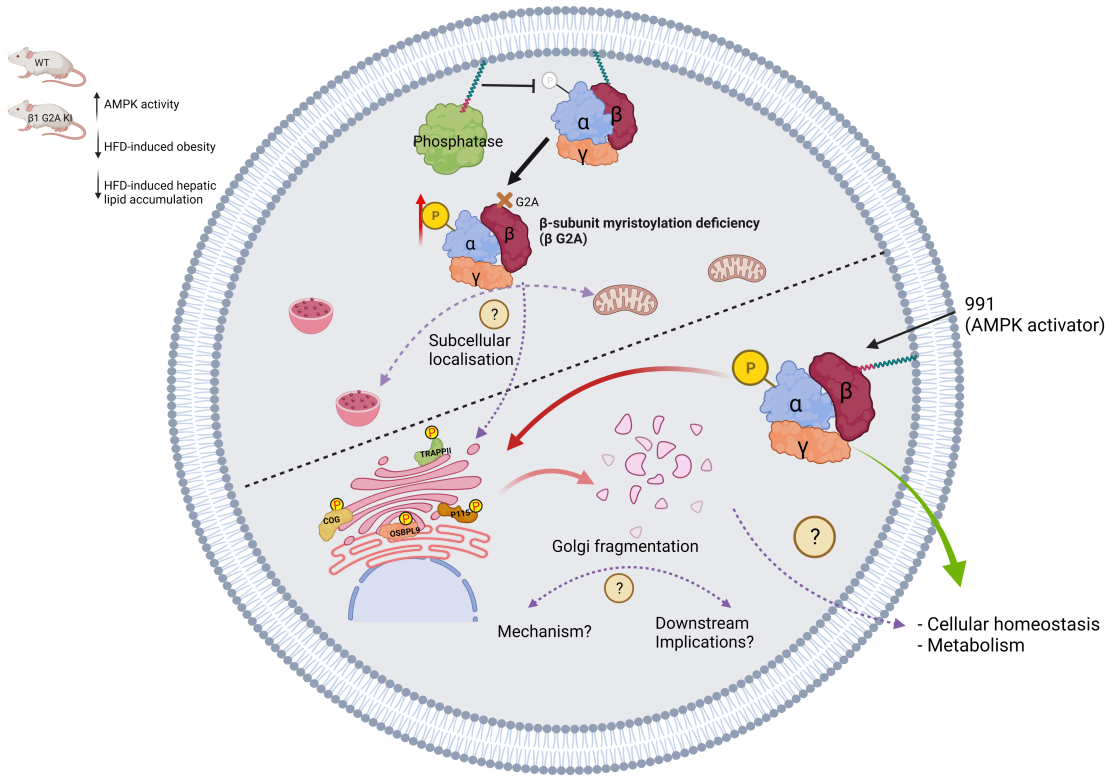

Created using BioRender

This work provides novel insights into the mechanism of AMPK regulation via β subunit myristoylation. Loss of myristoylation in the β subunit results in an enhanced cellular AMPK activity, characterised by an increase in basal phosphorylation of Thr172 AMPKα and its downstream substrates. We showed that this phenotype is partially due to disrupted interaction between phosphatases and AMPK. Immunofluorescence and PLA revealed an increased colocalisation between β1 and lysosomes in myristoylation-deficient (β1/2 G2A) MEFs. However, further investigation is needed to clarify AMPK localisation in different sub-cellular compartments using high-resolution imaging techniques. Interestingly, in mice,

genetic/constitutive loss of β1 myristoylation was metabolically beneficial at whole-body levels. We showed that β1 G2A mice were protected from HFD-induced obesity and aberrant hepatic lipid accumulation in the liver. The beneficial effects of β1-mediated AMPK activation on liver lipid metabolism are intriguing and provide a promising approach for therapeutic applications. In line with this, direct activation of AMPK through the ADaM site by PXL770, an orally bioavailable β1-selective AMPK activator, was demonstrated to inhibit *de novo* lipogenesis in rodents and is currently in clinical development for non-alcoholic steatohepatitis treatment (Gluais-Dagorn et al., 2022). Future studies using mice with mutation (G2A) in the β2 isoform will clarify if β2-specific AMPK activation leads to metabolic benefits with respect to other tissues, e.g., skeletal muscle and adipose, where β2 is predominantly expressed.

Although we extensively characterised phosphorylation of known AMPK substrates (ACC, Raptor, and ULK1), it is unknown whether loss of β1 myristoylation affects global substrate phosphorylation. We attempted to address this using MS-based phosphoproteomics; however, this aspect needs further in-depth analysis. It would also be interesting to identify tissue-specific substrate phosphorylation (e.g., identifying upregulated proteins from hepatocytes of β1 G2A KI mice). Our phosphoproteomics screen detected >200 proteins in WT MEFs in response to 991, which were specifically regulated by AMPK. Interestingly, a large proportion of the proteins were involved in Golgi/ER regulation. In addition, I showed that pharmacological activation of AMPK induces Golgi fragmentation in multiple cell types. I validated OSBPL9 which is known to regulate Golgi structure/function and cholesterol trafficking as a novel AMPK substrate. These findings link AMPK to Golgi signalling, which opens up new avenues for investigation and therapeutic potential of AMPK. Future studies should use relevant cell models to study the physiological/pathological relevance of AMPK-mediated OSBPL9 phosphorylation. Even though it is well known that AMPK favours serine to threonine, we have identified Thr335 on OSBPL9 to be phosphorylated by AMPK. It would be of great interest to explore what physiological implication this phosphorylation has, for instance, by using KI cell and mouse models (carrying T335A point mutation) and monitoring changes in different mechanisms that OSBPL9 is known to be involved (e.g., Golgi structure, cholesterol trafficking, protein glycosylation, and ER-Golgi transport). Golgi fragmentation is extensively studied in the context of neurological disorders where it is correlated to abnormal protein accumulation or impairment of protein trafficking (Joshi et al., 2014, Rendón et al., 2013). To address the mechanism and downstream implications of AMPK-induced Golgi fragmentation, an appropriate model, e.g., neuronal cell lines, could be used to investigate if AMPK is linked to specific neuronal pathologies via modulation of Golgi structure.

Overall, this study expands our understanding of the regulation and novel biological roles of AMPK. This will advance future studies to elucidate the significance of AMPK in the treatment of metabolic as well as non-metabolic disorders.

5 Materials and Methods

5.1 Antibodies and reagents

R=Rabbit; M=Mouse; S=Sheep; WB= Western blot; IP= Immunoprecipitation; IF= Immunofluorescence

Table 5.1: List of primary antibodies used in the study

S.N.	Primary antibodies	Species	Applications	Supplier
1	pS79 ACC (#3661)	R	WB	Cell Signaling Technology
2	ACC (#3676)	R	WB	
3	pS792 Raptor (#2083)	R	WB	
4	Raptor (#2280)	R	WB	
5	pT172 AMPKα (#2535)	R	WB	
6	AMPKα (#2532)	R	WB	
7	pS555 ULK1 (#5869)	R	WB	
8	ULK1 (#6439)	R	WB	
9	AMPKα1 (#2795)	R	WB	
10	AMPKβ1 (#12063)	R	WB	
11	AMPKβ2 (#4148)	R	WB	
12	AMPKβ1/2 (#4150)	R	WB	
13	phospho-AMPK substrate motif (#5759)	R	WB, IP	
14	SH3BP4 (#55935)	R	WB	
15	BiP (#3183)	R	WB	
16	pS51 eIF2α (#9721)	R	WB	
17	Total eIF2α (#9722)	R	WB	
18	Vinculin (#4650)	R	WB	

S.N.	Primary antibodies	Species	Applications	Supplier
19	AMPKβ1 (#27201)	M	IP, IF	Signalway
20	PPM1A (#ab14824)	M	WB	Abcam
21	PPM1A (#12961-1-AP)	R	WB, IP, IF	Proteintech
22	PPM1B (#13193-1-AP)	R	WB, IP, IF	
23	PPP2CA (#13482-1-AP)	R	WB, IP, IF	
24	MYPT1 (#22117-1-AP)	R	WB, IP	Proteintech
25	P115 (#13509-1-AP)	R	WB	
26	COG3 (#11130-1-AP)	R	WB	
27	GBF1 (#25183-1-AP)	R	WB	
28	OSBPL9 (#11879-1-AP)	R	WB	
29	pT335 OSBPL9 (YZ#7882)	R	WB	Yenzym antibodies
30	pS909 MYPT1	S	WB	Custom made (Dundee)
31	NMT1/2 (#ab186123)	R	WB	Abcam
32	FLAG (#F7425)	M	WB, IF	Sigma/Merck
33	Tubulin (#T6074)	M	WB	
34	GAPDH (#G8795)	M	WB	
35	β-Actin (#A2228)	M	WB	
36	AMPKα2 (#07-363)	R	WB	
37	GM130 ((#610822)	M	IF	BD Biosciences
38	β-tubulin Cy3 (#C4585)	M	IF	Sigma
39	LAMP1 (#ab24170)	R	IF	Abcam

Table 5.2: List of secondary antibodies used in the study.

S.N.	Secondary antibodies and dyes	Applications	Supplier
1	Vicia Villosa Biotinylated (#B-1235-2)	IF	Vector Lab
2	Streptavidin AF680 (#S21378)	WB, IF	Invitrogen
	Streptavidin AF488 (#S11223)	IF	
	Streptavidin AF790 (#S11378)	WB	
3	Hoechst	IF	
4	Rabbit IgG AF680 (#A21109)	WB	
5	Mouse IgG AF680 (#A21057)	WB	
6	Rabbit IgG AF790 (#A27041)	WB	
7	Mouse IgG AF800 (#A32720)	WB	
	Rabbit IgG FITC (#ab6717)	IF	Abcam
8	Mouse IgG AF 647 (#ab150115)	IF	
9	Rabbit IgG AF647 (#ab150083)	IF	

siRNA oligonucleotides ON-TARGETplus SMARTPool targeting mouse PPM1A (L-040052-00-0010), mouse PPM1B (L-040053-00-0010), mouse PPP2CA (L-040657-00-0005), mouse PPP2CB (L-041905-00-0005), mouse NMT1 (L-062260-01-0010), and human OSBPL9 (#L-009912-00-0010) were obtained from horizon discovery. Scrambled/negative control siRNA (#SIC005) was obtained from Sigma. For Golgi imaging, CellLight™ Golgi-RFP, BacMam (#C10593) was obtained from Invitrogen. AMPK activator 991 (#1219739-36-3) was obtained from Spirochem, MK-8722 (#1394371-71) from Glixx Laboratories, AICAR (#2627-69-2) from Apollo Scientific, and A769662 (#S2697) from Selleckchem. Thapsigargin (#T9033) and Nocodazole (#31430-18-9 487928) were obtained from Sigma and NMT1/2 inhibitor IMP-1088 (#25366) from Cayman chemical. Cell culture reagents were purchased from Invitrogen.

5.2 Cell culture

U-2 Osteosarcoma (U2OS) Flp-In T-Rex cells were kind gifts from John Rouse (MRC PPU, University of Dundee). The KO cell lines (U2OS AMPKα1/α2 DKO, β1 KO, β2KO and β1/2 DKO) were generated by Horizon discovery using the CRISPR-Cas9 approach. Cells were maintained in DMEM-high glucose, Glutamax (Thermo Fischer, #10566016) supplemented with 10% Fetal Bovine Serum, 1% Penicillin/Streptomycin and 1% Sodium Pyruvate. To maintain the FlpIn sites, cells were maintained in 10μg/ml Blasticidin (Thermo Fischer, #A1113903) and 100μg/ml Zeocin (Thermo Fischer, #R25001).

Mouse embryonic fibroblasts (MEFs) were isolated from homozygous WT, β1-G2A KI or β1/β2-G2A DKI embryos at days 12–13 post coitum. The head and internal organs were removed, and the remaining embryo body was minced and trypsinised. After adding DMEM supplemented with 10% FBS and 1% penicillin-streptomycin, cells were centrifuged (500 g, 5 min, 4 °C) and the medium replaced. The cell suspension was passed through a 40-μm cell strainer and plated in 10-cm dishes. Cells were cultured in DMEM supplemented with 10% FBS and 1% penicillin-streptomycin and passaged at 1:2 or 1:4 when confluent. MEFs were immortalised by transfection with an SV40 prominent T-antigen expression construct using Fugene HD transfection reagent (Promega) and were maintained in DMEM-high glucose, Glutamax supplemented with 10% Fetal Bovine Serum and 1% Penicillin/Streptomycin.

5.3 Transient transfection

Transient transfections were carried out using FUGENE HD transfection reagent (E231A, Promega). Briefly, cells were plated in 10-cm dishes a day before transfection. The next day, the transfection complex was prepared by adding DNA in a serum-free medium and FUGENE transfection reagent (1:3.5 DNA: FUGENE ratio). The mixture was incubated for 10 minutes at room temperature. Cells were washed and incubated with fresh complete DMEM. A transfection complex was added to each plate. 24h post-transfection, old media were replaced with fresh complete DMEM. Cells were treated and harvested 48h post-transfection

for analysis.

5.4 Plasmids

Plasmids encoding human OSBPL9 ((NM_148908), SH3BP4 (NM_014521), COG3 (NM_031431), P115 (NM_003715) and GBF1 (NM_004193) were purchased from OriGene. All plasmid constructs and mutagenesis for these plasmids were generated using standard molecular biology techniques by the cloning team at MRCPPU Reagents and Services (*https://mrcppureagents.dundee.ac.uk*). For AMPK β subunit expression in stable U2OS cell lines, human FLAG-β1 or -β2 were cloned into a pcDNA5-FRT vector under the CMV promoter. Site-directed mutagenesis was carried out according to the QuikChange method (Stratagene) using KOD polymerase (Novagen). Sequences were verified utilising the BigDyeR Terminator 3.1 kit on a 3500XL Genetic analyser (ABI-Invitrogen).

5.5 siRNA knockdown

siRNA knockdown was performed using Lipofectamine RNAiMAX transfection reagent (#133778075, Invitrogen). Briefly, cells were seeded in a 6-well plate (for immunoblotting) and μ-slide 8-well chamber (#80826, ibidi) (for immunofluorescence) a day before transfection. The next day indicated siRNAs were introduced into cells per the manufacturer's instructions. Cells were subjected to treatment and analysis 48 hours post-transfection.

5.6 Stable cell line generation

Stable cell lines were generated using the FlpIn DNA recombination system. Briefly, 1M β1/2 DKO U2OS cells (containing FRT site) were plated in a 10cm dish in a medium containing selection of antibiotics. On the day of transfection, cells were washed once with PBS, and cDNA constructs encoding FLAG-AMPK β1 WT or β1 S108A mutant were transfected along with pOG44 (1:9) using FUGENE HD transfection reagent (Promega #E2311). 24h post-transfection, the medium was replaced with fresh medium without additional antibiotics. 48h post-transfection, cells were trypsinised and divided into two 20cm culture dishes containing fresh medium. 24h later, cells were cultured in a medium containing 200μg/ml of Hygromycin B (Thermo Fischer, #10687010). The medium was replaced every 2-3 days until resistant colonies appeared. Single colonies were isolated using cloning rings (Sigma, #C1059) and were expanded and maintained in a selection medium containing 200μg/ml of Hygromycin B.

5.7 Homogenous Time-Resolved Fluorescence (HTRF) Assay

Dose-dependent cellular AMPK activation was monitored by FRET-based HTRF assay using phospho-ACC (Ser79) cellular kit (Cisbio, #64ACCPET) and phospho-AMPK (Thr172) cellular kit (Cisbio, #64MPKPET). Briefly, cells were seeded in a 96-well plate at a density of 5x104 cells per well a day before treatment. The next day, cells were treated with an increasing concentration of AMPK activator diluted in serum-free medium (50µl per well, 12 concentrations) for a required period. Post-treatment, cells were lysed in 50µl per well of phospho-total protein lysis buffer 1 (Cisbio, #64KL1DF) containing 1:100 phospho and total protein blocking reagent (Cisbio, #64KB1ACC) and left shaken at room temperature for 30min. D2-antibodies and Cryptate-antibodies were diluted (1:40) in the detection buffer. In a 384-well plate, 16µl lysate and 4µl antibodies solution were added per well. The plate was wrapped with a plastic seal and incubated at room temperature, protected from light. The next day, FRET was measured using a Spectramax microplate reader (Molecular Devices) according to the manufacturer's protocol.

5.8 Immunoblotting

Cells were homogenised in lysis buffer (50mM Tris-HCl Ph 7.5, 1mM EDTA, 1mM EGTA, 0.27M Sucrose, 1% Triton X-100, 20mM Glycerol-2-phosphate disodium, 50mM NaF, 5mM Na2P2O7.10H20) containing protease and phosphatase inhibitors. For immunoblotting, 20 µg protein was resolved using Bolt 4-12%, Bis-Tris mini protein gels (#NW04125BOX, Thermo Fisher Scientific). Protein gels were transferred onto nitrocellulose membranes (#926-31092, LI-COR Biosciences) and incubated in primary antibody diluted in Tris-buffered saline/0.1% Tween 20 containing 5% BSA overnight at 4 °C. After 1-hour incubation with secondary antibody at room temperature; membranes were scanned using Odyssey CLx Infrared Scanner. The volume densities of the protein signals were quantified using Image Studio™ software (LI-COR Biosciences).

5.9 Immunoprecipitation

For endogenous proteins, 5µl of the primary antibody was coupled to 5µl of packed Protein G Sepharose beads (17-0618-01, GE Healthcare). 500µg protein lysate was added to the beads-antibody conjugate. For FLAG-tagged proteins, 200µg protein lysate was added to 10µl of packed ANTI-FLAG® M2 Affinity Gel (A2220, Millipore), and the tubes were incubated on a vibrating shaker (Vibramax) at 4 °C overnight. The beads/immune complex were washed three times with cold lysis buffer, resuspended in 25µl of 1x Laemmli sample buffer containing 1 mM DTT, and boiled at 95 °C for 5 min. The eluted proteins were separated by SDS-PAGE followed by immunoblotting.

5.10 AMPK activity assay

For the AMPK activity assay, AMPKa1 (custom-made antibody) (ref) was immunoprecipitated overnight at 4 °C from 250μg of MEF cell lysates pre-conjugated to Protein-G Sepharose beads. The immunoprecipitants were subjected to *in vitro* kinases assay as previously described in detail (Scott et al., 2008).

5.11 Click chemistry

To assess the myristoylation of AMPKβ1 or PP1MA/B, click chemistry was performed using Click-IT myristic acid, azide (12-azidododecanoic acid) kit (C10268, Thermo Fisher Scientific). Briefly, 1 x 106 cells were plated in a 10-cm dish and experiments were performed when cells were 80% confluent. Cells were washed with PBS, and a complete fresh medium containing indicated concentrations of myristic acid-azide was added and incubated at 37 °C for indicated time points. Cells were lysed, and AMPKβ1 or PPM1A/B were immunoprecipitated from cell lysates (500 μg) as described. The immunoprecipitants were subjected to click chemistry reaction using 40 μM biotin-alkyne solution, and proteins were subjected to methanol: chloroform precipitation following the manufacturer's protocol. The dried protein precipitates were resolubilised in Laemmli sample buffer, separated by SDS-PAGE and subjected to immunoblotting as described. The myristoylated proteins were detected using Streptavidin Alexa Fluor conjugates.

5.12 Immunofluorescence

For immunofluorescence, 3 x 104 cells were plated per well in a μ-Slide 8 well (Ibidi). Cells were incubated with an AMPK activator (10 μM 991) or vehicle for 1 hour, washed with PBS, and fixed in 4% paraformaldehyde for 15 min at room temperature under a fume hood. Cells were then washed 3x with PBS-TritonX 0.01%. Cells were permeabilised and blocked with PBS-Saponin 0.1% containing 5% BSA for 1 hour at room temperature. The solution was aspirated and the primary antibody diluted in PBS- TritonX 0.01% was added to the cells and incubated in the dark at 4 °C overnight. The next day, cells were washed 3x with PBS-TritonX 0.01%, 5 min each. Secondary antibody diluted in PBS- TritonX 0.01% was added to the cells and incubated for 45 min at room temperature in the dark. Cells were washed 3x with PBS- TritonX 0.01%, 5 min each. To stain nuclei, Hoechst 33258 (#62249, Invitrogen) diluted 1:5000 in PBS was added to the cells and incubated for 5 min at room temperature in the dark. Cells were washed 3x with PBS and mounted in 100μl Fluoromount G mounting medium (#00-4958-02, Invitrogen) per well. Image acquisition was made on the SP8 confocal microscope (Leica) using the same settings for each condition.

5.13 Proximity Ligation Assay

Proximity ligation assay was carried out using Duolink In Situ Red Starter Kit Mouse/Rabbit (DUO92101, Sigma-Aldrich) following the manufacturer's instructions. Briefly, 2.5 x 104 cells per well were seeded in a μ-slide angiogenesis chamber (#81506, Ibidi). 24 hours later, cells were fixed in 4% Paraformaldehyde for 15min at room temperature. Cells were washed 3x with PBS-TritonX-100 (0.01%), permeabilised and blocked with PBS-Saponin 0.1% containing 5% BSA for 1 hour at room temperature. Required primary antibodies diluted in Duolink antibody dilution buffer (1:100 AMPKβ1 (#27201, Signalway Antibody), 1:250 PPM1A (#12961-1, Proteintech Group), 1:250 PPM1B (#13193-1, Proteintech Group), 1:250 PPP2C (#13482-1-AP, Proteintech Group), 1:250 LAMP1 (#ab24170, Abcam)) were added to cells and incubated at 4 °C overnight protected from light. The next day, cells were washed 3x with PBS-TritonX, 5 min per wash. Proximity Ligation Assay probes (Rabbit Plus and Mouse Minus) diluted in antibody dilution buffer were added and incubated at 37 °C for 1 hour, protected from light. Cells were washed 2x with PBS-TritonX, 5 min each wash. 15μl ligation mix was added to each well and incubated at 37 °C for 30 min, followed by a washing step. 15μl amplification mixture was added to each well and incubated at 37 °C for 100 min, protected from light. Cells were washed 2x with PBS-TritonX, 5 min each wash. 15 ul mounting medium containing DAPI was added to each well. Image acquisition was made on Leica SP8 confocal microscope using the same settings for each condition.

5.14 Image processing and quantification

Image processing and analysis were done using ImageJ/Fiji using the Common Tools Plugin (BIOP, EPFL) as described previously (Schmit et al., 2019). For quantification of mean intensity and number of dots per cell in PLA experiments or number of Golgi particles, an ImageJ script was used to define the Hoechst-stained nucleus as Region of Interest (ROI) in each cell, and required parameters from the Red channel were measured for each ROI (cell). An ImageJ macro was used for colocalisation analysis, automatically detecting each nucleus and measuring colocalisation between the two channels. The macro is deposited in the **Appendix section A.3.2**.

5.15 Phosphoproteomics analysis

Protein digestion and phosphoenrichment were performed by the EasyPhos method as previously described (Robles et al., 2017). Tryptic peptides were separated on an in-house packed 50 cm column (inner diameter 75 μm, 1.8 μm C18 beads, Dr. Maisch GmbH) using an Easy nano-flow high-performance-LC (HPLC) system. The HPLC system was coupled via a nanoelectrospray ion source to a Q Exactive™ HFX Hybrid Quadrupole-Orbitrap™ Mass Spectrometer (Thermo Fischer Scientific, Germany). Mass spectra were generated by the data-dependent acquisition (DDA) with automatic switching between MS and MS/MS.

Precursor ions were picked using the top-10 method. Tandem spectra were generated using high collision dissociation (HCD). MS spectra were acquired in the Orbitrap analyser. Raw mass spectra files were processed in MaxQuant v 1.6.0.1. MS/MS spectra were searched against the decoy UniProt-mouse database (December 2017 release) with forward and reverse sequences. The search included variable modification of serine (S), threonine (T) and tyrosine (Y). The S/T/Y output file from MaxQuant was imported into Perseus software. The rest of the bioinformatics analyses were performed in R studio v.4.1.2. The prediction of AMPK substrates was performed on the sites upregulated with 991 in the WT MEFs. Individual Log2 intensities from 991-treated samples were subtracted from the mean of control-treated samples (delta score). Delta Log2 intensities were z-score transformed. The kinase-substrate prediction analysis was done by first scoring the kinase-substrate relationship (Mouse PhosphoSitePlus annotation), followed by a machine learning approach based on adaptive sampling (PhosR package). Volcano plots were plotted with ggplot (tidyverse).

6 Glossary

25-OHC	25-hydroxycholesterol	18, 19
ACC	acetyl-CoA carboxylase	15, 25, 53
ADaM	Allosteric Drug and Metabolite	2, 4, 8
ADP	adenosine diphosphate	1–3, 12
AICAR	5-Aminoimidazole-4-carboxamide ribonucleotide	4, 8, 13
AID	Auto-Inhibitory Domain	2, 3
AMP	adenosine monophosphate	1–5, 10, 12, 13
AMPK	AMP-activated Protein Kinase	vii, xv, 1–13, 24
ATP	adenosine triphosphate	1, 3, 6, 10, 13
CaMKK2	calcium/calmodulin-dependent protein kinase kinase 2	2, 12, 13
CBM	Carbohydrate Binding Module	2, 3, 5, 7, 8, 63
CBS	Cystathionine Beta Synthase	2, 3
CERT	Ceramide Transfer Protein	18
CRTC3	CREB Regulated Transcription Coactivator 3	53
CTD	C-Terminal Domain	2, 3
DKO	double knock-out	24
ER	Endoplasmic Reticulum	17, 51, 68
FCCP	Carbonyl cyanide-p-trifluoromethoxyphenylhydrazone	22

FFAT	two phenylalanines (FF) in an acidic tract	20
FRET	Fluorescence Resonance Energy Transfer	25
FRT	Flp recombination target	24
G2A	Glycine2-to-Alanine	45
H/E	Hematoxylin/Eosin	47, 48
HMG-CoA	3-hydroxy-3-methylglutaryl coenzyme A	15, 18
HTRF	Homogenous Time-Resolved Fluorescence	25, 26
KI	knock-in	8
KO	knock-out	7, 8, 24
LAMP1	Lysosomal Associated Membrane Protein 1	36, 65
LC	Liquid Chromatography	51
LKB1	Liver kinase B1	2, 12, 13
MCS	Membrane Contact Site	18, 20
MFF	Mitochondrial Fission Factor	21, 53
MS	Mass Spectrometry	51
mTOR	mammalian target of rapamycin	17
MYPT1	Myosin phosphatase-targeting subunit 1	53
NMT	N-myristoyltransferase	9
NMTs	N-myristoyltransferases	66
ORD	oxysterol-binding protein-related domain	20
ORO	Oil Red O	47
ORPs	oxysterol-binding protein-related proteins	18, 19
OSBP	Oxysterol-Binding Protein	18–20
OSBPL9	Oxysterol-binding protein like 9	53
OSBPLs	Oxysterol-binding protein like proteins	19
PC	phosphatidylcholine	20
PH	pleckstrin homology	19
PI	phosphoinositides	18
PI(4)P	phosphatidylinositol 4-phosphate	21
PKD	protein kinase D	19
PPP12R1A	Protein phosphatase 1 regulatory subunit 12A	53
PS	phosphatidylserine	20
RA	Rheumatoid Arthritis	11

SBI	SBI-020696531	6
SID	Sequence Interacting Domain	2, 3
SIKs	salt-inducible kinases	53
SOCE	store-operated calcium entry	16
STIM1	stromal interaction molecule 1	16
STRAD	STE-20 related adaptor protein	12
TBC1D1	TBC1 domain family member 1	53
TGN	Trans Golgi Network	17
TR-FRET	Time-resolved-Fluorescence resonance energy transfer	25
VAP-A	Vesicle-Associated Membrane Protein-Associated Protein A	20
VSVG	vesicular stomatitis virus G	21
VVL	Vicia Villosa	58
WT	wild type	8, 24

A Appendix

A.1 Appendix Figures

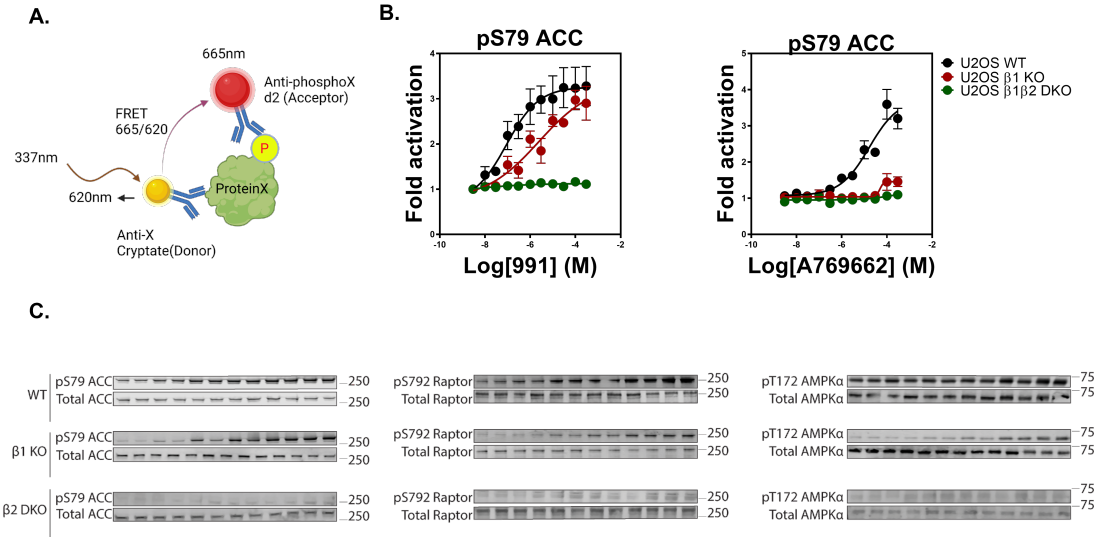

Figure A.1: **Characterisation of U2OS cells** (A) Schematic representation of HTRF assay. (B) Dose-response curves showing Ser79 ACC phosphorylation in U2OS WT, β1 KO and β1/2 DKO cells in response to increasing doses of 991 and A769662 represented as fold activation (value at 0μM set to 1). Graphs are representative of three independent experiments and error bars represent mean ± s.e.m. (C) Lysates from HTRF assay were subjected to immunoblot analysis to determine phosphorylation of ACC, Raptor, and AMPKα.

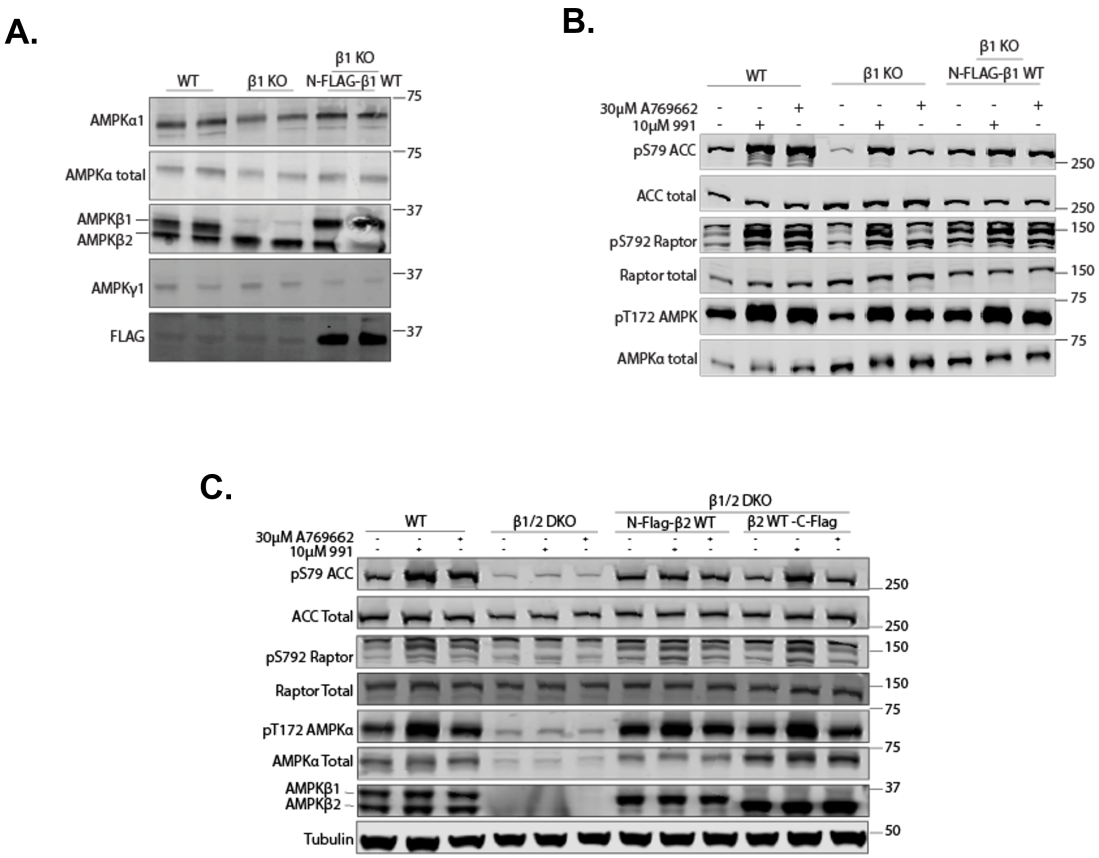

Figure A.2: **Characterisation of stable U2OS cell lines expressing β1 or β2 isoforms** Immunoblots showing (A) expression of AMPK subunits and (B) phosphorylation of AMPKα and its substrates (ACC and Raptor)in response to 991 or A769662 in U2OS WT, β1 KO cells or stable cells expressing N-FLAG-β1 WT in β1 KO background. (C) Immunoblots showing phosphorylation of AMPK substrates in U2OS WT, β1/2 DKO cells or stable cells expressing N-FLAG or C-FLAG-β2 WT in β1/2 DKO background in response to 991 or A769662.

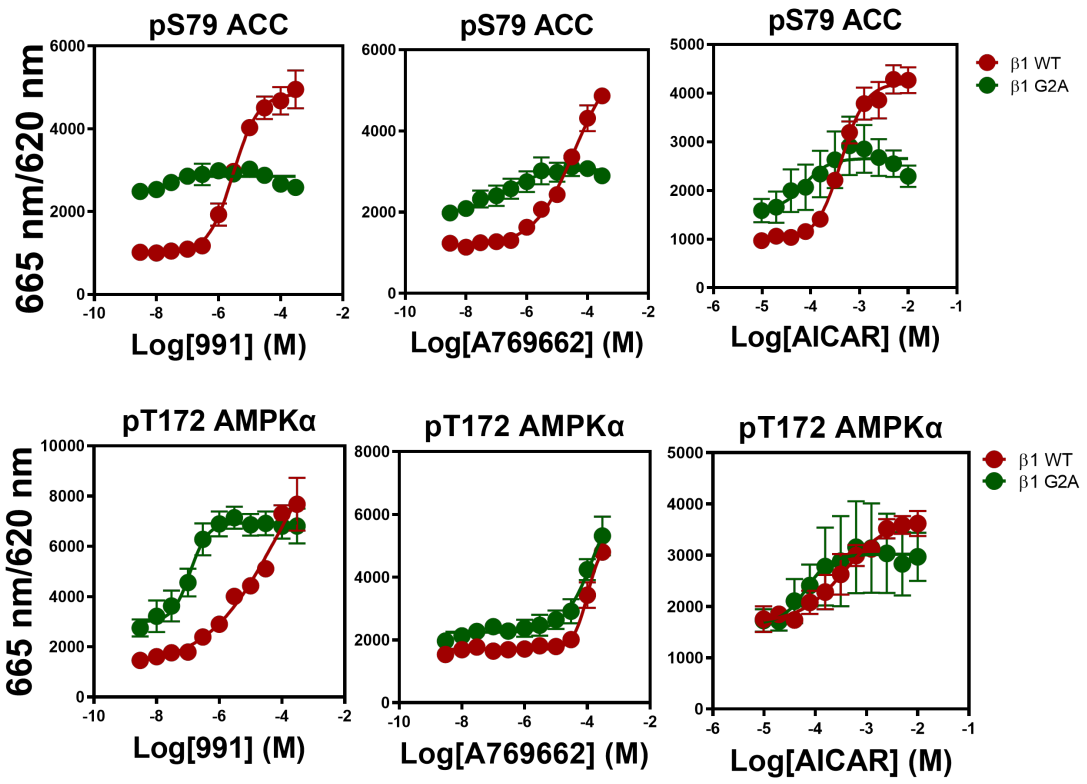

Figure A.3: **Enhanced AMPK activity in β1 G2A U2OS cells by HTRF assay** HTRF results showing dose-response curves of ACC or AMPKα phosphorylation in stable U2OS cell lines expressing C-terminally FLAG tagged β1 WT or G2A in response to increasing doses of 991, A769662 or AICAR. Values are shown as FRET ratio 665nm/620nm. Error bars represent mean ± s.e.m. from three independent experiments.

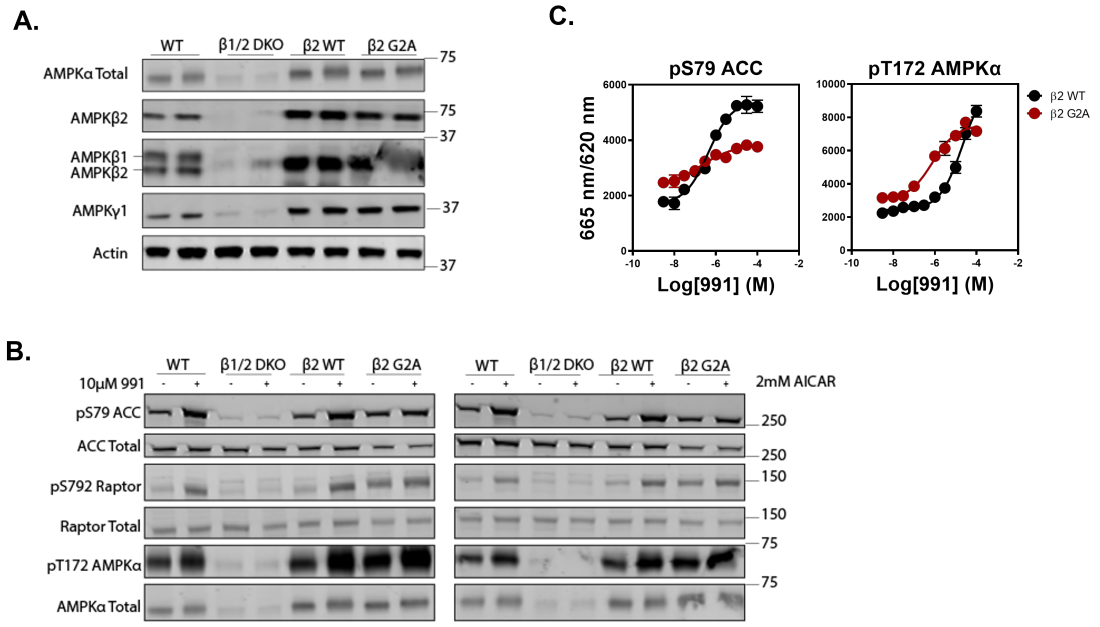

Figure A.4: **Characterisation of U2OS β2 G2A stable cell lines** (A) Immunoblots showing expression of AMPK subunits or (B) phosphorylation of AMPK substrates in U2OS WT, β1/2 DKO cells or stable cells expressing C-FLAG-β2 WT or β2 G2A in β1/2 DKO background. (C) HTRF results showing dose-response curves of ACC or AMPKα phosphorylation in the respective stable cell lines in response to increasing doses of 991. Values are shown as FRET ratio 665nm/620nm. Error bars represent mean ± s.e.m. from three independent experiments.

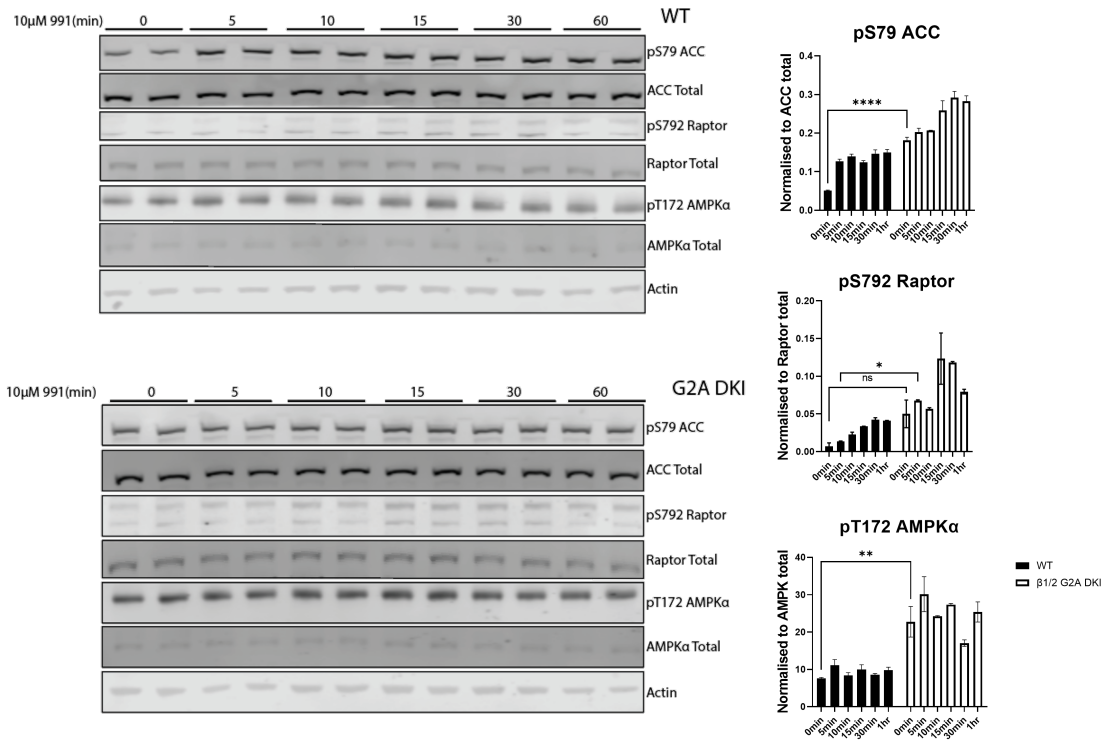

Figure A.5: **991 kinetics in MEFs** Immunoblots and respective quantification showing phosphorylation of AMPK substrates in WT or β1/2 G2A DKI MEFs in response to 10μM 991 for different time points (upto 60min). * P<0.1, ** P<0.01, **** P<0.0001 represents genotype differences measured by two-way ANOVA and Šídák's post-hoc test.

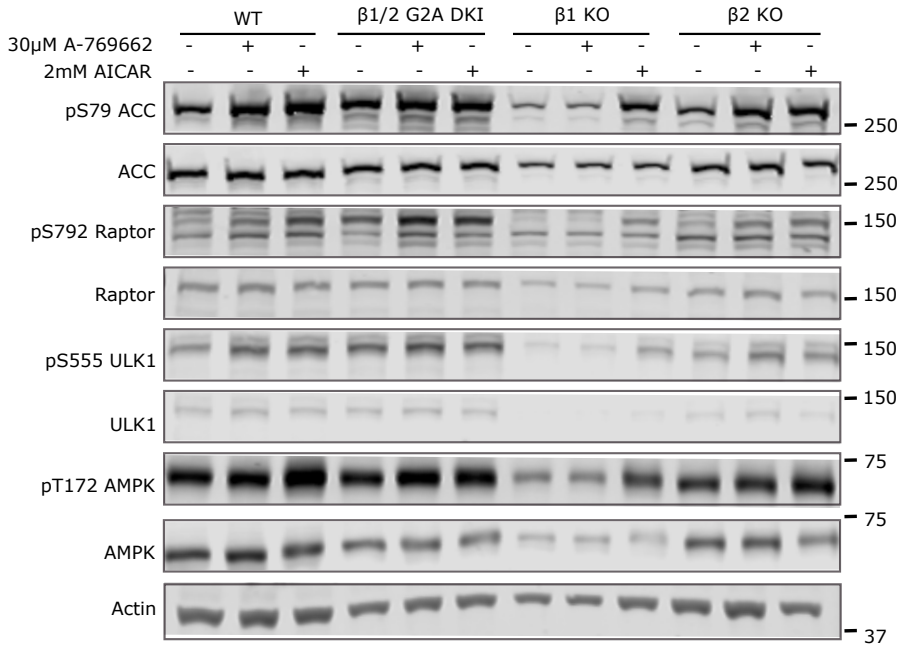

Figure A.6: **AMPK signalling in MEFs in response to A769662 and AICAR** Immunoblots showing phosphorylation of AMPK substrates in MEF cells in response to 30μM A769662 or 2mM AICAR for 30 minutes.

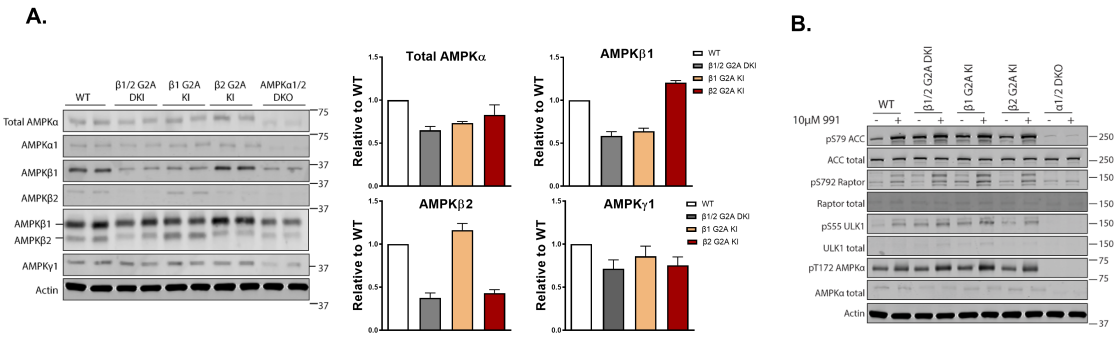

Figure A.7: **AMPK signalling in MEFs single G2A KI** (A) Immunoblots and respective quantification showing AMPK subunit/isoforms expression in MEFs (WT, β1/2 G2A DKI, β1 G2A KI, β2 G2A KI and α1/2 DKO). (B) Immunoblots showing phosphorylaton of AMPK substrates in respective MEFs.

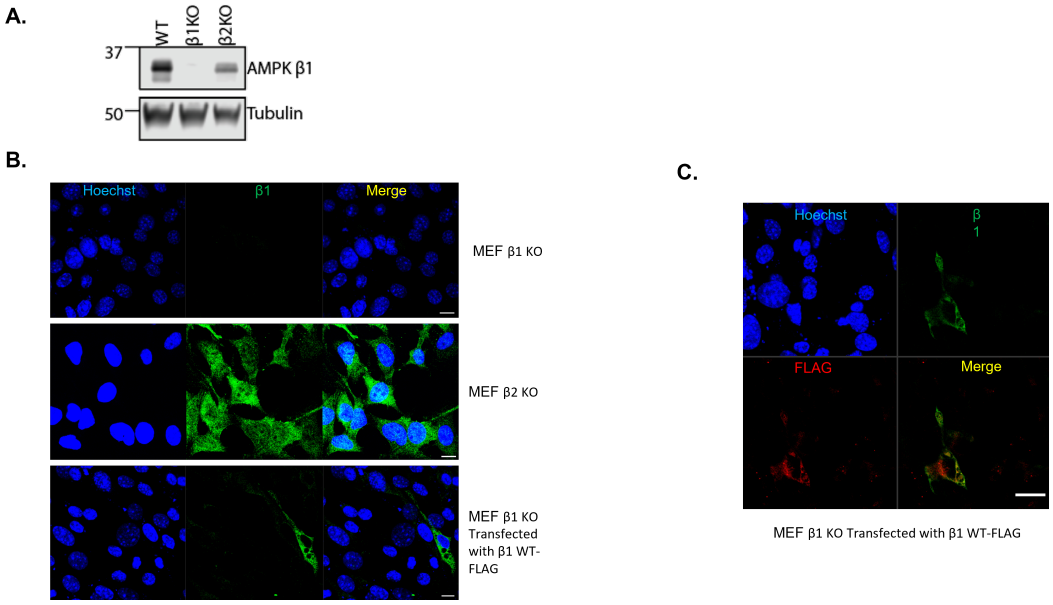

Figure A.8: **Validation of AMPKβ1-specific antibody** (A) Specificity of the β1 antibody was validated by immunoblot analysis in MEFs (β1 KO as control). (B) Immunofluorescence images of β1 KO and β2 KO MEFs or β1 KO MEFs transfected with a plasmid expressing β1 WT-FLAG and stained with β1-specific antibody (Green) or nuclear marker Hoechst (Blue). (C) Immunofluorescence images of β1 KO MEFs transfected with a plasmid expressing β1 WT-FLAG stained with β1-specific antibody (Green) and co-stained with FLAG antibody (Red) and nuclear marker Hoechst (Blue). Scale bar = 10μm.

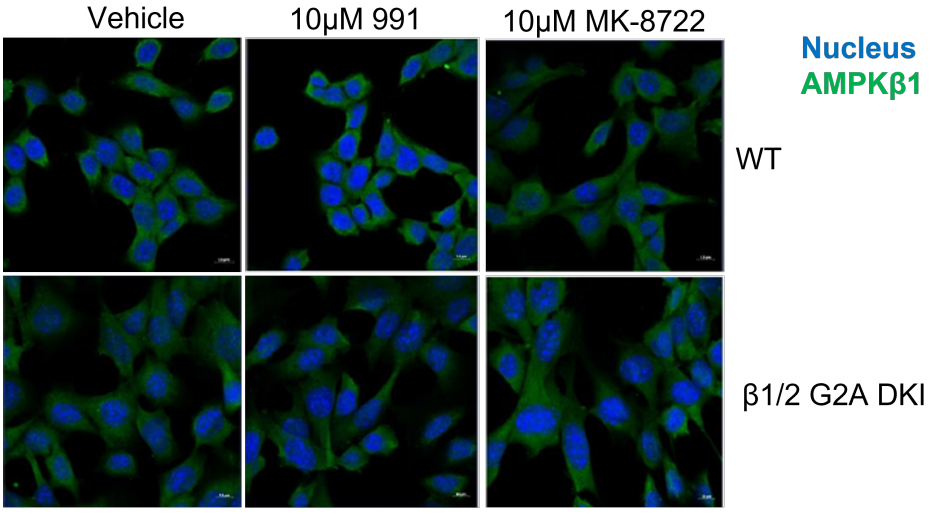

Figure A.9: **Localisation of β1 in MEFs** Immunofluorescence images of WT or β1/2 G2A DKI MEFs treated with vehicle (DMSO), 10μM 991 or 10μM MK-8722 and stained with β1-specific antibody (Green) or nuclear marker Hoechst (Blue). Scale bar = 10μm.

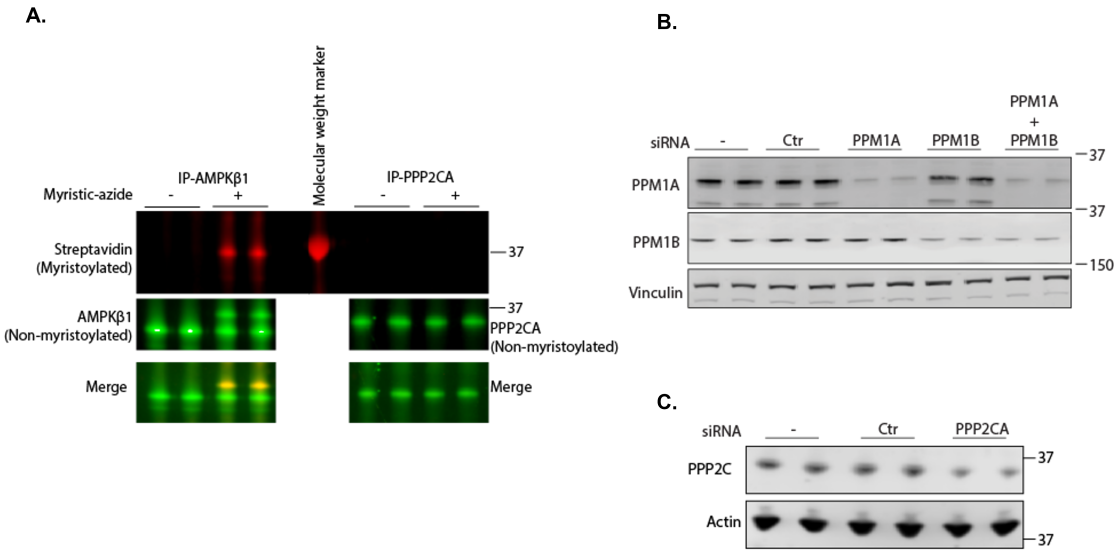

Figure A.10: **Validation of phosphatase antibodies** (A) Click chemistry showing myristoylation of β1 and absence of myrisotylation in a control phosphatase PPP2C as indicated by streptavidin blot (red channel). (B) WT MEFs were left untransfected or transfected with scrambled siRNA oligos (Ctr) or siRNA oligos targeting PPM1A or PPM1B or both PPM1A and PPM1B and subjetced to immunoblot analysis. (C) WT MEFs were left untransfected or transfected with scrambled siRNA oligos (Ctr) or siRNA oligos targeting PPP2C and subjected to immunoblot analysis.

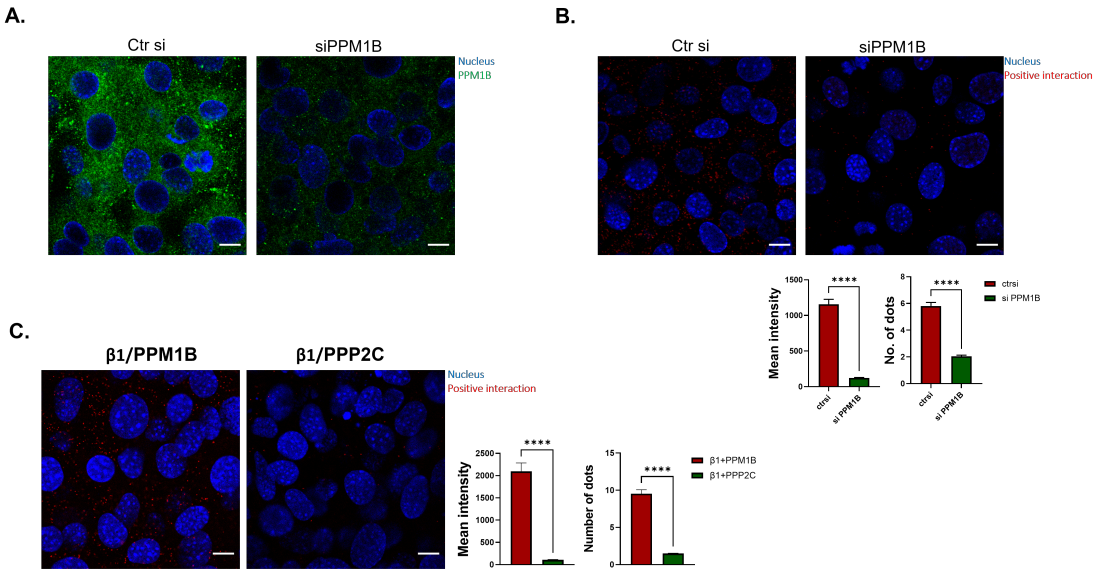

Figure A.11: **Proximity Ligation Assay** (A) Validation of PPM1B antibody in immunofluorescence using WT MEFs transfected with either scrambled siRNA oligos (Ctr si) or siRNA oligos targeting PPM1B and stained for PPM1B (Green) and nucleus (Blue). (B) Interaction/proximity of β1 and PPM1B was visualised using PLA in WT MEFs transfected with either scrambled siRNA oligos (Ctr si) or siRNA oligos targeting PPM1B. (C) Interaction/proximity of β1 and PPP2C was visualised using PLA in WT MEFs. Images are representative of two independent experiments. Signal was quantified as mean fluorescence intensity (relative to WT) or number of red dots per cell using ImageJ plugins. Scale bar = 10μm. ****P<0.0001 as determined by unpaired t-test. All data are mean ± s.e.m.

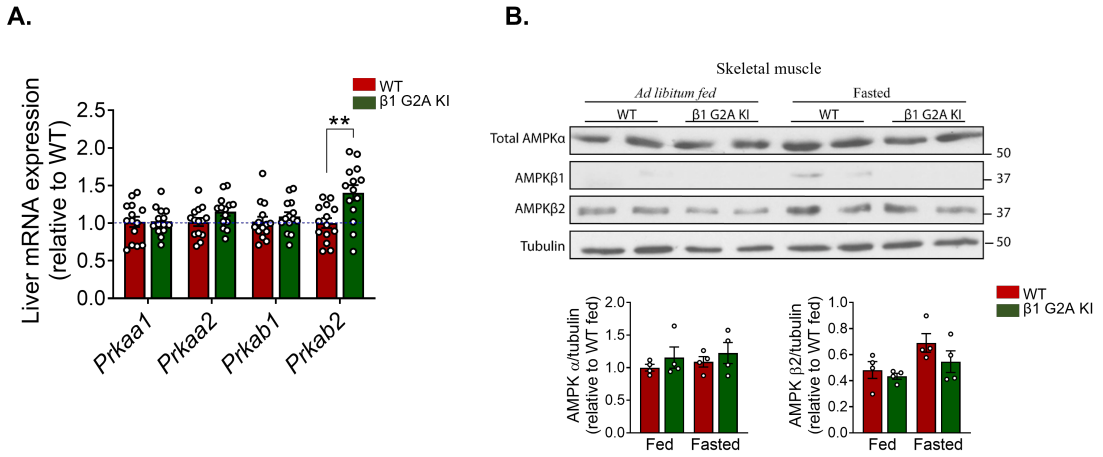

Figure A.12: **Characterisation of *in vivo* model** (A) mRNA expression analysis of AMPK α and β subunits in livers of *ad lbitum* fed β1 G2A and WT mice. (B) Tibialis anterior muscle was isolated from *ad libitum* fed or 16h fasted mice (male age-matched 20-24-week-old β1-G2A and WT) (n = 4-8) for immunoblot analysis and subsequent quantification. ** P<0.01 represents genotype differences measured by unpaired t-test.

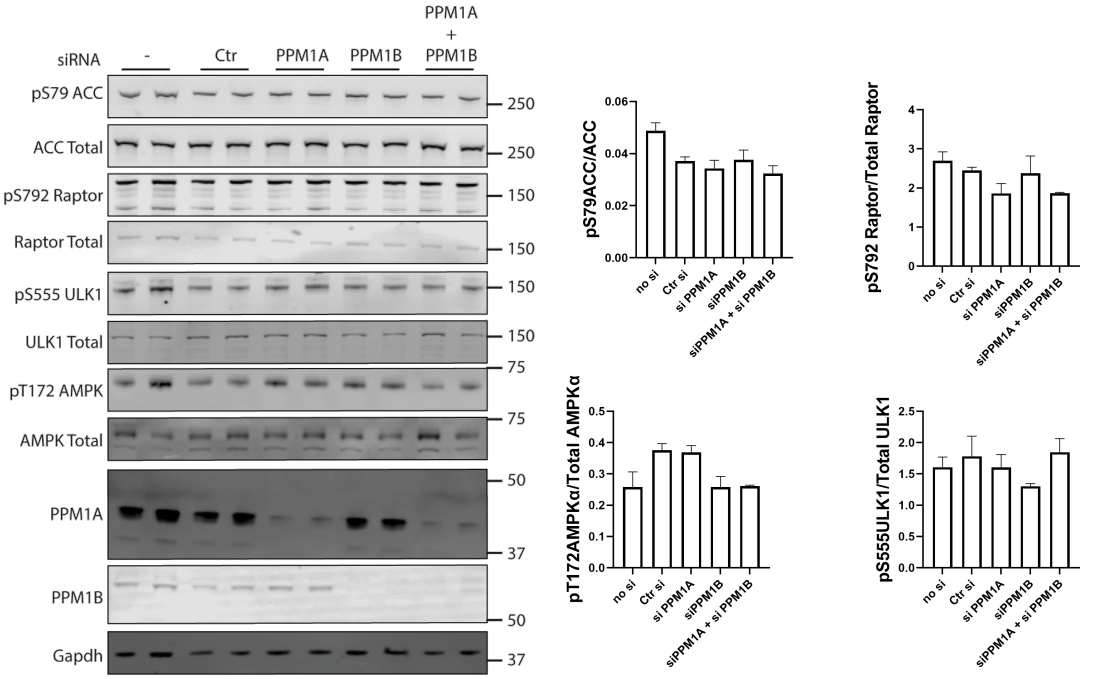

Figure A.13: **Effect of knockdown of phosphatases on AMPK signalling** WT MEFs were either left untransfeted or transfected with siRNA oligos as mentioned and subjected to immunoblot analysis and subsequent quantification. Results are representative of three independent experiments. All data are mean ± s.e.m.

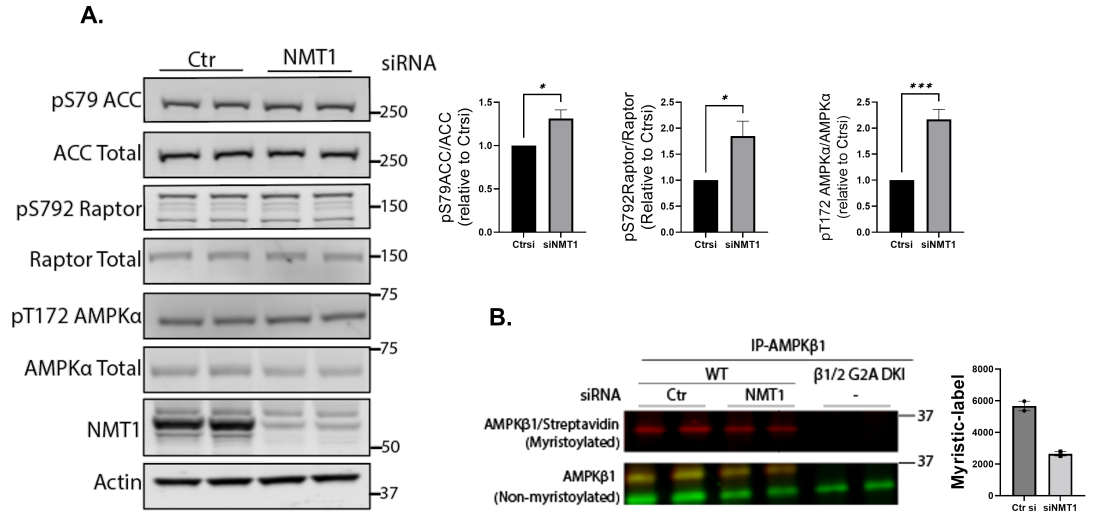

Figure A.14: **Effect of NMT1 knockdown on AMPK signalling** (A) WT MEFs were either left untransfeted or transfected with control siRNA oligos (Ctr) or targeting NMT1 and subjected to immunoblot analysis and subsequent quantification. Results are representative of three independent experiments. All data are mean ± s.e.m. (B) β1 myristoylation was asessed by click chemistry in WT MEFs after siRNA knockdown of NMT1. * P<0.1, *** P<0.001 represent genotype differences measured by unpaired t-test.

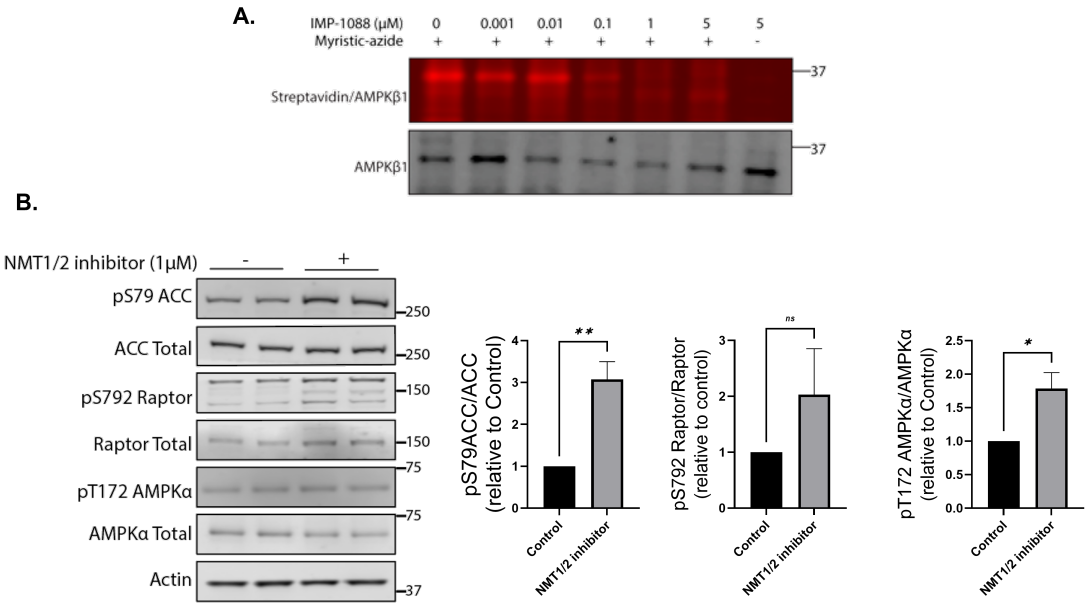

Figure A.15: **Effect of NMT1/2 chemical inhibition on AMPK signalling** (A) β1 myristoylation was asessed by click chemistry in WT MEFs after treatment with different doses of NMT1/2 inhibitor IMP-1088. (B) WT MEFs were either left untreated or treated with 1μM IMP-1088 for 16h and subjected to immunoblot analysis and subsequent quantification. Results are representative of three independent experiments. All data are mean ± s.e.m. * P<0.1, ** P<0.01 represent genotype differences measured by unpaired t-test.

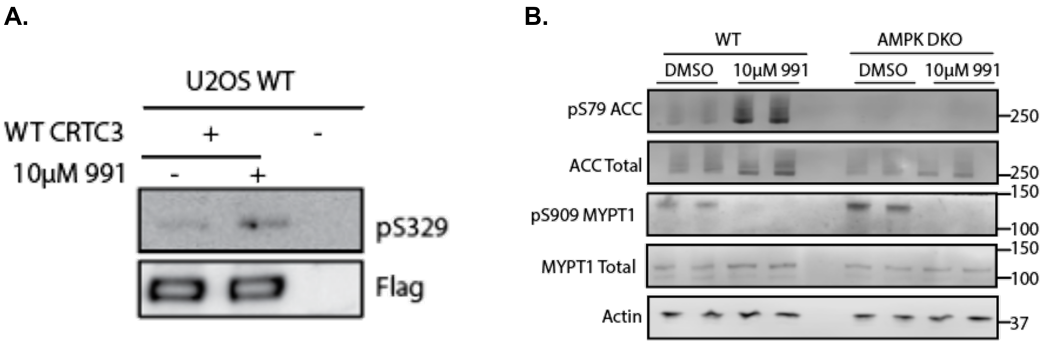

Figure A.16: **Investigating CRTC3 and MYPT1 as AMPK substrates** (A) U2OS WT cells transfected with FLAG-CRTC3 WT or left untransfected were treated with vehicle (-) or 991 (+) and subjected to immunoblot analysis. (B) MEFs treated with vehicle (DMSO) or 991 were subjected to immunoblot analysis.

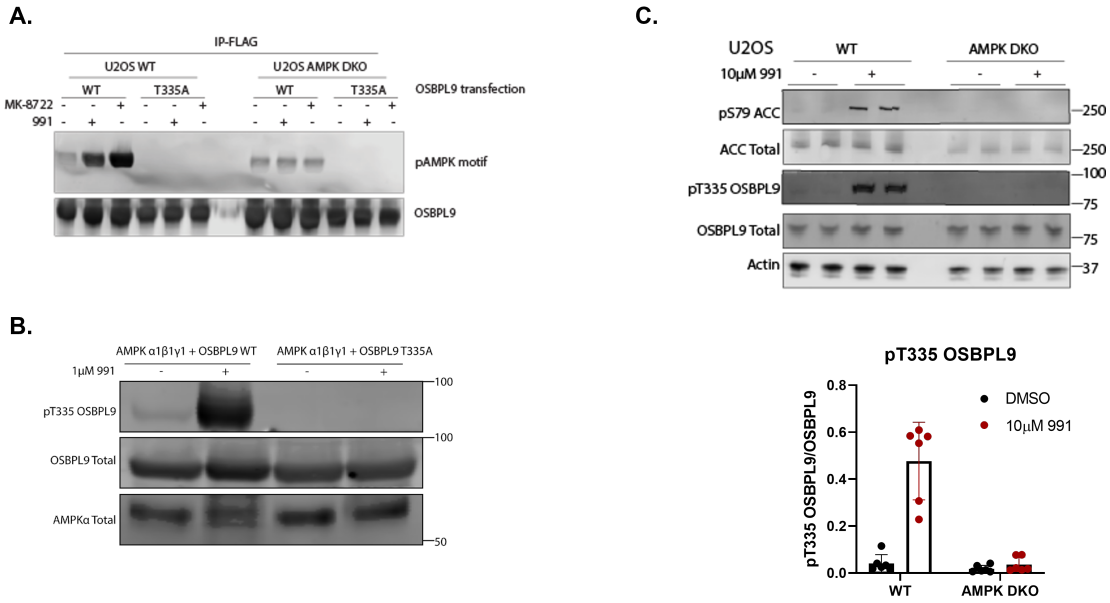

Figure A.17: **OSPBL9 is a novel AMPK substrate** (A) U2OS cells (WT or AMPK DKO) transiently expressing FLAG-tagged OSBPL9 WT or T335A were either left untreated or treated with AMPK activators MK-8722 or 991 (10μM for 30min), subjected to FLAG-immunoprecipitation and immunoblot analysis. (B) Kinase reaction using bacterially-expressed recombinant OSBPL9 (WT or T335A) and AMPK complex (α1β1γ1) pre-activated with 1μM 991 and assessment of phosphorylation of OSBPL9 Thr335 by immunoblot analysis. (C) Endogenous OSBPL9 phosphorylation (pThr335) in U2OS cells following treatment with vehicle (DMSO) or 10μM 991 was assessed by immunoblot analysis using phospho-specific antibody.

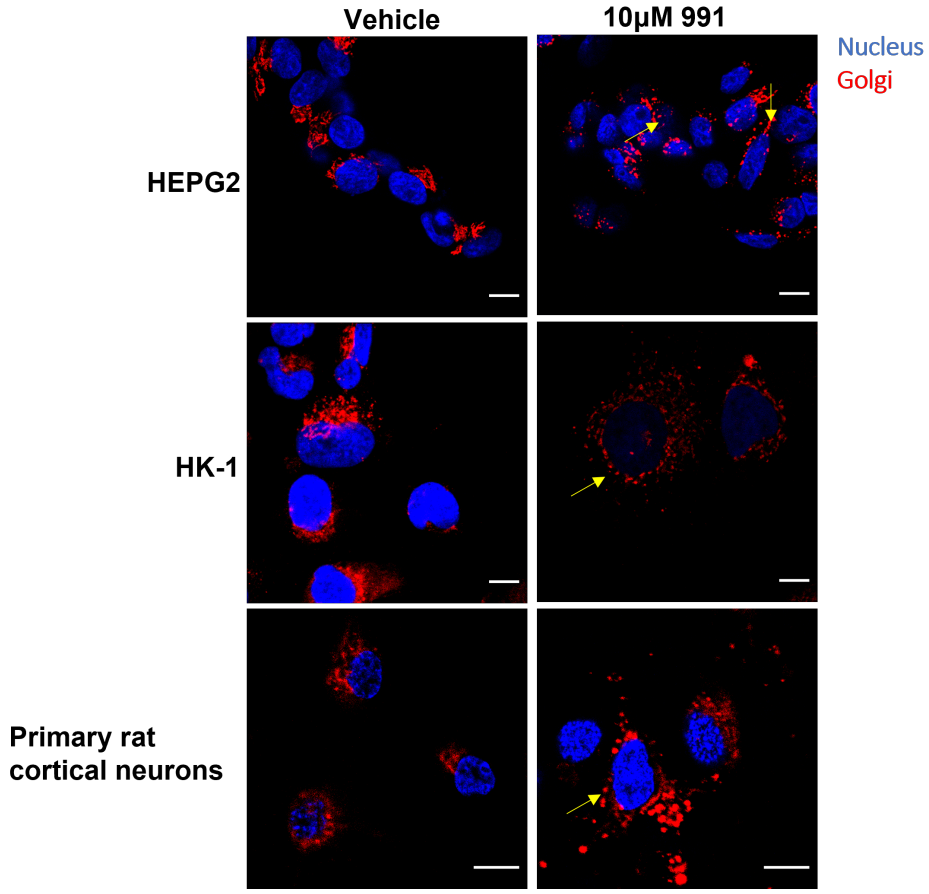

Figure A.18: **AMPK activation induces Golgi fragmentation in multiple cell types** Immunofluorescence images of HEPG2, Human Kidney (HK-1) cells and primary rat cortical neurons following treatment with vehicle (DMSO) or 10μM 991 for 30min and stained with Golgi marker Vicia Villosa (Red) and nuclear marker Hoechst (Blue). Scale bar = 10μm.

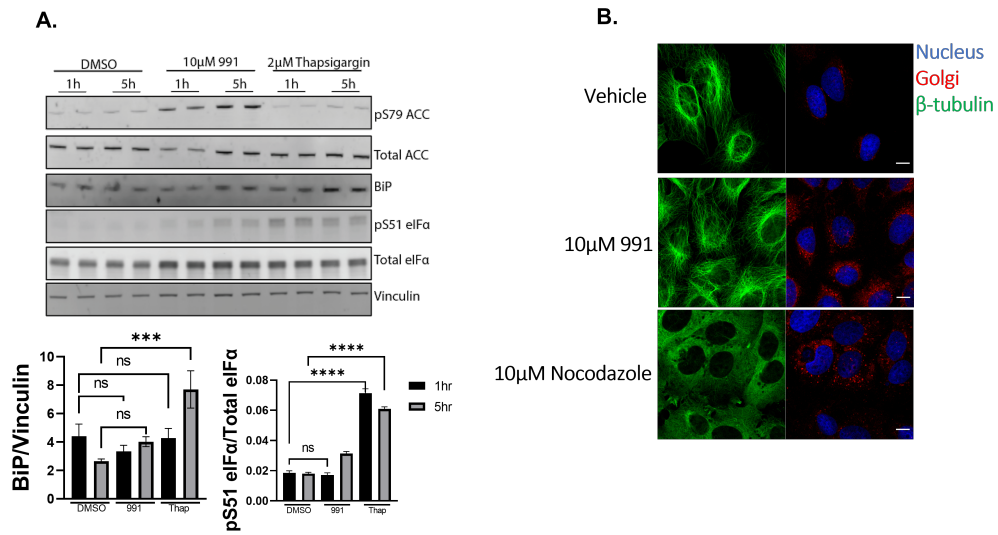

Figure A.19: **AMPK-induced Golgi fragmentation is not due to ER stress or microtubule disruption** (A) U2OS WT cells were treated with either vehicle (DMSO), 10μM 991 or 2μM Thapsigargin for 1h or 5h and subjected to immunoblot analysis and subsequent quantification of ER stress markers. All data are mean ± s.e.m. from two independent experiments. (B) Immunofluorescence images of U2OS WT cells treated with either vehicle (DMSO), 10μM 991 or 10μM Nocodazole for 30min and stained with Golgi marker (Red), β-tubulin (Green) and Hoechst (Blue). Scale bar = 10μm. Images are representative of three independent experiments. *** P<0.001, **** P<0.0001 represent treatment differences measured by ordinary one-way ANOVA.

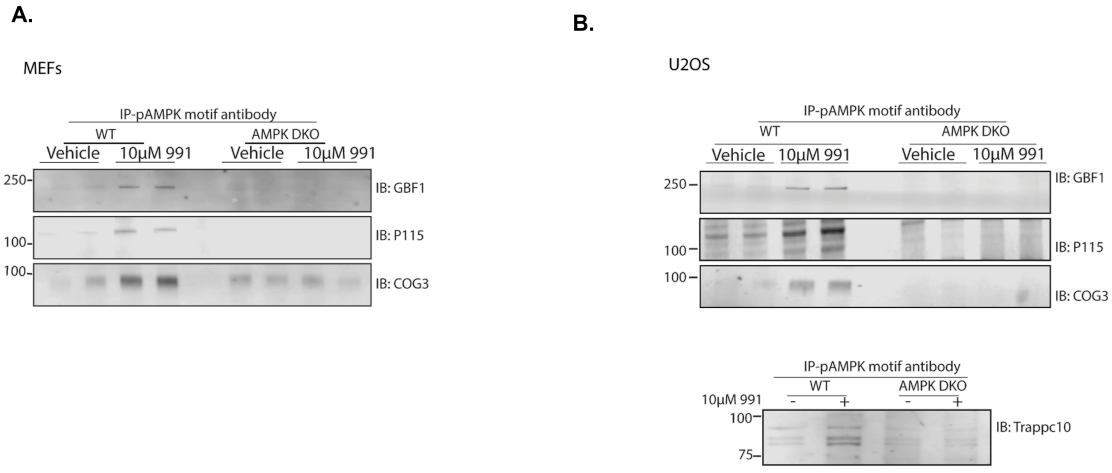

Figure A.20: **Biochemical Validation of AMPK substrates** WT or AMPK DKO (A) MEFs or (B) U2OS cells were treated with vehicle (DMSO) or 10μM 991 for 30min and lysates were immunoprecipitated using phospho-AMPK motif antibody and subjected to immunoblot analysis.

A.2 Appendix tables

Table A.1: Oxysterol-Binding protein and its isoforms

S.N.	ORP	Isoforms	Tissue expression	Characterised Localisation	Reported Functions
1.	OSBP		Ubiquitous	Golgi-ER	Catalyses sterol and PI(4)P transfer between ER-Golgi
2.	ORP1	ORP1L	Brain, Lung	ER-Late Endosome	Cholesterol efflux and endosomal positioning
		ORP1S	Heart, Skeletal muscle, macrophages	Nucleus	Sterol transfer from PM to lipid droplet
3.	ORP2		Ubiquitous	ER-Lipid droplets	Endocytosis, PM-ER sterol transport
4.	ORP3		Kidney, Thymus, macrophages	Not well-defined	Actin dynamics
5.	ORP4	ORP4L	Brain, heart, skeletal muscle	Vimentin	Ca2+ homeostasis, silencing causes apoptosis
		ORP4M		Vimentin	
		ORP4S	Brain, heart	Vimentin	
6.	ORP5		Heart, brain, liver, lung, kidney	ER-Mitochondria	PS transport to mitochondria
7.	ORP6		Brain, skeletal muscle	ER-Late Endosome	Cholesterol efflux from endosomes
8.	ORP7		Gastrointestinal tract	Not well-defined	Promotes proteosomal degradation of Golgi snare GS28
9.	ORP8		Macrophages, spleen, kidney, liver	ER-Mitochondria	PS transport to mitochondria
10.	ORP9	ORP9L	Brain, heart, kidney, liver	ER-Golgi	Golgi organisation and PI(4)P trafficking
		ORP9S	Liver	ER	Growth inhibition (dominant negative)
11.	ORP10	ORP10L		Microtubules	Negative regulator of hepatic lipid biosynthesis and apoB-100 secretion
		ORP10S		Nucleus	
12.	ORP11		Ovary, testis, brain, liver, kidney	Golgi-Early Endosome	Cellular triglyceride storage

Table A.2: 991-phosphorylated proteins from the phosphoproteomics screen involved in cytoskeleton/microtubule organisation

S.N.	Protein	AMPK motif present?	Previously identified?
1	specc1l - CytospinA	Yes	Yes
2	Dst - Dystonin	Yes	Yes
3	Gas2l - GAS2 like protein 1	No	Yes
4	Hsbp1 - Heat shock protein beta1	No	Yes
5	kif3a - Kinesin like protein KIF3A	Yes	Yes
6	map7d1 - MAP7 domain containing protein 1	Yes	Yes
7	map4 - Microtubule associated protein 4	Yes	Yes
8	map9 - microtubule associated protein 9	Yes	No
9	mast4 - Microtubule associated serine/threonine	Yes	Yes
10	Palld - palladin	Yes	Yes
11	Arhgap28 - Rho GTPase activating protein 28	Yes	No
12	Slain2 - SLAIN motif containing protien 2	Yes	Yes
13	Svil - Supervillin	Yes	Yes

Table A.3: 991-phosphorylated proteins from the phosphoproteomics screen involved in ER/Golgi regulation

S.N.	Protein	AMPK motif present?	Previously identified?
1	C2cd2l - Phospholipid transfer protein C2CD2L	Yes	Yes
2	Spag9 - C Jun amino terminal kinase interacting protein 4	Yes	Yes
3	COG3 - Conserved oligomeric Golgi complex subunit 3	Yes	No
4	cdk16 - Cyclin-dependent kinase 16	No	Yes
5	Dync1i2 - ytoplasmic dynein 1 intermediate chain 2	No	Yes
6	Dennd4c - DENN domain-containing protein 4C	Yes	Yes
7	Rnf139 - E3 ubiquitin-protein ligase RNF139	No	No
8	Gapvd1 - GTPase activating protein and VPS9 domain containing protein 1	Yes	Yes
9	Itsn2 - Intersectin 2	Yes	Yes
10	Pgrmc1 - Membrane-associated progesterone receptor component 1	No	Yes
11	OSBPL8 - Oxysterol-binding protein-related protein 8	No	No
12	Pi4kb - hosphatidylinositol 4-kinase beta	Yes	Yes
13	Dopey1 - Protein Dopey 1	Yes	No
14	Rer1 - Protein RER1	No	No
15	Rab11fip1 - Rab11 family-interacting protein 1	Yes	Yes
16	Rabsn - Rabenosyn	Yes	No
17	Ralbp1 - RalBP1-associated Eps domain- containing protein 2	Yes	Yes
18	SH3BP4 - SH3 domain-binding protein 4	Yes	Yes
19	Snx17 - Sorting nexin-17	Yes	Yes
20	Tjap1 - Tight junction-associated protein 1	No	Yes
21	Trappc10 - Trafficking protein particle complex subunit 10	Yes	No
22	Trappc12 - Trafficking protein particle complex subunit 12	No	Yes
23	Tmcc1 - Transmembrane and coiled-coil domains protein 1	Yes	Yes
24	OSBPL9 - Oxysterol-binding protein-related protein 9	Yes	Yes

Table A.4: Complete list of 991-phosphorylated proteins in WT MEFs

S.N.	Site	score	-5	-4	-3	-2	-1	0	+1	+2	+3	+4	+5
1	PPP1R12A;S909;	0.99	L	G	R	S	A	S	Y	S	Y	L	E
2	MFF;S146;	0.93	L	V	R	N	D	S	I	P	V	L	R
4	NUMA1;S1835;	0.86	L	R	A	T	S	S	T	Q	S	L	A
5	TBC1D1;S231;	0.86	M	R	K	S	F	S	Q	P	G	L	R
6	ACACA;S79;	0.85	M	R	S	S	M	S	G	L	H	L	V
7	RPTOR;S722;	0.84	L	R	S	V	S	S	Y	G	N	I	R
8	CRTC3;S329;	0.82	L	Q	S	S	R	S	N	P	S	I	Q
9	OSBPL9;S216;	0.80	L	T	H	S	S	S	G	N	S	L	K
10	TNS1;S623;	0.80	L	F	R	S	Q	S	F	P	D	V	E
11	DCUN1D4;S11;	0.79	K	R	R	P	A	S	G	D	D	L	S
12	PHACTR4;S430;	0.79	K	R	R	P	A	S	G	D	D	L	S
13	DNMT1;S22;	0.79	L	G	R	T	R	S	L	P	I	T	I
14	TAGLN2;S163;	0.78	P	R	R	S	K	S	D	S	D	T	L
15	CRTC2;S612;	0.78	N	P	R	N	F	S	D	N	Q	L	Q
16	ZNF609;S1057;	0.78	C	S	R	H	G	S	G	P	N	I	I
17	SMCR8;S488;	0.78	L	T	K	A	P	S	L	T	D	L	V
18	MID1;S92;	0.78	L	S	K	S	D	S	Q	A	S	L	T
19	SEC16A;S1377;	0.77	Q	K	A	S	V	S	G	P	N	S	P
20	LNP;S411;	0.77	L	R	S	T	H	S	L	P	S	R	R
21	WNK1;S2118;	0.77	V	L	R	A	D	S	V	P	N	L	E
22	ARHGAP35;S770;	0.77	L	N	L	V	S	S	T	A	S	I	K
23	RIF1;S387;	0.76	S	R	G	S	A	S	P	G	L	S	P
24	MAP4;S901;	0.76	L	A	T	T	V	S	A	P	D	L	K
25	TRIM28;S473;	0.76	M	K	R	S	R	S	G	E	G	E	V
26	SREK1IP1;S97;	0.75	K	R	S	Y	S	S	A	T	E	E	D
27	CRTC2;S612;	0.74	C	S	R	H	G	S	G	P	N	I	I
28	GM8797;S57;	0.74	D	G	R	T	L	S	D	Y	N	I	Q
29	SRRM1;S760;	0.74	R	S	V	S	G	S	P	E	P	A	A
30	SCRIB;S1457;	0.74	R	L	R	M	Q	S	P	E	L	P	A
31	MID1;S96;	0.74	V	S	G	P	N	S	P	S	E	T	R
32	MYADM;S22;	0.74	S	T	T	V	G	S	A	R	A	L	T
33	RBBP6;S1665;	0.74	S	S	P	S	V	S	P	S	R	S	H
34	IQCE;S65;	0.74	L	V	R	S	P	S	N	I	S	V	Q
35	DLG5;S1231;	0.73	S	Q	G	S	N	S	L	P	S	S	A
36	SLC4A7;S263;	0.72	L	A	S	P	Q	S	A	P	G	N	L
37	DOCK7;S30;	0.72	G	Q	Y	S	G	S	P	Q	L	L	K
38	DOPEY1;S1261;	0.72	R	Q	R	S	H	S	S	I	Q	F	S
39	DCAF10;S96;	0.72	S	Q	A	K	L	S	P	S	S	S	P
40	NUMA1;S1838;	0.71	T	S	S	T	Q	S	L	A	R	L	G

41	ZFML;S1571;	0.70	L	K	I	S	P	**S**	P	E	L	N	L
42	COG3;S533;	0.70	L	R	K	S	G	**S**	T	D	S	L	N
43	PGRMC2;S98;	0.70	K	K	R	D	F	**S**	L	E	Q	L	R
44	SLC12A2;S75;	0.69	L	G	P	T	P	**S**	Q	S	R	F	Q
45	AHNAK;S4648;	0.69	G	A	F	D	G	**S**	V	P	K	I	E
46	SNX17;S437;	0.69	L	S	S	K	L	**S**	A	V	S	L	R
47	HS1BP3;S3;	0.69	_	_	_	M	Q	**S**	P	A	V	L	R
48	STIM2;S299;	0.68	L	T	E	T	K	**S**	M	I	F	S	P
49	ULK1;S622;	0.67	P	P	I	L	G	**S**	P	T	K	A	G
50	CASC3;S115;	0.67	K	V	E	L	K	**S**	E	A	N	D	A
51	MLLT4;S1780;	0.66	R	Q	R	L	F	**S**	Q	G	Q	D	V
52	KIF5B;S945;	0.66	V	R	G	G	G	**S**	F	V	Q	N	N
53	LARP4;S395;	0.66	G	D	G	P	L	**S**	R	S	S	S	R
54	MCPH1;S383;	0.66	F	K	S	D	Q	**S**	P	P	S	T	I
55	SIN3A;S941;	0.66	R	D	K	S	D	**S**	P	A	I	Q	L
56	FSD1;S296;	0.65	K	G	R	T	A	**S**	P	V	N	S	P
57	TANC1;S455;	0.64	G	T	P	L	L	**S**	P	S	S	S	T
58	URB1;S17;	0.64	P	S	S	A	A	**S**	P	A	G	T	V
59	TCOF1;S593;	0.64	S	A	S	L	S	**S**	P	A	L	A	K
60	TRP53BP2;S485;	0.64	L	R	K	N	Q	**S**	S	E	D	I	L
61	INCENP;S211;	0.64	S	V	T	V	N	**S**	L	K	A	T	P
62	MAST4;S2325;	0.64	M	I	K	S	D	**S**	L	P	S	F	R
63	BMP2K;S1012;	0.63	R	R	D	S	Q	**S**	S	N	E	F	L
64	ULK1;S614;	0.63	D	F	L	Q	R	**S**	P	L	P	P	I
65	CSNK1E;S405;	0.63	S	R	L	A	A	**S**	Q	T	S	V	P
66	COBLL1;S352;	0.62	M	V	R	T	G	**S**	L	Q	L	S	S
67	PNPLA2;S374;	0.62	V	R	N	N	L	**S**	L	G	D	A	L
68	RIPK1;S254;	0.62	E	Y	P	D	Q	**S**	P	V	L	Q	R
69	EPB41L2;S630;	0.62	L	K	H	Q	A	**S**	I	S	E	L	K
70	SNX17;S440;	0.62	K	L	S	A	V	**S**	L	R	G	I	G
71	SMCR8;S497;	0.62	L	T	V	P	L	**S**	P	H	V	V	R
72	NOP14;S96;	0.62	Y	N	S	N	I	**S**	P	E	E	K	M
73	SLC4A8;S210;	0.62	T	V	S	P	Q	**S**	A	T	N	L	E
74	SRSF4;S297;	0.61	P	S	R	H	D	**S**	K	S	R	S	R
75	SLC9A1;S606;	0.61	I	P	S	A	V	**S**	T	V	S	M	Q
76	G3BP2;T227;	0.60	E	E	K	S	A	**T**	P	P	P	A	E
77	MFF;S124;	0.60	L	V	R	N	D	**S**	I	V	T	P	S
78	SLC9A1;S603;	0.60	M	G	K	I	P	**S**	A	V	S	T	V
79	AGPAT9;S68;	0.60	L	K	N	S	A	**S**	V	G	I	I	Q
80	SKA3;S324;	0.60	S	K	P	N	S	**S**	S	T	D	L	E
81	ZAK;S649;	0.60	L	S	R	N	F	**S**	S	L	N	L	S
82	MAGOHB;S62;	0.59	T	S	K	I	G	**S**	L	I	D	V	N
83	TAF6;S653;	0.59	Q	E	A	G	D	**S**	P	P	P	A	P
84	ZFYVE19;S280;	0.59	Y	H	L	P	D	**S**	D	E	D	E	E

85	CNKSR3;S142;	0.59	R	K	G	S	E	**S**	P	N	S	F	L
86	TAX1BP3;S61;	0.59	Y	V	T	R	V	**S**	E	G	G	P	A
87	SLC9A1;S609;	0.59	A	V	S	T	V	**S**	M	Q	N	I	H
88	CD2AP;S580;	0.58	D	G	K	R	N	**S**	V	D	E	L	R
89	CIC;S2284;	0.58	Q	S	L	A	T	**S**	P	R	A	I	L
90	SLC4A7;S238;	0.58	I	P	L	V	R	**S**	F	A	D	I	G
91	SH3BP4;S278;	0.57	P	E	Q	F	Q	**S**	R	E	D	F	R
92	FARP2;S389;	0.57	P	K	Q	S	V	**S**	F	T	D	G	L
93	SLC9A1;S609;	0.57	A	V	S	T	V	**S**	M	Q	N	I	H
94	CSNK1E;S408;	0.57	A	A	S	Q	T	**S**	V	P	F	D	H
95	CDK17;S59;	0.57	M	P	R	N	G	**S**	R	L	D	I	V
96	IRS2;T517;	0.56	S	H	R	S	N	**T**	P	E	S	I	A
97	BCL9L;T933;	0.56	H	L	K	S	P	**T**	L	S	Q	V	H
98	RPRD2;S309;	0.56	E	D	M	E	L	**S**	D	V	E	D	D
99	SRRM1;S758;	0.55	S	S	R	S	V	**S**	G	S	P	E	P
100	G3BP2;S225;	0.55	E	L	E	E	K	**S**	A	T	P	P	P
101	WDR4;S440;	0.55	S	P	F	P	G	**S**	P	E	Q	T	K
102	COG3;S536;	0.55	S	G	S	T	D	**S**	L	N	P	R	P
103	SRRM2;S356;	0.55	S	R	R	E	I	**S**	S	S	P	T	S
104	DPYSL2;S542;	0.54	S	G	F	S	L	**S**	G	A	Q	I	D
105	MAP1B;S1422;	0.54	G	R	R	S	E	**S**	P	F	E	G	K
106	STIM1;S512;	0.54	Q	L	G	L	G	**S**	Q	R	L	V	E
107	BRPF1;T141;	0.54	K	E	N	T	E	**T**	P	A	A	T	P
108	DMRTA1;S468;	0.54	M	I	R	E	P	**S**	H	L	P	S	K
109	CCDC88A;S1636;	0.54	K	S	L	S	V	**S**	S	D	F	L	G
110	ARHGAP23;S166;	0.54	P	G	A	L	V	**S**	P	R	L	E	R
111	SRSF4;S291;	0.54	K	A	K	S	H	**S**	P	S	R	H	D
112	SLC4A4;S248;	0.54	N	L	T	S	S	**S**	L	N	D	I	S
113	SLC9A1;S606;	0.53	I	P	S	A	V	**S**	T	V	S	M	Q
114	NES;S839;	0.52	K	V	S	Q	V	**S**	L	E	S	L	E
115	STAU1;S307;	0.52	T	F	F	E	P	**S**	P	G	D	E	N
116	ERCC5;S384;	0.52	D	A	G	S	I	**S**	P	R	T	C	A
117	RANBP2;S1101;	0.52	T	F	S	F	G	**S**	K	N	T	L	T
118	NME1;S120;	0.52	N	I	I	H	G	**S**	D	S	V	K	S
119	MAP1B;S1420;	0.51	V	L	G	R	R	**S**	E	S	P	F	E
120	TPR;S2149;	0.51	A	E	A	I	H	**S**	P	Q	V	A	G
121	CAMSAP2;T440;	0.51	S	A	Q	S	S	**T**	P	N	R	G	I
122	CLSPN;S1265;	0.51	V	F	H	T	L	**S**	P	T	K	A	E
123	MARCKS;T79;	0.51	S	G	S	A	A	**T**	P	A	A	A	E
124	OSBPL9;S219;	0.51	S	S	S	G	N	**S**	L	K	R	P	D
125	SRRM2;S679;	0.51	L	R	R	S	L	**S**	G	S	S	P	C
126	DENND5A;T1055;	0.50	E	R	P	C	R	**T**	P	P	L	Q	Q

127	BCL9L;T933;	0.50	H	L	K	S	P	**T**	L	S	Q	V	H
128	KIDINS220;S1583;	0.50	L	N	R	T	P	**S**	T	V	T	L	N
129	SLC39A10;S593;	0.50	E	A	Q	Q	E	**S**	P	P	K	N	Y
130	WDR24;S594;	0.50	Q	D	K	A	D	**S**	P	H	V	S	G
131	NA;S44;	0.50	L	K	G	S	R	**S**	S	E	L	L	G
132	BCL9L;S21;	0.49	R	E	A	P	G	**S**	P	P	L	S	P
133	HSP90AA1;S231;	0.49	R	D	K	E	V	**S**	D	D	E	A	E
134	TANC1;T451;	0.49	Q	D	L	P	G	**T**	P	L	L	S	P
135	SLC4A4;T245;	0.49	T	H	R	N	L	**T**	S	S	S	L	N
136	WDR24;S598;	0.49	D	S	P	H	V	**S**	G	N	E	A	D
137	NFIB;S294;	0.49	Y	P	S	P	N	**S**	P	A	A	G	S
138	SRRM1;S756;	0.49	V	S	S	S	R	**S**	V	S	G	S	P
139	LARP4B;S655;	0.48	N	T	P	P	K	**S**	P	Q	_	_	_
140	ARID1A;S697;	0.48	G	I	R	G	P	**S**	P	S	P	V	G
141	SRRM1;S760;	0.48	R	S	V	S	G	**S**	P	E	P	A	A
142	FMNL3;T95;	0.48	L	D	P	N	V	**T**	R	K	K	F	R
143	GUCY1B2;S731;	0.48	D	G	K	E	A	**S**	T	P	R	N	Q
144	PKP2;S188;	0.48	P	R	Y	A	R	**S**	E	I	L	G	L
145	NFIB;S264;	0.47	Q	R	S	L	S	**S**	P	P	S	S	K
146	SNX7;S8;	0.47	G	E	R	L	A	**S**	G	S	S	E	L
147	ZNF768;S36;	0.47	P	A	G	N	T	**S**	E	N	E	E	G
148	SRRM1;S878;	0.47	R	K	E	T	E	**S**	E	A	E	D	D
149	FKBP1A;S9;	0.46	Q	V	E	T	I	**S**	P	G	D	G	R
150	AHNAK;T3094;	0.46	G	S	K	V	Q	**T**	P	E	V	D	V
151	GSE1;S826;	0.45	M	L	R	E	R	**S**	P	S	P	P	A
152	BRPF1;T145;	0.45	E	T	P	A	A	**T**	P	K	S	G	K
153	GSE1;S828;	0.45	R	E	R	S	P	**S**	P	P	A	V	Q
154	PPFIA1;S238;	0.45	T	N	G	K	R	**S**	S	D	G	S	L
155	UHRF1BP1L;S952;	0.44	L	F	K	S	A	**S**	D	T	N	L	Q
156	TNC;S1485;	0.44	E	P	Q	E	I	**S**	L	P	S	P	E
157	DENND4C;S987;	0.44	I	V	K	V	P	**S**	G	L	F	D	T
158	CARHSP1;S31;	0.43	R	T	R	D	R	**S**	P	S	P	L	R
159	ARHGDIA;S47;	0.42	D	K	D	D	E	**S**	L	R	K	Y	K
160	PHIP;S659;	0.42	Q	D	L	R	R	**S**	G	E	A	G	V
161	SIPA1L1;S1544;	0.41	F	H	A	L	S	**S**	P	Q	S	P	F
162	CDC20;T59;	0.41	R	T	P	G	R	**T**	P	G	K	S	S
163	DDX59;S150;	0.41	S	L	R	P	S	**S**	P	Q	R	V	A
164	ABI1;S183;	0.40	T	Q	K	P	P	**S**	P	P	V	S	G
165	ELMSAN1;S988;	0.40	P	N	A	P	G	**S**	A	G	I	Q	T
166	LMOD1;S507;	0.40	G	S	P	K	P	**S**	P	Q	P	S	P
167	CDC20;T55;	0.40	H	S	A	G	R	**T**	P	G	R	T	P
168	PDZD8;S960;	0.39	D	L	V	E	P	**S**	P	K	H	T	P

169	CALD1;S490;	0.39	E	W	L	T	K	**S**	P	D	G	N	K
170	NPM1;T198;	0.38	K	S	V	R	D	**T**	P	A	K	N	A
171	POLA2;T130;	0.38	S	S	T	P	E	**T**	P	L	T	K	R
172	HIST1H1B;S18;	0.37	A	P	V	E	K	**S**	P	A	K	K	K
173	SRRM2;S677;	0.37	K	S	L	R	R	**S**	L	S	G	S	S
174	CHAF1B;S417;	0.37	T	H	Q	G	S	**S**	P	G	S	R	S
175	TOM1;S486;	0.35	L	P	N	L	A	**S**	P	S	A	E	G
176	DTL;S675;	0.34	K	A	E	N	S	**S**	P	R	S	P	S
177	DTL;S678;	0.34	N	S	S	P	R	**S**	P	S	S	Q	T
178	LMOD1;S511;	0.33	P	S	P	Q	P	**S**	P	K	P	A	P
179	SRRM2;S1281;	0.33	S	R	E	R	S	**S**	S	A	S	P	E
180	FOXM1;S329;	0.33	P	L	E	P	G	**S**	P	Q	S	P	E
181	SPIRE1;S267;	0.33	F	L	P	I	S	**S**	T	P	Q	P	E
182	CAST;S121;	0.32	A	S	P	V	Q	**S**	T	P	S	K	P
183	MSH6;S14;	0.32	S	F	F	P	K	**S**	P	A	L	G	D
184	NOL8;S888;	0.32	S	R	F	L	E	**S**	D	S	E	D	E
185	EZH2;T377;	0.32	N	S	R	C	Q	**T**	P	I	K	M	K
186	SRRM2;S1284;	0.32	R	S	S	S	A	**S**	P	E	L	K	D
187	AHNAK;S5059;	0.32	E	G	P	H	L	**S**	L	K	G	P	G
188	XRN2;S499;	0.32	R	K	A	E	D	**S**	D	S	E	P	E
189	SETD1A;S481;	0.31	A	S	P	A	R	**S**	G	S	P	A	P
190	MATR3;T740;	0.30	K	N	E	E	N	**T**	E	P	G	A	E
191	OSBP;S380;	0.30	T	G	S	N	I	**S**	G	A	S	S	D
192	RNF139;T667;	0.29	E	F	N	D	D	**T**	D	_	_	_	_
193	SRRM2;S682;	0.28	S	L	S	G	S	**S**	P	C	P	K	Q
194	CMTR1;S50;	0.28	S	A	T	S	L	**S**	G	S	D	S	E
195	ATRX;S626;	0.28	P	R	E	E	I	**S**	D	H	E	N	N
196	COBLL1;T272;	0.28	A	S	A	P	A	**T**	P	L	V	S	K
197	PDLIM7;T251;	0.27	H	S	Q	P	A	**T**	P	T	P	L	Q
198	CBX3;S93;	0.27	G	T	K	R	K	**S**	L	S	D	S	E
199	FRS2;T227;	0.27	N	A	E	S	N	**T**	P	K	E	E	P
200	IWS1;S306;	0.26	R	K	G	L	H	**S**	S	D	S	E	E
201	SLC9A1;S697;	0.26	A	H	K	L	D	**S**	P	T	L	S	R
202	SAFB;S626;	0.26	K	R	S	V	V	**S**	F	D	K	V	K
203	LMOD1;S503;	0.26	A	L	A	K	G	**S**	P	K	P	S	P
204	SAFB;S623;	0.26	S	R	E	K	R	**S**	V	V	S	F	D
205	MARCKSL1;S22;	0.25	E	A	A	G	A	**S**	P	A	K	A	N
206	RPLP2;S105;	0.25	E	E	S	E	E	**S**	D	D	D	M	G
207	NUFIP2;T88;	0.24	Q	Q	H	Q	E	**T**	P	K	K	K	T
208	TOX4;T176;	0.23	D	R	L	S	T	**T**	P	S	P	T	N
209	TOM1;S496;	0.23	G	P	P	R	P	**S**	P	G	T	A	P
210	ULK1;S718;	0.23	S	G	S	T	D	**S**	L	Q	E	K	P
211	ATRX;S644;	0.19	S	D	L	R	R	**S**	P	R	V	K	T
212	MARCKSL1;T14;	0.17	P	R	G	D	V	**T**	A	E	E	A	A

A.3 ImageJ macro for quantification

A.3.1 Quantification of PLA signal or number of Golgi particles per cell

Macro to calculate PLA spots/intensity and Golgi particles per cell

```
#@ImagePlus imp
import ij.*;
import ij.process.*;
import ij.gui.*;
import java.awt.*;
import ij.plugin.*;
import ij.plugin.frame.RoiManager
import ij.measure.ResultsTable

nuc_ch = 1;
spot_ch = 2;
IJ.run("Set Measurements...", "area mean shape display redirect=None decimal=3");

def rt = ResultsTable.getResultsTable()
if ( rt == null) rt = new ResultsTable()

RoiManager rm = RoiManager.getRoiManager();
rm.reset()

//ImagePlus imp = IJ.getImage()
image_name = imp.getTitle()
def imp_win   = WindowManager.getCurrentWindow()
IJ.run(imp, "Select None", "");

nuc_imp = new Duplicator().run(imp, nuc_ch, nuc_ch, 2, 2, 2, 2)
//IJ.setRawThreshold(nuc_imp, 20, 255, null)
Prefs.blackBackground = true
IJ.run(nuc_imp, "Convert to Mask", "")
IJ.run(nuc_imp, "Fill Holes", "");
IJ.run(nuc_imp, "Median...", "radius=2");
IJ.run(nuc_imp, "Watershed", "slice");
nuc_imp.setTitle("nuc")
nuc_imp.show()

voronoi_imp = nuc_imp.duplicate()
IJ.run(voronoi_imp, "Voronoi", "");
IJ.setRawThreshold(voronoi_imp, 1, 255, null)
IJ.run(voronoi_imp, "Convert to Mask", "")
IJ.run(voronoi_imp, "Invert", "");
voronoi_imp.setTitle("voronoi")

voronoi_imp.show()

// So here we have cell approximation
IJ.run(voronoi_imp, "Analyze Particles...", "size=5-Infinity add");
def cell_rois = rm.getRoisAsArray()
rm.reset();

spot_imp = new Duplicator().run(imp, spot_ch, spot_ch, 1, 1, 1, 1)
//IJ.setRawThreshold(spot_imp, 20, 255, null)
Prefs.blackBackground = true;
IJ.setAutoThreshold(spot_imp, "MaxEntropy dark");
```

```
53 IJ.run(spot_imp, "Convert to Mask", "method=MaxEntropy background=Dark only black
     ");
54 //IJ.run(spot_imp, "Convert to Mask", "")
55 spot_imp.setTitle(image_name+"_spot")
56 spot_imp.show()
57
58 def allrois
59 cell_rois.eachWithIndex{ roi , idx->
60
61     roi.setName("cell"+idx+"-")
62     rm.addRoi(roi);
63     spot_imp.setRoi(roi)
64
65     IJ.run(spot_imp, "Analyze Particles...", "size=0-Infinity add");
66     temp_rois = rm.getRoisAsArray()
67
68     if (temp_rois != null){
69
70         temp_rois.eachWithIndex{ subroi, subidx ->
71             if (subroi!=roi) subroi.setName("cell"+idx+"-spot"+subidx)
72         }
73
74         allrois = [allrois, temp_rois].flatten()
75     }
76     rm.reset();
77 }
78
79 allrois.each{ rm.addRoi(it) }
80 rm. runCommand("Measure")
81
82 return
83
84 IJ.run("Close All", "");
```

A.3.2 Quantification of colocalisation between two channels

Macro to measure colocalisation between two channels per cell

```
1  //Before you start, put DAPI, fluorescence 1 and fluorescence 2 images for the
     analysis in separate folders.
2
3  dir2=getDirectory("save folder for DAPI");
4  dir3=getDirectory("save folder for fluor 1");
5  dir4=getDirectory("save folder for fluor 2");
6  dir5=getDirectory("temp folder");
7
8  list2=getFileList(dir2);
9  list3=getFileList(dir3);
10 list4=getFileList(dir4);
11
12 for (i = 0; i < list2.length; i++) {
13     open(dir2+list2[i]);
14     name=getTitle();
15     run("8-bit");
16
17     run("Convert to Mask", "method=Huang background=Dark only black");
18
19     run("Set Scale...", "distance=0 known=0 unit=pixel");
20
21     run("Analyze Particles...", "size=5000-Infinity clear include add slice");
22
23     close();
24
25     open(dir2+list2[i]);
26     rename("DAPI");
27     run("8-bit");
28     //open(dir3+list3[i]);
29     run("Bio-Formats Importer", "open=["+dir3+list3[i]+"] autoscale color_mode=
         Default rois_import=[ROI manager] view=Hyperstack stack_order=XYCZT");
30     rename("delete");
31     run("Stack to RGB");
32     run("8-bit");
33     rename("C1");
34     selectWindow("delete");
35     close();
36     //run("8-bit");
37     run("Subtract Background...", "rolling=5 sliding");
38     //open(dir4+list4[i]);
39     run("Bio-Formats Importer", "open=["+dir4+list4[i]+"] autoscale color_mode=
         Default rois_import=[ROI manager] view=Hyperstack stack_order=XYCZT");
40     rename("delete");
41     run("Stack to RGB");
42     run("8-bit");
43     rename("C2");
44     selectWindow("delete");
45     close();
46     //run("8-bit");
47     run("Subtract Background...", "rolling=5 sliding");
48
49     run("Images to Stack");
50
51     count=roiManager("count");
52     n=0;
```

```
53
54      for (a = 0; a < count; a++) {
55          roiManager("select", n);
56          run("Enlarge...", "enlarge=70 pixel");
57
58          run("Duplicate...", "duplicate");
59
60          n=n+1;
61          saveAs("Tiff", dir5+name+"_cell_"+n);
62          close();
63
64      }
65
66      run("Close All");
67      roiManager("reset");
68      call("java.lang.System.gc");
69
70  }
71
72
73      list5=getFileList(dir5);
74
75      for (b = 0; b < list5.length; b++) {
76          open(dir5+list5[b]);
77          run("Select None");
78          name3=getTitle();
79
80          IJ.log("");
81          IJ.log(name3);
82
83          run("Stack to Images");
84
85          run("Coloc 2", "channel_1=C1 channel_2=C2 roi_or_mask=<None>
              threshold_regression=Costes display_images_in_result
              li_histogram_channel_1 li_histogram_channel_2 li_icq spearman'
              s_rank_correlation manders'_correlation kendall's_tau_rank_correlation
              2d_intensity_histogram costes'_significance_test psf=3
              costes_randomisations=10");
86          run("Close All");
87          call("java.lang.System.gc");
88
89      }
```

A.4 Personal contributions

For the first part of my thesis (β subunit myristoylation), I performed all the experiments in U2OS cells and MEFs. I generated results for all the main figures (except Figures **2.15 and 2.16**) and all the Appendix Figures (except Appendix Figures **A.9** and **A.12**).

For the second part of my thesis (novel AMPK substrates), I performed all the cellular and biochemical experiments, including validation of AMPK substrates and microscopy experiments. I generated results for all the main figures (except Figures **2.18 and 2.19**) and all the Appendix Figures.

I contributed to the design, planning and execution of the experiments and interpretation and analysis of the results. Prof. Kei Sakamoto conceived the project and supervised me, assisted by Dr. Matthew Sanders for the first part and Dr. Andreas Wiederkehr for the second part.

Individual contributions:

- Dr. Bruce E. Kemp and Dr. Sandra Galic generated the G2A KI mice.
- Natalie Kozlov and Dr. Sandra Galic performed *in vivo* experiments and AMPK signalling in hepatocytes in Figures **2.15 and 2.16**.
- Dr. Florentina Negoita performed imaging of β1 in Appendix **A.9**.
- Jeppe K. Larsen and Dr. Atul Deshmukh performed phosphoproteomics analysis in Figures **2.18 and 2.19**.
- Dr. Maria Deak performed molecular cloning and mutagenesis of AMPKβ subunits to generate stable U2OS cell lines and rest of the cloning and mutagenesis were performed at MRCPPU, Dundee.
- Romain Guiet (BIOP, EPFL) assisted with the generation of macro for Golgi count and Dr. Sandra Galic/Gavin Tjin (SVI, Melbourne) assisted with the colocalisation quantification.

A.5 List of co-authored publications

- **Neopane, K.**, Kozlov, N., Segal, L. M., Negoita, F., Brink, R., Hoque, A., McAloon, L., Yu, D., Ling, N., Sanders. M., Oakhill, J., Scott, J. W., Steinberg, G. R., Loh, K., Kemp, B. E., Sakamoto, K., Galic, S. "Blocking AMPK β1 myristoylation enhances AMPK activity and protects mice from high-fat diet-induced obesity and hepatic steatosis", *under revision (Cell Reports)*.

- Sanders, M. J., Ratinaud, Y., **Neopane, K.**, Bonhoure, N., Day, E. A., Ciclet, O., Pinta, M.N., Day, E., Deak, M., Brinon, B., Steinberg, G., Barron, D., Sakamoto, K. (2022). Natural (dihydro)phenanthrene plant compounds are direct activators of AMPK through its allosteric drug and metabolite binding site. Journal of Biological Chemistry, 101852. doi:10.1016/j.jbc.2022.101852

- Ahwazi, D.*, **Neopane, K.***, Markby, G. R., Kopietz, F., Ovens, A. J., Dall, M., Hassing, A.S., Graesle, P., Alshuweishi, Y., Treebak, J.T., Salt, I. P., Goransson, O., Zeqiraj, E., Scott, J.W., Sakamoto, K. (2021). Investigation of the specificity and mechanism of action of the ULK1/AMPK inhibitor SBI-0206965. Biochemical Journal, 478(15), 2977-2997. doi:10.1042/bcj20210284 *Contributed equally

Blocking AMPK β1 myristoylation enhances AMPK activity and protects mice from high-fat diet-induced obesity and hepatic steatosis.

Katyayanee Neopane[1,2,13], Natalie Kozlov[3,13], Lisa Murray-Segal[3], Florentina Negoita[4], Robert Brink[5], Ashfaqul Hoque[6], Luke M. McAloon[3,7], Dingyi Yu[3], Naomi X.Y. Ling[6], Matthew J. Sanders[1], Jonathan S. Oakhill[6,9], John W. Scott[7,8,12], Gregory R. Steinberg[10], Kim Loh[9,11], Bruce E. Kemp[3,9,12], Kei Sakamoto[4,14,*] and Sandra Galic[3,9,14,*]

[1]Nestlé Institute of Health Sciences, Nestlé Research, Societé des Produits Nestlé S.A., 1015 Lausanne, Switzerland.
[2]School of Life Sciences, École polytechnique fédérale de Lausanne, Lausanne 1015, Switzerland.
[3]Protein Chemistry and Metabolism, St. Vincent's Institute of Medical Research, Melbourne, Victoria 3065, Australia.
[4]Novo Nordisk Foundation Center for Basic Metabolic Research, University of Copenhagen, Copenhagen, Denmark.
[5]Immunology Division, Garvan Institute of Medical Research, Darlinghurst, New South Wales 2010, Australia.
[6]Metabolic Signalling, St. Vincent's Institute of Medical Research, Fitzroy, Victoria 3065, Australia.
[7]Neurometabolism, St. Vincent's Institute of Medical Research, Fitzroy, Victoria 3065, Australia.
[8]The Florey Institute of Neuroscience and Mental Health, Parkville 3052, Australia.
[9]Department of Medicine, University of Melbourne, Parkville 3010, Australia.
[10]Division of Endocrinology and Metabolism, Departments of Medicine and Biochemistry and Biomedical Sciences, McMaster University, Hamilton, ON, Canada.
[11]Diabetes and Metabolic Disease, St. Vincent's Institute of Medical Research, Fitzroy, Victoria 3065, Australia.
[12]Mary McKillop Institute for Health Research, Australian Catholic University, Melbourne 3000, Victoria, Australia.
[13]These authors contributed equally.
[14]These authors contributed equally.

***Correspondence:**

sgalic@svi.edu.au
kei.sakamoto@sund.ku.dk

SUMMARY

The AMP-activated protein kinase (AMPK) is a master regulator of cellular energy homeostasis and a therapeutic target for metabolic diseases. The co/post-translational N-

myristoylation of glycine-2 (Gly2) of the AMPK β-subunit has been suggested to regulate the distribution of the kinase between the cytosol and membranes through a "myristoyl-switch" mechanism. However, the relevance of AMPK myristoylation for metabolic signaling in cells and *in vivo* is unknown. Here, we generated knock-in mice with a Gly2-to-alanine point mutation of the AMPK β1 subunit (β1-G2A). We demonstrate that non-myristoylated AMPK β1 has reduced stability but is associated with increased kinase activity and phosphorylation of the Thr172 activation site in the AMPK α-subunit. Using proximity ligation assays, we show that loss of β1 myristoylation impedes the co-localization of the phosphatase PPM1A/B with AMPK in cells. Mice carrying the β1-G2A mutation have reduced adiposity, hepatic lipid accumulation and insulin resistance. These results show that AMPK β1-subunit myristoylation may be an alternative strategy for activating AMPK and improving metabolic health.

KEYWORDS

Signal transduction, AMPK, phosphatase, myristoylation

INTRODUCTION

The AMP-activated protein kinase (AMPK) is a cellular energy sensor that is activated by low energy conditions and phosphorylates a wide range of substrates, including key metabolic proteins and transcription factors, in order to restore energy homeostasis (Hardie et al., 2012). In response to cellular energy deficit signaled by an increase in the AMP/ATP ratio, AMPK redirects metabolism away from ATP-consuming processes and promotes ATP-generating pathways, allowing the cell to match its activity with the available energy supply. For example, AMPK phosphorylation and inhibition of HMG-CoA reductase and acetyl-CoA carboxylase (ACC) suppresses the energy-consuming reactions of cholesterol and fatty acid synthesis, respectively (Carling et al., 1987; Sim and Hardie, 1988). Concomitant with reduced fatty acid synthesis, AMPK-mediated reduction of intracellular malonyl-CoA levels, the product of the ACC-catalyzed reaction, reduces malonyl-CoA inhibition of mitochondrial carnitine palmitoyl transferase-1 and stimulation of ATP generation through fatty acid β-oxidation. Additionally, AMPK regulates the activity of a multitude of metabolic and non-metabolic substrates, including key proteins involved in glucose metabolism, protein synthesis, mitochondrial biogenesis, autophagy and cell proliferation. Studies using genetic and pharmacologic modulation of AMPK activity *in vivo* have also demonstrated a pivotal role for AMPK as a key regulator of whole-body energy metabolism linking AMPK activation to improved exercise capacity and glucose disposal, and suppression of obesity, hepatic steatosis and inflammation

(Gluais-Dagorn et al., 2021; Narkar et al., 2008; Smith et al., 2016). These findings highlight AMPK's potential as a pharmacological target for metabolic diseases, including type 2 diabetes, cardiovascular disease and obesity and emphasize the need for a better understanding of the structural, molecular and physiological determinants of AMPK action.

AMPK is a heterotrimeric complex consisting of a catalytic α subunit and two regulatory subunits, β and γ, each with different isoforms (α1, α2, β1, β2, γ1, γ2, γ3) and encoded by separate genes (Hardie, 2011; Steinberg and Kemp, 2009). The α subunit contains the catalytic domain that is under physiological conditions activated by phosphorylation of Thr172 by upstream kinases, including liver kinase B1 (LKB1) and calcium-calmodulin-dependent kinase kinase-2 (CaMKK2) (Hardie, 2011; Steinberg and Kemp, 2009). Conversely, AMPK is inactivated by Thr172 dephosphorylation by protein phosphatases, including members of the metal-dependent protein phosphatase (PPM) family, protein phosphatase 2A (PP2A) and protein phosphatase PPM1A/B (also known as PP2Cα/β) (Chida et al., 2013; Davies et al., 1995; Sanders et al., 2007; Steinberg et al., 2006). AMPK is also allosterically activated, which is mediated by binding of AMP to three nucleotide-binding sites of the γ subunit. Furthermore, binding of AMP and ADP helps maintain AMPK activity by protecting Thr172 from dephosphorylation (Davies et al., 1995; Sanders et al., 2007; Xiao et al., 2011). The C-terminal sequence of the β-subunit functions to anchor α- and γ-subunits for assembly of the AMPK heterotrimer core, while a central carbohydrate-binding module (CBM) permits AMPK association with glycogen (Hoffman et al., 2020; Polekhina et al., 2003). The β subunit also undergoes N-terminal myristoylation of Gly2, which occurs in both, the β1 and β2 isoforms (Mitchelhill et al., 1997; Oakhill et al., 2010; Warden et al., 2001). This modification facilitates AMPK association with intracellular membranes in response to AMP and nutrient stress, suggesting that similar to other myristoylated proteins, AMPK may undergo a ligand-induced "myristoyl switch" between membrane-bound and cytoplasmic forms (Oakhill et al., 2010; Warden et al., 2001). Such a mechanism may allow AMPK to effectively sense and transduce energy stress signals, by enabling interaction with membrane-bound signaling proteins. While an AMPK myristoyl switch hypothesis has not been unequivocally validated, several subsequent studies confirmed the importance of the myristoyl group for AMPK association with lysosomal (Wen et al., 2019; Zhang et al., 2013) and mitochondrial (Liang et al., 2015) membranes and phosphorylation by kinases, including LKB1 (Zhang et al., 2013) and Unc-51-like kinase 1 (ULK1) (Dite et al., 2017).

Despite indications that myristoylation is an important component of AMPK function, the role of β-subunit myristoylation at the whole organism level remains unknown. In the current study

we generated mice with whole-body alanine knock-in mutations of the myristoylation site Gly2 of the β-subunit and focused on investigating the importance of β1-isoform myristoylation for metabolic signaling *in vivo*. We found that loss of myristoylation prevented the co-localization of PP2Cα/β to AMPK and resulted in increased basal phosphorylation of α-Thr172 and AMPK substrates in cells. Furthermore, these changes were associated with reduced adiposity, hepatic lipid accumulation and protection from high-fat diet-induced insulin resistance, overall demonstrating that disruption of AMPK myristoylation has striking beneficial effects on metabolic health.

RESULTS

Ablation of AMPK β Gly-2 myristoylation enhances cellular AMPK activity.

To investigate the role of AMPK β-subunit myristoylation in the regulation of endogenous AMPK function, we used CRISPR/Cas9 gene targeting to generate two whole-body knock-in (KI) mouse lines on a C57BL/6 background carrying β-glycine-2 to alanine (G2A) point mutations of the β1 (**Fig. S1A**) and β2 (**Fig. S1B**) subunits, respectively. We inter-crossed these strains to generate AMPK β1/β2-G2A double knock-in (DKI) mice, which were subsequently used for the isolation of β1/β2-G2A DKI mouse embryonic fibroblasts (MEFs). To verify that myristoylation of endogenous AMPK β1, the predominant β isoform in MEFs, was detectable in wild-type (WT), but absent in β1/β2-G2A DKI MEFs, we took a click chemistry approach (Kim et al., 2017). The MEFs were treated with increasing doses of azido-myristic acid (5 - 50 μM) for up to 24 hours followed by immunoprecipitation and visualization of myristoylated AMPK β1 by immunoblotting (**Fig. S2A and B**). We observed that AMPK β1 was most robustly myristoylated (>50%) when cells were incubated with azido-myristic acid at ≥ 25 μM for 24 hours. Under this condition, we confirmed myristoylation of β1 was only detectable in WT, but not in β1/β2-G2A DKI MEFs (**Fig. 1A**).

Analysis of AMPK subunit/isoform expression in AMPK β1/β2-G2A DKI MEFs revealed that α, β1 and β2 subunit protein levels were reduced by ~50, 75 and 90%, respectively, indicating a protective effect of β-subunit myristoylation on AMPK protein stability (**Fig. 1B**). To determine whether the stoichiometry of AMPK heterotrimer formation was retained in the G2A mutant, we immunoprecipitated AMPK β1 from β1/β2-G2A DKI MEF lysates and analyzed the presence of AMPK subunits in the pull-down. We confirmed that relative interaction of β1 with α and γ subunits was comparable between WT and G2A mutant (**Fig. S2C**). To investigate the effect of AMPK β myristoylation on AMPK activity and signaling in cells, we left WT and

β1/β2-G2A DKI MEFs untreated or treated with increasing doses of the specific allosteric AMPK activator 991 (Bultot et al., 2016; Xiao et al., 2013) for 1 hour. 991 robustly increased phosphorylation of AMPK substrates including ACC, Raptor and ULK1 in WT MEFs (**Fig. 1C**). In contrast, phosphorylation of AMPK α and its substrates was markedly higher in untreated β1/β2-G2A DKI compared to WT cells, with only modest changes in the phosphorylation of AMPK α and its substrates with 991 treatment (**Fig. 1C)** Consistent with these observations, AMPK α1 activity in the untreated/basal condition was ~3-fold higher in β1/β2-G2A DKI compared to WT MEFs (**Fig. S2D**). We also analyzed MEFs derived from AMPK β1-G2A single KI mice and observed enhanced phosphorylation of ACC and ULK1 in the untreated/basal state (**Fig. 1D**). Collectively, we have shown that loss of AMPK β myristoylation is associated with enhanced Thr172 phosphorylation and activity of endogenous AMPK in cells.

Blocking AMPK β Gly-2 myristoylation disrupts co-localization with PPM1A/B

To investigate whether the altered signaling of the non-myristoylated AMPK β-G2A mutant was associated with changes in subcellular localization, we performed immunofluorescence analysis of AMPK β1 localization in β1/β2-G2A DKI MEFs after having confirmed specificity of the AMPK β1 antibody using β1 KO MEFs. Consistent with our previous study (Warden et al., 2001), we found that β1 was widely distributed across the cytosol with some peripheral membrane staining (**Fig. S3**). However, we did not observe any apparent differences in β1 subcellular distribution between WT and β1/β2-G2A DKI MEFs (**Fig. S3**). Furthermore, AMPK activation using treatment with 991 or another allosteric activator MK-8722 did not provoke any detectable changes in β1 localization (**Fig. S3**), suggesting that the observed effect of the G2A mutation on AMPK signaling in response to allosteric activation was likely independent of effects on subcellular distribution.

We next hypothesized that enhanced AMPK α-Thr172 phosphorylation coupled with increased cellular AMPK activity observed in β1/β2-G2A DKI MEFs was due to disrupted co-localization with AMPK phosphatases. It has been previously reported that PPM1A and PPM1B are myristoylated in HeLa cells (Chida et al., 2013). To verify that PPM1A and PPM1B are also myristoylated in MEFs, we performed a click chemistry analysis in WT MEFs transfected with siRNA targeting PPM1A or PPM1B or siRNA with a nonsense/scrambled sequence as control. We detected myristoylated PPM1A and PPM1B in non-transfected and

control siRNA-transfected MEFs in the presence of myristic acids (**Fig. 2A**). In contrast, myristoylation of PPM1A and PPM1B was ablated in cells transfected with siRNA targeting PPM1A or PPM1B (**Fig. 2A**).

We next examined whether AMPK β1 and PPM1A/PPM1B co-localize in cells. We took advantage of the proximity ligation assay which permits visualization and quantification of protein-protein interactions *in situ* at endogenous protein levels (Alam, 2018). As shown in **Fig. 2B**, under fluorescence microscopy we observed a cluster of signals (dots) enriched in WT MEFs, indicating proximity of AMPK β1 and PPM1A/PPM1B. Specificity of this interaction was verified, as depletion of PPM1B by siRNA (**Fig. S4A**) resulted in ablation of the signals/dots (**Fig. S4B**). The number of dots, as well as the mean intensity of the fluorescence signal was significantly reduced in AMPK β1/β2-DKI and absent in AMPK β1 KO MEFs (**Fig. 2B**). This is consistent with a previous study where ectopic expression of non-myristoylated G2A mutants of PPM1A or PPM1B was associated with blunted dephosphorylation of AMPK α-Thr172 in Hela cells (Chida et al., 2013). Taken together, we show that ablation of AMPK myristoylation results in a significant reduction of AMPK-phosphatase interactions, possibly contributing to enhanced AMPK phosphorylation and activity.

Blocking AMPK β1 Gly2 myristoylation protects from high-fat diet-induced hepatic steatosis.

To determine the effect of disrupted AMPK myristoylation in an *in vivo* setting, we focused on investigating the specific role of β1 myristoylation in metabolic regulation using β1-G2A KI mice. We first investigated AMPK subunit expression and signaling in various metabolically relevant tissues isolated from male β1-G2A KI and WT littermates that were either fed *ad libitum* or fasted for 16 hours. In liver, a tissue with predominant expression of the β1 isoform in rodents (Wu et al., 2013), we found that, consistent with our findings in MEFs, blocking β1 myristoylation resulted in a reduced abundance (~50%) of the β1 subunit in both the fed and fasted state (**Fig. 3A and 3B**). This was accompanied by a ~ 2-fold increase in β2 (**Fig. 3A and 3C**) and a drop in total AMPK α (~40%, **Fig. 3A and 3D**) and AMPK γ1 (~70%, **Fig. 3A**), the predominant γ subunit in rodent liver (Wu et al., 2013). qPCR analyses confirmed that the increase in β2 levels was at least in part due to an upregulation of *Prkab2* gene expression, whereas the reduction in β1 and α subunit abundance was independent of changes in mRNA expression (**Fig. 3E**) indicative of increased posttranslational turnover.

Despite decreased AMPK α protein levels, livers from β1-G2A KI mice had overall elevated ACC phosphorylation (**Fig. 3A and 3F**) reflecting increased cellular AMPK activity. To investigate this further, we measured kinase activity of AMPK complexes using AMPK α immunoprecipitated from β1-G2A KI and WT liver homogenates and accounted for the difference in AMPK abundance by normalizing activity to the amount of α subunit recovered. We found an overall genotype effect on AMPK specific activity ($P<0.0001$) with a 2.3-fold increase in homogenates from β1-G2A mice compared to WT in the fasted state (**Fig. 3G**). This finding correlated with an overall increase in AMPK α-Thr172 phosphorylation (genotype effect $P<0.027$) (**Fig. 3H**), suggesting that β1 myristoylation *in vivo* has an inhibitory effect on Thr172 phosphorylation and AMPK activity.

Consistent with negligible expression levels of AMPK β1 in skeletal muscle (Wu et al., 2013), blocking β1 myristoylation had no measurable effects on AMPK α- and β-subunit expression or AMPK α-Thr172 and ACC Ser212 phosphorylation in this tissue (**Fig. S5A-S5E**). Similarly, we did not observe any significant differences in AMPK expression and signaling in β1-G2A KI and WT subcutaneous white fat (**Fig. S6A-S6F**), likely due to the predominant expression of AMPK β2 in differentiated adipocytes (Katwan et al., 2019). In contrast, β1-G2A KI brown adipose tissue showed many of the changes in AMPK biology observed in liver, albeit to a lesser degree, including reduced AMPK β1- and α-subunit expression and increased ACC phosphorylation indicative of an overall increase in AMPK activity (**Fig. S6G-S6L**). These results suggest that the metabolic effect of the β1-G2A mutation *in vivo* may be predominantly a consequence of altered signaling in liver and brown adipose tissue.

Myristoylation of the AMPK β-subunit has previously been suggested to be a prerequisite for AMP-induced stimulation of α-Thr172 phosphorylation (Oakhill et al., 2010). To investigate the effect of the β1-G2A mutation on AMPK signaling in a system that allows for greater control of intracellular AMP levels, we isolated primary hepatocytes from AMPK β1-G2A and WT mice and analyzed ACC phosphorylation as a readout of cellular AMPK activity in response to 5-Aminoimidazole-4-carboxamide ribonucleotide (AICAR), a pro-drug for the AMP analog ZMP. β1-G2A hepatocytes showed significantly increased basal and similar levels of AICAR-stimulated ACC phosphorylation (**Fig. 3I and 3J**). Furthermore, ACC phosphorylation was maintained for a longer period in β1-G2A cells (**Fig. 3I and 3J**) and correlated with prolonged α-Thr172 phosphorylation (**Fig. S7A**). A similar pattern of elevated basal and comparable maximal ACC phosphorylation was observed in hepatocytes treated with the β1-selective AMPK activator A769662 (Scott et al., 2008) (**Fig. S7B and S7C**).

To assess the consequences of increased ACC phosphorylation in β1-G2A liver for hepatic lipid accumulation *in vivo*, we analyzed fat content in liver tissue from β1-G2A mice and WT controls fed a chow or obesity-inducing high-fat diet (HFD). There was no difference in the overall area of Oil Red O lipid stain in livers from chow-fed AMPK β1-G2A and WT mice and no apparent morphological difference as assessed by Haematoxylin/Eosin (H/E) staining (**Fig. S7D and S7E**). However, after 12 weeks of high-fat feeding, livers from β1-G2A mice had significantly smaller lipid droplets (**Fig. 3K and S7E**) and reduced fat content as assessed by nuclear magnetic resonance (NMR) analysis of liver biopsies (**Fig. S7F**). Furthermore, quantification of liver triglyceride content revealed decreased levels in β1-G2A livers from chow-fed (**Fig. 3L**) and HFD-fed mice (**Fig. 3M**) across all conditions examined. In comparison, there were only minor differences in liver glycogen content between genotypes (**Fig. S7G and S7H**) indicating a predominant effect of the β1-G2A mutation on lipid metabolism.

Hepatic lipid content in the postprandial state (Timlin and Parks, 2005) and under conditions of hyperglycemia and hyperinsulinemia in obesity (Eissing et al., 2013; Lewis et al., 2002; Smith et al., 2020) is substantially impacted by increased rates of fatty acid esterification and *de novo* lipogenesis, while lipid removal through oxidation and VLDL export is less affected (Lewis et al., 2002; Postic and Girard, 2008). In contrast, liver fatty acid catabolism is increased with fasting to generate ketone bodies as the major energy supply for the brain in times of energy deprivation (Kersten et al., 1999), with adipose tissue lipolysis as the main source of fatty acids used in this process. To investigate whether the reduced liver lipid content in β1-G2A may have been indirectly impacted by altered AMPK signaling and inhibited triglyceride lipolysis in adipose tissue, we assessed phosphorylation of hormone-sensitive lipase (HSL) Ser565, an AMPK phosphorylation site previously reported to have inhibitory effects on lipolysis (Garton and Yeaman, 1990; Watt et al., 2006). We found no measurable difference in HSL Ser565 phosphorylation in subcutaneous white fat during the *ad libitum* or fasted states (**Fig. S7I**), consistent with our previous observation that blocking AMPK β1 myristoylation had no significant impact on AMPK signaling in this tissue. We next analyzed the capacity for *de novo* triglyceride synthesis by measuring rates of ^{3}H-acetate incorporation in primary hepatocytes isolated from β1-G2A and WT mice. We found that β1-G2A cells had reduced basal and insulin-induced *de novo* triglyceride synthesis, while the lipid-lowering effect of A769662 was not significantly different between genotypes (**Fig. 3N**). The decreased lipogenic capacity of β1-G2A hepatocytes was likely due to increased suppression of ACC activity and

not gene expression differences as qPCR analyses of β1-G2A livers showed either no change or a possibly compensatory increase in a number of lipogenic genes examined (**Fig. S7J**). We also assessed effects on fatty acid catabolism by measuring the conversion of ^{14}C-palmitate to acid-soluble metabolites. We found a modest increase in basal oxidation rates in β1-G2A hepatocytes (**Fig 3O**), while treatment with A769662 had no significant additional effect on oxidation in G2A cells.

Collectively, these results indicate that deletion of β1 myristoylation maintains AMPK in an active state, altering lipid metabolism in hepatocytes and preventing hepatic lipid accumulation during high-fat feeding.

AMPK β1-G2A KI mice have reduced adiposity and improved insulin sensitivity on HFD.

To investigate the effect of non-myristoylated AMPK β1 on whole-body metabolism, we measured body mass and adiposity of male β1-G2A mice and age-matched WT controls fed a chow or HFD over a period of 12 weeks. There was no significant difference in body weight progression in chow-fed mice, however β1-G2A mice were partially protected from body weight gain during high-fat feeding (**Fig. 4A**). This was not attributable to differences in lean mass (**Fig. 4B**) but was instead due to a significant reduction in total body fat mass, which was to a smaller degree also detectable in chow-fed animals (**Fig. 4C**). Epididymal visceral fat pads dissected from age-matched β1-G2A mice and WT littermates at the end of the 12-week feeding period were significantly smaller in β1-G2A animals in both, chow- and HFD-fed conditions (**Fig. 4D**). We also observed a shift to significantly smaller lipid droplets in adipocytes from inguinal subcutaneous adipose tissue from β1-G2A animals in both, chow- and HFD-fed conditions (**Fig. 4E and 4F**). To investigate whether browning of subcutaneous fat deposits contributed to the lean phenotype of β1-G2A mice, we performed immunohistochemical analysis of UCP1 expression in inguinal fat tissue of chow- and HFD-fed β1-G2A and WT control mice. We did not observe any detectable UCP1-associated signal in any of the tissue sections examined (**Fig. S8A**). Similarly, immunoblot analysis revealed only a spurious UCP1 signal in tissues from chow-fed animals independent of genotype (**Fig. S8B**), suggesting that that loss of β1 myristoylation does not result in increased thermogenic capacity in subcutaneous tissue. A recent study using mice with widespread expression of a gain-of-function AMPK mutant (γ1-D316A) showed that chronic AMPK activation protects from diet-induced obesity, likely by promoting a UCP1-independent increase in the oxygen consumption rate in white adipose tissue due to increased mitochondrial content and expression

of skeletal muscle-associated genes (Pollard et al., 2019). To assess whether a similar mechanism may contribute to the obesity-resistant phenotype of β1-G2A mice, we analyzed the mRNA expression of genes involved in UCP1-independent thermogenesis in inguinal fat from HFD-fed β1-G2A and WT control mice. There were no significant differences in the transcription of any of the genes examined (**Fig. S8C**). Similarly, protein levels of mitochondrial electron-transport-chain proteins in inguinal fat of chow- and HFD-fed mice were comparable between genotypes (**Fig. S8D**). Taken together these results suggest that the reduced adiposity of β1-G2A mice is independent of functional changes within white adipose tissue.

We have shown that in addition to effects in the liver, non-myristoylated AMPK β1 also had measurable effects on ACC Ser79/Ser212 phosphorylation in brown fat, indicative of increased overall AMPK activity in this tissue. AMPK has previously been found to be crucial for maintaining UCP1 expression and thermogenesis in brown fat depots (Mottillo et al., 2016), suggesting that the reduced adiposity of HFD-fed β1-G2A may have been due to increased brown fat activity. H/E staining of brown fat tissue sections showed indeed smaller adipocyte size and reduced fat content in tissue isolated from HFD-fed β1-G2A animals compared to WT controls (**Fig. 4G**). Analysis of *Ucp1* mRNA levels in brown fat revealed no difference in expression in tissue from chow-fed animals, however, HFD-fed β1-G2A mice showed a modest increase in *Ucp1* expression, indicating a possible increase in thermogenic capacity. mRNA expression analysis of several other genes involved in brown fat lipid metabolism confirmed an increased adaptation to fatty acid utilization versus synthesis in brown fat of HFD-fed β1-G2A mice (**Fig. 4H**).

To investigate whether the changes in the brown fat gene expression pattern in high-fat diet-fed mice were associated with differences in whole-body energy expenditure, we performed calorimetry analysis using the Columbus Laboratory Animal Monitoring System over a period of 48 hours. We found that non-myristoylated AMPK β1 had no statistically significant effect on energy expenditure (**Fig. S9A and S9B**). To account for any potential confounding effects stemming from differences in adiposity, we performed regression analysis of the average rate of energy expended over a 24-hour period per unit change in lean mass (**Fig. S9C**) and ANCOVA analysis of the mean difference in energy expenditure in a given time period with lean mass as covariate (**Fig. S9D**). Analyses showed the expected effect of diet and mass on metabolic rate without revealing any significant genotype differences. In addition, cumulative food intake (**Fig. S9E and S9F**), substrate preference (as determined by the respiratory

exchange ratio (VCO_2/VO_2)) (**Fig. S9G and S9H**) and ambulatory activity (**Fig. S9I and S9J)** were also unaffected by the β1-G2A mutation, suggesting that any potential activating impact of non-myristoylated β1 on thermogenesis did not translate into any measurable effects on whole-body energy balance in high-fat diet-fed mice.

To investigate the potential therapeutic consequences of the anti-obesity effect of non-myristoylated AMPK, we measured insulin and glucose tolerance in β1-G2A KI mice and WT littermates on chow and HFD. There was no effect of genotype in blood glucose handling in response to insulin (**Fig. S10A and S10B**) or glucose (**Fig. S10C and S10D**) in chow-fed animals. Accordingly, serum insulin (**Fig. S10E**) and blood glucose (**Fig. S10F**) concentrations in the fed and fasted states were similar in β1-G2A and WT mice. However, under HFD-fed conditions, β1-G2A mice had increased glucose clearance after insulin injection (**Fig. 5A and 5B**) without any measurable effects on glucose tolerance (**Fig. 5C and 5D**). Consistent with this, blood glucose levels were similar in β1-G2A and WT mice (**Fig. 5E**) but were maintained on the background of significantly lower serum insulin concentrations in β1-G2A animals (**Fig. 5F**), suggesting improvements in insulin sensitivity, a notion also supported by a significantly lower HOMA IR (**Fig. 5G**).

DISCUSSION

In this study, we have described the role of AMPK β1-Gly2 myristoylation in the regulation of AMPK signaling and whole-body energy metabolism. In contrast to previous studies that have almost exclusively relied on cellular overexpression methods to investigate AMPK β-myristoyl group function, we have utilized a CRISPR-Cas9-generated Gly2-to-Ala knock-in system, which enabled us to disrupt myristoylation of the endogenous AMPK β protein.

We found that ablation of Gly2 myristoylation resulted in a destabilization of the β-subunit protein, independent of changes in gene expression. This finding is consistent with the recently proposed mechanism, by which N-myristoylation functions to protect N-terminal glycine degrons from proteasomal degradation by Cullin-RING E3 ligase complexes, $Cul2^{ZYG11B}$ and $Cul2^{ZER1}$ (Timms et al., 2019). However, the substitution of Gly-2 for Ala was also reported to enhance protein stability in this context (Timms et al., 2019), suggesting that other ubiquitin systems may contribute to the increased degradation of the β-G2A protein. Examples are the E3 ligases CIDEA, RNF44, UBE2O and CRBN, which have all been suggested to promote β-subunit degradation (Qi et al., 2008; Yang et al., 2020).

Despite reduced total cellular levels of AMPK complex components, basal phosphorylation of all AMPK substrates examined was significantly increased in cells expressing non-myristoylated (G2A) AMPK β and correlated with increased basal α-Thr172 phosphorylation and AMPK activity. Using purified AMPK complexes *in vitro* (Oakhill et al., 2010; Warden et al., 2001), we, and others, have previously reported that loss of β myristoylation results in enhanced AMPK activation in the basal condition. The increase in kinase activity was found to be at least in part independent of α-Thr172 phosphorylation and was suggested to be a consequence of changed subunit interactions in the absence of the myristoyl group (Warden et al., 2001). The structural basis for the increased activity is not entirely clear but may involve disruptions in the normal functioning of a "myristoyl switch" mechanism, by which the myristoyl group is normally buried in a putative hydrophobic binding pocket (switch OFF) and moves out in response to activating conditions enabling AMPK to interact with membrane associated proteins (switch ON) (Ali et al., 2016; Oakhill et al., 2010). It is possible that non-myristoylated AMPK mimics a perpetual "switch ON" conformation that alleviates AMPK autoinhibition even in the absence of activating conditions. In support of this, we previously reported an interaction between a short, β1-conserved sequence in the N-terminal region of the β2-isoform and the α2 autoinhibitory domain in the disengaged position, itself associated with higher basal AMPK activity and resistance to Thr172 dephosphorylation (Chen et al., 2009). Clearly, more detailed structural studies, ideally interrogating myristoylated AMPK complexes, are required to understand the precise mechanism.

An additional important aspect of AMPK myristoyl-group function is the targeting of AMPK to subcellular membranes in response to activating stimuli. Multiple studies overexpressing fluorescently tagged AMPK β G2A protein have shown the importance of the myristoyl group for the targeting of AMPK to subcellular structures (Liang et al., 2015; Oakhill et al., 2010; Warden et al., 2001; Wen et al., 2019; Zhang et al., 2013) and into the vicinity of upstream kinases (LKB1 (Zhang et al., 2013), ULK1 (Dite et al., 2017)) and downstream signaling proteins (Raptor/mTORC1 (Wen et al., 2019), ATG16 complex (Liang et al., 2015)). However, overexpression methods may introduce artifacts (Moore and Murphy, 2009) that result in mislocalizations of the tagged protein. Using immunofluorescence analysis of natively expressed non-myristoylated protein, we did not detect any discernible effects of the G2A mutation on subcellular localization. This finding would be consistent with the generally accepted view that myristoylation alone is not sufficient for membrane association in the absence of a second lipid modification or a stretch of basic sequence (Resh, 2013), both of

406 which are not present in the β-subunit. However, there are two caveats associated with this
407 study. Firstly, a more detailed analysis of AMPK localization using higher-resolution imaging
408 may uncover previously unrecognized changes in the distribution of the non-myristoylated
409 mutant. Secondly, previous studies have suggested that the putative myristoyl switch
410 mechanism may be most important during rising AMP levels and glucose deprivation (Oakhill
411 et al., 2010), conditions, which have not been explored in our study.

412 Basal phosphorylation of α-Thr172 and AMPK substrates in G2A cells were close to saturating
413 levels, as treatments with various AMPK activators (allosteric or ZMP--induced) had only
414 modest effects or were entirely ineffective at eliciting further increases. Furthermore, time
415 course analyses of AICAR-stimulated hepatocytes showed a pattern of prolonged
416 phosphorylation of α-Thr172 and ACC Ser79, indicating a delay in deactivation of the non-
417 myristoylated mutant. Our current data suggest that the AMPK myristoyl group may provide a
418 separate layer of regulation of AMPK activity by facilitating the spatial targeting of
419 myristoylated α-Thr172 phosphatases to AMPK for effective deactivation. In cell-free assays,
420 AMPK α-Thr172 has been shown to be dephosphorylated by recombinant/purified protein
421 phosphatases, including PP1, PP2A, and PPM1A (Carling et al., 1989; Davies et al., 1995). In
422 cellular studies, RNAi-mediated knockdown of PPM1A/B or PPM1E resulted in reduced
423 dephosphorylation of AMPK α (Chida et al., 2013; Voss et al., 2011). Chida *et al*. demonstrated
424 that ectopically/stably expressed PPM1A/B Gly-2 are myristoylated in HeLa cells and that the
425 overexpressed WT PPM1A/B, but not G2A mutant caused a large decrease in AMPK α
426 phosphorylation. We further extended this observation and showed here that endogenous
427 PPM1A/B are myristoylated in cells and they are in close proximity with endogenous AMPK
428 β1 WT, but to a significantly lower extent with the G2A mutant. These results suggest that
429 myristoylation of PPM1A/B and AMPK β may promote their co-localization and at least partly
430 contribute to keeping AMPK α-Thr172 phosphorylation at a low level in cells.

431 At the whole-body level, the increased AMPK α-Thr172 phosphorylation and kinase activity
432 of the non-myristoylated mutant had profound effects on adiposity and liver lipid metabolism,
433 reminiscent of the previously described phenotype of a whole-body gain-of-function γ1-
434 D316A transgenic mouse model (Pollard et al., 2019). However, in contrast to the γ1-D316A
435 mutation which affects both, AMPK β1- and β2-complexes, study of the AMPK G2A mutation
436 enabled us to determine the metabolic consequences of β1-specific AMPK activation. We
437 found that loss of β1 myristoylation was sufficient to afford a partial protection from HFD-
438 induced obesity with reduced lipid accumulation across all fat depots examined. In contrast to

the phenotype of γ1-D316A transgenic mice, which displayed increased oxygen consumption associated with a dramatic induction of a skeletal-muscle gene signature in subcutaneous fat (Pollard et al., 2019), ablation of β1 myristoylation had no measurable effects on thermogenic, mitochondrial or muscle-like protein and gene expression in white fat tissue. This was likely due to the predominant expression of the β2 isoform in differentiated adipocytes (Katwan et al., 2019). Future studies using mice with β2-specific Gly-2 myristoylation ablation may clarify whether AMPK activation through lack of myristoylation has the potential to remodel adipose tissue function.

In contrast, β1 is the principal AMPK β subunit in mouse liver. Consistent with this, β1-G2A mice showed substantial reductions in liver fat accumulation, particularly under conditions of a HFD, which were likely due to increased ACC inhibition leading to reduced lipid synthesis and modest increases in fatty acid oxidation. This finding is entirely consistent with numerous previous mouse models of whole-body or liver-specific AMPK activation (Garcia et al., 2019; Pollard et al., 2019; Woods et al., 2017) and confirms that AMPK activation in the liver is a viable strategy for prevention of HFD-induced hepatic steatosis.

In addition to the anti-steatotic effect in the liver, ablation of AMPK β1 myristoylation also resulted in reduced lipid deposition in white and brown adipose tissue depots suggesting that β1-G2A mice were suffering from an overall negative energy balance. Our analysis of AMPK subunit expression and signaling in metabolically relevant tissues revealed a potential role of myristoylated AMPK β1 in brown fat, in accordance with our previous report showing a predominant expression of the β1-subunit in this tissue type (Rhein et al., 2021). AMPK is known to be required for effective brown fat thermogenesis by maintaining mitochondrial integrity and function (Mottillo et al., 2016) and possibly by promoting the upregulation of thermogenic genes (Zhang et al., 2014). Consistent with this, we found elevated expression of UCP1 and genes involved in fat catabolism in brown fat of HFD-fed β1-G2A mice. However, these changes did not correlate with significant impacts on whole-body energy expenditure, suggesting that the AMPK activation associated with loss of myristoylation in brown fat did not elicit increases in heat dissipation sufficient to affect energy balance. It is possible that the effects of small increases in brown fat activity may become apparent when accumulated over a longer time period. Alternatively, the reduced adiposity of HFD-fed β1-G2A mice may have been a consequence of altered AMPK biology in the liver. Previous studies have reported significant extra-hepatic benefits, including reduced white adipose tissue expansion, associated with liver-specific AMPK activation (Garcia et al., 2019; Yang et al., 2008). AMPK activation

has been shown to alter the expression profile of the liver secretome, possibly affecting hepatokines capable of modifying whole-body metabolism (Garcia et al., 2019). Future studies may reveal whether a similar mechanism contributes to the reduced adiposity of β1-G2A mice.

Overall, loss of AMPK β1 myristoylation produces a phenotype characterized by increased basal AMPK Thr172 phosphorylation and activity, an effect that may at least partially be due to inhibited interactions with AMPK phosphatases. *In vivo*, these effects produce an overall metabolically beneficial outcome, by combining lowered hepatic lipid accumulation with reduced HFD-induced increases in adiposity leading to improvements in insulin sensitivity.

ACKNOWLEDGEMENTS

This work was supported by grants from the Australian Research Council (Grant DP170101196), the National Health & Medical Research Council of Australia (Grant 1085460 to BEK, SG and GRS, Grant 1145836 to SG, KL, GRS and BEK, Grant 1145265 to JSO and BEK) and supported in part by the Victorian Government Operational Infrastructure Support Scheme. Novo Nordisk Foundation Center for Basic Metabolic Research is an independent Research Center based at the University of Copenhagen, Denmark, and partially funded by an unconditional donation from the Novo Nordisk Foundation (Grant number NNF18CC0034900).

AUTHOR CONTRIBUTIONS

Conceptualization, B.E.K., K.S. and S.G.; Methodology, K.S, S.G., K.L., R.B.; Investigation, K.N., N.K., L.M.-S., A.H., L.M.M., D.Y., N.X.Y.L., F.N. and S.G.; Formal Analysis, K.N., N.K., L.M.-S., A.H., D.Y., J.W.S., K.S, and S.G.; Funding Acquisition, S.G., K.S., G.R.S., J.S.O. and B.E.K.; Supervision, K.S., M.J.S., S.G., K.L., J.S.O.; Writing-Original Draft, K. S. and S.G. Writing-Review & Editing, K.N., F.N., A.H., M.J.S., J.O.S., J.W.S., G.R.S., K.L., B.E.K., K.S. and S.G.

DECLARATION OF INTERESTS

Katyayanee Neopane and Matthew J Sanders are current, and Kei Sakamoto was a former employee of Societé des Produits Nestlé (Switzerland).

FIGURE LEGENDS

Fig. 1: **Lack of AMPKβ Gly-2 myristoylation results in enhanced AMPK phosphorylation and activity in cells.**

(A) Wild-type (WT) or AMPK β1/2-G2A double knock-in (DKI) mouse embryonic fibroblasts (MEFs) were incubated with azido-myristic acid (25 μM) for 24 hours. AMPK β1 was immunoprecipitated and click chemistry reaction was performed using biotin-alkyne followed by immunoblot analysis. Myristoylated and total β1 was detected by Streptavidin-AF680 or total β1 antibody and visualized by LI-COR Odyssey Blot Imager. Data shown are representative immunoblots from three independent experiments. (B) Immunoblots of the AMPK subunit isoforms in WT, β1/2-G2A DKI and β1 knockout (KO) MEFs and quantification of AMPK subunit isoform expression in β1/2-G2A DKI MEFs relative to WT The immunoblots shown are representative of three independent experiments. (C) Immunoblots and quantification of phosphorylation of AMPK and its substrates in the presence or absence of increasing concentrations of 991 for 30 min in WT or β1/2-G2A DKI MEFs. The phospho-signal was normalized to respective total protein and expressed as relative to vehicle-treated WT. Red arrow indicates band of interest. (D) WT or β1-G2A KI MEFs were treated with 10 μM 991 for 30 min and lysed for immunoblot analysis. Shown are representative immunoblots from two independent experiments. * P<0.05, ** P<0.01, *** P<0.001, *** P<0.0001 are differences between genotypes. # P<0.05, ## P<0.01, ### P<0.001, #### P <0.0001 represent 991 effects compared to vehicle control as determined by unpaired t-test or two-way ANOVA. All data are mean ± s.e.m.

Fig. 2: **PPM1A and PPM1B are myristoylated and co-localize with AMPK β1 in cells.**

(A) Wild-type (WT) mouse embryonic fibroblasts (MEFs) were incubated with azido-myristic acid for 16 hours. Cells were left untransfected (-) or transfected with scrambled siRNA (Control) or siRNA targeting PPM1A or PPM1B for 48 hours. Immunoprecipitated PPM1A (left panel) or PPM1B (right panel) was subjected to click chemistry reaction followed by immunoblot analysis. Myristoylated and total PPM1A or PPM1B was detected by Streptavidin-AF680 or total PPM1A or PPM1B antibodies and visualized by LI-COR Odyssey Blot Imager. (B) Co-localization of AMPK β1 and PPM1A (upper panel) or PPM1B (lower panel) was visualized by proximity ligation assay (PLA) in β1 knock-out (KO), WT or β1/2-G2A double knock-in (DKI) MEFs. Representative images shown were from at least two independent

experiments. Signal was quantified as mean fluorescence intensity (relative to WT) or number of dots per given field using ImageJ plugins. Scale bar = 10 μm. ****P<0.0001 as determined by unpaired t-test. All data are mean ± s.e.m.

Fig. 3. Ablation of AMPK β1 myristoylation increases liver AMPK activity and protects from high-fat diet-induced hepatic steatosis.

(A) Male age-matched 20-24-week-old β1-G2A and wild-type (WT) mice (n = 6-16) were fed *ad libitum* or fasted for 16 hours and livers isolated for immunoblot analysis. Densitometry analysis of (B) AMPK β1, (C) AMPK β2 and (D) AMPK pan α normalized to pan-actin signal. (E) mRNA expression analysis of AMPK α and β subunits in liver of *ad libitum* fed AMPK β1-G2A mice and WT controls (n = 14). (F) Densitometry analysis of ACC1/2 Ser79/Ser212 phosphorylation relative to ACC1 signal in immunoblots shown in A (n = 8). (G) Kinase activity of AMPK pan α immunoprecipitated from *ad libitum* fed and 16 hour-fasted β1-G2A and WT mice normalized for AMPK α recovered, as determined using separate immunoblots processed in parallel (n = 8). (H) Densitometry analysis of AMPK α-Thr172 phosphorylation in immunoblots shown in A and normalized for AMPK pan α (n = 12-16). (I) Time course of ACC1/2 Ser79/Ser212 and AMPK α-Thr172 phosphorylation in response to 0.25 mM AICAR in primary hepatocytes isolated from β1-G2A and WT mice. Total ACC was detected by enhanced chemoluminescence using streptavidin-HRP. Shown are representative immunoblots from 3-6 hepatocyte preparations. (J) Densitometry analysis of ACC1/2 Ser79/Ser212 phosphorylation of immunoblot shown in I, normalized to streptavidin-HRP signal (n = 6). (K) Haematoxylin & Eosin (H/E, top panel) and Oil Red O (ORO, bottom panel) staining of *ad libitum* fed β1-G2A mice and WT littermate controls on high-fat diet (HFD). Shown are representative images from n = 6 mice per condition. Scale bar, 50 μm for H/E and 20 μm for ORO. (L, M) Triglyceride content in liver tissue from *ad libitum* fed and 16-hour fasted β1-G2A and WT mice on (L) chow (n = 8-11) and (M) HFD (n = 7-10). (N) Triglyceride synthesis (n = 6) and (O) oxidation rates of [^{14}C]-palmitic acid to acid soluble metabolites (n = 7) in β1-G2A and WT primary hepatocytes. * P<0.05, ** P<0.01, *** P<0.001, **** P<0.0001 represent genotype differences. # P<0.05, ## P<0.01, ### P<0.001, #### P<0.0001 represent treatment effects as determined by two-way ANOVA and Šídák's post-hoc test. mRNA expression data (E) were analyzed by unpaired t-test. All data are mean ± s.e.m.

Fig. 4. AMPK β1-G2A mice show reduced adiposity and adaptations for increased brown fat lipid catabolism on a high-fat diet.

Male AMPK β1-G2A and wild-type (WT) mice were fed a chow (n=24-28) or high-fat diet (HFD) (n = 10-11) from 6 weeks of age and body mass and body composition measured weekly for 12-13 weeks. (A) Weekly body mass progression. (B) Weekly lean mass and (C) weekly fat mass as determined by nuclear magnetic resonance. (D) Epididymal fat pad mass relative to total body mass at 19-22 weeks of age (n=13-17 chow, n=19-21 HFD). (E) Haematoxylin/eosin-stained inguinal subcutaneous adipose tissue sections from chow (20-24-week-old) and HFD-fed (19-22-week-old) β1-G2A and WT mice. Representative sections from 6 mice per condition and genotype are shown. Scale bar 100 μm. (F) Frequency distribution of average adipocyte area of sections shown in (E) as analyzed from 3-4 representative images from 6 mice per condition and genotype. To enhance clarity, distributions of cells with area > 4000 μm^2 have been omitted from the graph. (G) Haematoxylin/eosin staining of interscapular brown adipose tissue sections from chow (20-24-week-old) and HFD-fed (19-22-week-old) β1-G2A and WT mice. Representative sections from 6 mice per condition and genotype are shown. Scale bar 50 μm. (H) mRNA expression analysis of *Ucp1* in brown adipose tissue of 20-24-week-old chow (n = 8-10) and *Ucp1* and genes involved in fatty acid oxidation or fatty acid synthesis in 19-22-week-old HFD-fed (n = 10-11) β1-G2A and WT mice. With the exception of (F), * $P<0.05$, ** $P<0.01$, *** $P<0.001$ represent genotype differences. Analyses of progression of body mass and body composition (A-C) were performed using repeated-measures two-way ANOVA with Šídák's post-hoc test. D and H were analyzed by unpaired t-test. Frequency distribution in F was calculated by GraphPad Prism software and differences within each area bin analyzed by multiple t-tests and corrected for multiple comparisons using the Holm- Šídák method. * $P<0.05$, ** $P<0.01$ represent differences between genotypes on chow diet; ## $P<0.01$ are differences between genotypes on HFD. All data are mean ± s.e.m.

Fig. 5. AMPK β1-G2A mice have improved insulin sensitivity with high-fat feeding.

(A) HFD-fed AMPK β1-G2A and WT mice (n = 24-25, 12 weeks of age) were fasted for 4 hours and subjected to an IPITT (1.2 U/kg lean mass) and (B) the area under the curve (AUC) analyzed. (C) IPGTT (1 g D-glucose/kg lean mass) of HFD-fed AMPK β1-G2A and WT mice (n=24-25, 13 weeks of age) fasted for 6 hours with AUC shown in (D). (E) Blood glucose (n=10-11) and (F) serum insulin (n=7-11) concentrations of *ad libitum* fed and 16 hour-fasted 19-20-week-old β1-G2A mice and WT littermates on HFD. (G) HOMA IR calculated from 16 h fasted glucose and insulin levels (n=10-11). * $P<0.05$, ** $P<0.01$ represent genotype differences. # $P<0.05$, ## $P<0.01$, #### $P<0.0001$ represent treatment differences. Analyses were performed by ordinary two-way ANOVA and Šídák's post-hoc test or unpaired t-test. All data are mean ± s.e.m.

MATERIAL AND METHODS

Antibodies and reagents

Antibodies against ACC (#3676), ACC1 (#4190), phospho-ACC (S79; #3661), Raptor (#2280), phospho-Raptor (S792; #2083), phospho-ULK1 (S555; #5869), AMPKα (#2532, Figure 1; #5831, Figures 3, 5, S4), AMPKα2 (#2757), phospho-AMPKα (T172; #2535), AMPKβ1 (#12063), AMPKβ2 (#4148), AMPKβ1/2 (#4150), pan-actin (#4968, Figure 3) and α/β-tubulin (#2148) were purchased from Cell Signaling Technology. Antibodies against AMPKγ1 (#ab32508, Figures 1, S2), PPM1A (#ab14824) and total OXPHOS rodent antibody cocktail (#ab1104113) were purchased from Abcam. Antibodies against AMPKα1 (#07-350) and β-actin (#A2228, Figure 1) were purchased from Sigma, AMPKγ1 (#1569-1, Figure 3A) from Epitomics, ULK1 (#20986-1-AP), PPM1A (#12961-1-AP) and PPM1B (#13193-1) from Proteintech Group and UCP1 (#UCP11-A) from Alpha Diagnostic. Antibodies against HSL and phospho-HSL (S565) were previously described (Watt et al., 2006). Antibody against AMPKβ1 (#27201) for immunoprecipitation and immunofluorescence was obtained from Signalway Antibody. Pan AMPKα (2-20) antibody used for immunoprecipitation in AMPK activity assays in liver tissue was generated in-house (Hamilton et al., 2001). AMPKα1 antibody used for assays of AMPK activity in MEFs was previously described (Bultot et al., 2016). Secondary antibodies for western blotting shown in Figures 1 and S2, Alexa FluorTM 680 Goat anti-rabbit IgG (H+L) (#A21109), Alexa FluorTM 680 Goat anti-mouse IgG (H+L) (#A21057), and Goat anti-Rabbit IgG (H+L) Highly Cross-Adsorbed Secondary Antibody Alexa Fluor 790 (#A11369), Streptavidin conjugates Alexa Fluor 680 (#S21378) and Alexa Fluor 790 (#S11378) were obtained from Invitrogen. Secondary antibodies used for immunoblotting shown in Figures 3 and S5-S7, HRP-conjugated Goat anti-Rabbit IgG (#P0448) and HRP-conjugated Goat anti-Mouse IgG (#P0447) were from Agilent Dako. HRP-conjugates streptavidin for detection of ACC in Figures 3, S5 and S7 (#ab7403) was purchased from Abcam. Proximity Ligation Assay kit (Duolink In Situ Red Starter Kit Mouse/Rabbit) was obtained from Sigma. siRNA oligonucleotides ON-TARGETplus SMARTPool targeting mouse PPM1A (#L-040052-00-0010) and mouse PPM1B (#L-040053-00-0010) were obtained from Horizon Discovery. Scrambled/negative control siRNA (#SIC005) was obtained from Sigma. 991 (5-[[6-chloro-5-(1-methylindol-5-yl)-1H-benzimidazol-2-yl]oxy]-2-methyl-benzoic acid) (CAS#: 129739-36-2) was synthesized by Spirochem (Basel, Switzerland) as

previously described (Ducommun et al., 2015). MK-8722 was obtained from Glixx Laboratories Inc (#GLXC-11445).

Animals

Prkab1^{G2A} (β1-G2A) and *Prkab2*^{G2A} (β2-G2A) KI mice were produced by the Mouse Engineering Garvan/ABR (MEGA) Facility using CRISPR/Cas9 gene targeting in C57BL/6J mouse embryos following established molecular and animal husbandry techniques (Yang et al., 2014). Single guide RNAs (sgRNA) were based on target sites in exon 2 of *Prkab1* (GAGCAGCGAGCGCGCCGCGC*TGG*) and *Prkab2* (TACCAGCGAGCGGGTGTCC*GGG*) (protospacer-associated motif = PAM italicised and underlined). In each case the specific sgRNA (15 ng/μl) was microinjected into the nucleus and cytoplasm of C57BL/6J zygotes together with polyadenylated *S. pyogenes* Cas9 mRNA (30 ng/μl) and a gene-specific 150 base single-stranded, anti-sense, deoxy-oligonucleotide homologous recombination substrate (15 ng/μl). For *Prkab1* the oligonucleotide encoded the G2A (GGC>GCC) substitution plus a PAM-inactivating silent mutation in the L11 codon (CTG>CTC), whilst for *Prkab2* the oligonucleotide encoded the G2A (GGA>GCA) substitution plus a PAM-inactivating silent mutation in the G11 codon (GGG>GGC) (**Fig. S1**). Founder males heterozygous for alleles that had been successfully modified by homologous recombination were backcrossed with C57BL/6J females to establish the β1-G2A and β2 G2A lines.

Breeding of β1-G2A and β2 G2A mouse lines was performed using heterozygous carriers of the KI mutation with biannual backcrosses to the C57BL/6Arc strain. For genotyping, tail samples were analyzed by TransnetYX using TaqMan-based real-time PCR. Mice homozygous for either the β1-G2A or β2-G2A mutation were crossed to generate β1/β2-G2A DKI mice for the isolation of mouse embryonic fibroblasts. Homozygous β1-G2A KI mice and WT mice derived from the same heterozygous founders were used for all other experiments. The study included only male mice due to limited availability of females for age-matched cohorts for metabolic studies while ensuring that sufficient females were available for colony maintenance. Mice were housed in pathogen-free microisolator cages on a 12-hour light-dark cycle. Mice were fed a standard chow diet (9% fat, 20% protein and 29% starch, with 12.8 MJ/kg of digestible energy, Barastoc, Ridley Agriproducts, Pakenham, Australia) or placed at 6-7 weeks of age on a HFD (23.5% fat, 18.4% protein and 22.8% starch, with 17 MJ/kg digestible energy, Specialty Feeds, Glen Forrest, Australia) for 12-13 weeks with *ad libitum*

access to water. For all experiments, mice were age-matched within two-four weeks of age, but otherwise randomized to their respective groups. The St. Vincent's Hospital (Melbourne, Australia) Animal Ethics Committee approved all experimental procedures (AEC 025/15 and AEC 013/19) in accordance with the National Health and Medical Research Council of Australia's (NHMRC) guidelines for the Ethical and Humane Use of Animals in research and Australian code of practice for the care and use of animals for scientific purposes (8th Edition 2013).

Generation of mouse embryonic fibroblasts

Mouse embryonic fibroblasts (MEFs) were isolated from homozygous WT, β1-G2A KI or β1/β2-G2A DKI embryos at days 12–13 post coitum. The head and internal organs were removed, and the remaining embryo body minced and trypsinized. After adding DMEM supplemented with 10% FBS and 1% penicillin-streptomycin, cells were centrifuged (500 g, 5 min, 4 °C) and medium replaced and the cell suspension was passed through a 40-μm cell strainer and plated in 10-cm dishes. Cells were cultured in DMEM supplemented with 10% FBS and 1% penicillin-streptomycin and passaged at 1:2 or 1:4 when confluent. MEFs were immortalized by transfection with an SV40 large T-antigen expression construct using Fugene HD transfection reagent (Promega).

Metabolic studies

Body composition analysis was performed by nuclear magnetic resonance imaging (Whole Body Composition Analyzer (EchoMRI)). Analysis of metabolic parameters, including energy expenditure, ambulatory activity, food intake and substrate preference was performed in 13-14-week-old mice using the Comprehensive Laboratory Animal Monitoring System (CLAMS, Columbus Instruments). Mice were individually housed with free access to water and either a standard laboratory chow or HFD and kept on a 12-hour light/dark cycle and temperature controlled at 21 °C throughout the experiment. Volumes of oxygen consumption (VO_2) and carbon dioxide production (VCO_2), food intake and ambulatory activity were measured continuously in 18-min intervals for 48 hours after a 24-hour acclimatization period. Food intake was recorded via scale measurement of a center-feeder while ambulatory activity was determined by the breaking of infrared beams within the cages. Respiratory exchange ratio (RER = VCO_2/VO_2) and energy expenditure (Heat = $(3.815+1.232*RER)*VO_2$) were

calculated from the measured gas exchange data. Energy expenditure data were normalized to lean mass measured at day 1 of the experiment.

Blood glucose concentrations were measured in 22-23-week-old chow-fed and 20-21-week-old HFD-fed mice on tail blood using a hand-held glucometer (Accu-Check Performa, Roche Diagnostics). For measurement of serum insulin concentrations, whole blood samples were collected using the submandibular method from 20-21-week-old chow and 19-20-week-old HFD-fed mice and left to clot at room temperature for 30 min followed by centrifugation at 1,500 g for 10 min. Insulin concentration was determined from supernatants using a mouse insulin ELISA (#10-1247-01, Mercodia).

Tissues for biochemical and histological analyses were dissected from 20-24-week-old chow or 19-22-week-old HFD-fed mice anaesthetized by ketamine/xylazine injection and snap-frozen in liquid nitrogen until further analyses or fixed in 10% formalin.

For glycogen measurements, tissue was homogenized in ddH_2O on ice using a hand-held homogenizer. After heating at 100 °C for 10 min, samples were centrifuged at 18,000 g for 10 min and glycogen concentrations determined from the supernatant using the Glycogen Assay Kit (#ab65620, Abcam). For triglyceride assays, liver tissue was homogenized in 6.5% NP-40/ddH2O at room temperature. Triglycerides were solubilized using 5 cycles of heating at 90 °C for 3 min and cooling to room temperature. Samples were centrifuged at 21,000 g, 4 °C and supernatants assayed using the Triglyceride Assay Kit (cat# ab65336, Abcam). Separate liver biopsies from the same animals were assayed for total fat content using the biopsy function of the EchoMRI Body Composition Analyzer.

Insulin and glucose tolerance testing

Tolerance tests were performed in 13-14-week-old chow- and 12-13-week-old HFD-fed mice. For insulin tolerance testing, mice were fasted for 4 hours followed by intraperitoneal insulin (Humulin, Eli Lilly) injection with 0.6 IU/kg lean mass for chow-fed animals and 1.2 IU/kg for HFD-fed animals. For glucose tolerance tests, mice were fasted for 6 hours and injected with 2 g D-glucose/kg lean mass for the chow-fed condition and 1 g D-glucose/kg lean mass for HFD-fed mice. D-glucose (Sigma-Aldrich) was dissolved in saline. Blood glucose concentrations were measured from tail blood using a hand-held glucometer (AccuCheck Performa, Roche Diagnostics). The area under the curve was analyzed using GraphPad Prism Software.

Histological analyses

For haematoxylin/eosin (H/E) staining, tissue samples from chow-fed (20-24 weeks) or HFD-fed (age 19-22 weeks) mice were fixed at room temperature for 48 hours in 10% neutral buffered formalin and transferred to 70% ethanol. After processing, samples were embedded in paraffin and sectioned at 5 μm using a microtome. Sections were de-waxed in histolene and after rehydration stained in Mayer's haematoxylin for 5 min, followed by blueing in Scott's tap water and incubation with eosin for 3 min. Samples were dehydrated and mounted using dibutylphthalate polystyrene xylene. Subcutaneous adipocyte size was determined by measuring the area of cells in 3-4 representative images per section and 6 mice per genotype using ImageJ. The frequency distribution of the number of cells per area size (bin 100 μm^2) was calculated using GraphPad Prism 9 software. For Oil Red O (ORO) staining, tissues were frozen in O.C.T. compound (#4583, Tissue-Tek®) and sectioned on a cryostat at 8 μm. Sections were fixed in 10% buffered formalin, washed in water and 60% isopropanol before staining in 60% ORO working solution for 15 min (stock solution: 1% ORO powder in isopropanol). The slides were then washed in 60% isopropanol and distilled water. To counterstain, sections were stained in Mayer's haematoxylin for 1 min and mounted with Faramount mounting medium (#S3025, Dako). The area of ORO staining was determined from averages of 3 representative images per mouse with 6 mice per diet and genotype using the thresholding function in ImageJ. Images were taken using a Leica DM-RB light microscope and relayed with an Olympus DP72 camera.

For UCP1 immunohistochemistry, subcutaneous adipose tissue was fixed with 10% formalin, embedded in paraffin and sectioned on a microtome at a thickness of 5 μm. Sections were de-waxed in histolene and after rehydration boiled in citrate antigen retrieval buffer (10 mM sodium citrate, pH 6.5) for 15 min. Endogenous peroxidases were quenched by incubation with 3% H_2O_2 in PBS for 15 min. Sections were blocked by incubation with 5% normal goat serum (NGS) in PBS for 40 min, followed by 15 min incubations each with avidin D and biotin (Avidin/Biotin Blocking Kit, #SP-2001, Vector Laboratories). Primary rabbit anti-UCP1 antibody (#ab10983, Abcam) was added at a concentration of 1: 500 in PBS/5% NGS for 2 hours at room temperature. After subsequent washes with PBS, sections were incubated with secondary biotinylated goat anti-rabbit antibody (#E0432, Agilent Technologies) at 1:1250 in PBS/5% NGS for 1 hour at room temperature. Following washes in PBS, secondary antibody binding was detected by incubating sections with VECTASTAIN ABC Peroxidase kit (#PK-

4005, Vector Laboratories) and DAB substrate kit (#SK-4100, Vector Laboratories) as per manufacturer's instructions. Sections were counterstained, dehydrated and mounted using dibutylphthalate polystyrene xylene. Images were taken under bright-field conditions using an Olympus BX61 microscope and Olympus DP71 camera.

Western blotting

Cells and tissues were homogenized in lysis buffer containing protease and phosphatase inhibitors as previously described (Ducommun et al., 2014; Scott et al., 2008). For immunoblotting of MEF lysates, 20 μg protein was resolved using Bolt 4-12%, Bis-Tris mini protein gels (#NW04125BOX, Thermo Fisher Scientific). Protein gels were transferred onto nitrocellulose membranes (#926-31092, LI-COR Biosciences) and incubated in primary antibody diluted in Tris-buffered saline/0.1% Tween 20 containing 5 % BSA overnight at 4 °C. After 1-hour incubation with secondary antibody conjugated to AF-680 at room temperature, membranes were scanned using Odyssey CLx Infrared Scanner. For immunoblotting of tissue homogenates, 20-50 μg total lysate was separated via SDS-PAGE, followed by transfer to an Immobilon-P PVDF membrane (Merck Millipore). Membranes were incubated overnight at 4 °C with primary antibody in PBS-Tween 20, followed by incubation with HRP-conjugated secondary antibodies in PBS-Tween 20 supplemented with 2.5 % skim milk. Proteins were detected by enhanced chemoluminescence and exposure to Super RX Medical X-ray Film (Fujifilm). Total ACC was determined by overnight incubation with streptavidin-HRP. To control for protein loading, signal obtained for phosphorylated ACC and AMPK were normalized to total ACC or AMPK α signal obtained from the same membrane after incubation in Restore PLUS Western blot stripping buffer (#46430, Thermo Fisher Scientific). The volume densities of the protein signals were quantified using Image Studio™ software (LI-COR Biosciences).

Immunoprecipitation

5μl of AMPKβ1 (#27201, Signalway Antibody), 5μl PP1MA (#ab14824, Abcam), or 2μg PP1MB (#13193-1, Proteintech Group) antibody was coupled to 5 μl of packed Protein G Sepharose beads (17-0618-01, GE Healthcare). 200 μg protein lysate was added to the beads-antibody conjugate and the tubes were incubated on a vibrating shaker (Vibramax) at 4 °C overnight. The beads/immune-complex were washed 3 times with cold lysis buffer and

resuspended in 25 µl of 1x Laemmli sample buffer containing 1 mM DTT and boiled at 95 °C for 5 min. The eluted proteins were separated by SDS-PAGE followed by immunoblotting.

Immunofluorescence

For immunofluorescence, 3 x 10^4 cells were plated per well in a µ-Slide 8 well (#80826, Ibidi). Cells were incubated with AMPK activator (10 µM 991 or MK-8722) or vehicle for 1 hour, followed by fixation in 4% paraformaldehyde for 15 min at room temperature. Cells were washed 3x with PBS-TritonX 0.01%., permeabilized and blocked with PBS-Saponin 0.1% containing 5% BSA for 1 hour at room temperature. Solution was aspirated and primary antibody diluted in PBS-TritonX 0.01% was added to the cells and incubated in the dark at 4 °C overnight. Next day, cells were washed 3x with PBS-TritonX 0.01%, 5 min each. Secondary antibody diluted in PBS- TritonX 0.01% was added to the cells and incubated for 45 min at room temperature in dark. Cells were washed 3x with PBS-TritonX 0.01%, 5 min each. To stain nuclei, Hoechst 33258 (#94403, Sigma) diluted 1:5000 in PBS was added to the cells and incubated for 5 min at room temperature. Cells were washed 3x with PBS and mounted using Fluoromount G mounting medium (#F4680, Sigma). Image acquisition was done on Zeiss780 confocal microscope using same settings for each condition.

siRNA knockdown

siRNA knockdown was carried out using Lipofectamine RNAiMAX transfection reagent (#133778075, Invitrogen). Briefly, cells were seeded in a 6-well plate a day before transfection. Next day, indicated siRNAs were introduced into cells as per the manufacturer's instructions. Cells were harvested 48 hours post-transfection for analysis.

Proximity ligation assay

Proximity ligation assay was carried out using Duolink In Situ Red Starter Kit Mouse/Rabbit (DUO92101, Sigma-Aldrich) following manufacturer's instruction. Briefly, 2.5 x 10^4 cells per well were seeded in a µ-slide angiogenesis chamber (#81506, Ibidi). 24 hours later, cells were fixed in 4% Paraformaldehyde for 15min at room temperature. Cells were washed 3x with PBS-TritonX-100 (0.01%), permeabilized and blocked with PBS-Saponin 0.1% containing 5% BSA for 1 hour at room temperature. Primary antibodies diluted in Duolink antibody dilution

buffer (1:100 AMPKβ1 (#27201, Signalway Antibody), 1:250 PPM1A (#12961-1, Proteintech Group) and 1:250 PPM1B ((#13193-1, Proteintech Group). were added to cells and incubated at 4 °C overnight protected from light. Next day, cells were washed 3x with PBS-TritonX, 5 min per wash. Proximity Ligation Assay probes (Rabbit Plus and Mouse Minus) diluted in antibody dilution buffer were added and incubated at 37 °C for 1 hour protected from light. Cells were washed 2x with PBS-TritonX, 5 min each wash. 15 µl ligation mix was added in each well and incubated at 37 °C for 30 min, followed by a washing step. 15 µl amplification mixture was added in each well and incubated at 37 °C for 100 min protected from light. Cells were washed 2x with PBS-TritonX, 5 min each wash. 15 ul mounting medium containing DAPI was added in each well. Image acquisition was done on Leica SP8 confocal microscope using same settings for each condition. Images were processed and analyzed in Fiji/ImageJ using the Common Tools Plugin (BioImaging And Optics Platform, École polytechnique fédérale de Lausanne). For quantification of mean intensity and number of spots per cell, an ImageJ script was used to define the Hoechst-stained nucleus as Region of Interest (ROI) in each cell and required parameters from the Red channel was measured for each ROI (cell).

Click chemistry

To assess myristoylation of AMPKβ1 or PP1MA/B click chemistry was performed using Click-IT myristic acid, azide (12-azidododecanoic acid) kit (C10268, Thermo Fisher Scientific). Briefly, 1 x 10^6 cells were plated in a 10-cm dish and experiments were performed when cells were 80% confluent. Cells were washed with PBS and fresh complete medium containing indicated concentrations of myristic acid-azide was added and incubated at 37 °C for indicated time points. Cells were lysed and AMPKβ1 or PPM1A/B were immunoprecipitated from cell lysates (500 µg) as described. The immunoprecipitants were subjected to click chemistry reaction using 40 µM biotin-alkyne solution and proteins subjected to methanol:chloroform precipitation following manufacturer's protocol. The dried protein precipitates were resolubilized in Laemmli sample buffer, separated by SDS-PAGE and subjected to immunoblotting as described. The myristoylated proteins were detected using Streptavidin Alexa Fluor conjugates.

Gene expression analysis

For mRNA expression analysis, liver and adipose tissue from 20-24-week-old mice were homogenized in Tri-Reagent (Sigma-Aldrich) and RNA isolated as per manufacturer's instructions. 500 ng of RNA was used to generate cDNA using the SuperScript IV Reverse Transcriptase Synthesis System (#18091050, Life Technologies). The PCR reaction was performed using the AmpliTaq Gold DNA Polymerase Kit (#4311806, Life Technologies) and specific TaqMan Gene Expression Assays (Thermo Fisher Scientific) on a Corbett Rotorgene 3000 (Corbett Research). The critical threshold (Ct) was manually set in the exponential phase and the Ct values determined by the Corbett Rotorgene instrument software. Relative expression was calculated using the comparative Ct ($2^{-\Delta\Delta Ct}$) method and normalized to eukaryotic 18S rRNA for liver samples and β-actin for adipose tissue analysis. The following TaqMan Gene Expressions were used: *Prkab1*, Mm01257133_m1; *Prkab2*, Mm01201921_m1; *Prkaa1*, Mm01296700_m1; *Prkaa2*, Mm01264789_m1; *Ucp1*, Mm01244861_m1; *Ppara*, Mm00440939_m1; *Ppargc1a*, Mm00447183_m1; *Cpt1b*, Mm00487200_m1, *Acadl*, Mm00599660_m1, *Acadm*, Mm00431611_m1; *Elovl3*, Mm00468164_m1; *Fasn*, Mm00662319_m1; *Scd1*, Mm00772290_m1; *Srebf1*, Mm00550338_m1; *Acaca*, Mm01304277_m1; *Acacb*, Mm01204683_m1; *Cs*, Mm00466043_m1; *Sdhd*, Mm00546511_m1; *Hadh*, Mm00492535_m1; *Ryr1*, Mm01175811_m1; *Atp2a1*, Mm01275320_m1; *Ckmt2*, Mm01285553_m1; *Myh4*, Mm01332541_m1; *Actb*, Mm02619580_g1; 18S, Hs99999901_s1.

AMPK activity assays

For AMPK activity assays, total AMPKα (pan-α antibody (Hamilton et al., 2001)) or AMPKa1 (custom-made antibody (Bultot et al., 2016)) was immunoprecipitated overnight at 4 °C from 1 mg of liver tissue homogenate or 250 ug of MEF cell lysates pre-conjugated to Protein-A Agarose or Protein-G Sepharose beads, respectively. The immunoprecipitants were subjected to *in vitro* kinases assay as previously described in detail (Scott et al., 2008).

De novo lipogenesis and fatty acid oxidation assays

Primary hepatocytes were isolated by collagenase perfusion and maintained in Medium 199 supplemented with 10% foetal bovine serum as previously described (Dzamko et al., 2010). The following day, cells were cultured for 2 hours in serum-free M199 followed by incubation with 5 μCi/mL [^{3}H] acetate (sodium) (Perkin Elmer) and 0.5 mM sodium acetate for 3 hours.

Medium was then removed and cells washed with PBS before lipid extraction using chloroform:methanol (2:1). For determination of triglyceride synthesis, the lipid fraction was removed, dried using a SpeedVac vacuum concentrator and redissolved in chloroform:methanol (2:1) supplemented with triglyceride standard (Sigma Aldrich) before separation on thin-layer chromatography (TLC) UNISIL silica GF plates (#40011, Analtech) in heptane:isopropylether:glacial acetic acid, 60:40:3. Plates were sprayed with dicholoroflurescein (0.02% w/v in EthOH) to visualize lipids and the triglyceride fraction was removed for liquid scintillation counting using a Tri-Carb 4810TR Liquid Scintillation Analyzer (Perkin Elmer). Triglyceride synthesis rates were calculated as nmol of ^{3}H-labeled acetate incorporated per milligram of cell protein per hour.

For fatty acid oxidation experiments, hepatocytes were incubated in serum-free Medium 199 for 2 hours followed by incubation with 0.5 μCi/ml [1-^{14}C]palmitic acid (Perkin Elmer), 0.25 mM palmitate (conjugated to 2% BSA) and 1 mM carnitine for 4 h. Medium was removed and cells acidified with 5% $HClO_4$ for 45 min at room temperature. The acid precipitate was removed by centrifugation and radioactivity of the supernatant measured by liquid scintillation counting to determine ^{14}C incorporation into acid soluble metabolites (ASM). Oxidation rates were calculated nmol of ^{14}C-labeled ASM per milligram of cell protein per hour.

Statistical analyses

All data are presented as mean ± s.e.m. and subjected to statistical analysis using GraphPad Prism 9 software. Sample size was estimated from our previously published studies (Dzamko et al., 2010; Fullerton et al., 2013). Statistical significance was determined using two-tailed unpaired t-test for a single variable unless otherwise stated. 1) Age-dependent body weight and body composition changes of mice on chow or HFD, 2) time-dependent metabolic parameters measured in CLAMS and 3) changes in blood glucose concentrations in tolerance tests were analyzed by repeated measures 2-way ANOVA followed by Šídák's post-hoc test. To evaluate the effect of body composition on energy expenditure, linear regression analysis and analysis of covariance (ANCOVA) with lean mass as covariate was performed using CalR (Mina et al., 2018). All remaining data comparing two variables (genotype, treatment) were analyzed by ordinary 2-way ANOVA with Šídák's post-hoc test. Significance was accepted at $P<0.05$.

REFERENCES

Alam, M.S. (2018). Proximity Ligation Assay (PLA). Curr Protoc Immunol *123*, e58.

Ali, N., Ling, N., Krishnamurthy, S., Oakhill, J.S., Scott, J.W., Stapleton, D.I., Kemp, B.E., Anand, G.S., and Gooley, P.R. (2016). beta-subunit myristoylation functions as an energy sensor by modulating the dynamics of AMP-activated Protein Kinase. Sci Rep *6*, 39417.

Bultot, L., Jensen, T.E., Lai, Y.C., Madsen, A.L., Collodet, C., Kviklyte, S., Deak, M., Yavari, A., Foretz, M., Ghaffari, S., et al. (2016). Benzimidazole derivative small-molecule 991 enhances AMPK activity and glucose uptake induced by AICAR or contraction in skeletal muscle. Am J Physiol Endocrinol Metab *311*, E706-E719.

Carling, D., Clarke, P.R., Zammit, V.A., and Hardie, D.G. (1989). Purification and characterization of the AMP-activated protein kinase. Copurification of acetyl-CoA carboxylase kinase and 3-hydroxy-3-methylglutaryl-CoA reductase kinase activities. Eur J Biochem *186*, 129-136.

Carling, D., Zammit, V.A., and Hardie, D.G. (1987). A common bicyclic protein kinase cascade inactivates the regulatory enzymes of fatty acid and cholesterol biosynthesis. FEBS Lett *223*, 217-222.

Chen, L., Jiao, Z.H., Zheng, L.S., Zhang, Y.Y., Xie, S.T., Wang, Z.X., and Wu, J.W. (2009). Structural insight into the autoinhibition mechanism of AMP-activated protein kinase. Nature *459*, 1146-1149.

Chida, T., Ando, M., Matsuki, T., Masu, Y., Nagaura, Y., Takano-Yamamoto, T., Tamura, S., and Kobayashi, T. (2013). N-Myristoylation is essential for protein phosphatases PPM1A and PPM1B to dephosphorylate their physiological substrates in cells. Biochem J *449*, 741-749.

Davies, S.P., Helps, N.R., Cohen, P.T., and Hardie, D.G. (1995). 5'-AMP inhibits dephosphorylation, as well as promoting phosphorylation, of the AMP-activated protein kinase. Studies using bacterially expressed human protein phosphatase-2C alpha and native bovine protein phosphatase-2AC. FEBS Lett *377*, 421-425.

Dite, T.A., Ling, N.X.Y., Scott, J.W., Hoque, A., Galic, S., Parker, B.L., Ngoei, K.R.W., Langendorf, C.G., O'Brien, M.T., Kundu, M., et al. (2017). The autophagy initiator ULK1 sensitizes AMPK to allosteric drugs. Nat Commun *8*, 571.

Ducommun, S., Deak, M., Sumpton, D., Ford, R.J., Nunez Galindo, A., Kussmann, M., Viollet, B., Steinberg, G.R., Foretz, M., Dayon, L., et al. (2015). Motif affinity and mass spectrometry proteomic approach for the discovery of cellular AMPK targets: identification of mitochondrial fission factor as a new AMPK substrate. Cell Signal *27*, 978-988.

Ducommun, S., Ford, R.J., Bultot, L., Deak, M., Bertrand, L., Kemp, B.E., Steinberg, G.R., and Sakamoto, K. (2014). Enhanced activation of cellular AMPK by dual-small molecule treatment: AICAR and A769662. Am J Physiol Endocrinol Metab *306*, E688-696.

Dzamko, N., van Denderen, B.J., Hevener, A.L., Jorgensen, S.B., Honeyman, J., Galic, S., Chen, Z.P., Watt, M.J., Campbell, D.J., Steinberg, G.R., et al. (2010). AMPK beta1 deletion reduces appetite, preventing obesity and hepatic insulin resistance. J Biol Chem *285*, 115-122.

Eissing, L., Scherer, T., Todter, K., Knippschild, U., Greve, J.W., Buurman, W.A., Pinnschmidt, H.O., Rensen, S.S., Wolf, A.M., Bartelt, A., et al. (2013). De novo lipogenesis in human fat and liver is linked to ChREBP-beta and metabolic health. Nat Commun *4*, 1528.

Fullerton, M.D., Galic, S., Marcinko, K., Sikkema, S., Pulinilkunnil, T., Chen, Z.P., O'Neill, H.M., Ford, R.J., Palanivel, R., O'Brien, M., et al. (2013). Single phosphorylation sites in Acc1 and Acc2 regulate lipid homeostasis and the insulin-sensitizing effects of metformin. Nat Med *19*, 1649-1654.

Garcia, D., Hellberg, K., Chaix, A., Wallace, M., Herzig, S., Badur, M.G., Lin, T., Shokhirev, M.N., Pinto, A.F.M., Ross, D.S., et al. (2019). Genetic Liver-Specific AMPK Activation Protects against Diet-Induced Obesity and NAFLD. Cell Rep *26*, 192-208 e196.

Garton, A.J., and Yeaman, S.J. (1990). Identification and role of the basal phosphorylation site on hormone-sensitive lipase. Eur J Biochem *191*, 245-250.

Gluais-Dagorn, P., Foretz, M., Steinberg, G.R., Batchuluun, B., Zawistowska-Deniziak, A., Lambooij, J.M., Guigas, B., Carling, D., Monternier, P.A., Moller, D.E., et al. (2021). Direct AMPK Activation Corrects NASH in Rodents Through Metabolic Effects and Direct Action on Inflammation and Fibrogenesis. Hepatol Commun.

Hamilton, S.R., Stapleton, D., O'Donnell, J.B., Jr., Kung, J.T., Dalal, S.R., Kemp, B.E., and Witters, L.A. (2001). An activating mutation in the gamma1 subunit of the AMP-activated protein kinase. FEBS Lett *500*, 163-168.

Hardie, D.G. (2011). AMP-activated protein kinase: an energy sensor that regulates all aspects of cell function. Genes Dev *25*, 1895-1908.

Hardie, D.G., Ross, F.A., and Hawley, S.A. (2012). AMPK: a nutrient and energy sensor that maintains energy homeostasis. Nat Rev Mol Cell Biol *13*, 251-262.

Hoffman, N.J., Whitfield, J., Janzen, N.R., Belhaj, M.R., Galic, S., Murray-Segal, L., Smiles, W.J., Ling, N.X.Y., Dite, T.A., Scott, J.W., et al. (2020). Genetic loss of AMPK-glycogen binding destabilises AMPK and disrupts metabolism. Mol Metab *41*, 101048.

Katwan, O.J., Alghamdi, F., Almabrouk, T.A., Mancini, S.J., Kennedy, S., Oakhill, J.S., Scott, J.W., and Salt, I.P. (2019). AMP-activated protein kinase complexes containing the beta2 regulatory subunit are up-regulated during and contribute to adipogenesis. Biochem J *476*, 1725-1740.

Kersten, S., Seydoux, J., Peters, J.M., Gonzalez, F.J., Desvergne, B., and Wahli, W. (1999). Peroxisome proliferator-activated receptor alpha mediates the adaptive response to fasting. J Clin Invest *103*, 1489-1498.

Kim, S., Yang, X., Li, Q., Wu, M., Costyn, L., Beharry, Z., Bartlett, M.G., and Cai, H. (2017). Myristoylation of Src kinase mediates Src-induced and high-fat diet-accelerated prostate tumor progression in mice. J Biol Chem *292*, 18422-18433.

Lewis, G.F., Carpentier, A., Adeli, K., and Giacca, A. (2002). Disordered fat storage and mobilization in the pathogenesis of insulin resistance and type 2 diabetes. Endocr Rev *23*, 201-229.

Liang, J., Xu, Z.X., Ding, Z., Lu, Y., Yu, Q., Werle, K.D., Zhou, G., Park, Y.Y., Peng, G., Gambello, M.J., et al. (2015). Myristoylation confers noncanonical AMPK functions in autophagy selectivity and mitochondrial surveillance. Nat Commun *6*, 7926.

Mina, A.I., LeClair, R.A., LeClair, K.B., Cohen, D.E., Lantier, L., and Banks, A.S. (2018). CalR: A Web-Based Analysis Tool for Indirect Calorimetry Experiments. Cell Metab *28*, 656-666 e651.

Mitchelhill, K.I., Michell, B.J., House, C.M., Stapleton, D., Dyck, J., Gamble, J., Ullrich, C., Witters, L.A., and Kemp, B.E. (1997). Posttranslational modifications of the 5'-AMP-activated protein kinase beta1 subunit. J Biol Chem *272*, 24475-24479.

Moore, I., and Murphy, A. (2009). Validating the location of fluorescent protein fusions in the endomembrane system. Plant Cell *21*, 1632-1636.

Mottillo, E.P., Desjardins, E.M., Crane, J.D., Smith, B.K., Green, A.E., Ducommun, S., Henriksen, T.I., Rebalka, I.A., Razi, A., Sakamoto, K., et al. (2016). Lack of Adipocyte AMPK Exacerbates Insulin Resistance and Hepatic Steatosis through Brown and Beige Adipose Tissue Function. Cell Metab *24*, 118-129.

Narkar, V.A., Downes, M., Yu, R.T., Embler, E., Wang, Y.X., Banayo, E., Mihaylova, M.M., Nelson, M.C., Zou, Y., Juguilon, H., et al. (2008). AMPK and PPARdelta agonists are exercise mimetics. Cell *134*, 405-415.

Oakhill, J.S., Chen, Z.P., Scott, J.W., Steel, R., Castelli, L.A., Ling, N., Macaulay, S.L., and Kemp, B.E. (2010). beta-Subunit myristoylation is the gatekeeper for initiating metabolic stress sensing by AMP-activated protein kinase (AMPK). Proc Natl Acad Sci U S A *107*, 19237-19241.

Polekhina, G., Gupta, A., Michell, B.J., van Denderen, B., Murthy, S., Feil, S.C., Jennings, I.G., Campbell, D.J., Witters, L.A., Parker, M.W., et al. (2003). AMPK beta subunit targets metabolic stress sensing to glycogen. Curr Biol *13*, 867-871.

Pollard, A.E., Martins, L., Muckett, P.J., Khadayate, S., Bornot, A., Clausen, M., Admyre, T., Bjursell, M., Fiadeiro, R., Wilson, L., et al. (2019). AMPK activation protects against diet induced obesity through Ucp1-independent thermogenesis in subcutaneous white adipose tissue. Nat Metab *1*, 340-349.

Postic, C., and Girard, J. (2008). Contribution of de novo fatty acid synthesis to hepatic steatosis and insulin resistance: lessons from genetically engineered mice. J Clin Invest *118*, 829-838.

Qi, J., Gong, J., Zhao, T., Zhao, J., Lam, P., Ye, J., Li, J.Z., Wu, J., Zhou, H.M., and Li, P. (2008). Downregulation of AMP-activated protein kinase by Cidea-mediated ubiquitination and degradation in brown adipose tissue. EMBO J *27*, 1537-1548.
Resh, M.D. (2013). Covalent lipid modifications of proteins. Curr Biol *23*, R431-435.
Rhein, P., Desjardins, E.M., Rong, P., Ahwazi, D., Bonhoure, N., Stolte, J., Santos, M.D., Ovens, A.J., Ehrlich, A.M., Sanchez Garcia, J.L., et al. (2021). Compound- and fiber type-selective requirement of AMPKgamma3 for insulin-independent glucose uptake in skeletal muscle. Mol Metab *51*, 101228.
Sanders, M.J., Grondin, P.O., Hegarty, B.D., Snowden, M.A., and Carling, D. (2007). Investigating the mechanism for AMP activation of the AMP-activated protein kinase cascade. Biochem J *403*, 139-148.
Scott, J.W., van Denderen, B.J., Jorgensen, S.B., Honeyman, J.E., Steinberg, G.R., Oakhill, J.S., Iseli, T.J., Koay, A., Gooley, P.R., Stapleton, D., et al. (2008). Thienopyridone drugs are selective activators of AMP-activated protein kinase beta1-containing complexes. Chem Biol *15*, 1220-1230.
Sim, A.T., and Hardie, D.G. (1988). The low activity of acetyl-CoA carboxylase in basal and glucagon-stimulated hepatocytes is due to phosphorylation by the AMP-activated protein kinase and not cyclic AMP-dependent protein kinase. FEBS Lett *233*, 294-298.
Smith, B.K., Marcinko, K., Desjardins, E.M., Lally, J.S., Ford, R.J., and Steinberg, G.R. (2016). Treatment of nonalcoholic fatty liver disease: role of AMPK. Am J Physiol Endocrinol Metab *311*, E730-E740.
Smith, G.I., Shankaran, M., Yoshino, M., Schweitzer, G.G., Chondronikola, M., Beals, J.W., Okunade, A.L., Patterson, B.W., Nyangau, E., Field, T., et al. (2020). Insulin resistance drives hepatic de novo lipogenesis in nonalcoholic fatty liver disease. J Clin Invest *130*, 1453-1460.
Steinberg, G.R., and Kemp, B.E. (2009). AMPK in Health and Disease. Physiol Rev *89*, 1025-1078.
Steinberg, G.R., Michell, B.J., van Denderen, B.J., Watt, M.J., Carey, A.L., Fam, B.C., Andrikopoulos, S., Proietto, J., Gorgun, C.Z., Carling, D., et al. (2006). Tumor necrosis factor alpha-induced skeletal muscle insulin resistance involves suppression of AMP-kinase signaling. Cell Metab *4*, 465-474.
Timlin, M.T., and Parks, E.J. (2005). Temporal pattern of de novo lipogenesis in the postprandial state in healthy men. Am J Clin Nutr *81*, 35-42.
Timms, R.T., Zhang, Z., Rhee, D.Y., Harper, J.W., Koren, I., and Elledge, S.J. (2019). A glycine-specific N-degron pathway mediates the quality control of protein N-myristoylation. Science *365*.
Voss, M., Paterson, J., Kelsall, I.R., Martin-Granados, C., Hastie, C.J., Peggie, M.W., and Cohen, P.T. (2011). Ppm1E is an in cellulo AMP-activated protein kinase phosphatase. Cell Signal *23*, 114-124.
Warden, S.M., Richardson, C., O'Donnell, J., Jr., Stapleton, D., Kemp, B.E., and Witters, L.A. (2001). Post-translational modifications of the beta-1 subunit of AMP-activated protein kinase affect enzyme activity and cellular localization. Biochem J *354*, 275-283.
Watt, M.J., Holmes, A.G., Pinnamaneni, S.K., Garnham, A.P., Steinberg, G.R., Kemp, B.E., and Febbraio, M.A. (2006). Regulation of HSL serine phosphorylation in skeletal muscle and adipose tissue. Am J Physiol Endocrinol Metab *290*, E500-508.
Wen, Z., Jin, K., Shen, Y., Yang, Z., Li, Y., Wu, B., Tian, L., Shoor, S., Roche, N.E., Goronzy, J.J., et al. (2019). N-myristoyltransferase deficiency impairs activation of kinase AMPK and promotes synovial tissue inflammation. Nat Immunol *20*, 313-325.
Woods, A., Williams, J.R., Muckett, P.J., Mayer, F.V., Liljevald, M., Bohlooly, Y.M., and Carling, D. (2017). Liver-Specific Activation of AMPK Prevents Steatosis on a High-Fructose Diet. Cell Rep *18*, 3043-3051.
Wu, J., Puppala, D., Feng, X., Monetti, M., Lapworth, A.L., and Geoghegan, K.F. (2013). Chemoproteomic analysis of intertissue and interspecies isoform diversity of AMP-activated protein kinase (AMPK). J Biol Chem *288*, 35904-35912.
Xiao, B., Sanders, M.J., Carmena, D., Bright, N.J., Haire, L.F., Underwood, E., Patel, B.R., Heath, R.B., Walker, P.A., Hallen, S., et al. (2013). Structural basis of AMPK regulation by small molecule activators. Nat Commun *4*, 3017.
Xiao, B., Sanders, M.J., Underwood, E., Heath, R., Mayer, F.V., Carmena, D., Jing, C., Walker, P.A., Eccleston, J.F., Haire, L.F., et al. (2011). Structure of mammalian AMPK and its regulation by ADP. Nature *472*, 230-233.

Yang, H., Wang, H., and Jaenisch, R. (2014). Generating genetically modified mice using CRISPR/Cas-mediated genome engineering. Nat Protoc *9*, 1956-1968.
Yang, J., Maika, S., Craddock, L., King, J.A., and Liu, Z.M. (2008). Chronic activation of AMP-activated protein kinase-alpha1 in liver leads to decreased adiposity in mice. Biochem Biophys Res Commun *370*, 248-253.
Yang, M., Zhang, D., Zhao, Z., Sit, J., Saint-Sume, M., Shabandri, O., Zhang, K., Yin, L., and Tong, X. (2020). Hepatic E4BP4 induction promotes lipid accumulation by suppressing AMPK signaling in response to chemical or diet-induced ER stress. FASEB J *34*, 13533-13547.
Zhang, Y.L., Guo, H., Zhang, C.S., Lin, S.Y., Yin, Z., Peng, Y., Luo, H., Shi, Y., Lian, G., Zhang, C., et al. (2013). AMP as a low-energy charge signal autonomously initiates assembly of AXIN-AMPK-LKB1 complex for AMPK activation. Cell Metab *18*, 546-555.
Zhang, Z., Zhang, H., Li, B., Meng, X., Wang, J., Zhang, Y., Yao, S., Ma, Q., Jin, L., Yang, J., et al. (2014). Berberine activates thermogenesis in white and brown adipose tissue. Nat Commun *5*, 5493.

Figure 1

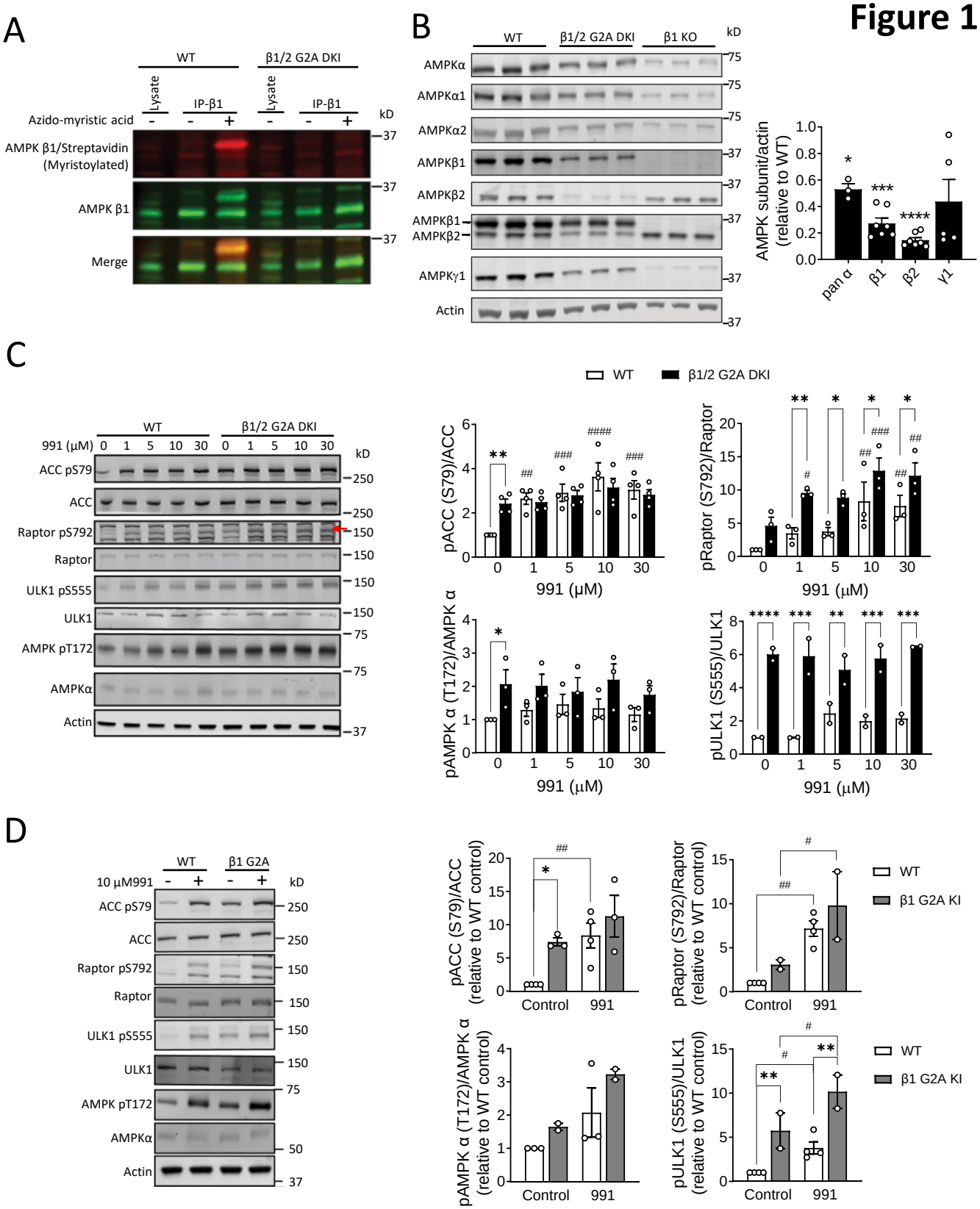
A
WT
β1/2 G2A DKI
Lysate
IP-β1
Azido-myristic acid
kD
AMPK β1/Streptavidin (Myristoylated)
AMPK β1
Merge
B
WT
β1/2 G2A DKI
β1 KO
kD
AMPKα
AMPKα1
AMPKα2
AMPKβ1
AMPKβ2
AMPKγ1
Actin
AMPK subunit/actin (relative to WT)
pan α
β1
β2
γ1
C
991 (μM)
ACC pS79
ACC
Raptor pS792
Raptor
ULK1 pS555
ULK1
AMPK pT172
AMPKα
Actin
pACC (S79)/ACC
pRaptor (S792)/Raptor
pAMPK α (T172)/AMPK α
pULK1 (S555)/ULK1
991 (μM)
D
10 μM991
β1 G2A
pACC (S79)/ACC (relative to WT control)
pRaptor (S792)/Raptor (relative to WT control)
pAMPK α (T172)/AMPK α (relative to WT control)
pULK1 (S555)/ULK1 (relative to WT control)
Control
991
β1 G2A KI

Figure 2

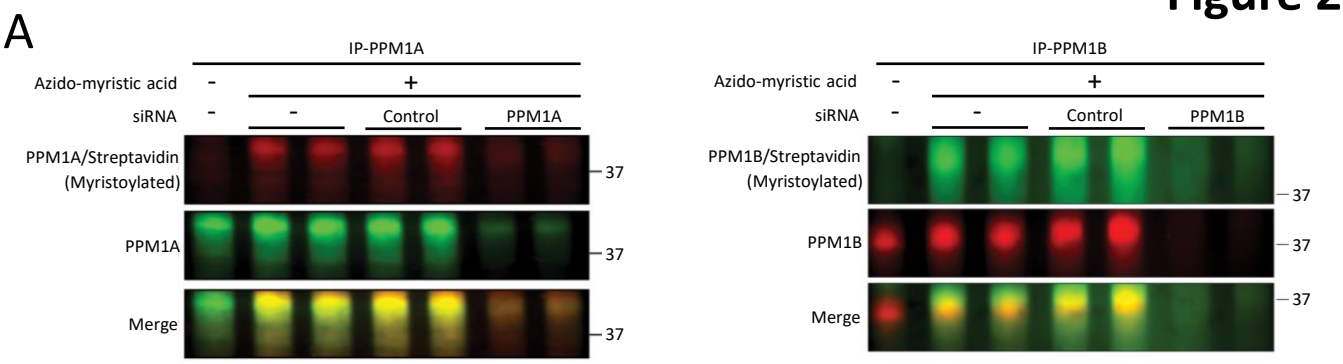
A
IP-PPM1A
Azido-myristic acid
siRNA
Control
PPM1A
PPM1A/Streptavidin (Myristoylated)
PPM1A
Merge
37
IP-PPM1B
PPM1B
PPM1B/Streptavidin (Myristoylated)

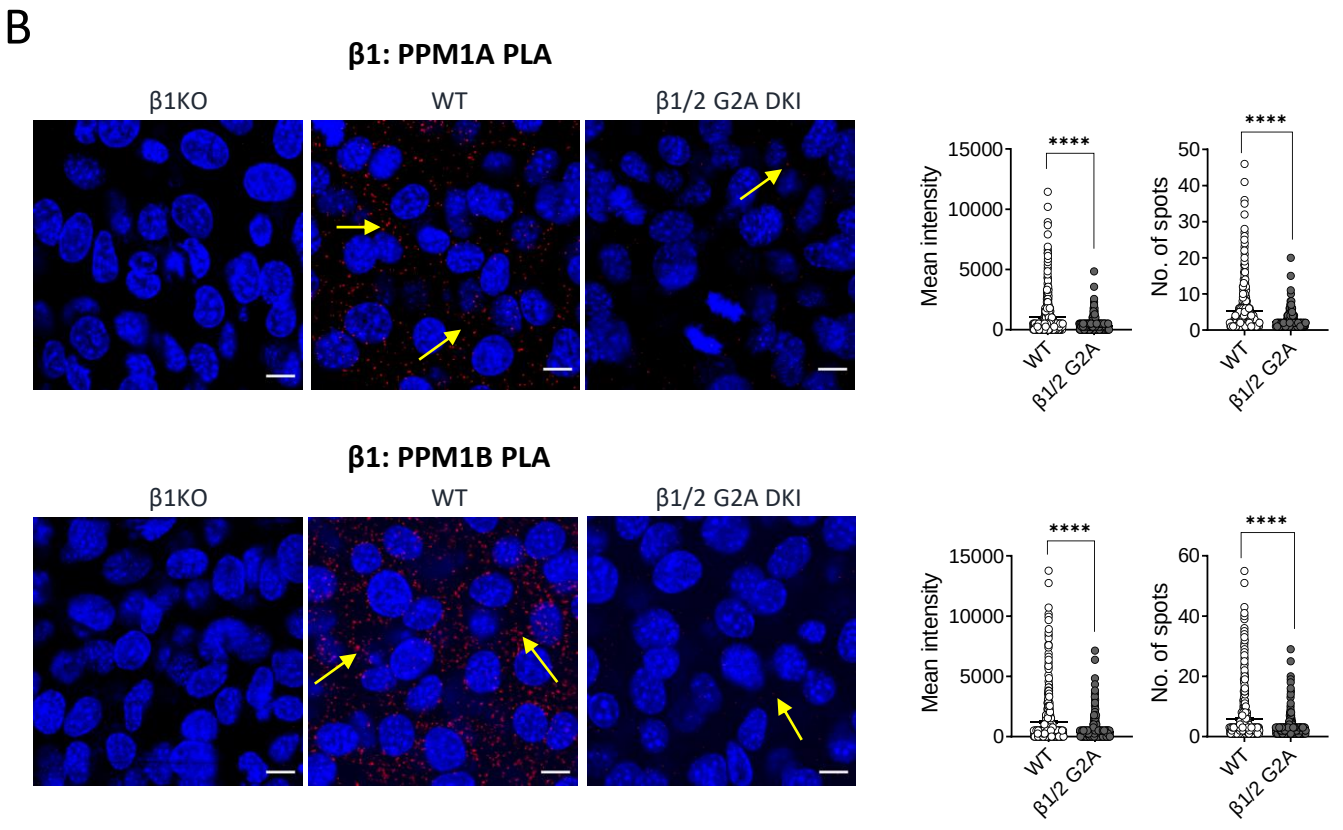
B
β1: PPM1A PLA
β1KO
WT
β1/2 G2A DKI
Mean intensity
No. of spots
****
β1: PPM1B PLA

Figure 3

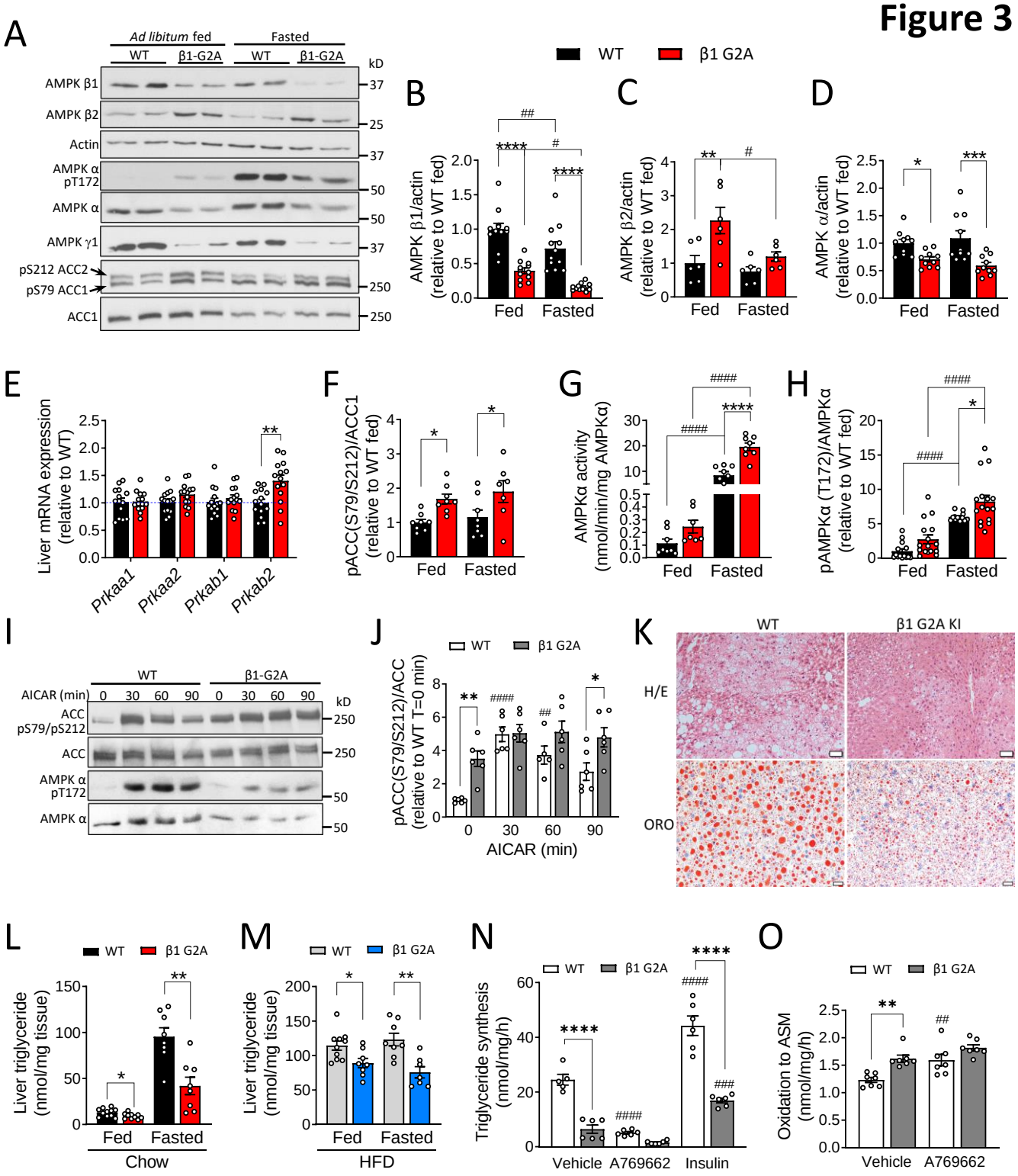
A
Ad libitum fed
Fasted
WT
β1-G2A
WT
β1-G2A
kD
AMPK β1
AMPK β2
Actin
AMPK α pT172
AMPK α
AMPK γ1
pS212 ACC2
pS79 ACC1
ACC1
37
25
37
50
50
37
250
250
WT
β1 G2A
B
AMPK β1/actin (relative to WT fed)
C
AMPK β2/actin (relative to WT fed)
D
AMPK α/actin (relative to WT fed)
Fed
Fasted
E
Liver mRNA expression (relative to WT)
Prkaa1
Prkaa2
Prkab1
Prkab2
F
pACC(S79/S212)/ACC1 (relative to WT fed)
G
AMPKα activity (nmol/min/mg AMPKα)
H
pAMPKα (T172)/AMPKα (relative to WT fed)
I
WT
β1-G2A
AICAR (min)
0
30
60
90
kD
ACC pS79/pS212
ACC
AMPK α pT172
AMPK α
250
250
50
50
J
pACC(S79/S212)/ACC (relative to WT T=0 min)
AICAR (min)
K
WT
β1 G2A KI
H/E
ORO
L
Liver triglyceride (nmol/mg tissue)
Chow
M
HFD
N
Triglyceride synthesis (nmol/mg/h)
Vehicle
A769662
Insulin
O
Oxidation to ASM (nmol/mg/h)
Vehicle
A769662

Figure 4

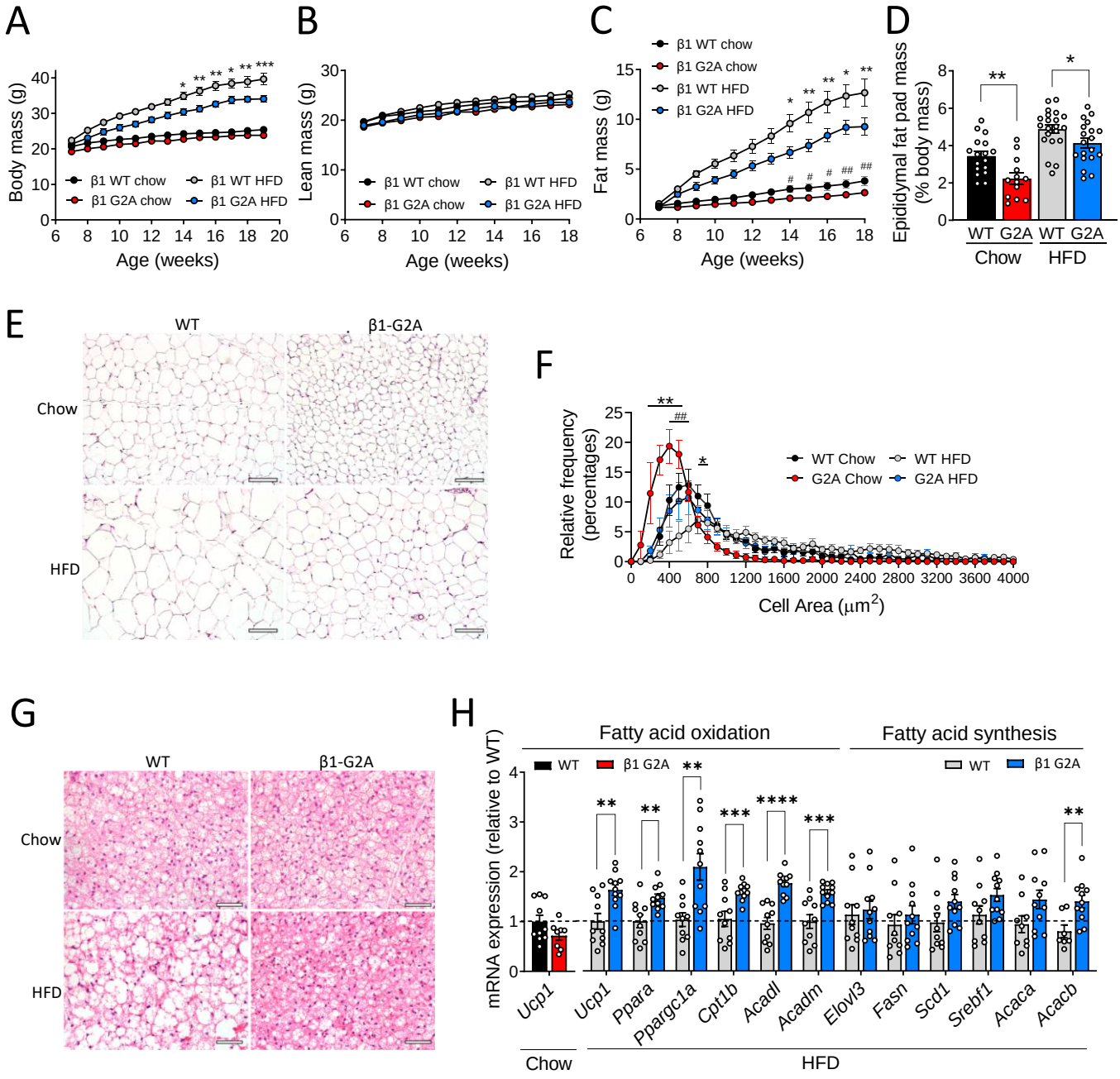
A
Body mass (g)
Age (weeks)
β1 WT chow
β1 G2A chow
β1 WT HFD
β1 G2A HFD
B
Lean mass (g)
Age (weeks)
C
Fat mass (g)
Age (weeks)
D
Epididymal fat pad mass (% body mass)
WT G2A WT G2A
Chow HFD
E
WT
β1-G2A
Chow
HFD
F
Relative frequency (percentages)
Cell Area (μm2)
WT Chow
G2A Chow
WT HFD
G2A HFD
G
WT
β1-G2A
Chow
HFD
H
Fatty acid oxidation
Fatty acid synthesis
WT
β1 G2A
mRNA expression (relative to WT)
Ucp1
Ucp1
Ppara
Ppargc1a
Cpt1b
Acadl
Acadm
Elovl3
Fasn
Scd1
Srebf1
Acaca
Acacb
Chow
HFD

Figure 5

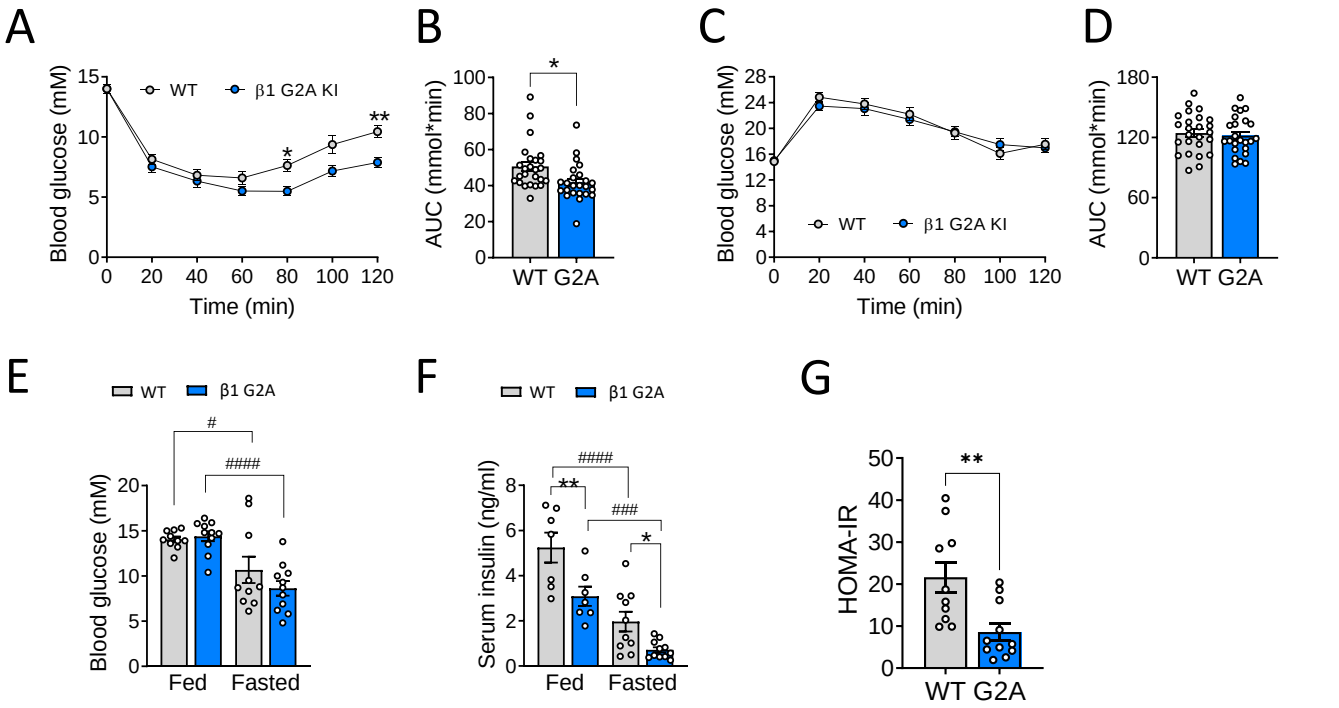
A
Blood glucose (mM)
WT
β1 G2A KI
Time (min)
B
AUC (mmol*min)
WT G2A
C
Blood glucose (mM)
WT
β1 G2A KI
Time (min)
D
AUC (mmol*min)
WT G2A
E
WT
β1 G2A
Blood glucose (mM)
Fed
Fasted
F
WT
β1 G2A
Serum insulin (ng/ml)
Fed
Fasted
G
HOMA-IR
WT G2A

Figure S1

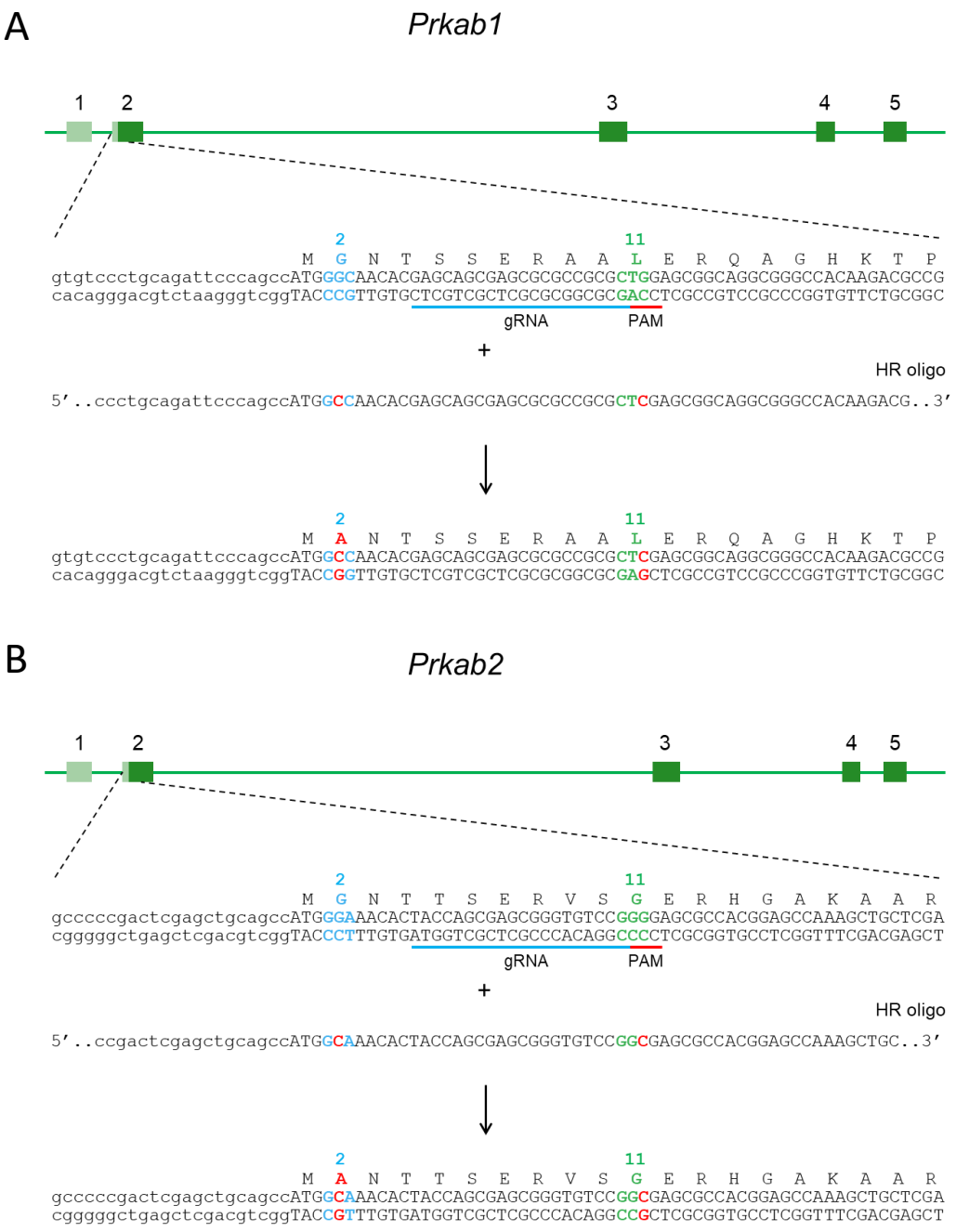
A
Prkab1
1 2 3 4 5
2 11
M G N T S S E R A A L E R Q A G H K T P
gtgtccctgcagattcccagccATGGGCAACACGAGCAGCGAGCGCGCCGCGCTGGAGCGGCAGGCGGGCCACAAGACGCCG
cacagggacgtctaagggtcggTACCCGTTGTGCTCGTCGCTCGCGCGGCGCGACCTCGCCGTCCGCCCGGTGTTCTGCGGC
gRNA
PAM
+
HR oligo
5'..ccctgcagattcccagccATGGCCAACACGAGCAGCGAGCGCGCCGCGCTCGAGCGGCAGGCGGGCCACAAGACG..3'
2 11
M A N T S S E R A A L E R Q A G H K T P
gtgtccctgcagattcccagccATGGCCAACACGAGCAGCGAGCGCGCCGCGCTCGAGCGGCAGGCGGGCCACAAGACGCCG
cacagggacgtctaagggtcggTACCGGTTGTGCTCGTCGCTCGCGCGGCGCGAGCTCGCCGTCCGCCCGGTGTTCTGCGGC
B
Prkab2
1 2 3 4 5
2 11
M G N T T S E R V S G E R H G A K A A R
gcccccgactcgagctgcagccATGGGAAACACTACCAGCGAGCGGGTGTCCGGGGAGCGCCACGGAGCCAAAGCTGCTCGA
cgggggctgagctcgacgtcggTACCCTTTGTGATGGTCGCTCGCCCACAGGCCCCTCGCGGTGCCTCGGTTTCGACGAGCT
gRNA
PAM
+
HR oligo
5'..ccgactcgagctgcagccATGGCAAACACTACCAGCGAGCGGGTGTCCGGCGAGCGCCACGGAGCCAAAGCTGC..3'
2 11
M A N T T S E R V S G E R H G A K A A R
gcccccgactcgagctgcagccATGGCAAACACTACCAGCGAGCGGGTGTCCGGCGAGCGCCACGGAGCCAAAGCTGCTCGA
cgggggctgagctcgacgtcggTACCGTTTGTGATGGTCGCTCGCCCACAGGCCGCTCGCGGTGCCTCGGTTTCGACGAGCT

Figure S2

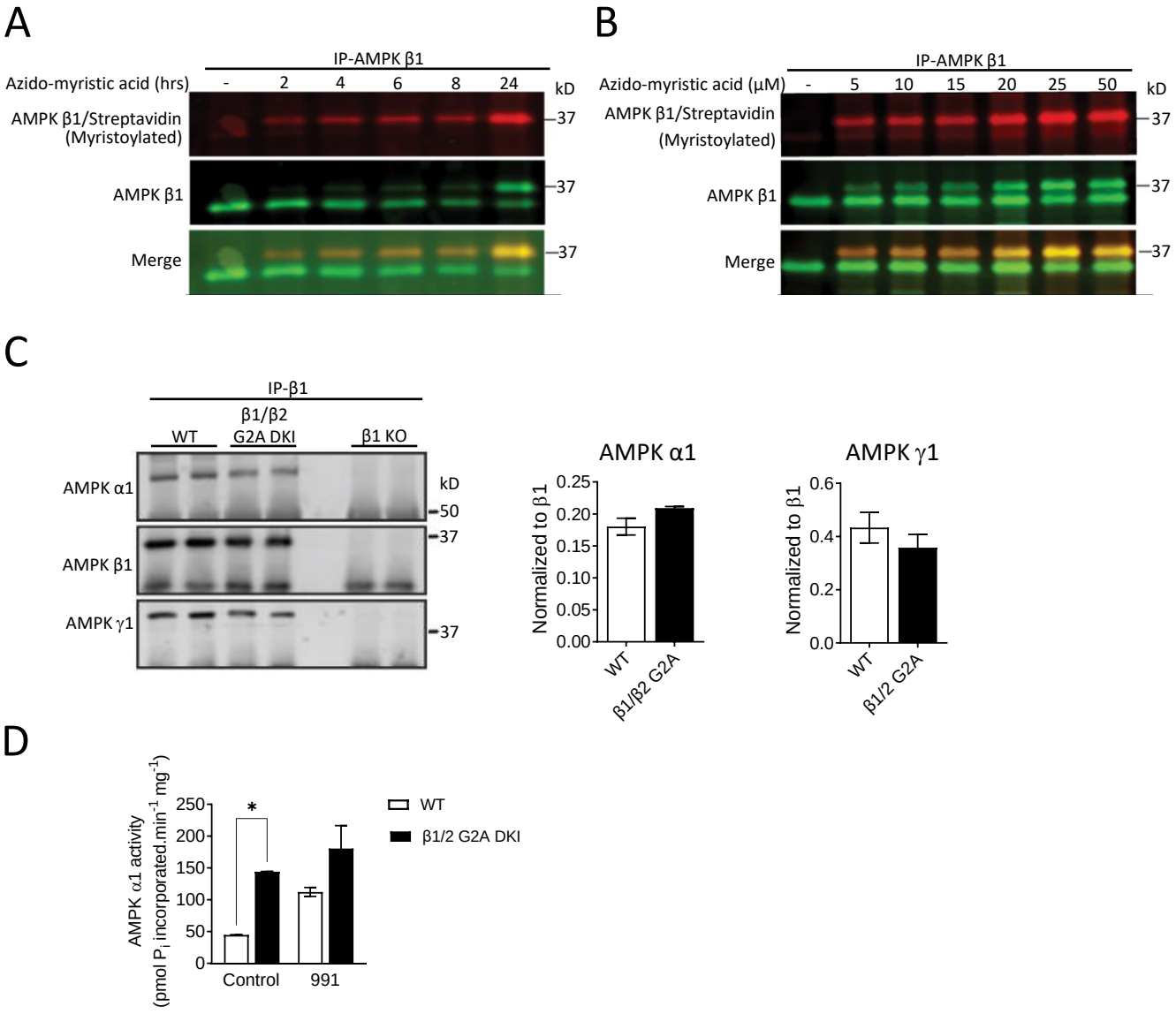
A
IP-AMPK β1
Azido-myristic acid (hrs)
- 2 4 6 8 24
kD
AMPK β1/Streptavidin (Myristoylated)
AMPK β1
Merge
37
B
IP-AMPK β1
Azido-myristic acid (μM)
- 5 10 15 20 25 50
kD
AMPK β1/Streptavidin (Myristoylated)
AMPK β1
Merge
37
C
IP-β1
β1/β2
WT
G2A DKI
β1 KO
AMPK α1
AMPK β1
AMPK γ1
kD
50
37
AMPK α1
Normalized to β1
0.25
0.20
0.15
0.10
0.05
0.00
WT
β1/β2 G2A
AMPK γ1
Normalized to β1
0.6
0.4
0.2
0.0
WT
β1/2 G2A
D
AMPK α1 activity
(pmol Pi incorporated.min-1 mg-1)
250
200
150
100
50
0
*
Control
991
WT
β1/2 G2A DKI

Figure S3

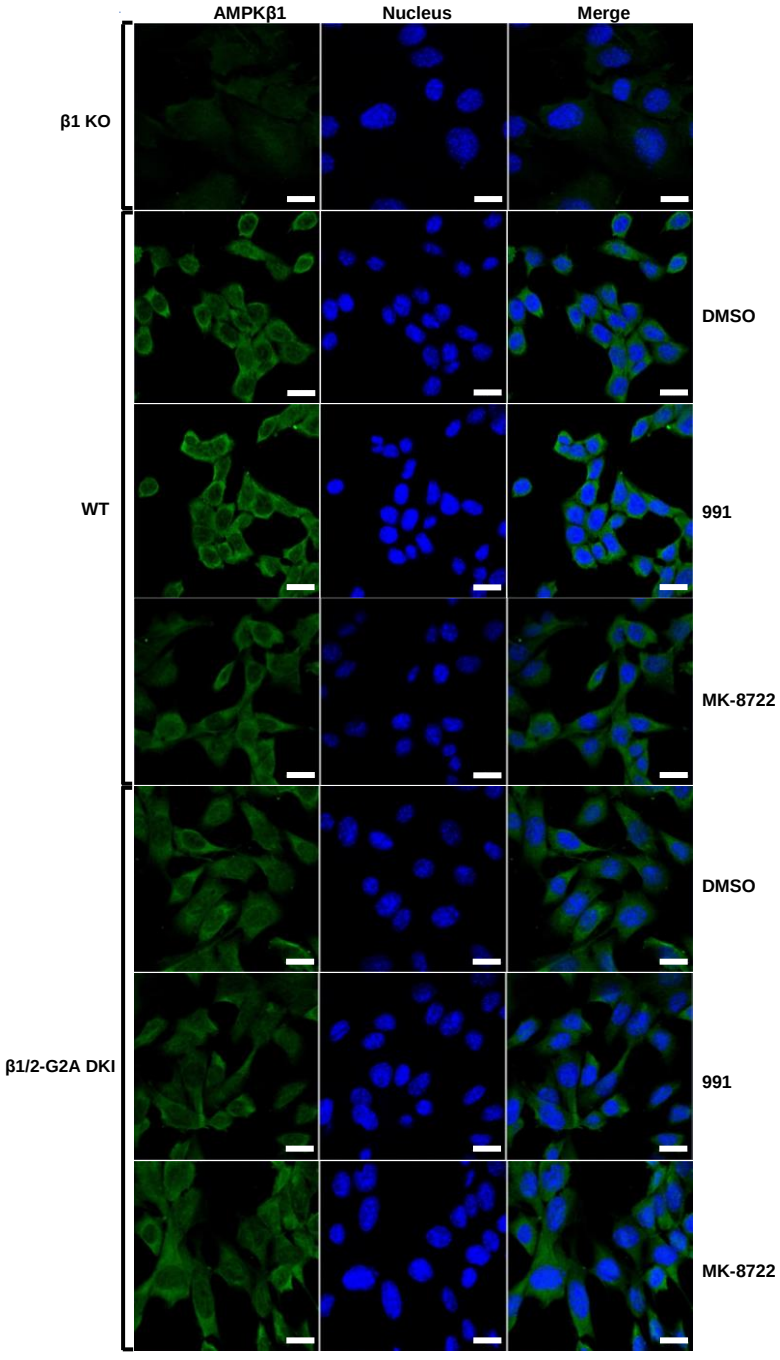
AMPKβ1
Nucleus
Merge
β1 KO
WT
β1/2-G2A DKI
DMSO
991
MK-8722
DMSO
991
MK-8722

Figure S4

A

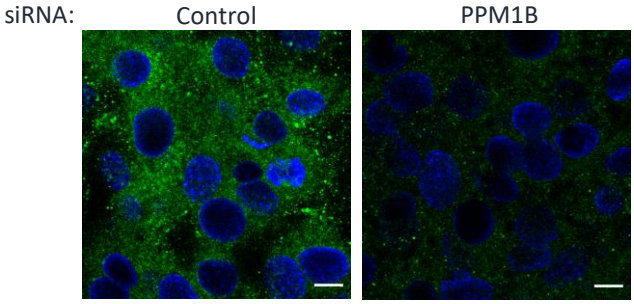
siRNA:
Control
PPM1B

B

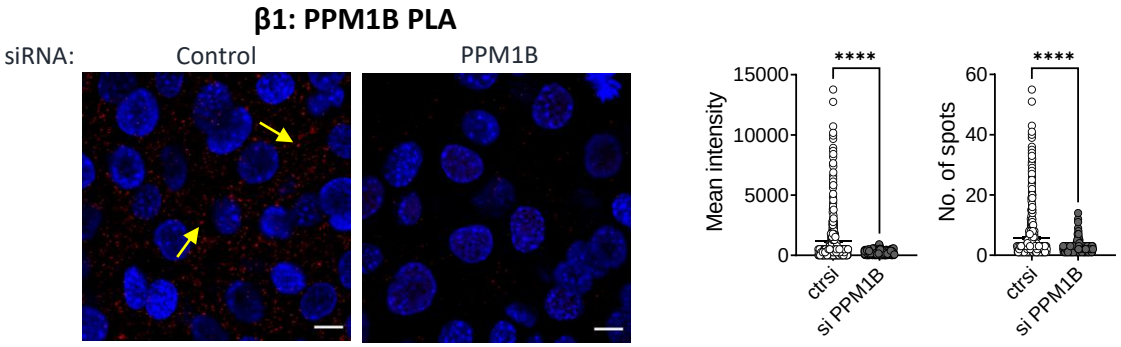
β1: PPM1B PLA
siRNA:
Control
PPM1B
Mean intensity
15000
10000
5000
0
****
ctrsi
si PPM1B
No. of spots
60
40
20
0
****
ctrsi
si PPM1B

Figure S5

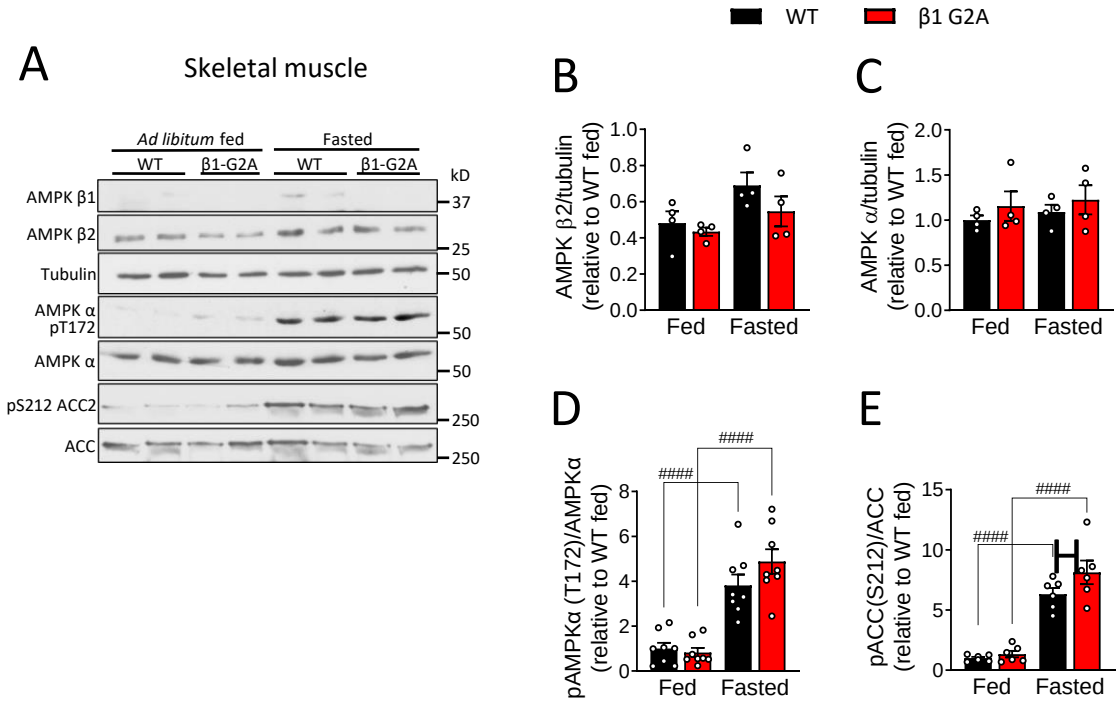
A
Skeletal muscle
Ad libitum fed
Fasted
WT
β1-G2A
WT
β1-G2A
kD
AMPK β1
AMPK β2
Tubulin
AMPK α pT172
AMPK α
pS212 ACC2
ACC
37
25
50
50
50
250
250
WT
β1 G2A
B
AMPK β2/tubulin (relative to WT fed)
Fed
Fasted
C
AMPK α/tubulin (relative to WT fed)
Fed
Fasted
D
pAMPKα (T172)/AMPKα (relative to WT fed)
####
####
Fed
Fasted
E
pACC(S212)/ACC (relative to WT fed)
####
####
Fed
Fasted

Figure S6

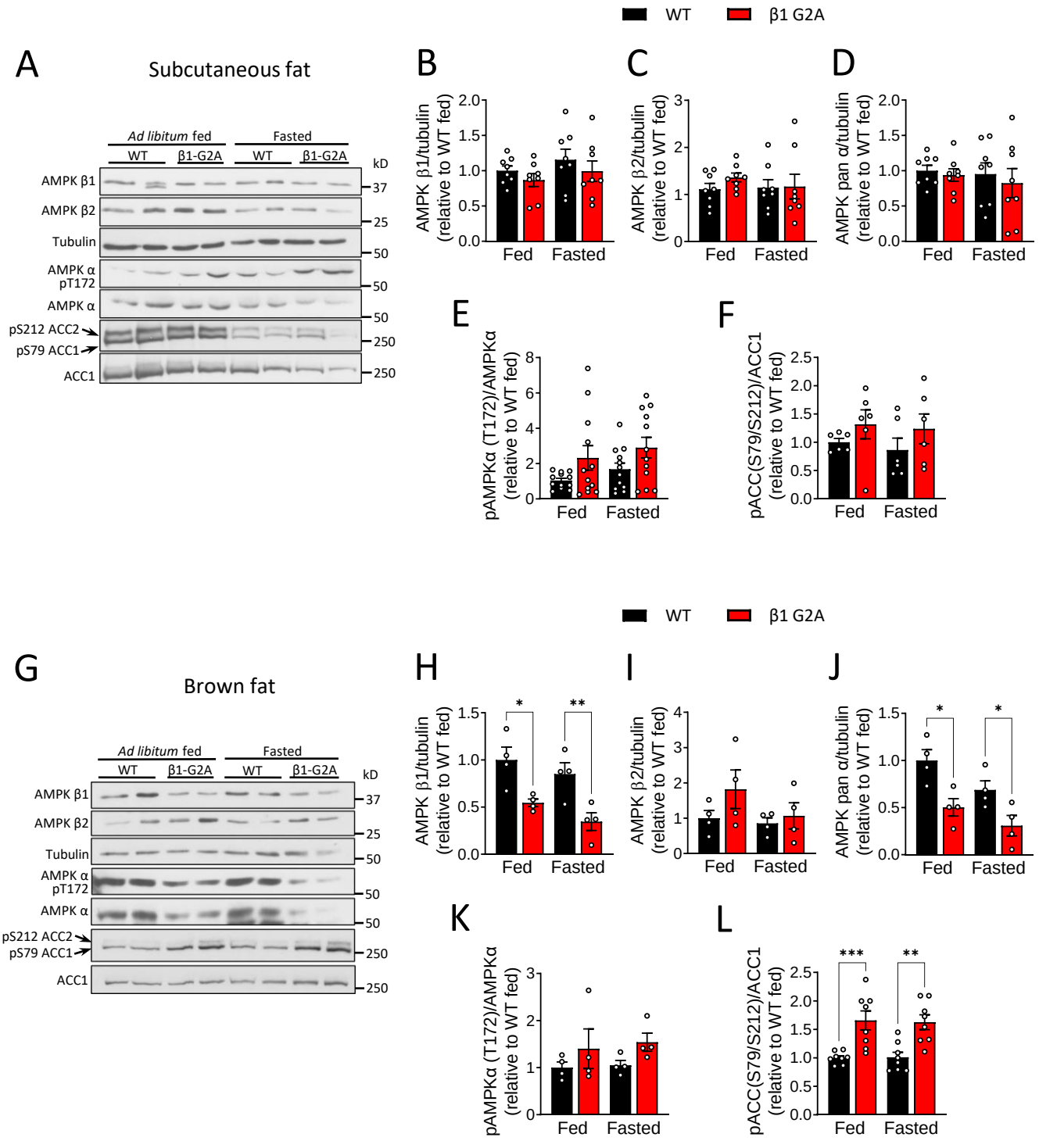
WT
β1 G2A
A
Subcutaneous fat
Ad libitum fed
Fasted
WT
β1-G2A
WT
β1-G2A
kD
AMPK β1
AMPK β2
Tubulin
AMPK α pT172
AMPK α
pS212 ACC2
pS79 ACC1
ACC1
37
25
50
50
50
250
250
B
AMPK β1/tubulin (relative to WT fed)
C
AMPK β2/tubulin (relative to WT fed)
D
AMPK pan α/tubulin (relative to WT fed)
E
pAMPKα (T172)/AMPKα (relative to WT fed)
F
pACC(S79/S212)/ACC1 (relative to WT fed)
Fed
Fasted
G
Brown fat
H
I
J
K
L
*
**
***

Figure S7

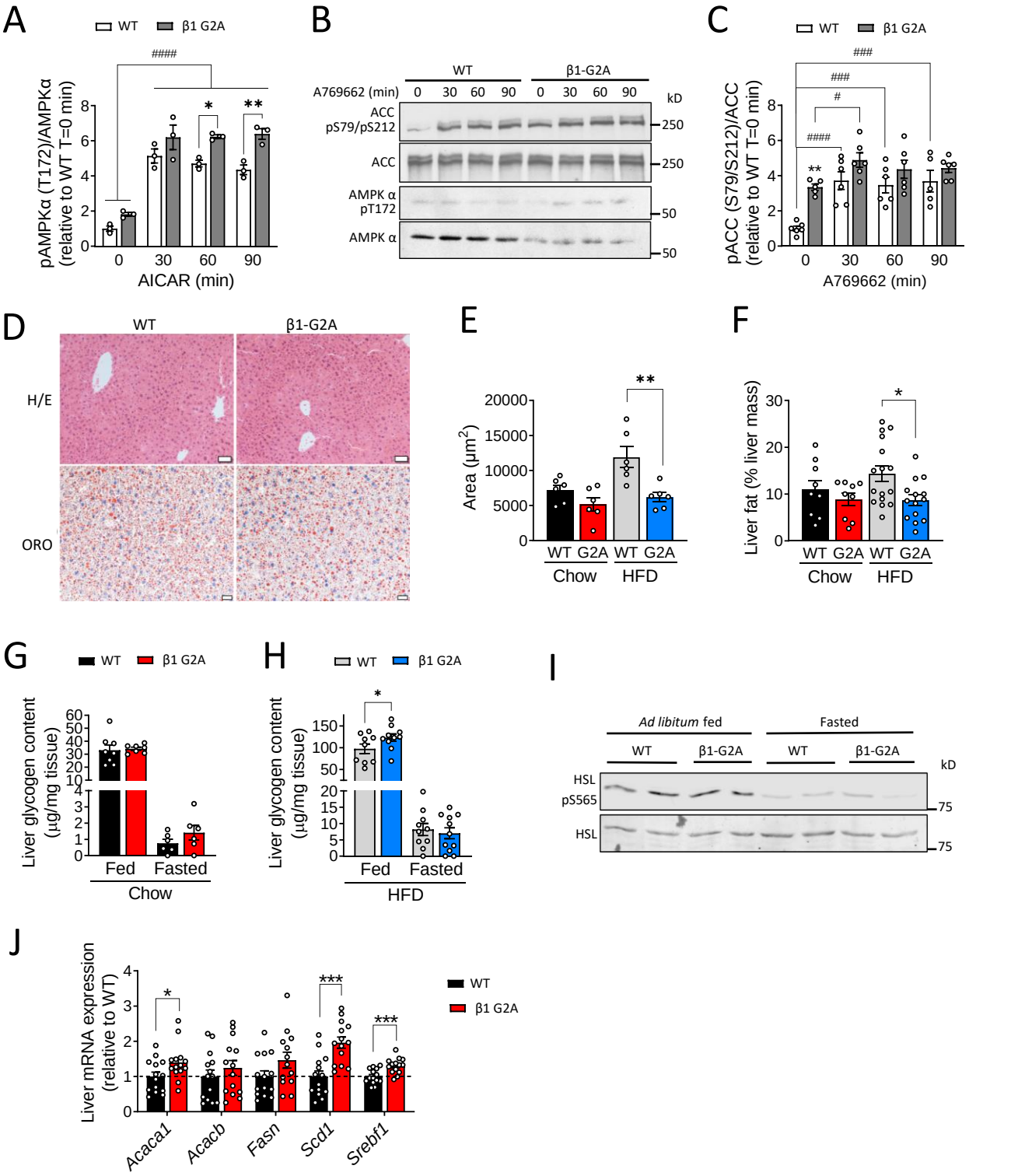
A
WT
β1 G2A
####
*
**
pAMPKα (T172)/AMPKα (relative to WT T=0 min)
AICAR (min)
B
WT
β1-G2A
A769662 (min)
0 30 60 90 0 30 60 90
kD
ACC pS79/pS212
ACC
AMPK α pT172
AMPK α
250
250
50
50
C
WT
β1 G2A
###
###
#
####
**
pACC (S79/S212)/ACC (relative to WT T=0 min)
A769662 (min)
D
WT
β1-G2A
H/E
ORO
E
**
Area (μm²)
WT G2A WT G2A
Chow HFD
F
*
Liver fat (% liver mass)
WT G2A WT G2A
Chow HFD
G
WT
β1 G2A
Liver glycogen content (μg/mg tissue)
Fed Fasted
Chow
H
WT
β1 G2A
*
Liver glycogen content (μg/mg tissue)
Fed Fasted
HFD
I
Ad libitum fed
Fasted
WT
β1-G2A
WT
β1-G2A
kD
HSL pS565
HSL
75
75
J
Liver mRNA expression (relative to WT)
*
***
***
WT
β1 G2A
Acaca1
Acacb
Fasn
Scd1
Srebf1

Figure S8

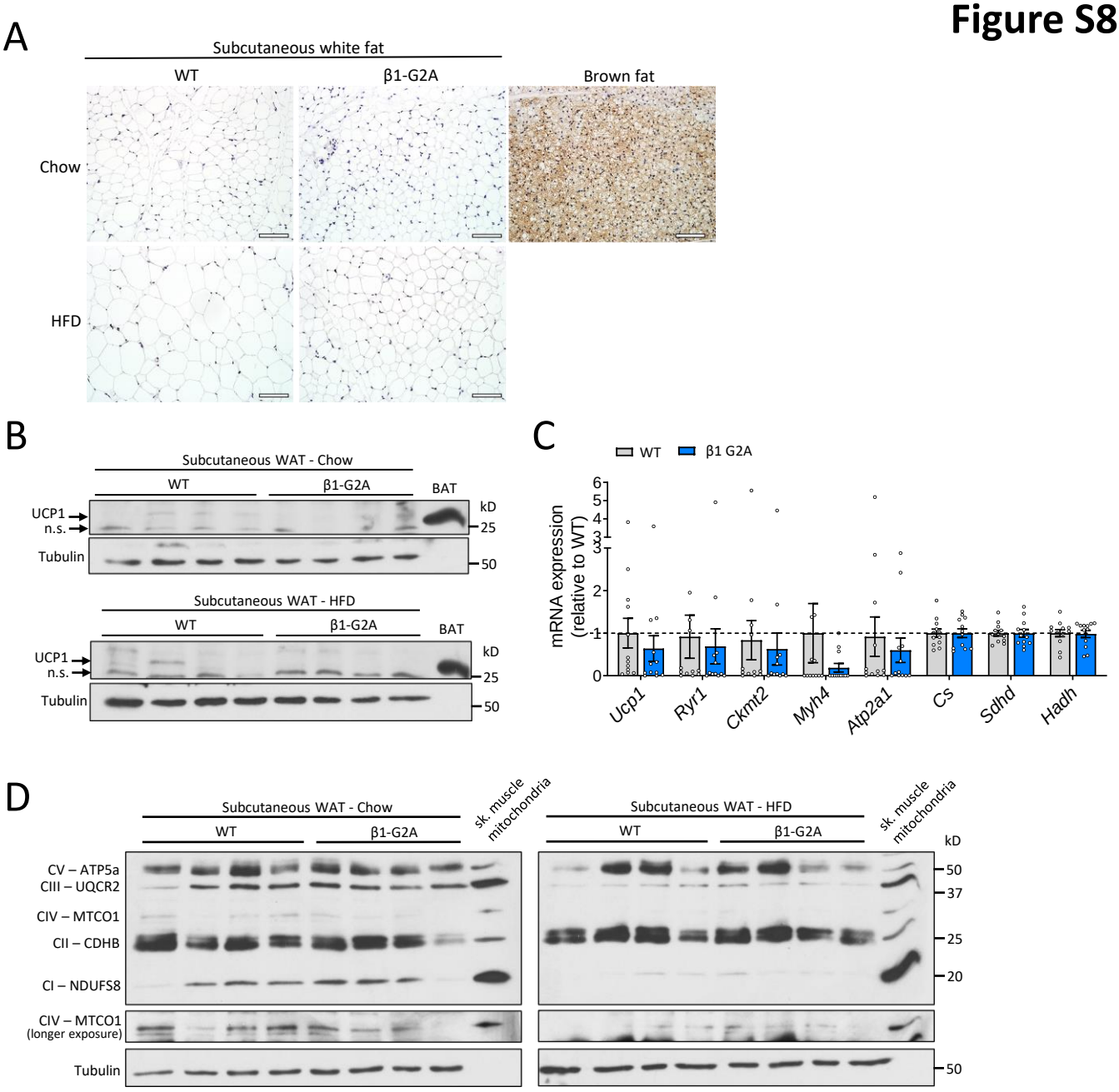
A
Subcutaneous white fat
WT
β1-G2A
Brown fat
Chow
HFD
B
Subcutaneous WAT - Chow
WT
β1-G2A
BAT
kD
UCP1
n.s.
25
Tubulin
50
Subcutaneous WAT - HFD
WT
β1-G2A
BAT
kD
UCP1
n.s.
25
Tubulin
50
C
WT
β1 G2A
mRNA expression (relative to WT)
0
1
2
3
4
5
6
Ucp1
Ryr1
Ckmt2
Myh4
Atp2a1
Cs
Sdhd
Hadh
D
Subcutaneous WAT - Chow
WT
β1-G2A
sk. muscle mitochondria
Subcutaneous WAT - HFD
WT
β1-G2A
sk. muscle mitochondria
kD
CV – ATP5a
CIII – UQCR2
CIV – MTCO1
CII – CDHB
CI – NDUFS8
CIV – MTCO1 (longer exposure)
Tubulin
50
37
25
20
50

Figure S9

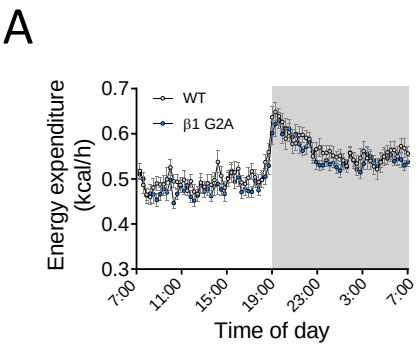

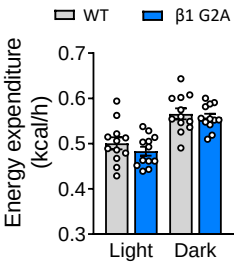

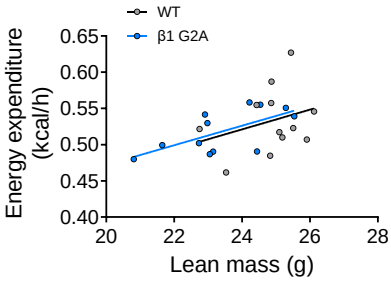

D

ANCOVA analysis of energy expenditure (kcal/time period) with lean mass as covariate

	Full day		Light		Dark	
Effect	Mass	Genotype	Mass	Genotype	Mass	Genotype
High-fat diet	0.0412*	0.6865	0.0724	0.8365	0.0368*	0.6278

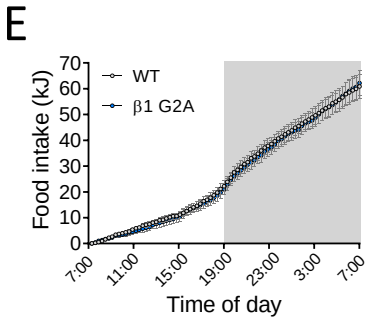

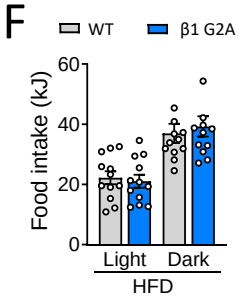

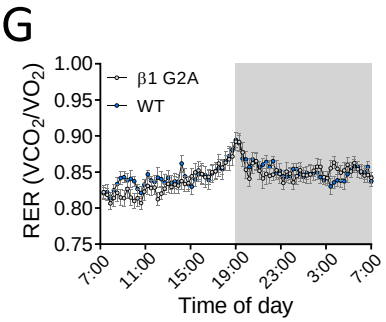

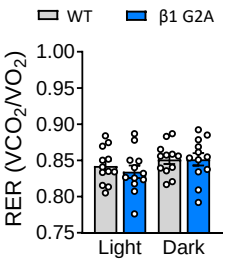

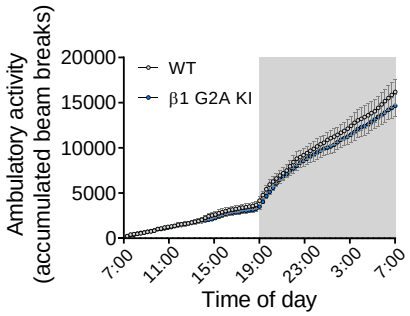

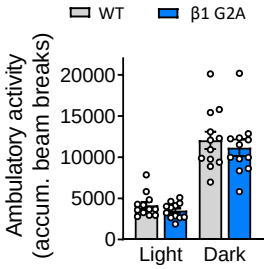

Figure S10

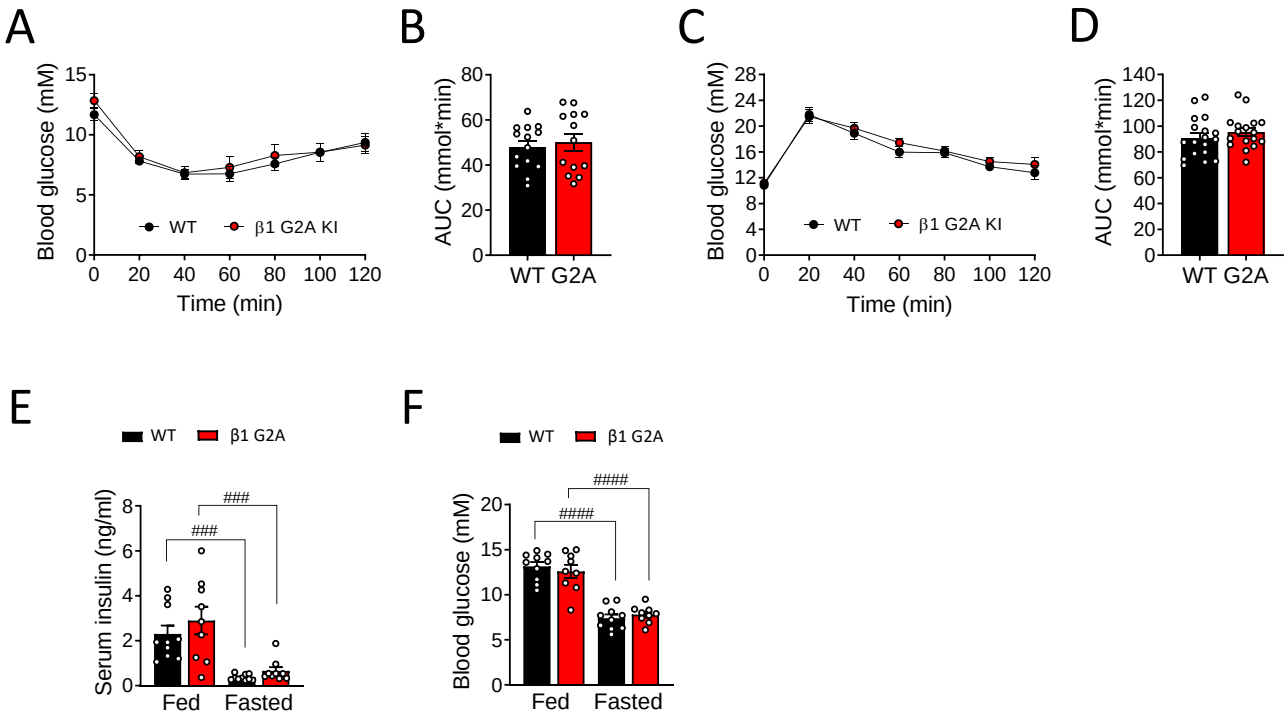
A
Blood glucose (mM)
Time (min)
WT
β1 G2A KI
B
AUC (mmol*min)
WT G2A
C
Blood glucose (mM)
Time (min)
WT
β1 G2A KI
D
AUC (mmol*min)
WT G2A
E
WT
β1 G2A
Serum insulin (ng/ml)
###
###
Fed
Fasted
F
WT
β1 G2A
Blood glucose (mM)
####
####
Fed
Fasted

FIGURE LEGENDS

Figure S1. Gene targeting strategy for the generation of AMPK β1-G2A and AMPK β2 G2A knock-in mice.

Prkab1^{G2A} (β1-G2A) and *Prka21*^{G2A} (β2 G2A) mice were generated using CRISPR/Cas9 gene targeting in C57BL/6J mouse embryos. Single guide RNAs (sgRNA) were based on target sites in exon 2 of *Prkab1* (GAGCAGCGAGCGCGCCGCGC*TGG*) and *Prkab2* (TACCAGCGAGCGGGTGTCC*GGG*) (protospacer-associated motif = PAM italicised and underlined). (A) For *Prkab1* the oligonucleotide encoded the G2A (GGC>GCC) substitution plus a PAM-inactivating silent mutation in the L11 codon (CTG>CTC). (B) For *Prkab2* the oligonucleotide encoded the G2A (GGA>GCA) substitution plus a PAM-inactivating silent mutation in the G11 codon (GGG>GGC).

Figure S2. Analysis of AMPK myristoylation, complex formation and kinase activity in β1/β2 G2A DKI MEFs.

(A) Wild-type (WT) mouse embryonic fibroblasts (MEFs) were incubated with azido-myristic acid for indicated duration of time (A) or at indicated concentrations (B) followed by cell lysis. Immunoprecipitated AMPKβ1 was subjected click chemistry reaction followed by immunoblot analysis. Myristoylated and total β1 was detected by Streptavidin-AF680 or total β1 antibody and visualized by LI-COR Odyssey Blot Imager. Data shown are representative immunoblots from three independent experiments. (C) Cell lysates from WT or β1/2 G2A double knock-in (DKI) MEFs were used for immunoprecipitation of AMPK β1 followed by immunoblotting analysis to determine heterotrimeric complex formation (with α and γ subunits). Representative immunoblots shown are from three independent experiments. (D) AMPKα1 was immunoprecipitated from vehicle (0.1% DMSO)- or 991 (10 μM)-treated WT or β1/2 G2A DKI MEFs and an *in vitro* AMPK activity assay was performed (n=2). * $P<0.05$ as analyzed by two-way ANOVA and Šídák's post-hoc test. All data are mean ± s.e.m.

Figure S3: Immunofluorescence microscopy analysis of AMPK β1 subunit localization in MEFs.

Immunofluorescence images of AMPK β1 (Green) and Hoechst (Nucleus) from wild-type (WT), β1/2 G2A double knock-in (DKI) or β1 knock-out (KO) MEFs untreated or treated with

vehicle (0.1% DMSO), 991 (10 μM) or MK-8722 (10 μM). Representative images shown are from three independent experiments. Scale bar = 10 μm.

Figure S4. Specificity of PPM1B antibody and co-localization between PPM1B and AMPK β1 in cells.

(A) Wild-type (WT) mouse embryonic fibroblasts (MEFs) were transfected with either siRNA targeting PPM1B or siRNA with a nonsense/scrambled sequence as control. Representative images shown were from at least two independent experiments. Immunofluorescence imaging was performed 48 hours following the transfection. (B) Co-localization of AMPK β1 and PPM1B was visualized by proximity ligation assay (PLA) in MEFs following transfection with either siRNA targeting PPM1B or siRNA with a nonsense/scrambled sequence (Control). Representative images shown were from at least two independent experiments. Signal was quantified as mean fluorescence intensity or number of dots per given field using ImageJ plugins. Scale bar = 10 μm. ****P<0.0001 as determined by unpaired t-test. All data are mean ± s.e.m.

Figure S5. Ablation of AMPK β1 myristoylation has no effect on AMPK subunit expression or AMPK signaling in skeletal muscle.

(A) Male age-matched 20-24-week-old β1-G2A and wild-type (WT) mice (n = 4-8) were fed *ad libitum* or fasted for 16 hours and tibialis anterior muscle isolated for immunoblot analysis. Densitometry analysis of (B) AMPK β2 and (C) AMPK pan α normalized to α,β-tubulin signal (n=4). (D) Densitometry analysis of AMPK α-Thr172 phosphorylation in immunoblots shown in A and normalized for AMPK pan α (n = 6). (E) Densitometry analysis of ACC Ser212 phosphorylation relative to total ACC signal as determined by incubation of membranes with streptavidin-HRP (n=8). #### P < 0.0001 are treatment differences as determined by two-way ANOVA with Šídák's post-hoc test. Shown are mean ± s.e.m.

Figure S6. Effects of the blocking of AMPK β1 myristoylation on AMPK subunit expression and signaling in brown and subcutaneous white adipose tissue.

(A) Male age-matched 20-24-week-old β1-G2A and wild-type (WT) mice (n = 6-12) were fed *ad libitum* or fasted for 16 hours and inguinal subcutaneous adipose tissue isolated for

immunoblotting. Densitometry analysis of (B) AMPK β1, (C) AMPK β2 and (D) AMPK pan α normalized to α,β-tubulin signal (n=8). (E) Densitometry analysis of AMPK α-Thr172 phosphorylation in immunoblots shown in A and normalized for AMPK pan α (n = 12). (F) Densitometry analysis of ACC1/2 Ser79/Ser212 phosphorylation relative to total ACC1 signal (n=6). (G) Male age-matched 20-24-week-old β1-G2A and wild-type (WT) mice (n = 4-8) were fed *ad libitum* or fasted for 16 hours and brown adipose tissue isolated for immunoblotting. Densitometry analysis of (B) AMPK β1, (C) AMPK β2 and (D) AMPK pan α normalized to α,β-tubulin signal (n=4). (E) Densitometry analysis of AMPK α-Thr172 phosphorylation normalized for AMPK pan α (n = 4). (F) Densitometry analysis of ACC1/2 Ser79/Ser212 phosphorylation relative to total ACC1 signal (n=8). * $P < 0.05$, ** $P < 0.01$, *** $P < 0.001$ represent genotype differences as determined by regular two-way ANOVA with Šídák's post-hoc test. Shown are mean ± s.e.m.

Figure S7. AMPK signaling and hepatic glycogen and lipid content in β1-G2A and wild-type liver.

(A) Densitometry analysis of immunoblot in Figure 3I showing a time course of AMPK α-Thr172 phosphorylation in primary β1-G2A and WT hepatocytes (n = 3 separate isolations) treated with 0.25 mM AICAR. (B) Time course of ACC Ser79/Ser212 and AMPK α-Thr172 phosphorylation in response to 10 μM A769662 in primary hepatocytes isolated β1-G2A and WT mice. Total ACC was detected using streptavidin-HRP. Shown are representative immunoblots from 6 separate hepatocyte preparations. (C) Densitometry analysis of ACC Ser79/Ser212 phosphorylation of immunoblot shown in C, normalized to streptavidin-HRP signal (n = 6). (D) Haematoxylin & Eosin (H/E, top panel) and Oil Red O (ORO, bottom panel) staining of 20-24-week-old *ad libitum* fed β1-G2A mice and WT littermate controls on chow diet. Shown are representative images from n = 6 per condition. Scale bar, 50 μm for H/E and 20 μm for ORO. (E) Quantification of the total area of ORO staining calculated from an average of 3 sections from 6 individual mice per genotype and condition. (F) Total tissue fat mass of livers from 20-24-week-old chow and 19-22-week-old high-fat diet (HFD)-fed β1-G2A and WT mice as determined by nuclear magnetic resonance. (G, H) Tissue glycogen content in livers from *ad libitum* fed and 16 hour-fasted β1-G2A mice and WT littermates after 12 weeks of (G) chow or (H) HFD feeding. (I) Immunoblot of HSL Ser565 phosphorylation in inguinal subcutaneous fat tissue from 20-24-week-old β1-G2A and wild-type (WT) mice fed *ad libitum* or fasted for 16 hours. (J) mRNA expression analysis of lipogenic genes in livers from 20-24-

week-old *ad libitum* fed β1-G2A and WT mice. * $P < 0.05$, ** $P < 0.01$, *** $P < 0.001$ represent genotype differences and # $P < 0.05$, ### $P < 0.001$, #### $P < 0.0001$ are treatment differences as determined by regular two-way ANOVA with Šídák's post-hoc test. E, F and J were analyzed using unpaired t-test. Shown are mean ± s.e.m.

Figure S8. Expression of thermogenic and mitochondrial proteins in subcutaneous adipose tissue from AMPK β1-G2A and wild-type mice on chow and high-fat diet.

(A) Immunohistochemistry analysis of UCP1 expression in inguinal subcutaneous adipose tissue sections from 20-24-week-old chow and 19-22-week-old high-fat diet (HFD)-fed β1-G2A KI and wild-type (WT) mice. Shown are representative images from tissue sections from 6 mice per genotype with a chow-fed WT brown fat tissue sample as control. Scale bar 100 μm. (B) Immunoblot of UCP1 protein expression with α,β-tubulin as loading control from subcutaneous tissue homogenates of 20-24 week-old chow and 19-22 week-old HFD-fed β1-G2A KI and WT mice. A WT brown fat tissue sample (0.5 μg) was included to control for successful detection of UCP1. Representative blots of n = 8 tissue samples are shown. (C) mRNA expression analysis of thermogenic and mitochondrial genes in inguinal subcutaneous fat tissue from HFD-fed β1-G2A and WT mice with β-actin as housekeeping gene (n = 12). (D) Immunoblot of mitochondrial OXPHOS proteins in subcutaneous tissue homogenates of 20-24-week-old chow and 19-22-week-old HFD-fed β1-G2A and WT mice. A crude skeletal muscle mitochondrial preparation was included to identify bands of interest. Representative blots of n = 8 tissue samples are shown. Data in C were analyzed by unpaired t-test and shown as means ± s.e.m.

Figure S9. Metabolic parameters of AMPK β1-G2A and wild-type mice on high-fat diet.

Male high-fat diet (HFD)-fed (n = 12) β1-G2A and wild-type (WT) mice at 13-14 weeks of age were subjected to analysis of metabolic parameters in Columbus Laboratory Animal Monitoring System cages over a 48-hour period at 21 °C. (A) Average energy expenditure over a 24-hour period. (B) Average energy expenditure within the light and dark cycle. (C) Regression plot comparing average energy expenditure (kcal/h) over 24 hours to lean body mass (g). (D) ANCOVA analysis of energy expenditure (lean mass as covariate) within the indicated time periods as determined using CalR. (E) Cumulative food intake over a 24-hour period and (F) average accumulated food intake within the light and dark cycle. (G) Respiratory

exchange ratio (RER) over a 24-hour period and (H) 12-hour average RER within the light and dark cycle. (I) Cumulative ambulatory activity over a 24-hour period and (J) average accumulated ambulatory activity within the light and dark cycles. Differences between genotypes at an individual time point (xy-graphs) or light/dark cycle (bar graphs) were analyzed by repeated-measures or ordinary two-way ANOVA, respectively, with Šídák's post-hoc test. Shown are mean ± s.e.m.

Figure S10. Insulin and glucose tolerance of AMPK β1-G2A and wild-type mice on chow diet.

Male chow-fed β1-G2A mice and wild-type (WT) littermates at 13-14 weeks of age were (A, n = 13-14) fasted for 4 hours and subjected to an IPITT (0.6 IU/kg lean mass) and (B) area under the curve (AUC) determined or (C, n = 17-18) fasted for 6 hours and subjected to an IPGTT (2 g D-glucose/kg lean mass) and (D) AUC analyzed. (E) Blood glucose (n = 9-10) and (F) serum insulin (n = 9-10) concentrations of *ad libitum* fed and 16 hour-fasted chow-fed β1-G2A mice and WT mice at 11-12 weeks of age. ### $P < 0.001$, #### $P < 0.0001$ represent treatment differences as analyzed by ordinary two-way ANOVA with Šídák's post-hoc test. IPITT and IPGTT data were analyzed by repeated-measures two-way ANOVA with Šídák's post-hoc test. AUC data were analyzed by unpaired t-test. All data are mean ± s.e.m.

Biochemical Journal (2021) **478** 2977–2997
https://doi.org/10.1042/BCJ20210284

PORTLAND PRESS

Research Article

Investigation of the specificity and mechanism of action of the ULK1/AMPK inhibitor SBI-0206965

Danial Ahwazi[1,*], Katyayanee Neopane[2,3,*], Greg R. Markby[1], Franziska Kopietz[4], Ashley J. Ovens[5,6], Morten Dall[1], Anna S. Hassing[1], Pamina Gräsle[1], Yazeed Alshuweishi[7,8], Jonas T. Treebak[1], Ian P. Salt[7], Olga Göransson[4], Elton Zeqiraj[9], John W. Scott[5,6,10] and Kei Sakamoto[1]

[1]Novo Nordisk Foundation Center for Basic Metabolic Research, University of Copenhagen, Copenhagen, Denmark; [2]Nestlé Institute of Health Sciences, Nestlé Research, Societé Produit de Nestlé S.A.; [3]School of Life Sciences, École polytechnique fédérale de Lausanne, Lausanne, Switzerland; [4]Department of Experimental Medical Science, Lund University, Lund, Sweden; [5]St Vincent's Institute of Medical Research, Fitzroy, Melbourne, Australia; [6]Mary MacKillop Institute for Health Research, Australian Catholic University, Melbourne, Australia; [7]Institute of Cardiovascular and Medical Sciences, College of Medical, Veterinary and Life Sciences, University of Glasgow, Glasgow, U.K.; [8]Department of Clinical Laboratory Sciences, King Saud University, Riyadh, Kingdom of Saudi Arabia; [9]Astbury Centre for Structural Molecular Biology, School of Molecular and Cellular Biology, Faculty of Biological Sciences, University of Leeds, Leeds, U.K.; [10]The Florey Institute of Neuroscience and Mental Health, Parkville, Melbourne, Australia

Correspondence: Kei Sakamoto (kei.sakamoto@sund.ku.dk)

SBI-0206965, originally identified as an inhibitor of the autophagy initiator kinase ULK1, has recently been reported as a more potent and selective AMP-activated protein kinase (AMPK) inhibitor relative to the widely used, but promiscuous inhibitor Compound C/Dorsomorphin. Here, we studied the effects of SBI-0206965 on AMPK signalling and metabolic readouts in multiple cell types, including hepatocytes, skeletal muscle cells and adipocytes. We observed SBI-0206965 dose dependently attenuated AMPK activator (991)-stimulated ACC phosphorylation and inhibition of lipogenesis in hepatocytes. SBI-0206965 (≥25 μM) modestly inhibited AMPK signalling in C2C12 myotubes, but also inhibited insulin signalling, insulin-mediated/AMPK-independent glucose uptake, and AICA-riboside uptake. We performed an extended screen of SBI-0206965 against a panel of 140 human protein kinases *in vitro*, which showed SBI-0206965 inhibits several kinases, including members of AMPK-related kinases (NUAK1, MARK3/4), equally or more potently than AMPK or ULK1. This screen, together with molecular modelling, revealed that most SBI-0206965-sensitive kinases contain a large gatekeeper residue with a preference for methionine at this position. We observed that mutation of the gatekeeper methionine to a smaller side chain amino acid (threonine) rendered AMPK and ULK1 resistant to SBI-0206965 inhibition. These results demonstrate that although SBI-0206965 has utility for delineating AMPK or ULK1 signalling and cellular functions, the compound potently inhibits several other kinases and critical cellular functions such as glucose and nucleoside uptake. Our study demonstrates a role for the gatekeeper residue as a determinant of the inhibitor sensitivity and inhibitor-resistant mutant forms could be exploited as potential controls to probe specific cellular effects of SBI-0206965.

Introduction

AMP-activated protein kinase (AMPK) is an important regulator of energy balance [1,2]. AMPK has long held promise as a therapeutic target for metabolic syndrome, as its activation in multiple metabolic tissues resulted in amelioration of insulin resistance and reduction in hyperglycemia in preclinical studies [3–5]. For example, active AMPK inhibits fatty acid biosynthesis in the liver through phosphorylation and inactivation of acetyl-CoA carboxylase-1 (ACC1) [6,7]. The activation of AMPK also leads to increased fatty acid oxidation through phosphorylation of ACC2 [8], and glucose uptake in skeletal muscle, at least in part through phosphorylation of TBC1D1 [9,10], a Rab GTPase-activating protein (GAP) which modulates trafficking of GLUT4-containing vesicles [11]. AMPK exists as hetero-complexes of three subunits; a catalytic α and two regulatory β and γ subunits.

*These authors contributed equally.

Received: 23 April 2021
Revised: 12 July 2021
Accepted: 13 July 2021

Accepted Manuscript online: 13 July 2021
Version of Record published: 10 August 2021

Biochemical Journal (2021) **478** 2977–2997
https://doi.org/10.1042/BCJ20210284

Each exists as multiple isoforms (α1/α2, β1/β2, γ1/γ2/γ3), generating up to 12 possible combinations [2]. AMPK is activated through phosphorylation of threonine 172 (Thr172) within the activation segment of the α subunit kinase domain [12]. The major upstream kinases phosphorylating Thr172 are liver kinase B (LKB1) and Ca^{2+}- calmodulin-dependent protein kinase kinase-2 (CaMKK2) [2]. The γ-subunits contain four tandem cystathionine β-synthase (CBS) motifs that bind adenine nucleotides. The binding of ADP and/or AMP to CBS motifs causes conformational changes that increase net Thr172 phosphorylation [13–15]. In addition, the binding of AMP, but not ADP, further increases AMPK activity through allosteric stimulation [13]. AMPK activity is, therefore, regulated in a multi-layered process, often involving a combination of posttranslational modifications and allosteric regulation [16].

To delineate cellular and physiological roles for AMPK, small-molecule activators have played important roles. The most widely used small-molecule activator of AMPK is 5-aminoimidazole-4-carboxamide riboside (AICAR), a prodrug of AMP-mimetic ZMP, which was used for probing the AMPK-dependent (and insulin-independent) stimulation of glucose uptake in skeletal muscle [17–19]. However, the specificity of AICAR has been challenged and numerous AMPK-independent actions of AICAR have been reported [20–23]. Specific allosteric activators and new mechanisms for their targeting of AMPK have recently been discovered. The crystallographic structures of AMPK trimeric complexes revealed that A-769662 (a member of the thieno-pyridone family [24]) and 991 (a benzimidazole derivative, also known as ex229) bind in an allosteric drug and metabolite (ADaM) pocket located at the interface of the α subunit (kinase domain N-lobe) and β subunit (carbohydrate-binding module) [25,26]. We and others have shown that 991, and its two related analogues with improved bioavailability (MK-8722, PF-739), are potent and highly specific AMPK activators [4,5,21,27]. Collectively, these activators and their analogues are exploited for drug development (e.g. for metabolic disorders) and have also been used extensively as research tools to delineate AMPK's molecular and physiological roles in cellular and organismal contexts [3].

In contrast, the availability of small-molecule AMPK inhibitors as research tools is vastly limited. The most widely utilised AMPK inhibitor, the pyrazolopyrimidine derivative Compound C (also known as Dorsomorphin), was originally discovered in a high-throughput screen and used to probe AMPK-dependent metabolic actions of metformin in hepatocytes [28]. Compound C is an ATP-competitive inhibitor and binds to the highly conserved active site of the AMPKα catalytic domain [29]. However, Compound C/Dorsomorphin inhibits several other kinases *in vitro* with similar or much greater potency than AMPK [30–32] and elicits numerous AMPK-independent biological effects [33].

SBI-0206965, a 2-aminopyrimidine derivative, was originally identified through screening a library of pyrimidine analogues as an ATP-competitive inhibitor of the autophagy initiator kinase ULK1, with the ability to inhibit ULK signalling and ULK1-mediated survival of lung cancer and glioblastoma cells when coupled with nutrient stress [34]. Interestingly, using cell-free phosphorylation of the AMPK and the ULK1 synthetic peptide substrate S108tide as a measure of kinase activity [35], it was recently reported that SBI-0206965 (used at 1 μM) was a more effective inhibitor of AMPK (80% inhibition) compared with ULK1 (63% inhibition) [32]. In addition, SBI-0206965 has demonstrated much higher potency and selectivity toward AMPK when directly compared with Compound C in cell-free assays, even though several other kinases (including JAK3, Src, FAK, Abl, Aurora A/B) were also selectively inhibited [32,34,36,37]. Mechanistically, a co-crystal structure of the AMPKα2 kinase domain-SBI-0206965 complex showed that the drug occupies a pocket that partially overlaps with the ATP-binding site; however, SBI-0206965 displayed mixed-competitive kinetics [32]. SBI-0206965 inhibits glucose deprivation-, AICAR-, A769662- or ionomycin-induced cellular AMPK activation, judged by phosphorylation of AMPK substrates, at doses ranging from 5 to 30 μM in multiple cell lines including HEK293, SH-SY5Y, mouse embryonic fibroblasts, or HUVECs [32,38,39] with no associated metabolic readouts of AMPK assessed.

In the current study, we initially sought to evaluate the effects of SBI-0206965 on AMPK signalling and metabolic readouts in multiple cell types, including hepatocytes, skeletal muscle cells, and adipocytes. We observed SBI-0206965 dose dependently attenuated AMPK-dependent stimulation of ACC phosphorylation and inhibition of lipogenesis with the direct AMPK activator 991 in mouse primary hepatocytes. SBI-0206965 (≥25 μM) only modestly inhibited AMPK signalling in C2C12 myotubes and adipocytes, but potently inhibited basal and AMPK-independent (or insulin-stimulated) glucose transport and nucleoside uptake. We next performed an extended (activity-based) screen of SBI-0206965 using a panel of 140 human protein kinases *in vitro* to test our hypothesis that SBI-0206965 would inhibit AMPK-related kinases, given the structural similarities of the kinase domains of AMPK and AMPK-related kinases [40,41]. This screen, together with molecular

Biochemical Journal (2021) 478 2977–2997
https://doi.org/10.1042/BCJ20210284

modelling and structure-guided mutagenesis, has identified that SBI-0206965 inhibits several kinases with equal or higher potency, including the AMPK-related kinases NUAK1, MARK3 and MARK4.

Materials and methods

Materials

5-Aminoimidazole-4-carboxamide ribonucleotide (AICAR, #OR1170T) was obtained from Apollo Scientific. 991 (#AOB8150) was purchased from Aobious. Insulin (#I9287) and SBI-0206965 (#SML1540) were obtained from MerckMilliporeSigma. A769662 (#3336) and S-(4-Nitrobenzyl)-6-thioinosine (NBMPR, #2924) were purchased from Tocris Bioscience. Deoxy-D-[1, 2-^{3}H]-glucose, [5, 6-^{3}H]-uridine, [1-^{14}C]-Acetic acid and [U-^{14}C]-D-glucose were purchased from PerkinElmer. Rotenone (#R8875) was obtained from MerckMilliporeSigma. Cell culture reagents were purchased from Thermo Fisher Scientific. All other materials, unless otherwise indicated, were from MerckMilliporeSigma.

Antibodies

AS160 (#07-741), Flag (#F7425), α-tubulin (#T6074), and phospho-TBC1D1 Ser237 (#07-2268) antibodies were purchased from MerckMilliporeSigma. ACC (#3676), phospho-ACC1 Ser79 (#3661), Akt (#4691), phospho-Akt Ser473 (#4060), phospho-Akt Thr308 (#9275) AMPKα (#2532), phospho-AMPKα Thr172 (#2535), phospho-AS160 Thr649 (#8881), ERK1/2 (#4695), phospho-ERK1/2 Thr202/Tyr204 (#4370), GSK3β (#9315), phospho-GSK3β Ser9 (#9322), HSP90 (#4874), p70S6K1 (#2708), phospho-p70S6K1 Thr389 (#9234), Raptor (#2280), phospho-Raptor Ser792 (#2083), TBC1D1 (#4629), ULK1 (#8054), phospho-ULK1 Ser555 (#5869), and vinculin (#13901) antibodies were purchased from Cell Signaling Technology.

Experimental animals

Animal experiments were performed in accordance with the European directive 2010/63/EU of the European Parliament and of the Council of the protection of animals used for scientific purposes. Ethical approval was given by the Danish Animal Experiments Inspectorate (#2015-15-0201-00796) or by the Regional Ethical Committee on Animal Experiments in Malmö/Lund (#5.8.18-18569/2018). Animal studies were conducted on C57BL/6NTac male mice (obtained from Taconic Biosciences) at 9–12 weeks of age in the animal facility at the Faculty of Health and Medical Sciences (University of Copenhagen) or 36- to 38-day-old Sprague-Dawley rats (obtained from Taconic Biosciences) in the animal facility at the Biomedical Centre (Lund University, Sweden). Animals were maintained on a standard chow diet and 12 : 12-h light–dark cycle.

Mouse primary hepatocytes isolation, culture, and lipogenesis assay

Mice were anesthetised via intraperitoneal injection of avertin, prepared from a stock of 1 g/ml tribromoethanol (#T48402, MerckMilliporeSigma) in 2-methyl-2-butanol (#152463, MerckMilliporeSigma), diluted 1 : 20 in saline, and dosed as 10 µl/g body weight. Hepatocytes were isolated by collagenase perfusion as previously described [42,43]. Hepatocytes were seeded in medium Eagle-199 (MEM-199) (#41150, Thermo Fisher Scientific) containing 100 U/ml penicillin G, 100 µg/ml streptomycin and 10% (vol/vol) FBS. Hepatocytes were left for attachment (3–4 h) and cultured overnight at 37°C with 5% CO_2 in MEM-199 supplemented with 100 U/ml penicillin G, 100 µg/ml streptomycin, 10 nM insulin, and 100 nM dexamethasone. Twenty-four hours after seeding, primary hepatocytes were incubated for 1 h for signalling studies as described [42] or 3 h with MEM-199 supplemented with 0.6 µCi/ml [^{14}C]-acetate in the presence of SBI-0206965 with 991 or vehicle (0.1% DMSO). Cells were harvested in 0.5 ml PBS, transferred into 1 ml 40% KOH and 2 ml methanol followed by 1 h incubation at 80°C. Lipids were saponified by acidifying the samples in 37% HCl and extracted with petroleum ether. Extracts were allowed to evaporate to dryness, then dissolved in Ultima Gold scintillation fluid for determination of [^{14}C]-acetate incorporation into lipids.

C2C12 skeletal muscle cell culture, treatment, and glucose uptake measurement

C2C12 (#CRL-1772, ATCC) myoblasts were cultured and differentiated into myotubes as described [44]. Fully differentiated C2C12 myotubes (day 4–5) were serum starved in DMEM for 4 h followed by 1 h incubation with bicarbonate-free media (DMEM, 20 mM HEPES, 0.2% BSA, pH 7.4). Cells were then pre-incubated in Krebs-Ringer HEPES (KRH) buffer (140 mM NaCl, 4.7 mM KCl, 2.5 mM $CaCl_2$, 1.25 mM $MgSO_4$, 10 mM

Biochemical Journal (2021) 478 2977–2997
https://doi.org/10.1042/BCJ20210284

HEPES, 1.2 mM KH_2PO_4, and 0.2% BSA) with vehicle (0.1% DMSO) or SBI-0206965 for 30 min followed by an additional 1 h incubation with 991 (10 μM) or insulin (100 nM). Cells were incubated in KRH buffer containing 50 μM [^{3}H]2-deoxyglucose (0.1 μCi/ml) for 5 min and the reaction was stopped by adding 25 mM glucose. The cells were washed in KRH buffer and harvested in ice-cold lysis buffer. Two-third of the lysate was used for immunoblot analysis and the remaining one-third was analysed by scintillation counting to measure 2-deoxyglucose uptake in the cells.

Ex vivo mouse skeletal muscle incubation

Mice were anesthetised by avertin (as described above) via intraperitoneal injection, and extensor digitorum longus (EDL) muscle was rapidly dissected and mounted in oxygenated (95% O_2 and 5% CO_2) and warmed (30°C) Krebs-Ringer buffer in a myograph system (820MS, Danish Myo Technology) as described [27,45]. The muscles were incubated in the presence of the indicated compounds or vehicle (0.1% DMSO) for 50 min before snap-frozen in liquid nitrogen.

Rat primary adipocyte isolation, culture, treatment, and glucose uptake assay

Adipocytes were isolated by collagenase digestion as described [46]. After isolation, primary adipocytes were stimulated directly (1 ml of 8–10% (v/v) cells per stimulation) as indicated in the figure legends. After stimulation, cells were washed in KRH buffer without BSA and lysed in lysis buffer. For glucose uptake, freshly isolated rat adipocytes were washed in glucose-free buffer containing 30 mM HEPES pH 7.4, 120 mM NaCl, 4 mM KH_2OPO_4, 1 mM $MgSO_4$, 0.75 mM $CaCl_2$, 10 mM $NaHCO_3$, 200 nM adenosine and 1% (w/v) BSA (incubation buffer). Adipocyte suspensions (400 μl of 5% (v/v) cells) were pre-incubated with SBI-0206965 or 0.1% DMSO for 30 min before being stimulated with 10 nM insulin or 10 μM cytochalasin B for 30 min. Subsequently, 100 μl incubation buffer containing 0.25 μl (0.025 μCi) [^{14}C]-glucose (275 mCi/mmol glucose; final glucose concentration = 0.18 μM) was added and cells were incubated for a further 30 min. Reactions were stopped by centrifuging 300 μl of each reaction in a Beckman microtube containing 75 μl dinonylphtalate. The adipocyte fraction was collected and subjected to liquid scintillation counting.

3T3-L1 adipocyte culture and glucose uptake

3T3-L1 fibroblasts were originally obtained from ATCC (#CL-173). The cells were cultured and differentiated into adipocytes as described previously [47] and used between passages 7 and 12. Experiments were performed at days 8–12 post differentiation. 2-deoxyglucose uptake assay and preparation of cell lysates were as described previously [46].

Cell and tissue extract preparation

Treated cells were washed once with PBS and lysed in ice-cold lysis buffer (containing 50 mM Tris–HCl, pH 7.5, 1 mM EGTA, 1 mM EDTA, 270 mM sucrose, 1% Triton X-100, 20 mM glycerol-2-phosphate, 50 mM NaF, 5 mM $Na_4P_2O_7$, 1 mM DTT, 0.1 mM PMSF, 1 mM benzamidine, 1 μM microcystin-LR, 1 μg/ml leupeptin, 1 μg/ml pepstatin A, and 1 mM Na_3VO_4). For mouse skeletal muscle tissue samples, ∼10 mg tissue was homogenised in 400 μl ice-cold lysis buffer using a Tissuelyser II (Qiagen) at 30 Hz for 30 s (x 2 sets). Cell or tissue lysates were clarified by centrifugation at 6000×***g*** for 10 min at 4°C, and total protein concentration was determined using Bradford reagent (#23200, ThermoFisher) and BSA as standard.

Immunoblot analysis

Protein lysates were denatured in Laemmli buffer at 95°C for 5 min. Twenty micrograms of protein was separated by SDS–PAGE on home-made Tris-glycine or pre-cast Novex 4–12% Bis-Tris gels (ThermoFisher) and transferred onto nitrocellulose or Immobilon-FL polyvinylidene difluoride membranes. Membranes were blocked for 45 min in TBST [Tris-buffered saline (20 mM Tris–HCl, pH 7.6, 137 mM NaCl) with 0.1% Tween 20] containing 5% skimmed milk. Blocked membranes were incubated overnight at 4°C in primary antibody diluted in TBST containing 4% BSA. Protein detection was performed with horseradish peroxidase-conjugated secondary antibodies and enhanced chemiluminescence (ECL) substrate or LI-COR IRdye-conjugated secondary antibodies and a LI-COR Odyssey infrared imaging system (LI-COR Biosciences). ECL signals were visualised using a ChemiDoc XRS+ system followed by analysis of band intensities with the software Image Lab 6.0

Biochemical Journal (2021) 478 2977–2997
https://doi.org/10.1042/BCJ20210284

(both from Bio-Rad). LI-COR signals were analysed and quantified using ImageStudioLite software (LI-COR Biosciences).

Protein expression constructs

AMPKα1 constructs (used in Figure 8) were made by the cloning team at Medical Research Council Protein Phosphorylation and Ubiquitylation Unit (MRC PPU) Reagents and Services (https://mrcppureagents.dundee.ac.uk/). The coding region of AMPKα1 (NM_006251.5) was amplified using oligonucleotides adding BglII and NotI restriction sites at the 5′ and 3′ end, respectively, and subcloned as a BglII/NotI insert into pcDNA5D-FRT/TO FLAG vector (DU41457) digested with BamHI and NotI to generate pcDNA5D-FRT/TO FLAG AMPKα1 (DU67861). The M104T mutant version of this plasmid was made according to the QuikChange method (Stratagene) using KOD polymerase (Novagen) to generate pcDNA5D-FRT/TO FLAG AMPKα1 M104T. Plasmid expression constructs for AMPK Flag-α1, β1-Myc, and HA-γ1 (used in Figure 7) were previously described [32]. Mutagenesis of Flag-α1 was performed as above using the QuikChange method. Note that the AMPKα1 construct used in Figure 7 is a variant of NM_006251.5 that starts at Met10 (the alternate initiation site), thus the gatekeeper methionine shown as M104 corresponds to M93. Plasmid constructs for full-length, N-terminal Flag-tagged human ULK1 (NM_003565.4) and the M92T mutant were generated by custom gene synthesis (Gene Universal) and cloned into pcDNA3.1(−) vector using XhoI/HindIII restriction sites. All constructs were sequence verified.

Protein production and kinase assays

Heterotrimeric human AMPK Flag-α1β1γ1 and human Flag-ULK1 were produced in mammalian cells as described [32,35]. For AMPK expression, the cells were triply transfected at 60% confluency using FuGene HD (Roche Applied Science) and 1 μg of pcDNA3 plasmid expression constructs for AMPK Flag-α1, β1-Myc, and HA-γ1, whereas for ULK1 expression the cells were transfected with 2 μg of pcDNA3.1(−) Flag-ULK1 plasmid. After 48 h, the transfected cells were harvested by rinsing with ice-cold PBS, followed by rapid lysis using 500 μl of lysis buffer.

AMPK and ULK1 activity were determined by phosphorylation of synthetic peptide substrates SAMS (HMRSAMSGLHLVKRR) and S108tide (KLPLTRSHNNFVARRR), respectively [32,35]. Briefly, recombinant AMPK or ULK1 was immunoprecipitated from 10 μg of transfected cultured cell lysate using 10 μl of anti-FLAG M2 agarose beads (50% (v/v)) (MerckMilliporeSigma), washed and then added to a 25 μl reaction containing assay buffer (50 mM HEPES-NaOH, pH 7.4, 1 mM DTT, and 0.02% (v/v) Brij-35), 200 μM synthetic peptide substrate (SAMS or S108tide), 200 μM [γ-^{32}P]-ATP (PerkinElmer), 5 mM $MgCl_2$, in the presence of Compound C (0–400 μM) or SBI-0206965 (0–400 μM). Reactions were performed at 30°C and terminated after 10 min by spotting 15 μl onto P81 phosphocellulose paper (Whatman). Radioactivity was quantified by liquid scintillation counting.

Homogeneous time-resolved fluorescence (HTRF) assay using AMPKα1 and α2 double KO (DKO) U2OS cells

U2OS FRT Flp-In T-REx cell line was a kind gift from John Rouse (University of Dundee) and dual deletion of *PRKAA1* and *PRKAA2* (that encode AMPKα1 and α2, respectively) was performed by Horizon Discovery using CRISPR–CAS9 technology. HTRF was employed for a higher throughput application, as well as more sensitive and quantitative detection of ACC phosphorylation (using the phospho-ACC 1/2 (Ser79) kit, # 64ACCPET, Cisbio). Briefly, cells were seeded in a 96-well plate at a density of 5×10^4 cells per well. The next day, cells were treated with increasing concentration of the indicated compounds diluted in a serum-free medium. Post-treatment, cells were lysed in 50 μl per well of phospho-total protein lysis buffer 1 (#64KL1FDF, Cisbio) containing 1 : 100 blocking reagent (#64KB1ACC, Cisbio) with continuous vibration at room temperature for 30 min. ACC (Ser79) D2- and Cryptate-antibodies were diluted (1 : 40) in the detection buffer. In a 384-well plate, 16 μl lysate and 4 μl antibody solution were added per well. The plate was incubated at room temperature with light protection. The next day, FRET (665 nm/620 nm) was measured using Spectramax microplate reader (Molecular Devices) according to the manufacturer instruction.

Biochemical Journal (2021) 478 2977–2997
https://doi.org/10.1042/BCJ20210284

Nucleotide and ZMP measurements

Nucleotides and ZMP were measured by liquid chromatography-mass spectrometry from perchlorate extracts of mouse primary hepatocytes, C2C12 myotubes, and mouse EDL muscle tissues as described previously [32,45]. Adenylate energy charge was calculated as:

$$\frac{(\mathrm{ATP} + 0.5\mathrm{ADP})}{(\mathrm{ATP} + \mathrm{ADP} + \mathrm{AMP})}$$

Uridine uptake

Uridine uptake assay was performed as described [48]. Briefly, C2C12 myotubes were washed once in uridine uptake buffer (20 mM Tris–HCl, 3 mM KH_2PO_4, 1 mM $MgCl_2$, 2 mM $CaCl_2$, 5 mM glucose, 130 mM NaCl, pH 7.4) before incubating at room temperature in 400 µl uridine uptake buffer containing vehicle (0.1% DMSO), NBMPR, or SBI-0206965. Thirty minutes following incubation, the buffer was aspirated and the new 400 µl uridine uptake buffer containing the compounds (DMSO, NBMPR, or SBI-0206965) and 0.1 µM (2 µCi/ml) [^{3}H]-uridine. After 1 min, uridine transport was terminated by washing the cells five times in ice-cold uridine uptake buffer containing cold 1 mM uridine. The cells were lysed in 200 µl 10% (w/v) SDS before scraping. The amount of uridine transported into the cells was determined by scintillation counting.

Adenosine kinase assay

Of human recombinant adenosine kinase (BioVision, #8024-AK), 0.5 µg was pre-incubated with non-nucleoside adenosine kinase inhibitor ABT-702 (Tocris, #2372) or vehicle (DMSO) for 30 min followed by a further incubation with or without increasing doses (0.1–10 µM) of SBI-0206965 for 60 min. Adenosine kinase activity was measured using the Universal Kinase Activity kit (R&D System, EA004) using adenosine (MerckMilliporeSigma, #A9251) as substrate according to the manufacturer protocol.

Protein kinase screen and IC_{50} determination

All protein kinases in the kinase panel were expressed, purified and assayed at the International Centre for Protein Kinase Profiling (http:// www.kinase-screen.mrc.ac.uk/), MRCPPU, University of Dundee, as previously described [30]. Briefly, all assays were carried out at room temperature. Assays were performed for 30 min (except Lck and PBK that were incubated for 15 min) using Multidrop Micro reagent dispensers (Thermo Electron Corporation) in a 96-well format. The concentration of magnesium acetate in the assays was 10 mM and [γ-^{33}P]ATP (~800 cpm/pmol) was used at either 5, 20, or 50 µM in order to be at or below the Km for ATP for each enzyme (described under 'kinase panel' in the webpage http://www.kinase-screen.mrc.ac.uk/services/premier-screen). The half-maximal inhibitory concentration (IC_{50}) values of the selected kinases against SBI-0206965 were performed by the International Centre for Kinase Profiling team and determined after carrying out assays at ten different concentrations of the compound.

Molecular docking

Molecular docking was performed using the SwissDock server [49] available at http://www.swissdock.ch/ (last accessed on 20 August 2020). The kinase domain structures of AMPKα2 (PDBid: 6BX6), ULK2 (PDBid: 6YID), MARK3 (PDBid: 2QNJ), MARK4 (PDBid: 5ES1) were prepared for docking using the Chimera plugin DOCKPREP after removal of water and ligand molecules [50,51]. The ligand SBI-0206965 (ZINC database entry: 253387916) was docked to each kinase structure using the default settings for 'accurate' docking, allowing flexibility for side chains within 3 Å of any atom of the ligand in its reference binding mode.

Statistical analysis

Results are indicated as means ± standard error mean (SEM). Two-way analysis of variance (ANOVA) with Tukey's post hoc analysis was used to determine differences between multiple treatment groups. Significance was set at $P < 0.05$.

Biochemical Journal (2021) **478** 2977–2997
https://doi.org/10.1042/BCJ20210284

Results

SBI-0206965 dose dependently attenuates 991-induced phosphorylation of ACC and inhibition of lipogenesis in primary hepatocytes

SBI-0206965 was reported to inhibit cellular AMPK activation, assessed by phosphorylation of ACC, at doses ranging from 5 to 30 μM in multiple cell lines including HEK293, SH-SY5Y, or HUVECs [32,38]. We observed that SBI-0206965 attenuates basal or 991-stimulated phosphorylation of AMPK substrates (ACC and Raptor) in a dose-dependent manner in primary mouse hepatocytes (Figure 1A,B). Phosphorylation of AMPKα T172 was modestly elevated with 991, and was further increased with increasing doses of SBI-0206965 (Figure 1A,B). Since a previous study noted that cellular incubations at high concentrations of SBI-0206965 may induce AMPKα T172 phosphorylation through fluctuations in AMP/ATP and ADP/ATP ratios [32], we measured the effect of SBI-0206965 on adenylate energy charge. We indeed observed that SBI-0206965 promoted phosphorylation of AMPKα T172 at higher doses (Supplementary Figure S1A), however, there was no reduction in adenylate energy charge (Supplementary Figure S1B).

Since activation of AMPK leads to inhibition of lipogenesis through phosphorylation of ACC1 in hepatocytes [6,7,42], we tested if SBI-0206965 treatment could prevent 991-induced suppression of lipogenesis. As previously reported [7,27], 991 potently inhibited lipogenesis in hepatocytes (Figure 1C). Co-treatment with SBI-0206965 attenuated 991-induced inhibition of lipogenesis in a dose-dependent manner. When co-treated with a 25 μM dose of SBI-0206965, the inhibitory effect of 991 was fully restored to the level comparable to the vehicle-treated state (Figure 1C). As shown in Figure 1D, we observed an inverse relationship between ACC phosphorylation and lipogenesis in response to increasing doses of SBI-0206965 with 991 (10 μM). These results demonstrate that SBI-0206965 is a useful tool compound to probe AMPK-dependent regulation of lipogenesis by small-molecule activators in primary hepatocytes.

SBI-0206965 potently inhibits glucose uptake in C2C12 myotubes and adipocytes

We next assessed the effects of SBI-0206965 on AMPK signalling and glucose uptake in C2C12 myotubes. SBI-0206965 (10 μM) alone modestly increased phosphorylation of AMPKα with no apparent effect on phosphorylation of AMPK substrates (ACC, Raptor, TBC1D1, ULK1) (Figure 2A,B and Supplementary Figure S1A). As anticipated, 991 (10 μM) enhanced phosphorylation of AMPK substrates to varying degrees. Treatment of C2C12 myotubes with increasing doses of SBI-0206965 in combination with 991 resulted in a dose-dependent decrease in Raptor phosphorylation, however, phosphorylation of ACC and ULK1 was only modestly decreased at doses up to 50 μM (Figure 2A,B). Notably, phosphorylation of TBC1D1, known to be involved in AMPK-mediated glucose uptake in skeletal muscle [9–11], was unchanged with SBI-0206965 (Figure 2A,B). In contrast, phosphorylation of extracellular signal-regulated kinase (ERK), used as control unrelated to AMPK signalling, was markedly inhibited with SBI-0206965 at 5 μM (Figure 2A). SBI-0206965 (10 μM) suppressed basal glucose uptake by more than 50%, whereas 991 stimulated glucose uptake by ∼2-fold and this was dose dependently reduced with SBI-0206965 (Figure 2C). Even though 5 μM SBI-0206965 had no apparent inhibitory effect on phosphorylation of AMPK substrates (Figure 2A,B), it was sufficient to fully inhibit 991-stimulated glucose uptake in C2C12 myotubes (Figure 2C). Contrary to the inhibitory effect of SBI-0206965 on phosphorylation of AMPK substrates, 991-stimulated phosphorylation of AMPKα T172 was further elevated with increasing doses of SBI-0206965 (Figure 2A). Consistent with the observation in hepatocytes (Supplementary Figure S1A) SBI-0206965 dose dependently promoted phosphorylation of AMPKα and there was no change in adenylate energy charge (Supplementary Figure 1C,D). Collectively, SBI-0206965 is a potent inhibitor for basal and 991-stimulated glucose uptake, although it promotes phosphorylation of AMPKα T172 and has only a modest inhibitory effect on phosphorylation of AMPK substrates in C2C12 myotubes.

Since we observed that SBI-0206965 potently inhibits basal and 991-stimulated glucose uptake with no detectable inhibition of TBC1D1 phosphorylation, we tested if SBI-0206965 suppresses insulin-stimulated (i.e. AMPK-independent) glucose uptake in C2C12 myotubes. SBI-0206965 doses ≥25 μM consistently inhibited insulin-stimulated phosphorylation of Akt and its downstream targets including AS160 (also known as TBC1D4), which plays a key role in regulating GLUT4 trafficking [11,52,53] (Figure 3A,B). We observed that basal and insulin-stimulated glucose uptake were robustly inhibited with SBI-0206965 (Figure 3C), which is consistent with a previous study using L6 myotubes and isolated mouse skeletal muscle *ex vivo* [54].

Biochemical Journal (2021) 478 2977–2997
https://doi.org/10.1042/BCJ20210284

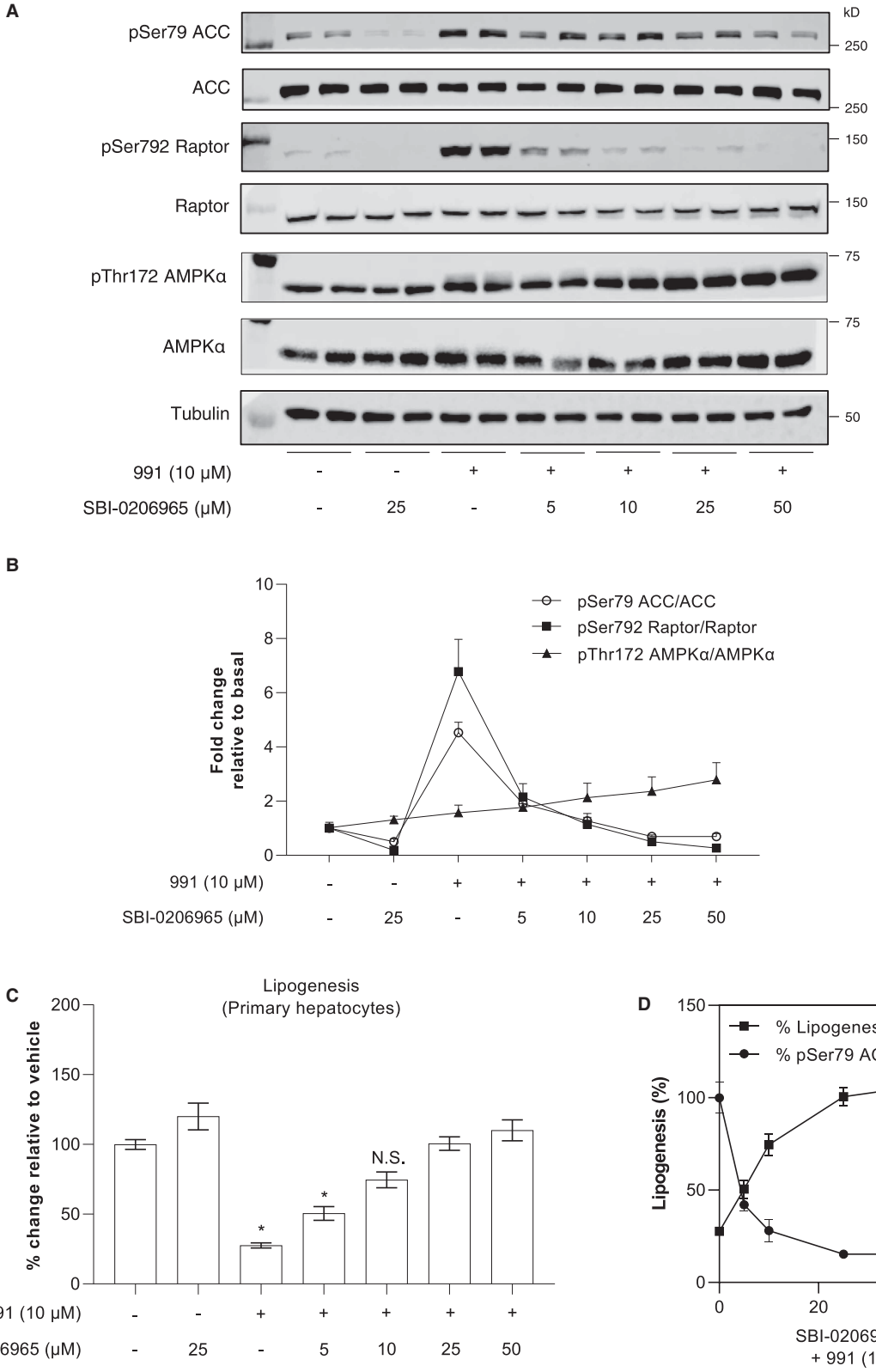

Figure 1. SBI-0206965 dose dependently attenuates 991-induced phosphorylation of ACC and inhibition of lipogenesis in mouse primary hepatocytes.

Part 1 of 2

(A,B) Mouse primary hepatocytes were pre-incubated for 30 min with vehicle (0.1% DMSO) or the indicated concentrations of SBI-0206965 followed by an additional incubation for 1 h with 991 (10 μM) or vehicle. Cell lysates were subjected to immunoblot analysis using the indicated antibodies.

Biochemical Journal (2021) **478** 2977–2997
https://doi.org/10.1042/BCJ20210284

Figure 1. SBI-0206965 dose dependently attenuates 991-induced phosphorylation of ACC and inhibition of lipogenesis in mouse primary hepatocytes. Part 2 of 2

Tubulin was used as a loading control. Representative images (A) and quantification of the indicated blots (B) from three independent experiments are shown ($n = 6$ per treatment). (C) Mouse hepatocytes were treated with the indicated concentrations of SBI-0206965 in the absence (vehicle) or presence of 991 (10 μM) and labelled with [^{14}C]-acetate for 3 h. Rates of fatty acid synthesis were estimated from incorporation [^{14}C]-acetate into saponifiable lipids. (D) Results from (B) and (C) (except vehicle and SBI-0206965 alone data) are plotted to visualise the inverse relationship between ACC phosphorylation and lipogenesis in response to increasing doses of SBI-0206965 in combination with 991 (10 μM). Results are expressed as percentage relative to the vehicle and represent the mean ± SEM for three independent experiments ($n = 6$–12 per treatment). *$P < 0.05$ (vehicle vs. indicated compound(s) treated). N.S.; not significant.

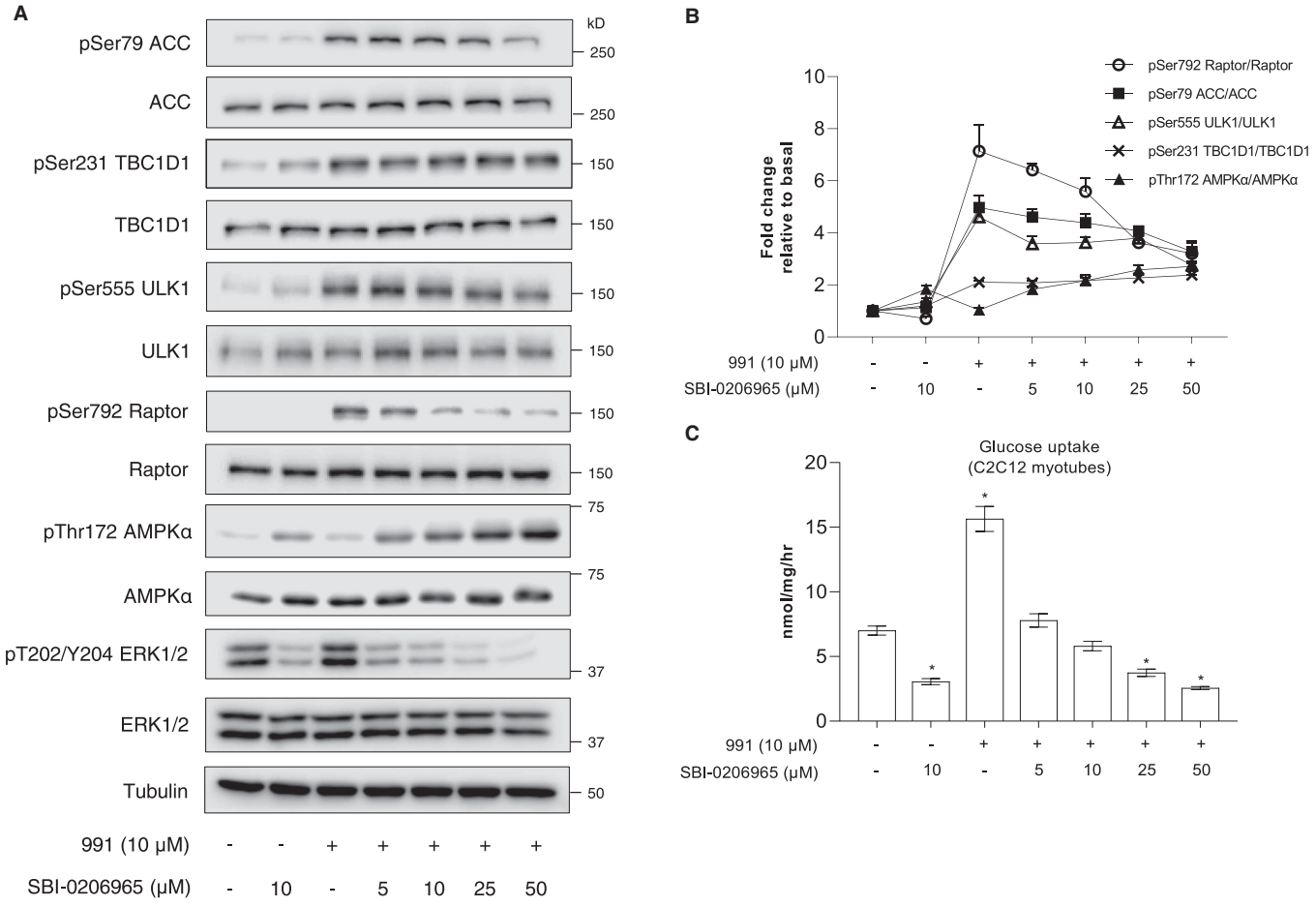

Figure 2. SBI-0206965 inhibits unstimulated and 991-stimulated glucose uptake with no apparent inhibition of TBC1D1 Ser231 phosphorylation in C2C12 myotubes.

(A,B) C2C12 myotubes were pre-incubated for 30 min with vehicle (0.1% DMSO) or the indicated concentrations of SBI-0206965 followed by an additional 1 h incubation with 991 (10 μM) or vehicle. Cell lysates were subjected to immunoblot analysis using the indicated antibodies. Tubulin was used as a loading control. Representative images (A) and quantification of the indicated blots (B) from three independent experiments are shown ($n = 3$ per treatment). (C) C2C12 myotubes were incubated with vehicle or the indicated compounds for 1 h followed by addition of [^{3}H]-2-deoxy-glucose and measurement of glucose uptake for 5 min ($n = 8$–9 per treatment). Results are expressed as mean ± SEM. *$P < 0.05$ (vehicle vs. indicated compound(s) treated).

Biochemical Journal (2021) **478** 2977–2997
https://doi.org/10.1042/BCJ20210284

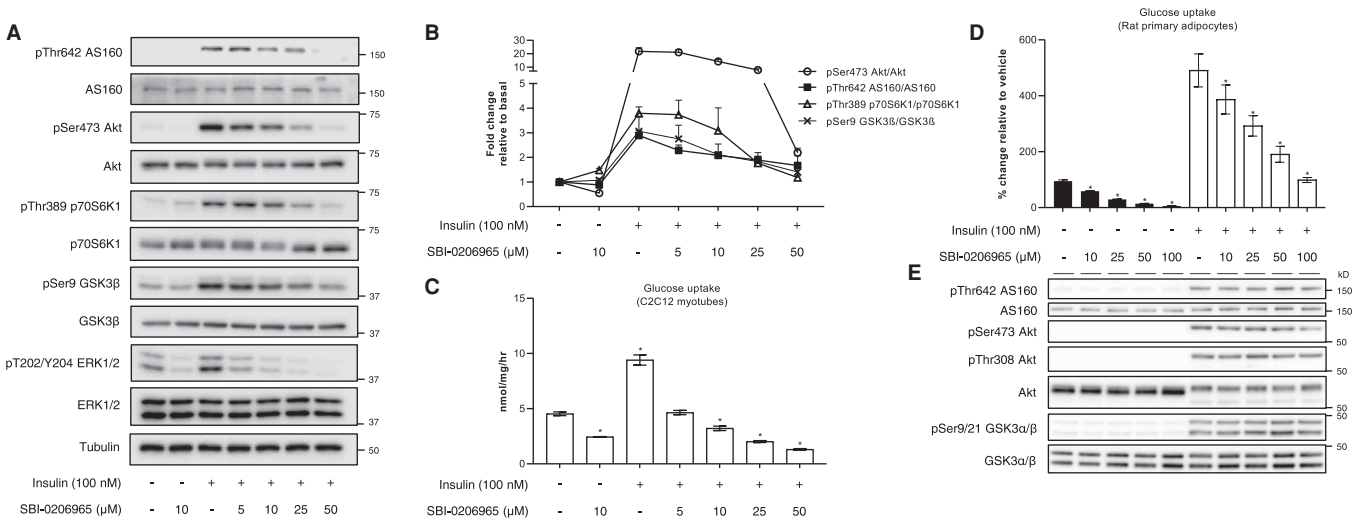

Figure 3. SBI-0206965 inhibits insulin-stimulated glucose uptake in C2C12 myotubes and rat primary adipocytes.

(**A**,**B**) C2C12 myotubes were pre-incubated for 30 min with vehicle (0.1% DMSO) or the indicated concentrations of SBI-0206965 followed by an additional incubation without (vehicle) or with insulin (100 nM) for 1 h. Cell lysates were subjected to immunoblot analysis using the indicated antibodies. Tubulin was used as a loading control. Representative images (**A**) and quantification of the indicated blots (**B**) from three independent experiments are shown ($n = 3$ per treatment). (**C**) C2C12 myotubes were incubated with vehicle or the indicated compounds for 1 h followed by addition of [^{3}H]-2-deoxy-glucose and measurement of glucose uptake for 5 min ($n = 6$ per treatment). (**D**,**E**) Rat primary adipocytes were pre-incubated with vehicle (0.1% DMSO) or the indicated concentrations of SBI-0206965 for 30 min before being stimulated with insulin (10 nM) for 30 min. The adipocytes were either lysed for immunoblot analysis (**E**, $n = 4$ per treatment) or incubated further 30 min with an addition of [^{14}C]-glucose for determination of glucose uptake (**D**, $n = 4$ per treatment). Results are expressed as mean ± SEM. *$P < 0.05$ (vehicle vs. indicated compound(s) treated).

Collectively, these results demonstrate that SBI-0206965 potently inhibits insulin-stimulated glucose uptake and modestly inhibits insulin signalling intermediaries in C2C12 myotubes.

To further examine if SBI-0206965 ubiquitously inhibits the glucose transport system in different cell types, we also treated rat primary adipocytes with SBI-0206965 in the presence or absence of insulin. Consistent with our observation in C2C12 myotubes, both basal and insulin-stimulated glucose uptake were dose dependently reduced in primary adipocytes (Figure 3D). However, contrary to the inhibitory effect on insulin signalling intermediaries in C2C12 myotubes (Figure 3A,B), SBI-0206965 had no effect on phosphorylation of Akt and its substrates (AS160 and GSK3α/β) in primary adipocytes (Figure 3E). We also assessed the effect of SBI-0206965 on 991-induced AMPK activation in primary adipocytes and observed that phosphorylation of Raptor, but not ACC, was only modestly reduced at 50 or 100 μM (Supplementary Figure S2A,B). We also used 3T3 L1 mouse adipocytes and observed that SBI-0206965 (30 μM) profoundly inhibited both basal and insulin-stimulated glucose uptake (Supplementary Figure S2C). Taken together, SBI-0206965 inhibits both stimulated and unstimulated glucose transport in multiple cell types.

SBI-0206965 inhibits the nucleoside transport system

AICAR is the most widely used compound to pharmacologically activate AMPK and probe AMPK's cellular and physiological functions, although its specificity has recently been challenged [20–22]. Upon uptake into cells, AICAR is converted to the monophosphate derivative, ZMP, which can accumulate to high levels, and mimics the effects of AMP on the AMPK pathway. Consistent with previous findings using HEK293 cells [32], we observed that SBI-0206965 potently inhibits AICAR uptake (measured as cellular ZMP accumulation) in both C2C12 myotubes and isolated mouse skeletal muscle (EDL) tissue *ex vivo* (Figure 4A,B). To determine if the reduced accumulation of ZMP was due to inhibition of the transport or conversion of AICAR to ZMP through phosphorylation by adenosine kinase, we measured the effect of SBI-0206965 on the activity of human recombinant adenosine kinase *in vitro*. We observed that while a non-nucleoside adenosine kinase inhibitor (ABT-702) potently inhibited adenosine kinase activity at 0.01 μM, SBI-0206965 had no effect on adenosine

Biochemical Journal (2021) **478** 2977–2997
https://doi.org/10.1042/BCJ20210284

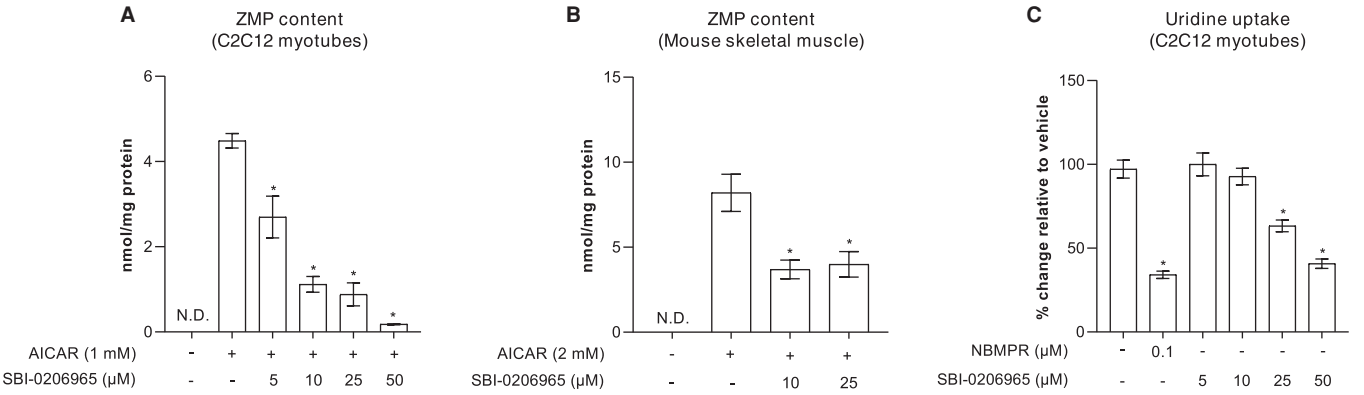

Figure 4. SBI-0206965 inhibits AICAR and uridine uptake in C2C12 myotubes.

(**A**,**B**) C2C12 myotubes or isolated mouse skeletal muscle (extensor digitorum longus) were pre-incubated for 30 min with vehicle (0.1% DMSO) or the indicated concentrations of SBI-0206965 followed by an additional 1-h incubation without (vehicle) or with AICAR (1 mM). Cell or tissue extracts were subjected to ZMP analysis by liquid chromatography-mass spectrometry. (**C**) C2C12 myotubes were incubated in the absence (vehicle) or presence of the indicated compounds for 30 min followed by an addition of [^{3}H]-uridine for 1 min for determination of uridine uptake. Results are expressed as mean ± SEM. *$P < 0.05$ (AICAR (A,B) or vehicle (C) vs. SBI-0206965 or NBMPR). N.D.; not detectable.

kinase up to 10 μM (Supplementary Figure S3). In line with these observations, SBI-0206965 also inhibited the uptake of uridine (ribonucleoside), although the potency was much more modest compared with NBMPR, a known inhibitor of nucleoside transporters [55] (Figure 4C). These results, together with a previous report [32], establish that SBI-0206965 inhibits the nucleoside transport system when used at ≥5–10 μM in multiple cell types and skeletal muscle tissue.

In vitro screen of SBI-0206965 against an extended panel of human protein kinases

Given the similarity of the kinase domain structure between AMPK and AMPK-related kinases (BRSK1, BRSK2, MARK1, MARK2, MARK3, MARK4, MELK, NUAK1, NUAK2, SIK1, SIK2, SIK3, SNRK) [40,41], we hypothesised that SBI-0206965 also inhibits several members of the AMPK-related kinases. In a previous study [32], among 13 members of the AMPK-related kinases only MARK3 was included in the screen. Notably, while AMPK was most potently inhibited (~80%) by SBI-0206965 (used at 0.25 μM), cross-reactivity with MARK3 (>40% inhibition) was also observed [32]. To gain a better understanding of SBI-0206965 selectivity we performed a screen against an expanded kinase panel consisting of 140 kinases, 49 of which overlap with a previous report [32]. Importantly, our panel includes 10 members of the AMPK-related kinases (BRSK1, BRSK2, MARK1, MARK2, MARK3, MARK4, MELK, NUAK1, SIK2, SIK3). Our results were similar to the results obtained in the previous screen [32] and SBI-0206965 robustly inhibited AMPK (~80%) and to a lesser degree (~30–50% inhibition) multiple other kinases (e.g. MARK3, MLK3, PAK4, Src, TrkA) (Figure 5A). Interestingly, our expanded screen revealed that SBI-0206965 also inhibits MLK1 and NUAK1 more potently than AMPK and ULK1/2, while an additional 25 kinases were inhibited by ≥25% (Figure 5B,C). We next determined the half-maximal inhibitory concentration (IC_{50}) of SBI-0206965 against AMPK and MLK1, as well as selected AMPK-related kinases (MARK3/4, NUAK1, SIK2). In line with the results of our single concentration screen (Figure 5C), we observed that IC_{50} values (ATP concentration = 20 μM) for MLK1 (0.071 μM) and NUAK1 (0.087 μM) were noticeably lower than AMPK (0.170 μM) (Figure 5D).

SBI-0206965 inhibits kinases that contain methionine at the gatekeeper residue

Structures of SBI-0206965 (Figure 6A) bound to AMPKα2 and ULK2 kinase domains have provided a detailed view of how this inhibitor engages the ATP-binding cleft of protein kinases (Figure 6B). Both structures revealed a compound binding mode that is characteristic of type I kinase inhibitors, taking advantage of the 'active-like' conformation of the kinase domain. SBI-0206965 engages the hinge region, the canonical DFG

PORTLAND PRESS

Biochemical Journal (2021) **478** 2977–2997
https://doi.org/10.1042/BCJ20210284

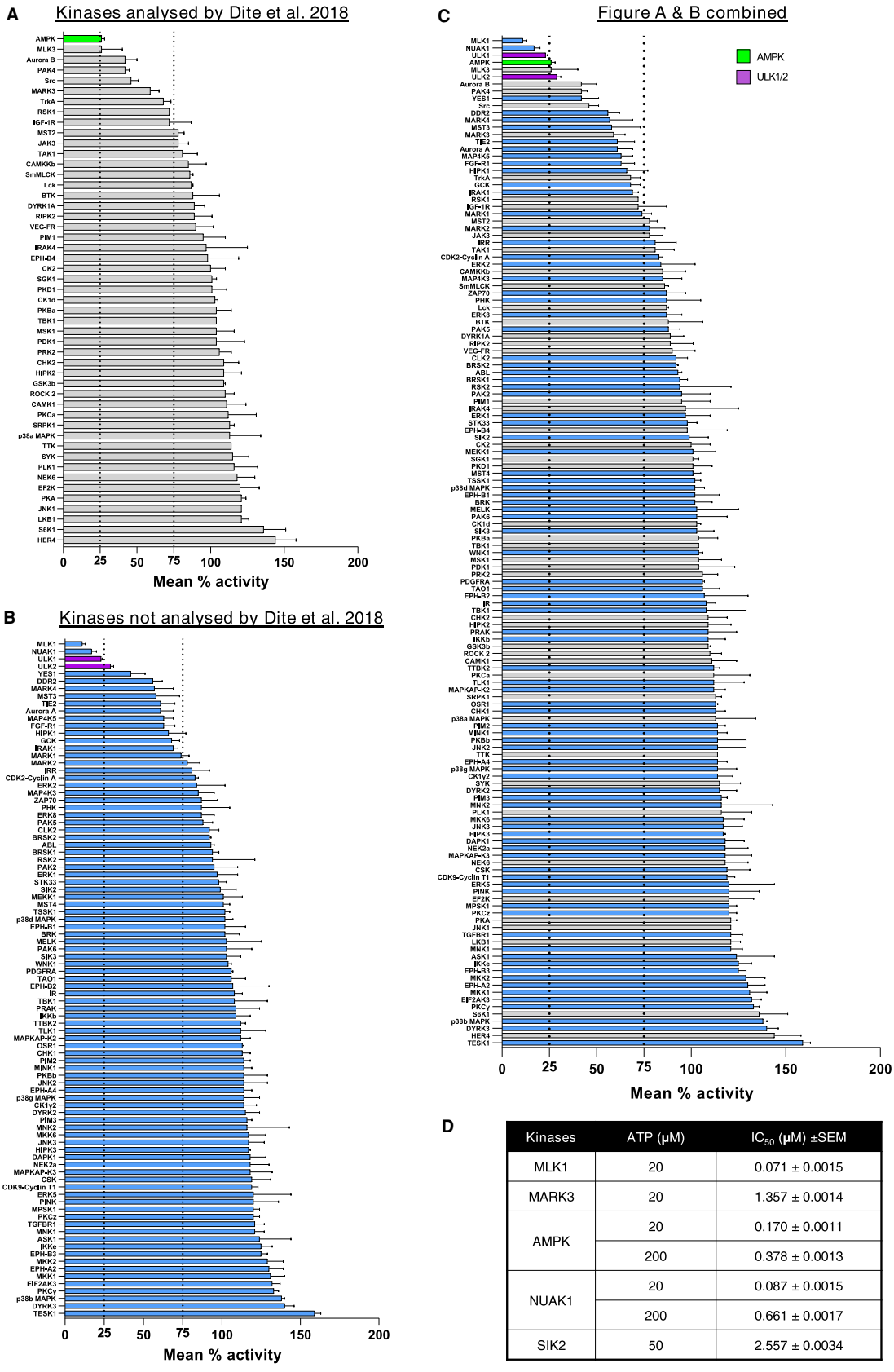

D

Kinases	ATP (μM)	IC_{50} (μM) ±SEM
MLK1	20	0.071 ± 0.0015
MARK3	20	1.357 ± 0.0014
AMPK	20	0.170 ± 0.0011
	200	0.378 ± 0.0013
NUAK1	20	0.087 ± 0.0015
	200	0.661 ± 0.0017
SIK2	50	2.557 ± 0.0034

Figure 5. Kinase selectivity profile for SBI-0206965. Part 1 of 2

(**A–C**) A screen of 140 human protein kinases ($n = 2$ per kinase, with or without 1 μM SBI-0206965) was performed *in vitro*

Biochemical Journal (2021) **478** 2977–2997
https://doi.org/10.1042/BCJ20210284

Figure 5. Kinase selectivity profile for SBI-0206965. Part 2 of 2

using the MRC-PPU Premier Screen service as described in Materials and methods. Results from the current profiling (140 kinases) were shown as; kinases profiled previously (49 kinases) by Dite *et al*. [32] (**A**) or not profiled (91 kinases) (**B**) or combined data from A and B (**C**). (**D**) The half-maximal inhibitory concentration (IC_{50}) values of the selected kinases against SBI-0206965 were performed using the indicated concentrations of ATP. Results are expressed as mean ± SEM.

motif and, importantly, the bromine atom fills the 'back pocket' next to the methionine 'gatekeeper' residue (Figure 6B). To gain a general overview of how SBI-0206965 may be interacting with MARK3 and MARK4 we performed molecular docking experiments using the SwissDock server [49]. As expected, SBI-0206965 engages MARK3 and MARK4 in a similar manner as AMPKα2 and ULK2 and binds in the ATP cleft with the bromine atom facing the methionine gatekeeper residue (Figure 6B). The position of docked SBI-0206965 was

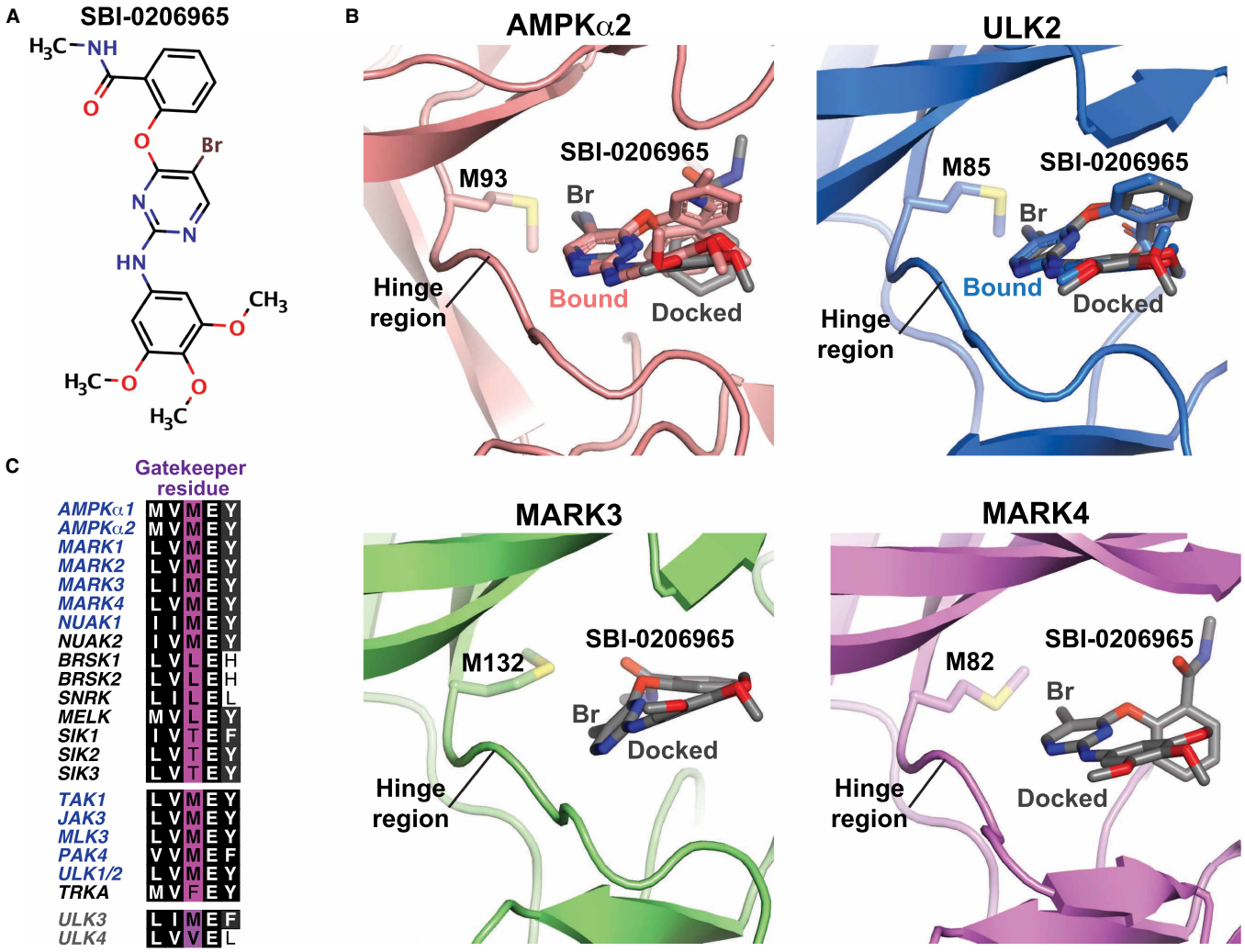

Figure 6. SBI-0206965 inhibitor engagement with kinase ATP-binding clefts.

(**A**) Chemical structure of SBI-0206965. (**B**) Kinase domain structures with bound and/or docked SBI-0206965 in the active site. SBI-0206965 engages the ATP-binding cleft near the hinge region and gatekeeper residue. Docked compound structures are shown in grey with coloured heteroatoms (red, oxygen; blue, nitrogen). Accession PDBid codes for bound compound structures: 6BX6, AMPKα2; 6YID, ULK2. (**C**) Gatekeeper residues of AMPK-related kinases (top panel) and a select set of kinases sensitive to SBI-0206965 (middle panel). Gatekeeper residues of ULK3 and ULK4 are shown (bottom panel).

Biochemical Journal (2021) 478 2977–2997
https://doi.org/10.1042/BCJ20210284

almost identical with the position of the bound compound to AMPKα2 and ULK2 (Figure 6B), thus validating our molecular docking approach for determining the general binding mode of SBI-0206965 to MARK3 and MARK4. Interestingly, we noticed that most SBI-0206965-sensitive kinases contain a large gatekeeper residue and a preference for methionine at this position (Figure 6C, Supplementary Figure S4).

Mutation of the gatekeeper methionine to threonine renders AMPK and ULK1 resistant to SBI-0206965 *in vitro*

We wondered if converting the gatekeeper residue methionine to an amino acid with a smaller side chain (e.g. threonine) would lead to loss of SBI-0206965 inhibition. We mutated the gatekeeper residue of AMPKα1 (M104 → Thr; M104T) or ULK1 (M92T) and expressed the respective mutant or wild type (WT) in mammalian cells. Immunoblot analysis showed that levels of total (AMPKα1 and ULK1) and AMPK α1-pThr172 were comparable between WT and the respective gatekeeper mutant (Figure 7A,B). We observed that both AMPKα1 M104T and ULK1 M92T mutants had lower activity *in vitro* compared with respective WT forms (Figure 7C, D). Despite the reduced basal activity, AMPKα1 M93T mutant was equally responsive to allosteric AMPK activators AMP and A-769662 (that bind the nucleotide-binding domain of γ subunit and ADaM site located at the interface of the α and β subunit, respectively [3]) compared with WT (Figure 7E,F). Notably, we observed a marked increase in SBI-0206965 IC_{50} for AMPKα1 M104T (∼20 fold) and ULK1 M92T (∼7-fold) compared with their respective WT control suggesting the importance of a methionine gatekeeper for SBI-0206965 inhibition. In contrast, the IC_{50} was virtually unchanged (within 2-fold difference) when Compound C, an ATP-competitive inhibitor that binds to the highly conserved active site of AMPK [29], was tested for inhibition of AMPK and ULK1 WT and mutant forms (Figure 7G–J).

Mutation of the gatekeeper methionine to threonine renders AMPK resistant to SBI-0206965 in cells

We next wanted to verify if *in vitro* results of the SBI-0206965-insensitive AMPK mutant (Figure 7G,H) can be recapitulated in a cellular context. We generated AMPKα1/α2 double knockout (DKO) U2OS cells (Supplementary Figure S5) and transfected the DKO cells with AMPKα1 WT or M104T mutant, which allowed us to avoid the influence of endogenous AMPKα in the mutant-expressing cells. The transfected cells were treated with vehicle or SBI-0206965 followed by incubation with vehicle or 991. Using a sensitive and quantitative HTRF assay, phosphorylation of ACC (Ser79) was measured as surrogate readout of cellular AMPK activity. As shown in Figure 8A, 991 equally increased ACC phosphorylation ∼2.5-fold in AMPKα1 WT- and M104T-expressing cells. Consistent with *in vitro* kinase activity data, the inhibitory effect of SBI-0206965 on ACC phosphorylation was blunted in AMPKα1 M104T-expressing cells compared with WT-expressing cells (Figure 8B). In contrast, the inhibitory effect of Compound C on ACC phosphorylation was similar between WT- and M104T-expressing cells (Figure 8C). Immunoblot analysis confirmed differential effects of SBI-0206965 on ACC phosphorylation (measured by HTRF assay, Figure 8A, B) in WT- and M104T-expressing cells and also consistent/comparable expression of the transfected WT and M104T mutant (Figure 8D). Collectively, we demonstrate the key role of a methionine gatekeeper for SBI-0206965-mediated inhibition of AMPK and have designed an inhibitor-insensitive mutant form of AMPK that can be used as control.

Discussion

The use of protein kinase inhibitors as tool compounds have transformed our ability to study cell signalling and resulting biological responses. However, for chemical probes to be useful a thorough analysis of their off-target effects is paramount. We have demonstrated that SBI-0206965 is not a highly selective inhibitor for either ULK1 or AMPK. In cell-free assays, SBI-0206965 inhibits MLK1/3, NUAK1 and also FAK [34] at the same levels as, or more robustly than ULK1 or AMPK. We also show that in intact cells, SBI-0206965 potently inhibits glucose and nucleoside uptake independent of its inhibition of AMPK activity. Analysis of co-crystal structures of AMPK-SBI-0206965 or ULK2-SBI-0206965 complex and computational modelling has revealed the importance of the gatekeeper methionine as a key determinant of SBI-0206965 sensitivity.

A previous study reported superior selectivity and preferable characteristics of SBI-0206965 for AMPK relative to Compound C, and a co-crystal structure of the AMPKα2 kinase domain (residues 6–278)-SBI-0206965 complex showed that the drug occupies a pocket that partially overlaps with the ATP-binding site [32]. The ATP-binding site is composed of the adenine pocket (near the hinge region), the ribose-interacting region, the

Biochemical Journal (2021) **478** 2977–2997
https://doi.org/10.1042/BCJ20210284

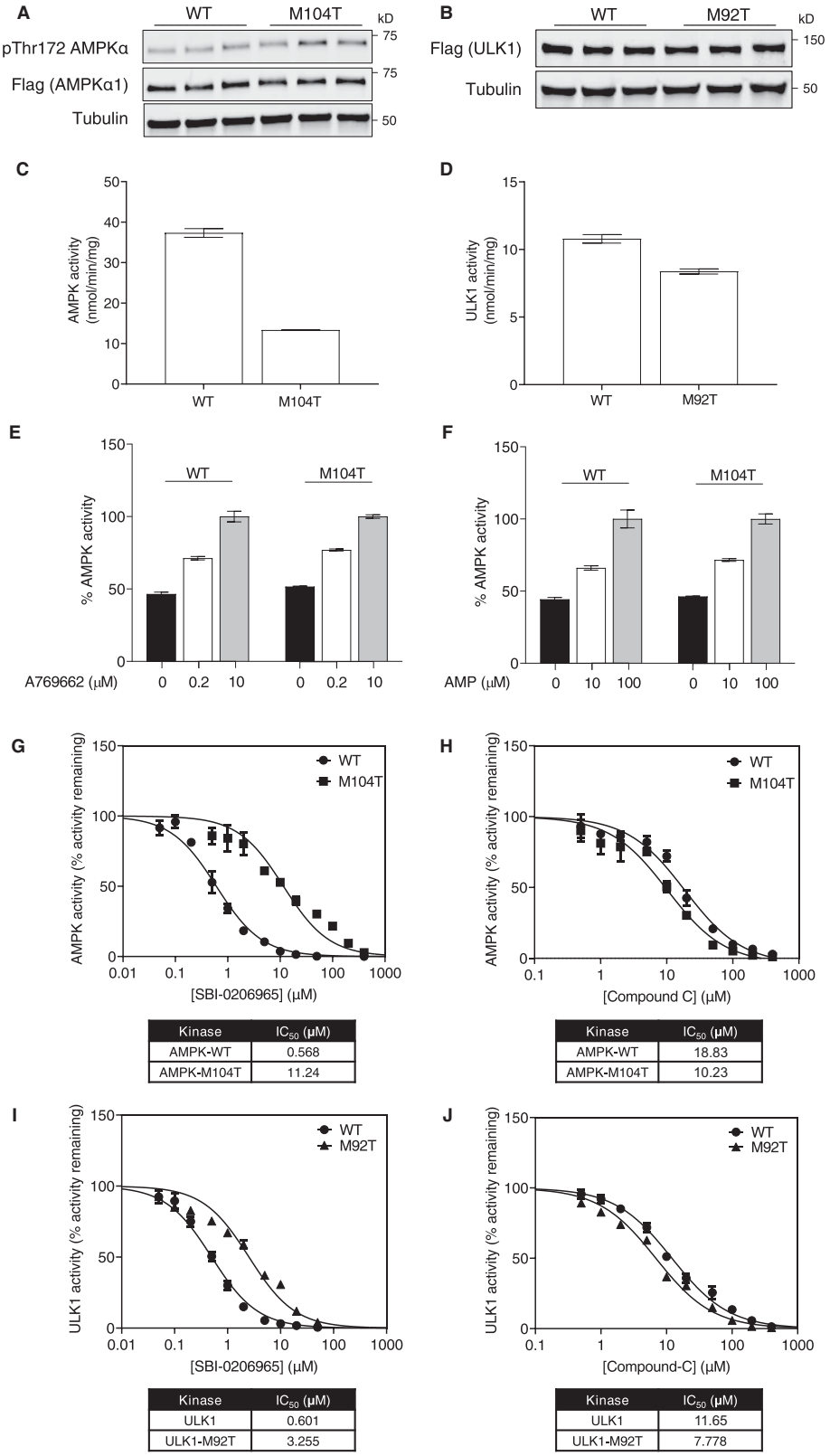

Kinase	IC_{50} (μM)
AMPK-WT	0.568
AMPK-M104T	11.24

Kinase	IC_{50} (μM)
AMPK-WT	18.83
AMPK-M104T	10.23

Kinase	IC_{50} (μM)
ULK1	0.601
ULK1-M92T	3.255

Kinase	IC_{50} (μM)
ULK1	11.65
ULK1-M92T	7.778

Figure 7. Mutation of gatekeeper methionine to threonine renders AMPK and ULK1 insensitive to SBI-0206965 in cell-free assay.

Part 1 of 2

(**A**–**J**) Immunopurified recombinant Flag-AMPKα1 (wild type (WT), M104T) complex or Flag-ULK1 (WT, M92T mutant) were

Biochemical Journal (2021) **478** 2977–2997
https://doi.org/10.1042/BCJ20210284

Figure 7. Mutation of gatekeeper methionine to threonine renders AMPK and ULK1 insensitive to SBI-0206965 in cell-free assay. Part 2 of 2

subjected to immunoblot analysis with the indicated antibodies (**A**,**B**) or *in vitro* kinase assay without (**C**,**D**) or with the indicated compounds (**E–J**). Results are expressed as mean ± SEM.

phosphate-coordinating region, the solvent accessible region, and the buried region [56,57]. The size and shape of the buried region is controlled by the gatekeeper residue, which serves as a molecular gate controlling the accessibility to this pocket and the nature of interactions with ligands (as seen in Figure 6C) [57,58]. In ∼73% of human kinases, a hydrophobic amino acid with a bulky side chain (Met, Phe, or Leu) is observed at that position, 22% have a small residue, such as Thr or Val and the remaining 5% have one of the remaining amino acids [57]. It has been reported that the amino acid distribution of the gatekeeper residue in some of the kinase groups differ significantly from the whole distribution. In particular, methionine is relatively more frequent (∼20 kinases) in the tyrosine kinase group than in the overall distribution [59]. We noticed that among the top 30 kinases inhibited by SBI-0206965 (>25% inhibition, Figure 5C) in the current screen, 25 kinases have medium (Met, Leu) or large gatekeepers (Phe, Tyr) and the other 4 kinases (YES, SRC, DDR2, TIE2, FGFR1) have a small gatekeeper (Thr, Ile, Val) (Supplementary Figure S4A). Notably, 19 out of 30 kinases (MLK1, NUAK1, ULK1, AMPK, MLK3, ULK2, Aurora B, PAK4, MARK4, MST3, MARK3, MAP4K5, GCK, IGF-1R, MARK1, MST2, MARK2, MARK2, JAK3, IRR, TAK1) have methionine in their gatekeeper residue. Consistent with this, out of the top 18 kinases whose binding/activity was shown to be inhibited by SBI-0206965 [34], seven of them (ULK1, ULK2, FAK, JAK3, JAK2, NUAK2, PAK1) have methionine in their gatekeeper residue. Nonetheless, it should also be noted that there are kinases with a methionine gatekeeper residue (e.g. JNKs), which are not selectively inhibited by SBI-0206965 [31,33].

We show here that converting the gatekeeper residue methionine of AMPKα1 (M104) or ULK1 (M92) to an amino acid with a smaller side chain (Thr) attenuated SBI-0206965 inhibition in a cell-free assay. Importantly, reintroducing WT or the M104T mutant of AMPKα1 into AMPKα1/α2 DKO U2O2 cells shows that the gatekeeper residue is also critical for efficient AMPK inhibition *in cellulo*. Interestingly, we observed that Compound C was not affected by mutations of the gatekeeper residue in AMPK and ULK1 *in vitro* or AMPK *in cellulo*. Structures of the AMPKα2 kinase domain bound to SBI-0206965 [32] and Compound C [29] show that SBI-0206965 contacts mainly the ATP pocket, hinge region and the gatekeeper region. In addition to the hinge and gatekeeper regions, Compound C interacts with the C-lobe αD helix and the activation segment, which has moved within the ATP-binding grove (Supplementary Figure S6). Therefore, Compound C is likely to be less reliant on interactions with the gatekeeper residue than SBI-0206965.

We and others [32,34] have observed that SBI-0206965 doses ≥25 μM increase phosphorylation of AMPKα T172 in multiple cell types, which may be due to off-target effects or cellular toxicity by reduced cellular adenylate energy charge as there was a trend toward reduced adenylate energy charge at 30 μM [32]. Contrary to this hypothesis, we did not observe reduced AMP/ATP, ADP/ATP ratio or adenylate energy charge in both C2C12 and primary hepatocytes with SBI-0206965 (up to 50 μM). We show that SBI-0206965 does not activate (>25%) upstream kinases (LKB1 or CaMKK2) that catalyse AMPKα T172 in the cell-free assay (Figure 5). It is unknown if SBI-0206965 inhibits a protein phosphatase that regulates AMPKα T172 or if inhibitor binding causes a conformational change that makes T172 less accessible to a phosphatase. Nonetheless, we observed that SBI-0206965-induced phosphorylation of AMPKα T172 was not accompanied by an increase but rather a decrease in AMPK substrate phosphorylation. This is presumably because SBI-0206965 binds the kinase domain and inhibits the catalytic activity of AMPK [32], negating the effect of increases in AMPKα T172 phosphorylation. This highlights the unreliability of using AMPKα T172 phosphorylation as a sole readout of cellular AMPK activity. In mouse embryonic fibroblasts (MEFs) and HEK293 cells, SBI-0206965 treatment at 10–50 μM (1 h) appeared to cause reduced activity of FAK, while mTOR, Akt, or ERK signalling were unaltered [34]. We observed that in C2C12 myotubes, but not adipocytes, Akt and ERK signalling were inhibited with ≥25 μM SBI-0206965.

In previous studies, SBI-0206965 was used to probe the effect of AMPK activators on glucose uptake in isolated rodent skeletal muscle *ex vivo*. It was reported that AICAR-mediated increase in phosphorylation of AMPK substrates (ACC, ULK1, or TBC1D1) was reduced with SBI-0206965 (used at 10 or 100 μM), which was accompanied by a profound reduction in glucose uptake in isolated rodent skeletal muscle *ex vivo* [54,60]. However, the results of these studies need to be cautiously interpreted as SBI-0206965 potently inhibits cellular

Biochemical Journal (2021) **478** 2977–2997
https://doi.org/10.1042/BCJ20210284

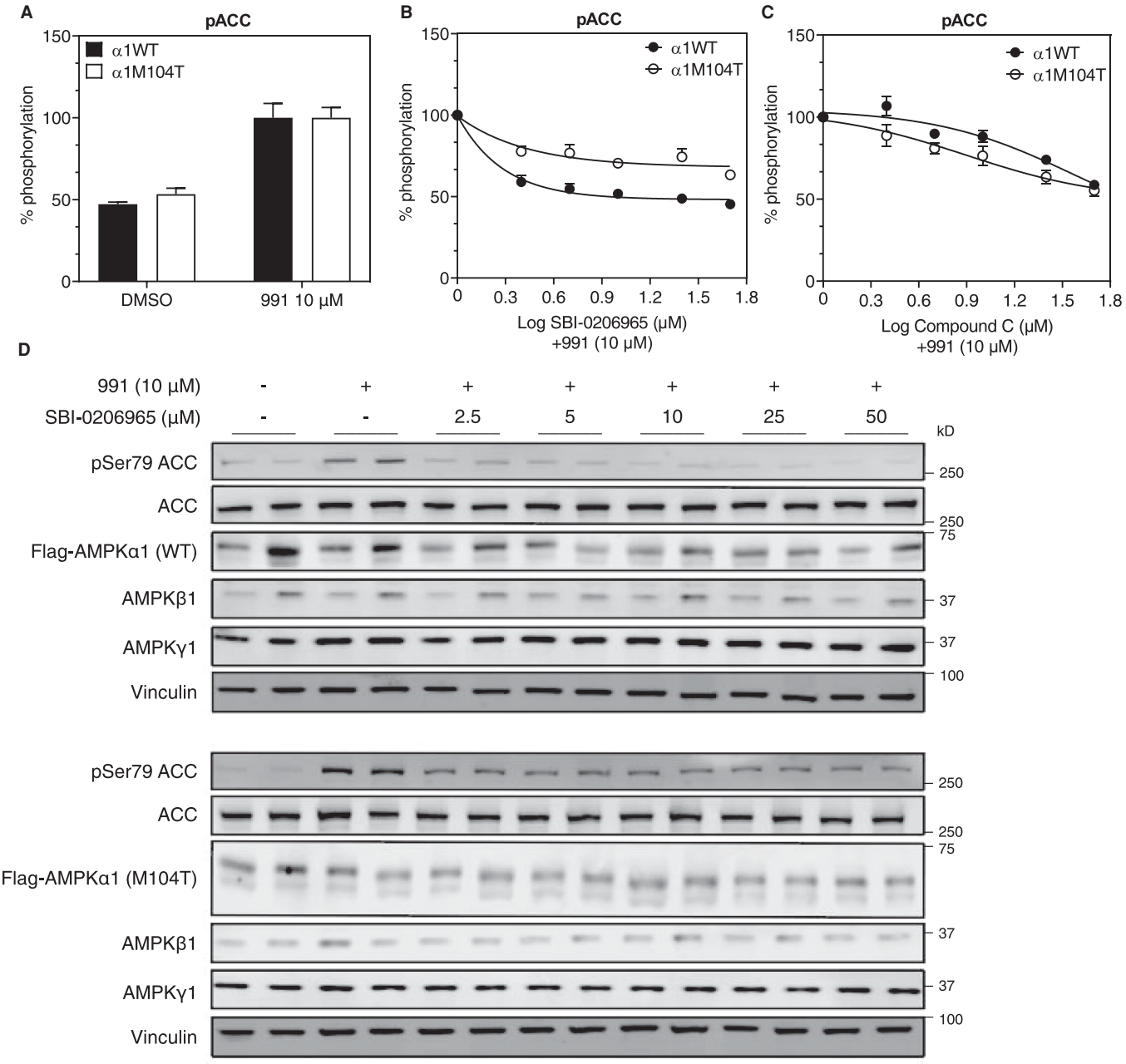

Figure 8. Mutation of gatekeeper methionine to threonine renders AMPK insensitive to SBI-0206965 in cells.

(**A**–**D**) cDNA constructs encoding Flag-AMPKα1 wild type (WT) or M104T mutant were transfected into AMPKα1/α2 double knockout (DKO) U2OS cells in 96-well plate. Forty-eight hours post transfection, cells were treated with indicated compounds for 1 h prior to cell lysis. Cell lysates were subjected to homogeneous time-resolved fluorescence (HTRF) assay, as described in the Materials and methods section, or immunoblot analysis. (**A**) Phosphorylation of ACC with vehicle (0.1% DMSO) or 991 (10 μM) using HTRF assay. Data are shown as % of 991-stimulated (100%) state. (**B**, **C**) % ACC phosphorylation (HTRF assay) relative to respective 991-stimulated value (100%) in response to increasing doses of SBI-0206965 or Compound C. (**D**) Immunoblot analysis of lysates from Flag-AMPKα1 WT (upper panel) or M104T mutant (lower panel) expressing cells using the indicated antibodies. Results are from three independent experiments ($n = 6$–9 per treatment) and are expressed as mean ± SEM.

uptake of AICAR (i.e. cellular accumulation of ZMP) at 10 μM in cultured cells and intact skeletal muscle tissue ([32] and the current study), and the above studies [54,60] did not report muscular ZMP content with AICAR in combination with SBI-0206965. Compound C also blocks cellular AICAR uptake through

Biochemical Journal (2021) **478** 2977–2997
https://doi.org/10.1042/BCJ20210284

competition for adenosine transporter binding sites, which accounts for its inhibitory effects on AICAR-mediated AMPK activation [61]. Based on the results reported in the previous [32,61] and the current study, we would strongly advise against the use of SBI-0206965 or Compound C in combination with AICAR when investigating cellular AMPK signalling and function.

A recent study reported that SBI-0206965 inhibits unstimulated and insulin-stimulated glucose transport in isolated skeletal muscle tissue and cultured L6 myotubes without apparent effect on GLUT4 translocation in L6 muscle cells [54]. This is reminiscent of the p38 MAPK inhibitor SB-203580, which was shown to inhibit insulin-stimulated glucose transport in skeletal muscle tissue/cells and adipocytes [62]. Using a SB-203580-resistant mutant of p38 MAPK, it was unambiguously shown that the inhibitory effect of SB-203580 on glucose transport was independent of p38 MAPK [63]. Along the same lines, it would be useful to utilise SBI-0206965-resistant mutant AMPK or ULK1 to probe drug selectivity towards respective kinase signalling pathways. For this purpose, we generated AMPKα1α2 DKO U2OS cells and transfected the DKO cells with AMPKα1 WT or M104T mutant, which allowed us to avoid the effect of SBI-0206965 on endogenous AMPKα in the mutant-expressing cells. A similar approach may be needed for the ULK pathway (e.g. use of ULK1/2 DKO cells and introduction of WT or M92T mutant). It would also be interesting to assess if the SBI-0206965-resistant mutant can be exploited to delineate drug selectivity towards the functional/physiological outputs of the kinases. However, it might be technically challenging since the SBI-0206965-resistant mutants display only a partial resistance to the inhibitor action.

In conclusion, while SBI-0206965 was reported as a highly selective inhibitor against ULK1 [34] and AMPK [32], we and others demonstrate that *in vitro* the compound is a potent inhibitor of several other kinases, including NUAK1, FAK, MLK1/3, and MARK3/4, all of which contain a methionine in their gatekeeper position. In addition to these kinases, SBI-0206965 also inhibits glucose and nucleoside transport systems; therefore, the drug effect on cell growth, metabolism or survival needs to be carefully assessed not only when studying kinase signalling cascades, but also when investigating nutrient and metabolite levels. Considering the cross-talk in kinase signalling networks and the myriad of roles that AMPK has in regulating metabolism, the field is still in need of a more selective and potent tool compound. Until more specific AMPK inhibitors are discovered, cautious use of the current tools and careful interpretations of results are advised. Our study has revealed inhibitor-insensitive mutant forms of AMPK and ULK1 that could be exploited as potential controls. We hope that our conclusions stimulate a search for better tool compounds and improved experimental design to probe AMPK and ULK1/2 functions.

Data availability

Data and reagents are available upon request to the corresponding author.

Competing Interests

The authors declare that there are no competing interests associated with the manuscript.

Funding

This work was financially supported by The Swedish Research Council (project grant Dnr 2017-01295), The Swedish Diabetes Foundation, Royal Physiographic Society of Lund and The Påhlsson Foundation (to O.G.). J. W.S. was supported by National Health and Medical Research Council (NHMRC) project grant (GNT1138102). This project was also supported in part by the Victorian Government's Operational Infrastructure Support Programme. A.J.O. is supported by a PhD scholarship funded by the Australian Catholic University. M.D. is supported by a postdoc fellowship and A.S.H. by a PhD scholarship from the Danish Diabetes Academy, which is funded by the Novo Nordisk Foundation (NNF17SA0031406). P.G. was supported by the Erasmus+ programme. Y.A. was supported by a research scholarship from King Saud University. E.Z. was supported by a Sir Henry Dale Fellowship (Wellcome Trust and the Royal Society; 200523/Z/16/Z). The Novo Nordisk Foundation Center for Basic Metabolic Research is an independent Research Center based at the University of Copenhagen, Denmark, and partially funded by an unconditional donation from the Novo Nordisk Foundation (Grant number NNF18CC0034900).

CRediT Author Contribution

Kei Sakamoto: Conceptualization, resources, supervision, funding acquisition, investigation, writing — original draft. **Danial Ahwazi**: Investigation, visualization, methodology, writing — review and editing. **Katyayanee**

Neopane: Investigation, visualization, methodology, writing — review and editing. **Greg R. Markby**: Investigation, methodology, writing — review and editing. **Franziska Kopietz**: Investigation, methodology, writing — review and editing. **Ashley J. Ovens**: Investigation, methodology, writing — review and editing. **Morten Dall**: Investigation, writing — review and editing. **Anna S. Hassing**: Investigation, writing — review and editing. **Pamina Graesle**: Investigation, writing — review and editing. **Yazeed Alshuweishi**: Investigation, writing — review and editing. **Jonas T. Treebak**: Supervision, methodology, writing — review and editing. **Ian P. Salt**: Supervision, writing — review and editing. **Olga Göransson**: Resources, supervision, writing — review and editing. **Elton Zeqiraj**: Conceptualization, investigation, visualization, writing — original draft. **John W. Scott**: Conceptualization, resources, supervision, investigation, visualization, methodology, writing — review and editing.

Acknowledgements
We thank Amy Ehrlich for her technical assistance and Sourav Banerjee for valuable input.

Abbreviations
ACC1, acetyl-CoA carboxylase-1; ADaM, allosteric drug and metabolite; AMPK, AMP-activated protein kinase; CaMKK2, Ca^{2+}-calmodulin-dependent protein kinase kinase-2; CBS, cystathionine β-synthase; ECL, enhanced chemiluminescence; EDL, extensor digitorum longus; LKB1, liver kinase B.

References
1 Hardie, D.G. and Sakamoto, K. (2006) AMPK: a key sensor of fuel and energy status in skeletal muscle. *Physiology (Bethesda)* **21**, 48–60 https://doi.org/10.1152/physiol.00044.2005
2 Hardie, D.G. (2011) AMP-activated protein kinase: an energy sensor that regulates all aspects of cell function. *Genes Dev.* **25**, 1895–1908 https://doi.org/10.1101/gad.17420111
3 Steinberg, G.R. and Carling, D. (2019) AMP-activated protein kinase: the current landscape for drug development. *Nat. Rev. Drug. Discov.* **18**, 527–551 https://doi.org/10.1038/s41573-019-0019-2
4 Cokorinos, E.C., Delmore, J., Reyes, A.R., Albuquerque, B., Kjobsted, R., Jorgensen, N.O. et al. (2017) Activation of skeletal muscle AMPK promotes glucose disposal and glucose lowering in non-human primates and mice. *Cell Metab.* **25**, 1147–1159.e1110 https://doi.org/10.1016/j.cmet.2017.04.010
5 Myers, R.W., Guan, H.P., Ehrhart, J., Petrov, A., Prahalada, S., Tozzo, E. et al. (2017) Systemic pan-AMPK activator MK-8722 improves glucose homeostasis but induces cardiac hypertrophy. *Science* **357**, 507–511 https://doi.org/10.1126/science.aah5582
6 Fullerton, M.D., Galic, S., Marcinko, K., Sikkema, S., Pulinilkunnil, T., Chen, Z.P. et al. (2013) Single phosphorylation sites in Acc1 and Acc2 regulate lipid homeostasis and the insulin-sensitizing effects of metformin. *Nat. Med.* **19**, 1649–1654 https://doi.org/10.1038/nm.3372
7 Boudaba, N., Marion, A., Huet, C., Pierre, R., Viollet, B. and Foretz, M. (2018) AMPK Re-activation suppresses hepatic steatosis but its downregulation does not promote fatty liver development. *EBioMedicine* **28**, 194–209 https://doi.org/10.1016/j.ebiom.2018.01.008
8 O'Neill, H.M., Lally, J.S., Galic, S., Thomas, M., Azizi, P.D., Fullerton, M.D. et al. (2014) AMPK phosphorylation of ACC2 is required for skeletal muscle fatty acid oxidation and insulin sensitivity in mice. *Diabetologia* **57**, 1693–1702 https://doi.org/10.1007/s00125-014-3273-1
9 Chen, Q., Xie, B., Zhu, S., Rong, P., Sheng, Y., Ducommun, S. et al. (2017) A Tbc1d1 (Ser231Ala)-knockin mutation partially impairs AICAR- but not exercise-induced muscle glucose uptake in mice. *Diabetologia* **60**, 336–345 https://doi.org/10.1007/s00125-016-4151-9
10 Kjobsted, R., Roll, J.L.W., Jorgensen, N.O., Birk, J.B., Foretz, M., Viollet, B. et al. (2019) AMPK and TBC1D1 regulate muscle glucose uptake after, but not during, exercise and contraction. *Diabetes* **68**, 1427–1440 https://doi.org/10.2337/db19-0050
11 Sakamoto, K. and Holman, G.D. (2008) Emerging role for AS160/TBC1D4 and TBC1D1 in the regulation of GLUT4 traffic. *Am. J. Physiol. Endocrinol. Metab.* **295**, E29–E37 https://doi.org/10.1152/ajpendo.90331.2008
12 Hawley, S.A., Davison, M., Woods, A., Davies, S.P., Beri, R.K., Carling, D. et al. (1996) Characterization of the AMP-activated protein kinase kinase from rat liver and identification of threonine 172 as the major site at which it phosphorylates AMP-activated protein kinase. *J. Biol. Chem.* **271**, 27879–27887 https://doi.org/10.1074/jbc.271.44.27879
13 Gowans, G.J., Hawley, S.A., Ross, F.A. and Hardie, D.G. (2013) AMP is a true physiological regulator of AMP-activated protein kinase by both allosteric activation and enhancing net phosphorylation. *Cell Metab.* **18**, 556–566 https://doi.org/10.1016/j.cmet.2013.08.019
14 Xiao, B., Sanders, M.J., Underwood, E., Heath, R., Mayer, F.V., Carmena, D. et al. (2011) Structure of mammalian AMPK and its regulation by ADP. *Nature* **472**, 230–233 https://doi.org/10.1038/nature09932
15 Oakhill, J.S., Steel, R., Chen, Z.P., Scott, J.W., Ling, N., Tam, S. et al. (2011) AMPK is a direct adenylate charge-regulated protein kinase. *Science* **332**, 1433–1435 https://doi.org/10.1126/science.1200094
16 Ovens, A.J., Scott, J.W., Langendorf, C.G., Kemp, B.E., Oakhill, J.S. and Smiles, W.J. (2021) Post-translational modifications of the energy guardian AMP-activated protein kinase. *Int. J. Mol. Sci* **22**, 1229 https://doi.org/10.3390/ijms22031229
17 Merrill, G.F., Kurth, E.J., Hardie, D.G. and Winder, W.W. (1997) AICA riboside increases AMP-activated protein kinase, fatty acid oxidation, and glucose uptake in rat muscle. *Am. J. Physiol.* **273**, E1107–E1112 https://doi.org/10.1152/ajpendo.1997.273.6.E1107
18 Hayashi, T., Hirshman, M.F., Kurth, E.J., Winder, W.W. and Goodyear, L.J. (1998) Evidence for 5′ AMP-activated protein kinase mediation of the effect of muscle contraction on glucose transport. *Diabetes* **47**, 1369–1373 https://doi.org/10.2337/diab.47.8.1369
19 Mu, J., Brozinick, Jr, J.T., Valladares, O., Bucan, M. and Birnbaum, M.J. (2001) A role for AMP-activated protein kinase in contraction- and hypoxia-regulated glucose transport in skeletal muscle. *Mol. Cell* **7**, 1085–1094 https://doi.org/10.1016/S1097-2765(01)00251-9

20 Guigas, B., Sakamoto, K., Taleux, N., Reyna, S.M., Musi, N., Viollet, B. et al. (2009) Beyond AICA riboside: in search of new specific AMP-activated protein kinase activators. *IUBMB Life* **61**, 18–26 https://doi.org/10.1002/iub.135
21 Collodet, C., Foretz, M., Deak, M., Bultot, L., Metairon, S., Viollet, B. et al. (2019) AMPK promotes induction of the tumor suppressor FLCN through activation of TFEB independently of mTOR. *FASEB J.* **33**, 12374–12391 https://doi.org/10.1096/fj.201900841R
22 Hunter, R.W., Hughey, C.C., Lantier, L., Sundelin, E.I., Peggie, M., Zeqiraj, E. et al. (2018) Metformin reduces liver glucose production by inhibition of fructose-1-6-bisphosphatase. *Nat. Med.* **24**, 1395–1406 https://doi.org/10.1038/s41591-018-0159-7
23 Foretz, M., Hebrard, S., Leclerc, J., Zarrinpashneh, E., Soty, M., Mithieux, G. et al. (2010) Metformin inhibits hepatic gluconeogenesis in mice independently of the LKB1/AMPK pathway via a decrease in hepatic energy state. *J. Clin. Invest.* **120**, 2355–2369 https://doi.org/10.1172/JCI40671
24 Cool, B., Zinker, B., Chiou, W., Kifle, L., Cao, N., Perham, M. et al. (2006) Identification and characterization of a small molecule AMPK activator that treats key components of type 2 diabetes and the metabolic syndrome. *Cell Metab.* **3**, 403–416 https://doi.org/10.1016/j.cmet.2006.05.005
25 Xiao, B., Sanders, M.J., Carmena, D., Bright, N.J., Haire, L.F., Underwood, E. et al. (2013) Structural basis of AMPK regulation by small molecule activators. *Nat. Commun.* **4**, 3017 https://doi.org/10.1038/ncomms4017
26 Calabrese, M.F., Rajamohan, F., Harris, M.S., Caspers, N.L., Magyar, R., Withka, J.M. et al. (2014) Structural basis for AMPK activation: natural and synthetic ligands regulate kinase activity from opposite poles by different molecular mechanisms. *Structure* **22**, 1161–1172 https://doi.org/10.1016/j.str.2014.06.009
27 Bultot, L., Jensen, T.E., Lai, Y.C., Madsen, A.L., Collodet, C., Kviklyte, S. et al. (2016) Benzimidazole derivative small-molecule 991 enhances AMPK activity and glucose uptake induced by AICAR or contraction in skeletal muscle. *Am. J. Physiol. Endocrinol. Metab.* **311**, E706–E719 https://doi.org/10.1152/ajpendo.00237.2016
28 Zhou, G., Myers, R., Li, Y., Chen, Y., Shen, X., Fenyk-Melody, J. et al. (2001) Role of AMP-activated protein kinase in mechanism of metformin action. *J. Clin. Invest.* **108**, 1167–1174 https://doi.org/10.1172/JCI13505
29 Handa, N., Takagi, T., Saijo, S., Kishishita, S., Takaya, D., Toyama, M. et al. (2011) Structural basis for compound C inhibition of the human AMP-activated protein kinase alpha2 subunit kinase domain. *Acta Crystallogr. D Biol. Crystallogr.* **67**, 480–487 https://doi.org/10.1107/S0907444911010201
30 Bain, J., Plater, L., Elliott, M., Shpiro, N., Hastie, C.J., McLauchlan, H. et al. (2007) The selectivity of protein kinase inhibitors: a further update. *Biochem. J.* **408**, 297–315 https://doi.org/10.1042/BJ20070797
31 Vogt, J., Traynor, R. and Sapkota, G.P. (2011) The specificities of small molecule inhibitors of the TGFss and BMP pathways. *Cell Signal.* **23**, 1831–1842 https://doi.org/10.1016/j.cellsig.2011.06.019
32 Dite, T.A., Langendorf, C.G., Hoque, A., Galic, S., Rebello, R.J., Ovens, A.J. et al. (2018) AMP-activated protein kinase selectively inhibited by the type II inhibitor SBI-0206965. *J. Biol. Chem.* **293**, 8874–8885 https://doi.org/10.1074/jbc.RA118.003547
33 Dasgupta, B. and Seibel, W. (2018) Compound C/Dorsomorphin: its use and misuse as an AMPK inhibitor. *Methods Mol. Biol.* **1732**, 195–202 https://doi.org/10.1007/978-1-4939-7598-3_12
34 Egan, D.F., Chun, M.G., Vamos, M., Zou, H., Rong, J., Miller, C.J. et al. (2015) Small molecule inhibition of the autophagy kinase ULK1 and identification of ULK1 substrates. *Mol. Cell* **59**, 285–297 https://doi.org/10.1016/j.molcel.2015.05.031
35 Dite, T.A., Ling, N.X.Y., Scott, J.W., Hoque, A., Galic, S., Parker, B.L. et al. (2017) The autophagy initiator ULK1 sensitizes AMPK to allosteric drugs. *Nat. Commun.* **8**, 571 https://doi.org/10.1038/s41467-017-00628-y
36 Chaikuad, A., Koschade, S.E., Stolz, A., Zivkovic, K., Pohl, C., Shaid, S. et al. (2019) Conservation of structure, function and inhibitor binding in UNC-51-like kinase 1 and 2 (ULK1/2). *Biochem. J.* **476**, 875–887 https://doi.org/10.1042/BCJ20190038
37 Ji, X., Zhang, X. and Li, Z. (2020) ULK1 inhibitor induces spindle microtubule disorganization and inhibits phosphorylation of Ser10 of histone H3. *FEBS Open Bio* **10**, 2452–2463 https://doi.org/10.1002/2211-5463.13000
38 Strembitska, A., Mancini, S.J., Gamwell, J.M., Palmer, T.M., Baillie, G.S. and Salt, I.P. (2018) A769662 inhibits insulin-stimulated Akt activation in human macrovascular endothelial cells independent of AMP-activated protein kinase. *Int. J. Mol. Sci* **19**, 3886 https://doi.org/10.3390/ijms19123886
39 Zachari, M., Longo, M. and Ganley, I.G. (2020) Aberrant autophagosome formation occurs upon small molecule inhibition of ULK1 kinase activity. *Life Sci. Alliance* **3**, e202000815 https://doi.org/10.26508/lsa.202000815
40 Alessi, D.R., Sakamoto, K. and Bayascas, J.R. (2006) LKB1-dependent signaling pathways. *Annu. Rev. Biochem.* **75**, 137–163 https://doi.org/10.1146/annurev.biochem.75.103004.142702
41 Lizcano, J.M., Goransson, O., Toth, R., Deak, M., Morrice, N.A., Boudeau, J. et al. (2004) LKB1 is a master kinase that activates 13 kinases of the AMPK subfamily, including MARK/PAR-1. *EMBO J.* **23**, 833–843 https://doi.org/10.1038/sj.emboj.7600110
42 Hunter, R.W., Foretz, M., Bultot, L., Fullerton, M.D., Deak, M., Ross, F.A. et al. (2014) Mechanism of action of compound-13: an alpha1-selective small molecule activator of AMPK. *Chem. Biol.* **21**, 866–879 https://doi.org/10.1016/j.chembiol.2014.05.014
43 Dall, M., Trammell, S.A.J., Asping, M., Hassing, A.S., Agerholm, M., Vienberg, S.G. et al. (2019) Mitochondrial function in liver cells is resistant to perturbations in NAD(+) salvage capacity. *J. Biol. Chem.* **294**, 13304–13326 https://doi.org/10.1074/jbc.RA118.006756
44 Ducommun, S., Ford, R.J., Bultot, L., Deak, M., Bertrand, L., Kemp, B.E. et al. (2014) Enhanced activation of cellular AMPK by dual-small molecule treatment: AICAR and A769662. *Am. J. Physiol. Endocrinol. Metab.* **306**, E688–E696 https://doi.org/10.1152/ajpendo.00672.2013
45 Rhein, P., Desjardins, E.M., Rong, P., Ahwazi, D., Bonhoure, N., Stolte, J. et al. (2021) Compound- and fiber type-selective requirement of AMPKgamma3 for insulin-independent glucose uptake in skeletal muscle. *Mol. Metab.* 101228 https://doi.org/10.1016/j.molmet.2021.101228
46 Kopietz, F., Alshuweish, Y., Bijland, S., Alghamdi, F., Degerman, E., Sakamoto, K. et al. (2021) A-769662 inhibits adipocyte glucose uptake in an AMPK-independent manner. *Biochem. J.* **478**, 633–646 https://doi.org/10.1042/BCJ20200659
47 Katwan, O.J., Alghamdi, F., Almabrouk, T.A., Mancini, S.J., Kennedy, S., Oakhill, J.S. et al. (2019) AMP-activated protein kinase complexes containing the beta2 regulatory subunit are up-regulated during and contribute to adipogenesis. *Biochem. J.* **476**, 1725–1740 https://doi.org/10.1042/BCJ20180714
48 Logie, L., Lees, Z., Allwood, J.W., McDougall, G., Beall, C. and Rena, G. (2018) Regulation of hepatic glucose production and AMPK by AICAR but not by metformin depends on drug uptake through the equilibrative nucleoside transporter 1 (ENT1). *Diabetes Obes. Metab.* **20**, 2748–2758 https://doi.org/10.1111/dom.13455

49 Grosdidier, A., Zoete, V. and Michielin, O. (2011) Swissdock, a protein-small molecule docking web service based on EADock DSS. *Nucleic Acids Res.* **39**, W270–W277 https://doi.org/10.1093/nar/gkr366
50 Lang, P.T., Brozell, S.R., Mukherjee, S., Pettersen, E.F., Meng, E.C., Thomas, V. et al. (2009) DOCK 6: combining techniques to model RNA-small molecule complexes. *RNA* **15**, 1219–1230 https://doi.org/10.1261/rna.1563609
51 Pettersen, E.F., Goddard, T.D., Huang, C.C., Couch, G.S., Greenblatt, D.M., Meng, E.C. et al. (2004) UCSF chimera–a visualization system for exploratory research and analysis. *J. Comput. Chem.* **25**, 1605–1612 https://doi.org/10.1002/jcc.20084
52 Chen, S., Wasserman, D.H., MacKintosh, C. and Sakamoto, K. (2011) Mice with AS160/TBC1D4-Thr649Ala knockin mutation are glucose intolerant with reduced insulin sensitivity and altered GLUT4 trafficking. *Cell Metab.* **13**, 68–79 https://doi.org/10.1016/j.cmet.2010.12.005
53 Sano, H., Kane, S., Sano, E., Miinea, C.P., Asara, J.M., Lane, W.S. et al. (2003) Insulin-stimulated phosphorylation of a Rab GTPase-activating protein regulates GLUT4 translocation. *J. Biol. Chem.* **278**, 14599–14602 https://doi.org/10.1074/jbc.C300063200
54 Knudsen, J.R., Madsen, A.B., Persson, K.W., Henriquez-Olguin, C., Li, Z. and Jensen, T.E. (2020) The ULK1/2 and AMPK inhibitor SBI-0206965 blocks AICAR and insulin-stimulated glucose transport. *Int. J. Mol. Sci* **21**, 2344 https://doi.org/10.3390/ijms21072344
55 Wright, N.J. and Lee, S.Y. (2019) Structures of human ENT1 in complex with adenosine reuptake inhibitors. *Nat. Struct. Mol. Biol.* **26**, 599–606 https://doi.org/10.1038/s41594-019-0245-7
56 Vulpetti, A. and Bosotti, R. (2004) Sequence and structural analysis of kinase ATP pocket residues. *Farmaco* **59**, 759–765 https://doi.org/10.1016/j.farmac.2004.05.010
57 Romano, V., de Beer, T.A. and Schwede, T. (2017) A computational protocol to evaluate the effects of protein mutants in the kinase gatekeeper position on the binding of ATP substrate analogues. *BMC Res. Notes* **10**, 104 https://doi.org/10.1186/s13104-017-2428-9
58 Elphick, L.M., Lee, S.E., Gouverneur, V. and Mann, D.J. (2007) Using chemical genetics and ATP analogues to dissect protein kinase function. *ACS Chem. Biol.* **2**, 299–314 https://doi.org/10.1021/cb700027u
59 Huang, D., Zhou, T., Lafleur, K., Nevado, C. and Caflisch, A. (2010) Kinase selectivity potential for inhibitors targeting the ATP binding site: a network analysis. *Bioinformatics* **26**, 198–204 https://doi.org/10.1093/bioinformatics/btp650
60 Choumessi, A.T., Johanns, M., Beaufay, C., Herent, M.F., Stroobant, V., Vertommen, D. et al. (2019) Two isoprenylated flavonoids from *Dorstenia psilurus* activate AMPK, stimulate glucose uptake, inhibit glucose production and lower glycemia. *Biochem. J.* **476**, 3687–3704 https://doi.org/10.1042/BCJ20190326
61 Fryer, L.G., Parbu-Patel, A. and Carling, D. (2002) Protein kinase inhibitors block the stimulation of the AMP-activated protein kinase by 5-amino-4-imidazolecarboxamide riboside. *FEBS Lett.* **531**, 189–192 https://doi.org/10.1016/S0014-5793(02)03501-9
62 Turban, S., Beardmore, V.A., Carr, J.M., Sakamoto, K., Hajduch, E., Arthur, J.S. et al. (2005) Insulin-stimulated glucose uptake does not require p38 mitogen-activated protein kinase in adipose tissue or skeletal muscle. *Diabetes* **54**, 3161–3168 https://doi.org/10.2337/diabetes.54.11.3161
63 Antonescu, C.N., Huang, C., Niu, W., Liu, Z., Eyers, P.A., Heidenreich, K.A. et al. (2005) Reduction of insulin-stimulated glucose uptake in L6 myotubes by the protein kinase inhibitor SB203580 is independent of p38MAPK activity. *Endocrinology* **146**, 3773–3781 https://doi.org/10.1210/en.2005-0404

Bibliography

Ahwazi, D., Neopane, K., Markby, G. R., Kopietz, F., Ovens, A. J., Dall, M., Hassing, A. S., Gräsle, P., Alshuweishi, Y., Treebak, J. T., Salt, I. P., Göransson, O., Zeqiraj, E., Scott, J. W., & Sakamoto, K. (2021). Investigation of the specificity and mechanism of action of the ULK1/AMPK inhibitor SBI-0206965. *Biochem. J.*, *478*(15), 2977–2997. https://doi.org/10.1042/BCJ20210284

Alam, M. S. (2018). Proximity ligation assay (pla). *Current protocols in immunology*, *123*(1), e58.

Aledavood, E., Gheeraert, A., Forte, A., Vuillon, L., Rivalta, I., Luque, F. J., & Estarellas, C. (2021). Elucidating the Activation Mechanism of AMPK by Direct Pan-Activator PF-739. *Front. Mol. Biosci.*, *8*, 760026. https://doi.org/10.3389/fmolb.2021.760026

Ali, N., Ling, N., Krishnamurthy, S., Oakhill, J. S., Scott, J. W., Stapleton, D. I., Kemp, B. E., Anand, G. S., & Gooley, P. R. (2016). B-subunit myristoylation functions as an energy sensor by modulating the dynamics of AMP-activated Protein Kinase. *Sci. Rep.*, *6*(1), 39417. https://doi.org/10.1038/srep39417

Altan-Bonnet, N., Sougrat, R., & Lippincott-Schwartz, J. (2004). Molecular basis for Golgi maintenance and biogenesis. *Curr. Opin. Cell Biol.*, *16*(4), 364–372. https://doi.org/10.1016/j.ceb.2004.06.011

Andersson, U., Filipsson, K., Abbott, C. R., Woods, A., Smith, K., Bloom, S. R., Carling, D., & Small, C. J. (2004). AMP-activated Protein Kinase Plays a Role in the Control of Food Intake. *J. Biol. Chem.*, *279*(13), 12005–12008. https://doi.org/10.1074/jbc.C300557200

Bailey Blackburn, J., Pokrovskaya, I., Fisher, P., Ungar, D., & Lupashin, V. V. (2016). COG Complex Complexities: Detailed Characterization of a Complete Set of HEK293T Cells Lacking Individual COG Subunits. *Front. Cell Dev. Biol.*, *4*. https://doi.org/10.3389/fcell.2016.00023

Banerji, S., Ngo, M., Lane, C. F., Robinson, C.-A., Minogue, S., & Ridgway, N. D. (2010). Oxysterol Binding Protein-dependent Activation of Sphingomyelin Synthesis in the Golgi Apparatus Requires Phosphatidylinositol 4-Kinase II␣. *Mol. Biol. Cell*, *21*, 10.

Banko, M. R., Allen, J. J., Schaffer, B. E., Wilker, E. W., Tsou, P., White, J. L., Villén, J., Wang, B., Kim, S. R., Sakamoto, K., Gygi, S. P., Cantley, L. C., Yaffe, M. B., Shokat, K. M., & Brunet, A. (2011). Chemical Genetic Screen for AMPKα2 Substrates Uncovers a Network of Proteins Involved in Mitosis. *Mol. Cell*, *44*(6), 878–892. https://doi.org/10.1016/j.molcel.2011.11.005

Bendayan, M., London, I., Kemp, B. E., Hardie, G. D., Ruderman, N., & Prentki, M. (2009). Association of AMP-activated Protein Kinase Subunits With Glycogen Particles as Revealed In Situ by Immunoelectron Microscopy. *J Histochem Cytochem.*, *57*(10), 963–971. https://doi.org/10.1369/jhc.2009.954016

Boncompain, G., & Weigel, A. V. (2018). Transport and sorting in the golgi complex: multiple mechanisms sort diverse cargo. *Current Opinion in Cell Biology*, *50*, 94–101.

Bultot, L., Jensen, T. E., Lai, Y.-C., Madsen, A. L. B., Collodet, C., Kviklyte, S., Deak, M., Yavari, A., Foretz, M., Ghaffari, S., Bellahcene, M., Ashrafian, H., Rider, M. H., Richter, E. A., & Sakamoto, K. (2016). Benzimidazole derivative small-molecule 991 enhances AMPK activity and glucose uptake induced by AICAR or contraction in skeletal muscle. *American Journal of Physiology-Endocrinology and Metabolism*, *311*(4), E706–E719. https://doi.org/10.1152/ajpendo.00237.2016

Burckhardt, C. J., Minna, J. D., & Danuser, G. (2021). Sh3bp4 promotes neuropilin-1 and α5-integrin endocytosis and is inhibited by akt. *Developmental cell*, *56*(8), 1164–1181.

Carling, D., Zammit, V. A., & Hardie, D. (1987). A common bicyclic protein kinase cascade inactivates the regulatory enzymes of fatty acid and cholesterol biosynthesis. *FEBS Lett.*, *223*(2), 217–222. https://doi.org/10.1016/0014-5793(87)80292-2

Chabin-Brion, K., Marceiller, J., Perez, F., Settegrana, C., Drechou, A., Durand, G., & Poüs, C. (2001). The Golgi Complex Is a Microtubule-organizing Organelle (S. R. Pfeffer, Ed.). *MBoC*, *12*(7), 2047–2060. https://doi.org/10.1091/mbc.12.7.2047

Cheung, P. C. F., Salt, I. P., Davies, S. P., Hardie, D. G., & Carling, D. (2000). Characterization of AMP-activated protein kinase γ-subunit isoforms and their role in AMP binding, 11.

Chida, T., Ando, M., Matsuki, T., Masu, Y., Nagaura, Y., Takano-Yamamoto, T., Tamura, S., & Kobayashi, T. (2013). N-Myristoylation is essential for protein phosphatases PPM1A and PPM1B to dephosphorylate their physiological substrates in cells. *Biochem. J.*, *449*(3), 741–749. https://doi.org/10.1042/BJ20121201

Chow, M., Newman, J. F. E., Filman, D., Hogle, J. M., Rowlands, D. J., & Brown, F. (1987). Myristylation of picornavirus capsid protein VP4 and its structural significance [Number: 6122]. *Nature*, *327*(6122), 482–486. https://doi.org/10.1038/327482a0

Clark, K., MacKenzie, K. F., Petkevicius, K., Kristariyanto, Y., Zhang, J., Choi, H. G., Peggie, M., Plater, L., Pedrioli, P. G., McIver, E., et al. (2012). Phosphorylation of crtc3 by the salt-inducible kinases controls the interconversion of classically activated and regulatory macrophages. *Proceedings of the National Academy of Sciences*, *109*(42), 16986–16991.

Crute, B. E., Seefeld, K., Gamble, J., Kemp, B. E., & Witters, L. A. (1998). Functional Domains of the α1 Catalytic Subunit of the AMP-activated Protein Kinase. *J. Biol. Chem.*, *273*(52), 35347–35354. https://doi.org/10.1074/jbc.273.52.35347

Dagon, Y., Hur, E., Zheng, B., Wellenstein, K., Cantley, L. C., & Kahn, B. B. (2012). p70S6 Kinase Phosphorylates AMPK on Serine 491 to Mediate Leptin's Effect on Food Intake. *Cell Metab.*, *16*(1), 104–112. https://doi.org/10.1016/j.cmet.2012.05.010

Dale, S., Wilson, W. A., Edelman, A. M., & Hardie, D. (1995). Similar substrate recognition motifs for mammalian AMP-activated protein kinase, higher plant HMG-CoA reductase kinase-A, yeast SNF1, and mammalian calmodulin-dependent protein

kinase I [Number: 2-3]. *FEBS Letters*, *361*(2-3), 191–195. https://doi.org/10.1016/0014-5793(95)00172-6

Darling, N. J., & Cohen, P. (2021). Nuts and bolts of the salt-inducible kinases (siks). *Biochemical Journal*, *478*(7), 1377–1397.

Davies, S. P., Helps, N. R., Cohen, P. T., & Hardie, D. G. (1995). 5-amp inhibits dephosphorylation, as well as promoting phosphorylation, of the amp-activated protein kinase. studies using bacterially expressed human protein phosphatase-2cα and native bovine protein phosphatase-2ac. *FEBS letters*, *377*(3), 421–425.

Dite, T. A., Langendorf, C. G., Hoque, A., Galic, S., Rebello, R. J., Ovens, A. J., Lindqvist, L. M., Ngoei, K. R., Ling, N. X., Furic, L., et al. (2018). Amp-activated protein kinase selectively inhibited by the type ii inhibitor sbi-0206965. *Journal of Biological Chemistry*, *293*(23), 8874–8885.

Dite, T. A., Ling, N. X., Scott, J. W., Hoque, A., Galic, S., Parker, B. L., Ngoei, K. R., Langendorf, C. G., O'Brien, M. T., Kundu, M., et al. (2017). The autophagy initiator ulk1 sensitizes ampk to allosteric drugs. *Nature communications*, *8*(1), 1–14.

Dong, Y., Zhang, M., Liang, B., Xie, Z., Zhao, Z., Asfa, S., Choi, H. C., & Zou, M.-H. (2010). Reduction of AMP-Activated Protein Kinase α2 Increases Endoplasmic Reticulum Stress and Atherosclerosis In Vivo. *Circulation*, *121*(6), 792–803. https://doi.org/10.1161/CIRCULATIONAHA.109.900928

Drake, J. C., Wilson, R. J., Laker, R. C., Guan, Y., Spaulding, H. R., Nichenko, A. S., Shen, W., Shang, H., Dorn, M. V., Huang, K., Zhang, M., Bandara, A. B., Brisendine, M. H., Kashatus, J. A., Sharma, P. R., Young, A., Gautam, J., Cao, R., Wallrabe, H., … Yan, Z. (2021). Mitochondria-localized AMPK responds to local energetics and contributes to exercise and energetic stress-induced mitophagy. *Proc. Natl. Acad. Sci. U.S.A.*, *118*(37), e2025932118. https://doi.org/10.1073/pnas.2025932118

Ducker, C. E., Upson, J. J., French, K. J., & Smith, C. D. (2005). Two N-Myristoyltransferase Isozymes Play Unique Roles in Protein Myristoylation, Proliferation, and Apoptosis. *Mol Cancer Res*, *3*(8), 463–476. https://doi.org/10.1158/1541-7786.MCR-05-0037

Ducommun, S., Deak, M., Sumpton, D., Ford, R. J., Núñez Galindo, A., Kussmann, M., Viollet, B., Steinberg, G. R., Foretz, M., Dayon, L., Morrice, N. A., & Sakamoto, K. (2015). Motif affinity and mass spectrometry proteomic approach for the discovery of cellular AMPK targets: Identification of mitochondrial fission factor as a new AMPK substrate. *Cell. Signal.*, *27*(5), 978–988. https://doi.org/10.1016/j.cellsig.2015.02.008

Ducommun, S., Deak, M., Zeigerer, A., Göransson, O., Seitz, S., Collodet, C., Madsen, A. B., Jensen, T. E., Viollet, B., Foretz, M., Gut, P., Sumpton, D., & Sakamoto, K. (2019). Chemical genetic screen identifies Gapex-5/GAPVD1 and STBD1 as novel AMPK substrates. *Cell. Signal.*, *57*, 45–57. https://doi.org/10.1016/j.cellsig.2019.02.001

Dzamko, N., van Denderen, B. J., Hevener, A. L., Jørgensen, S. B., Honeyman, J., Galic, S., Chen, Z.-P., Watt, M. J., Campbell, D. J., Steinberg, G. R., & Kemp, B. E. (2010). AMPK β1 Deletion Reduces Appetite, Preventing Obesity and Hepatic Insulin Resistance. *J. Biol. Chem.*, *285*(1), 115–122. https://doi.org/10.1074/jbc.M109.056762

Egan, D. F., Chun, M. G., Vamos, M., Zou, H., Rong, J., Miller, C. J., Lou, H. J., Raveendra-Panickar, D., Yang, C.-C., Sheffler, D. J., Teriete, P., Asara, J. M., Turk, B. E., Cosford, N. D., & Shaw, R. J. (2015). Small Molecule Inhibition of the Autophagy Kinase ULK1 and Identification of ULK1 Substrates. *Mol. Cell*, *59*(2), 285–297. https://doi.org/10.1016/j.molcel.2015.05.031

Emr, S., Glick, B. S., Linstedt, A. D., Lippincott-Schwartz, J., Luini, A., Malhotra, V., Marsh, B. J., Nakano, A., Pfeffer, S. R., Rabouille, C., Rothman, J. E., Warren, G., & Wieland, F. T. (2009). Journeys through the Golgi—taking stock in a new era. *J. Cell Biol.*, *187*(4), 449–453. https://doi.org/10.1083/jcb.200909011

Fassett, J. T., Hu, X., Xu, X., Lu, Z., Zhang, P., Chen, Y., & Bache, R. J. (2013). AMPK attenuates microtubule proliferation in cardiac hypertrophy [Number: 5]. *American Journal of Physiology-Heart and Circulatory Physiology*, *304*(5), H749–H758. https://doi.org/10.1152/ajpheart.00935.2011

Feng, D., Biftu, T., Romero, F. A., Kekec, A., Dropinski, J., Kassick, A., Xu, S., Kurtz, M. M., Gollapudi, A., Shao, Q., Yang, X., Lu, K., Zhou, G., Kemp, D., Myers, R. W., Guan, H.-P., Trujillo, M. E., Li, C., Weber, A., & Sebhat, I. K. (2018). Discovery of MK-8722: A Systemic, Direct Pan-Activator of AMP-Activated Protein Kinase. *ACS Med. Chem. Lett.*, *9*(1), 39–44. https://doi.org/10.1021/acsmedchemlett.7b00417

Finlay, D. K. (2019). N-myristoylation of ampk controls t cell inflammatory function. *Nature Immunology*, *20*(3), 252–254.

Garcia, D., Hellberg, K., Chaix, A., Wallace, M., Herzig, S., Badur, M. G., Lin, T., Shokhirev, M. N., Pinto, A. F., Ross, D. S., Saghatelian, A., Panda, S., Dow, L. E., Metallo, C. M., & Shaw, R. J. (2019). Genetic Liver-Specific AMPK Activation Protects against Diet-Induced Obesity and NAFLD [Number: 1]. *Cell Reports*, *26*(1), 192–208.e6. https://doi.org/10.1016/j.celrep.2018.12.036

Garcia, D., & Shaw, R. J. (2017). Ampk: mechanisms of cellular energy sensing and restoration of metabolic balance. *Molecular cell*, *66*(6), 789–800.

Gerlitz, G., Reiner, O., & Bustin, M. (2013). Microtubule dynamics alter the interphase nucleus [Number: 7]. *Cellular and Molecular Life Sciences*, *70*(7), 1255–1268. https://doi.org/10.1007/s00018-012-1200-5

Gluais-Dagorn, P., Foretz, M., Steinberg, G. R., Batchuluun, B., Zawistowska-Deniziak, A., Lambooij, J. M., Guigas, B., Carling, D., Monternier, P.-A., Moller, D. E., et al. (2022). Direct ampk activation corrects nash in rodents through metabolic effects and direct action on inflammation and fibrogenesis. *Hepatology communications*, *6*(1), 101–119.

Gonatas, N. K. (1997). The Golgi apparatus in disease. In E. G. Berger & J. Roth (Eds.), *The Golgi Apparatus* (pp. 247–273). Birkhäuser Basel. https://doi.org/10.1007/978-3-0348-8876-9_9

Göransson, O., McBride, A., Hawley, S. A., Ross, F. A., Shpiro, N., Foretz, M., Viollet, B., Hardie, D. G., & Sakamoto, K. (2007). Mechanism of action of a-769662, a valuable tool for activation of amp-activated protein kinase. *Journal of Biological Chemistry*, *282*(45), 32549–32560.

Gosavi, P., Houghton, F. J., McMillan, P. J., Hanssen, E., & Gleeson, P. A. (2017). The Golgi ribbon in mammalian cells negatively regulates autophagy by modulating mTOR activity. *J. Cell Sci.*, jcs.211987. https://doi.org/10.1242/jcs.211987

Gowans, G. J., & Hardie, D. G. (2014). AMPK: a cellular energy sensor primarily regulated by AMP. *Biochem. Soc. Trans.*, *42*(1), 71–75. https://doi.org/10.1042/BST20130244

Gowans, G. J., Hawley, S. A., Ross, F. A., & Hardie, D. G. (2013). AMP Is a True Physiological Regulator of AMP-Activated Protein Kinase by Both Allosteric Activation and Enhancing Net Phosphorylation. *Cell Metab.*, *18*(4), 556–566. https://doi.org/10.1016/j.cmet.2013.08.019

Guizzunti, G., & Seemann, J. (2016). Mitotic Golgi disassembly is required for bipolar spindle formation and mitotic progression. *Proc Natl Acad Sci USA*, *113*(43), E6590–E6599. https://doi.org/10.1073/pnas.1610844113

Hardie, D. G., Schaffer, B. E., & Brunet, A. (2016). Ampk: an energy-sensing pathway with multiple inputs and outputs. *Trends in cell biology*, *26*(3), 190–201.

Hawley, S. A., Boudeau, J., Reid, J. L., Mustard, K. J., Udd, L., Mäkelä, T. P., Alessi, D. R., & Hardie, D. G. (2003). Complexes between the LKB1 tumor suppressor, STRAD␣/
and MO25␣/
are upstream kinases in the AMP-activated protein kinase cascade. *J. Biol.*, 16.

Hawley, S. A., Davison, M., Woods, A., Davies, S. P., Beri, R. K., Carling, D., & Hardie, D. G. (1996). Characterization of the AMP-activated Protein Kinase Kinase from Rat Liver and Identification of Threonine 172 as the Major Site at Which It Phosphorylates AMP-activated Protein Kinase. *J. Biol. Chem.*, *271*(44), 27879–27887. https://doi.org/10.1074/jbc.271.44.27879

Hawley, S. A., Selbert, M. A., Goldstein, E. G., Edelman, A. M., Carling, D., & Hardie, D. G. (1995). 5-AMP Activates the AMP-activated Protein Kinase Cascade, and Ca2+/Calmodulin Activates the Calmodulin-dependent Protein Kinase I Cascade, via Three Independent Mechanisms. *J. Biol. Chem.*, *270*(45), 27186–27191. https://doi.org/10.1074/jbc.270.45.27186

Hayashi, N., & Titani, K. (2010). N-myristoylated proteins, key components in intracellular signal transduction systems enabling rapid and flexible cell responses [Number: 5]. *Proceedings of the Japan Academy, Series B*, *86*(5), 494–508. https://doi.org/10.2183/pjab.86.494

Herzig, S., & Shaw, R. J. (2018). Ampk: guardian of metabolism and mitochondrial homeostasis. *Nature reviews Molecular cell biology*, *19*(2), 121–135.

Hoffman, N. J., Parker, B. L., Chaudhuri, R., Fisher-Wellman, K. H., Kleinert, M., Humphrey, S. J., Yang, P., Holliday, M., Trefely, S., Fazakerley, D. J., et al. (2015). Global phosphoproteomic analysis of human skeletal muscle reveals a network of exercise-regulated kinases and ampk substrates. *Cell metabolism*, *22*(5), 922–935.

Horman, S., Vertommen, D., Heath, R., Neumann, D., Mouton, V., Woods, A., Schlattner, U., Wallimann, T., Carling, D., Hue, L., & Rider, M. H. (2006). Insulin Antagonizes Ischemia-induced Thr172 Phosphorylation of AMP-activated Protein Kinase α-Subunits in Heart

via Hierarchical Phosphorylation of Ser485/491. *J. Biol. Chem.*, *281*(9), 5335–5340. https://doi.org/10.1074/jbc.M506850200

Hunter, R. W., Treebak, J. T., Wojtaszewski, J. F., & Sakamoto, K. (2011). Molecular Mechanism by Which AMP-Activated Protein Kinase Activation Promotes Glycogen Accumulation in Muscle. *Diabetes*, *60*(3), 766–774. https://doi.org/10.2337/db10-1148

Hurley, R. L., Barré, L. K., Wood, S. D., Anderson, K. A., Kemp, B. E., Means, A. R., & Witters, L. A. (2006). Regulation of AMP-activated Protein Kinase by Multisite Phosphorylation in Response to Agents That Elevate Cellular cAMP. *J. Biol. Chem.*, *281*(48), 36662–36672. https://doi.org/10.1074/jbc.M606676200

Ireland, S., Ramnarayanan, S., Fu, M., Zhang, X., Zhang, J., Li, J., Emebo, D., & Wang, Y. (2020). Cytosolic Ca2+ Modulates Golgi Structure Through PKCα-Mediated GRASP55 Phosphorylation [Number: 3]. *iScience*, *23*(3), 100952. https://doi.org/10.1016/j.isci.2020.100952

Iseli, T. J., Walter, M., van Denderen, B. J. W., Katsis, F., Witters, L. A., Kemp, B. E., Michell, B. J., & Stapleton, D. (2005). AMP-activated Protein Kinase β Subunit Tethers α and γ Subunits via Its C-terminal Sequence (186-270). *J. Biol. Chem.*, *280*(14), 13395–13400. https://doi.org/10.1074/jbc.M412993200

Jackson, C. L. (2018). Activators and Effectors of the Small G Protein Arf1 in Regulation of Golgi Dynamics During the Cell Division Cycle. *Front. Cell Dev. Biol.*, *6*, 29. https://doi.org/10.3389/fcell.2018.00029

Jenne, D. E., Reomann, H., Nezu, J.-i., Friedel, W., Loff., S., Jeschke, R., Müller, O., Back, W., & Zimmer, M. (1998). Peutz-Jeghers syndrome is caused by mutations in a novel serine threoninekinase. *Nat Genet*, *18*(1), 38–43. https://doi.org/10.1038/ng0198-38

Jørgensen, S. B., Wojtaszewski, J. F. P., Viollet, B., Andreelli, F., Birk, J. B., Hellsten, Y., Schjerling, P., Vaulont, S., Neufer, P. D., Richter, E. A., & Pilegaard, H. (2005). Effects of α-AMPK knockout on exercise-induced gene activation in mouse skeletal muscle. *FASEB j.*, *19*(9), 1146–1148. https://doi.org/10.1096/fj.04-3144fje

Joseph, B. K., Liu, H.-Y., Francisco, J., Pandya, D., Donigan, M., Gallo-Ebert, C., Giordano, C., Bata, A., & Nickels, J. T. (2015). Inhibition of AMP Kinase by the Protein Phosphatase 2A Heterotrimer, PP2APpp2r2d. *J. Biol. Chem.*, *290*(17), 10588–10598. https://doi.org/10.1074/jbc.M114.626259

Joshi, G., Chi, Y., Huang, Z., & Wang, Y. (2014). Aβ-induced Golgi fragmentation in Alzheimer's disease enhances Aβ production. *Proc Natl Acad Sci USA*, *111*(13), E1230–E1239. https://doi.org/10.1073/pnas.1320192111

Kallemeijn, W. W., Lueg, G. A., Faronato, M., Hadavizadeh, K., Goya Grocin, A., Song, O.-R., Howell, M., Calado, D. P., & Tate, E. W. (2019). Validation and Invalidation of Chemical Probes for the Human N-myristoyltransferases [Number: 6]. *Cell Chemical Biology*, *26*(6), 892–900.e4. https://doi.org/10.1016/j.chembiol.2019.03.006

Kandutsch, A. A., & Chen, H. W. (1973). Inhibition of Sterol Synthesis in Cultured Mouse Cells by 7α-Hydroxycholesterol, 7β-Hydroxycholesterol, and 7-Ketocholesterol. *J. Biol. Chem.*, *248*(24), 8408–8417. https://doi.org/10.1016/S0021-9258(19)43148-7

Kim, H., Moon, S. Y., Kim, J.-S., Baek, C. H., Kim, M., Min, J. Y., & Lee, S. K. (2015). Activation of AMP-activated protein kinase inhibits ER stress and renal fibrosis. *American Journal of Physiology-Renal Physiology*, *308*(3), F226–F236. https://doi.org/10.1152/ajprenal.00495.2014

Kim, J., Yang, G., Kim, Y., Kim, J., & Ha, J. (2016). AMPK activators: mechanisms of action and physiological activities. *Exp Mol Med*, *48*(4), e224–e224. https://doi.org/10.1038/emm.2016.16

Kim, S., Alsaidan, O. A., Goodwin, O., Li, Q., Sulejmani, E., Han, Z., Bai, A., Albers, T., Beharry, Z., Zheng, Y. G., Norris, J. S., Szulc, Z. M., Bielawska, A., Lebedyeva, I., Pegan, S. D., & Cai, H. (2017). Blocking Myristoylation of Src Inhibits Its Kinase Activity and Suppresses Prostate Cancer Progression. *Cancer Res*, *77*(24), 6950–6962. https://doi.org/10.1158/0008-5472.CAN-17-0981

Kim, Y.-M., Stone, M., Hwang, T. H., Kim, Y.-G., Dunlevy, J. R., Griffin, T. J., & Kim, D.-H. (2012). SH3BP4 Is a Negative Regulator of Amino Acid-Rag GTPase-mTORC1 Signaling. *Mol. Cell*, *46*(6), 833–846. https://doi.org/10.1016/j.molcel.2012.04.007

Kola, B. (2008). Role of AMP-Activated Protein Kinase in the Control of Appetite. *J. Neuroendocrinol.*, *20*(7), 942–951. https://doi.org/10.1111/j.1365-2826.2008.01745.x

Lee, I. J., Lee, C.-W., & Lee, J.-H. (2015). CaMKKβ-AMPKα2 signaling contributes to mitotic Golgi fragmentation and the G2/M transition in mammalian cells. *Cell Cycle*, *14*(4), 598–611. https://doi.org/10.4161/15384101.2014.991557

Lehto, M., & Olkkonen, V. M. (2003). The OSBP-related proteins: a novel protein family involved in vesicle transport, cellular lipid metabolism, and cell signalling. *Biochimica et Biophysica Acta (BBA) - Molecular and Cell Biology of Lipids*, *1631*(1), 1–11. https://doi.org/10.1016/S1388-1981(02)00364-5

Liang, J., Xu, Z.-X., Ding, Z., Lu, Y., Yu, Q., Werle, K. D., Zhou, G., Park, Y.-Y., Peng, G., Gambello, M. J., & Mills, G. B. (2015). Myristoylation confers noncanonical AMPK functions in autophagy selectivity and mitochondrial surveillance. *Nat Commun*, *6*(1), 7926. https://doi.org/10.1038/ncomms8926

Ling, N. X., Kaczmarek, A., Hoque, A., Davie, E., Ngoei, K. R., Morrison, K. R., Smiles, W. J., Forte, G. M., Wang, T., Lie, S., et al. (2020). Mtorc1 directly inhibits ampk to promote cell proliferation under nutrient stress. *Nature metabolism*, *2*(1), 41–49.

Liu, X., Chhipa, R. R., Nakano, I., & Dasgupta, B. (2014). The AMPK Inhibitor Compound C Is a Potent AMPK-Independent Antiglioma Agent. *Mol Cancer Ther*, *13*(3), 596–605. https://doi.org/10.1158/1535-7163.MCT-13-0579

Lowe, M. (2011). Structural organization of the Golgi apparatus. *Curr. Opin. Cell Biol.*, *23*(1), 85–93. https://doi.org/10.1016/j.ceb.2010.10.004

Maeda, A., Uchida, M., Nishikawa, S., Nishino, T., & Konishi, H. (2018). Role of N-myristoylation in stability and subcellular localization of the CLPABP protein [Number: 1]. *Biochemical and Biophysical Research Communications*, *495*(1), 1249–1256. https://doi.org/10.1016/j.bbrc.2017.11.112

Mahlapuu, M., Johansson, C., Lindgren, K., Hjälm, G., Barnes, B. R., Krook, A., Zierath, J. R., Andersson, L., & Marklund, S. (2004). Expression profiling of the γ-subunit isoforms

of AMP-activated protein kinase suggests a major role for γ3 in white skeletal muscle. *American Journal of Physiology-Endocrinology and Metabolism*, *286*(2), E194–E200. https://doi.org/10.1152/ajpendo.00147.2003

Mao, L., Li, N., Guo, Y., Xu, X., Gao, L., Xu, Y., Zhou, L., & Liu, W. (2013). AMPK phosphorylates GBF1 for mitotic Golgi disassembly. *J. Cell Sci.*, jcs.121954. https://doi.org/10.1242/jcs.121954

Marley, A. E., Sullivan, J. E., Carling, D., Abbott, W. M., Smith, G. J., Taylor, I. W. F., Carey, F., & Beri, R. K. (1996). Biochemical characterization and deletion analysis of recombinant human protein phosphatase 2Cα. *Biochem. J.*, *320*(3), 801–806. https://doi.org/10.1042/bj3200801

Martin, D. D., Beauchamp, E., & Berthiaume, L. G. (2011). Post-translational myristoylation: fat matters in cellular life and death. *Biochimie*, *93*(1), 18–31.

Mesmin, B., Bigay, J., Moser von Filseck, J., Lacas-Gervais, S., Drin, G., & Antonny, B. (2013). A Four-Step Cycle Driven by PI(4)P Hydrolysis Directs Sterol/PI(4)P Exchange by the ER-Golgi Tether OSBP. *Cell*, *155*(4), 830–843. https://doi.org/10.1016/j.cell.2013.09.056

Mitchelhill, K. I., Michell, B. J., House, C. M., Stapleton, D., Dyck, J., Gamble, J., Ullrich, C., Witters, L. A., & Kemp, B. E. (1997). Posttranslational modifications of the 5-amp-activated protein kinase β1 subunit. *Journal of Biological Chemistry*, *272*(39), 24475–24479.

Miyamoto, L., Toyoda, T., Hayashi, T., Yonemitsu, S., Nakano, M., Tanaka, S., Ebihara, K., Masuzaki, H., Hosoda, K., Ogawa, Y., Inoue, G., Fushiki, T., & Nakao, K. (2007). Effect of acute activation of 5-AMP-activated protein kinase on glycogen regulation in isolated rat skeletal muscle. *J. Appl. Physiol.*, *102*(3), 1007–1013. https://doi.org/10.1152/japplphysiol.01034.2006

Miyamoto, T., Oshiro, N., Yoshino, K.-i., Nakashima, A., Eguchi, S., Takahashi, M., Ono, Y., Kikkawa, U., & Yonezawa, K. (2008). AMP-activated Protein Kinase Phosphorylates Golgi-specific Brefeldin A Resistance Factor 1 at Thr1337 to Induce Disassembly of Golgi Apparatus. *J. Biol. Chem.*, *283*(7), 4430–4438. https://doi.org/10.1074/jbc.M708296200

Miyamoto, T., Rho, E., Sample, V., Akano, H., Magari, M., Ueno, T., Gorshkov, K., Chen, M., Tokumitsu, H., Zhang, J., & Inoue, T. (2015). Compartmentalized AMPK Signaling Illuminated by Genetically Encoded Molecular Sensors and Actuators. *Cell Rep.*, *11*(4), 657–670. https://doi.org/10.1016/j.celrep.2015.03.057

Moore, F., Weekes, J., & Hardie, D. G. (1991). Evidence that AMP triggers phosphorylation as well as direct allosteric activation of rat liver AMP-activated protein kinase. A sensitive mechanism to protect the cell against ATP depletion. *Eur J Biochem*, *199*(3), 691–697. https://doi.org/10.1111/j.1432-1033.1991.tb16172.x

Morrow, M. E., Morgan, M. T., Clerici, M., Growkova, K., Yan, M., Komander, D., Sixma, T. K., Simicek, M., & Wolberger, C. (2018). Active site alanine mutations convert deubiquitinases into high-affinity ubiquitin-binding proteins [Number: 10]. *EMBO reports*, *19*(10). https://doi.org/10.15252/embr.201745680

Mu, J., Brozinick, J. T., Valladares, O., Bucan, M., & Birnbaum, M. J. (2001). A Role for AMP-Activated Protein Kinase in Contraction- and Hypoxia-Regulated Glucose Transport in Skeletal Muscle. *Mol. Cell*, *7*(5), 1085–1094. https://doi.org/10.1016/S1097-2765(01)00251-9

Nakano, A., Kato, H., Watanabe, T., Min, K.-D., Yamazaki, S., Asano, Y., Seguchi, O., Higo, S., Shintani, Y., Asanuma, H., Asakura, M., Minamino, T., Kaibuchi, K., Mochizuki, N., Kitakaze, M., & Takashima, S. (2010). AMPK controls the speed of microtubule polymerization and directional cell migration through CLIP-170 phosphorylation [Number: 6]. *Nature Cell Biology*, *12*(6), 583–590. https://doi.org/10.1038/ncb2060

Nakano, A., & Takashima, S. (2012). LKB1 and AMP-activated protein kinase: regulators of cell polarity. *Genes Cells*, *17*(9), 737–747. https://doi.org/10.1111/j.1365-2443.2012.01629.x

Nakatsu, F., & Kawasaki, A. (2021). Functions of Oxysterol-Binding Proteins at Membrane Contact Sites and Their Control by Phosphoinositide Metabolism. *Front. Cell Dev. Biol.*, *9*, 664788. https://doi.org/10.3389/fcell.2021.664788

Nelson, M. E., Parker, B. L., Burchfield, J. G., Hoffman, N. J., Needham, E. J., Cooke, K. C., Naim, T., Sylow, L., Ling, N. X., Francis, D., Norris, D. M., Chaudhuri, R., Oakhill, J. S., Richter, E. A., Lynch, G. S., Stöckli, J., & James, D. E. (2019). Phosphoproteomics reveals conserved exercise-stimulated signaling and AMPK regulation of store-operated calcium entry. *EMBO J*, *38*(24). https://doi.org/10.15252/embj.2019102578

Ngo, M., & Ridgway, N. D. (2009). Oxysterol binding protein–related protein 9 (orp9) is a cholesterol transfer protein that regulates golgi structure and function. *Molecular biology of the cell*, *20*(5), 1388–1399.

Nhek, S., Ngo, M., Yang, X., Ng, M. M., Field, S. J., Asara, J. M., Ridgway, N. D., & Toker, A. (2010). Regulation of Oxysterol-binding Protein Golgi Localization through Protein Kinase D–mediated Phosphorylation (V. Malhotra, Ed.). *MBoC*, *21*(13), 2327–2337. https://doi.org/10.1091/mbc.e10-02-0090

Novikoff, P. M., Novikoff, A. B., Quintana, N., & Hauw, J.-J. (1971). GOLGI APPARATUS, GERL, AND LYSOSOMES OF NEURONS IN RAT DORSAL ROOT GANGLIA, STUDIED BY THICK SECTION AND THIN SECTION CYTOCHEMISTRY. *J. Cell Biol.*, *50*(3), 859–886. https://doi.org/10.1083/jcb.50.3.859

Oakhill, J. S., Chen, Z.-P., Scott, J. W., Steel, R., Castelli, L. A., Ling, N., Macaulay, S. L., & Kemp, B. E. (2010). β-subunit myristoylation is the gatekeeper for initiating metabolic stress sensing by amp-activated protein kinase (ampk). *Proceedings of the National Academy of Sciences*, *107*(45), 19237–19241.

Obenauer, J. C., Cantley, L. C., & Yaffe, M. B. (2003). Scansite 2.0: proteome-wide prediction of cell signaling interactions using short sequence motifs. *Nucleic acids research*, *31*(13), 3635–3641.

Oligschlaeger, Y., Miglianico, M., Chanda, D., Scholz, R., Thali, R. F., Tuerk, R., Stapleton, D. I., Gooley, P. R., & Neumann, D. (2015). The Recruitment of AMP-activated Protein Kinase to Glycogen Is Regulated by Autophosphorylation. *J. Biol. Chem.*, *290*(18), 11715–11728. https://doi.org/10.1074/jbc.M114.633271

O'Neill, H. M., Maarbjerg, S. J., Crane, J. D., Jeppesen, J., Jorgensen, S. B., Schertzer, J. D., Shyroka, O., Kiens, B., van Denderen, B. J., Tarnopolsky, M. A., Kemp, B. E., Richter, E. A., & Steinberg, G. R. (2011). AMP-activated protein kinase (AMPK) 1 2 muscle null mice reveal an essential role for AMPK in maintaining mitochondrial content and glucose uptake during exercise. *Proc. Natl. Acad. Sci.*, *108*(38), 16092–16097. https://doi.org/10.1073/pnas.1105062108

Ovens, A. J., Scott, J. W., Langendorf, C. G., Kemp, B. E., Oakhill, J. S., & Smiles, W. J. (2021). Post-translational modifications of the energy guardian amp-activated protein kinase. *International journal of molecular sciences*, *22*(3), 1229.

Pang Ching, Y., Kobayashi, T., Tamura, S., & Grahame Hardie, D. (1997). Specificity of different isoforms of protein phosphatase-2A and protein phosphatase-2C studied using site-directed mutagenesis of HMG-CoA reductase. *FEBS Lett.*, *411*(2-3), 265–268. https://doi.org/10.1016/S0014-5793(97)00712-6

Park, S., Scheffler, T., Rossie, S., & Gerrard, D. (2013). AMPK activity is regulated by calcium-mediated protein phosphatase 2A activity. *Cell Calcium*, *53*(3), 217–223. https://doi.org/10.1016/j.ceca.2012.12.001

Peretti, D., Dahan, N., Shimoni, E., Hirschberg, K., & Lev, S. (2008). Coordinated Lipid Transfer between the Endoplasmic Reticulum and the Golgi Complex Requires the VAP Proteins and Is Essential for Golgi-mediated Transport (V. Malhotra, Ed.). *MBoC*, *19*(9), 3871–3884. https://doi.org/10.1091/mbc.e08-05-0498

Persico, A., Cervigni, R. I., Barretta, M. L., & Colanzi, A. (2009). Mitotic inheritance of the golgi complex. *FEBS letters*, *583*(23), 3857–3862.

Pietrangelo, A., & Ridgway, N. D. (2018). Bridging the molecular and biological functions of the oxysterol-binding protein family. *Cell. Mol. Life Sci.*, *75*(17), 3079–3098. https://doi.org/10.1007/s00018-018-2795-y

Pineda, C. T., Ramanathan, S., Fon Tacer, K., Weon, J. L., Potts, M. B., Ou, Y.-H., White, M. A., & Potts, P. R. (2015). Degradation of AMPK by a Cancer-Specific Ubiquitin Ligase [Number: 4]. *Cell*, *160*(4), 715–728. https://doi.org/10.1016/j.cell.2015.01.034

Pinkosky, S. L., Scott, J. W., Desjardins, E. M., Smith, B. K., Day, E. A., Ford, R. J., Langendorf, C. G., Ling, N. X., Nero, T. L., Loh, K., et al. (2020). Long-chain fatty acyl-coa esters regulate metabolism via allosteric control of ampk β1 isoforms. *Nature metabolism*, *2*(9), 873–881.

Pizzo, P., Lissandron, V., Capitanio, P., & Pozzan, T. (2011). Ca2+ signalling in the Golgi apparatus. *Cell Calcium*, *50*(2), 184–192. https://doi.org/10.1016/j.ceca.2011.01.006

Polekhina, G., Gupta, A., Michell, B. J., Van Denderen, B., Murthy, S., Feil, S. C., Jennings, I. G., Campbell, D. J., Witters, L. A., Parker, M. W., et al. (2003). Ampk β subunit targets metabolic stress sensing to glycogen. *Current biology*, *13*(10), 867–871.

Polekhina, G., Gupta, A., van Denderen, B. J., Feil, S. C., Kemp, B. E., Stapleton, D., & Parker, M. W. (2005). Structural Basis for Glycogen Recognition by AMP-Activated Protein Kinase. *Structure*, *13*(10), 1453–1462. https://doi.org/10.1016/j.str.2005.07.008

Presley, J. (1997). Cole nb, schroer ta, hirschberg k, zaal kj. *Lippincott-Schwartz J. ER-to-Golgi transport visualized in living cells. Nature*, *389*, 81–85.

Puustinen, P., Keldsbo, A., Corcelle-Termeau, E., Ngoei, K., Sønder, S. L., Farkas, T., Kaae Andersen, K., Oakhill, J. S., & Jäättelä, M. (2020). Dna-dependent protein kinase regulates lysosomal amp-dependent protein kinase activation and autophagy. *Autophagy*, *16*(10), 1871–1888.

Qi, J., Gong, J., Zhao, T., Zhao, J., Lam, P., Ye, J., Li, J. Z., Wu, J., Zhou, H.-M., & Li, P. (2008). Downregulation of AMP-activated protein kinase by Cidea-mediated ubiquitination and degradation in brown adipose tissue [Number: 11]. *The EMBO Journal*, *27*(11), 1537–1548. https://doi.org/10.1038/emboj.2008.92

Quentin, T., Kitz, J., Steinmetz, M., Poppe, A., Bär, K., & Krätzner, R. (2011). Different expression of the catalytic alpha subunits of the amp activated protein kinase-an immunohistochemical study in human tissue. *Histology and Histopathology, vol. 26, 2011*.

Quinn, J. M. W., Tam, S., Sims, N. A., Saleh, H., McGregor, N. E., Poulton, I. J., Scott, J. W., Gillespie, M. T., Kemp, B. E., & Denderen, B. J. W. (2010). Germline deletion of AMP-activated protein kinase β subunits reduces bone mass without altering osteoclast differentiation or function. *FASEB j.*, *24*(1), 275–285. https://doi.org/10.1096/fj.09-137158

Rabouille, C., Hui, N., Hunte, F., Kieckbusch, R., Berger, E. G., Warren, G., & Nilsson, T. (1995). Mapping the distribution of golgi enzymes involved in the construction of complex oligosaccharides. *Journal of cell science*, *108*(4), 1617–1627.

Rendón, W. O., Martínez-Alonso, E., Tomás, M., Martínez-Martínez, N., & Martínez-Menárguez, J. A. (2013). Golgi fragmentation is Rab and SNARE dependent in cellular models of Parkinson's disease. *Histochem Cell Biol*, *139*(5), 671–684. https://doi.org/10.1007/s00418-012-1059-4

Rhein, P., Desjardins, E. M., Rong, P., Ahwazi, D., Bonhoure, N., Stolte, J., Santos, M. D., Ovens, A. J., Ehrlich, A. M., Garcia, J. L. S., et al. (2021). Compound-and fiber type-selective requirement of ampkγ3 for insulin-independent glucose uptake in skeletal muscle. *Molecular metabolism*, *51*, 101228.

Ridgway, N. D., Dawson, P. A., Ho, Y. K., Brown, M. S., & Goldstein, J. L. (1992). Translocation of Oxysterol Binding Protein to Golgi Apparatus Triggered by Ligand Binding. *The Journal of Cell Biology*, *116*, 13.

Ridgway, N. D., Lagace, T. A., Cook, H. W., & Byers, D. M. (1998). Differential Effects of Sphingomyelin Hydrolysis and Cholesterol Transport on Oxysterol-binding Protein Phosphorylation and Golgi Localization. *J. Biol. Chem.*, *273*(47), 31621–31628. https://doi.org/10.1074/jbc.273.47.31621

Robles, M. S., Humphrey, S. J., & Mann, M. (2017). Phosphorylation is a central mechanism for circadian control of metabolism and physiology. *Cell metabolism*, *25*(1), 118–127.

Roder, K. (2022). The effects of glycine to alanine mutations on the structure of GPO collagen model peptides, 10.

Ross, F. A., MacKintosh, C., & Hardie, D. G. (2016). AMP-activated protein kinase: a cellular energy sensor that comes in 12 flavours. *FEBS J*, *283*(16), 2987–3001. https://doi.org/10.1111/febs.13698

Rousset, C. I., Leiper, F. C., Kichev, A., Gressens, P., Carling, D., Hagberg, H., & Thornton, C. (2015). A dual role for AMP-activated protein kinase (AMPK) during neonatal hypoxic-ischaemic brain injury in mice. *J. Neurochem.*, *133*(2), 242–252. https://doi.org/10.1111/jnc.13034

Russell, F. M., & Hardie, D. G. (2020). Amp-activated protein kinase: do we need activators or inhibitors to treat or prevent cancer? *International Journal of Molecular Sciences*, *22*(1), 186.

Sakamoto, K., Göransson, O., Hardie, D. G., & Alessi, D. R. (2004). Activity of LKB1 and AMPK-related kinases in skeletal muscle: effects of contraction, phenformin, and AICAR. *American Journal of Physiology-Endocrinology and Metabolism*, *287*(2), E310–E317. https://doi.org/10.1152/ajpendo.00074.2004

Sakamoto, K., McCarthy, A., Smith, D., Green, K. A., Grahame Hardie, D., Ashworth, A., & Alessi, D. R. (2005). Deficiency of LKB1 in skeletal muscle prevents AMPK activation and glucose uptake during contraction. *EMBO J*, *24*(10), 1810–1820. https://doi.org/10.1038/sj.emboj.7600667

Sanders, A. A. W. M., & Kaverina, I. (2015). Nucleation and Dynamics of Golgi-derived Microtubules. *Front. Neurosci.*, *9*. https://doi.org/10.3389/fnins.2015.00431

Sanders, M. J., Ratinaud, Y., Neopane, K., Bonhoure, N., Day, E. A., Ciclet, O., Lassueur, S., Pinta, M. N., Deak, M., Brinon, B., et al. (2022). Natural (dihydro) phenanthrene plant compounds are direct activators of ampk through its allosteric drug and metabolite–binding site. *Journal of Biological Chemistry*, *298*(5).

Sanz, P., Rubio, T., & Garcia-Gimeno, M. A. (2013). AMPKbeta subunits: more than just a scaffold in the formation of AMPK complex. *FEBS J*, *280*(16), 3723–3733. https://doi.org/10.1111/febs.12364

Schaffer, B. E., Levin, R. S., Hertz, N. T., Maures, T. J., Schoof, M. L., Hollstein, P. E., Benayoun, B. A., Banko, M. R., Shaw, R. J., Shokat, K. M., & Brunet, A. (2015). Identification of AMPK Phosphorylation Sites Reveals a Network of Proteins Involved in Cell Invasion and Facilitates Large-Scale Substrate Prediction. *Cell Metab.*, *22*(5), 907–921. https://doi.org/10.1016/j.cmet.2015.09.009

Schmit, N. E., Neopane, K., & Hantschel, O. (2019). Targeted protein degradation through cytosolic delivery of monobody binders using bacterial toxins. *ACS chemical biology*, *14*(5), 916–924.

Scott, J. W., van Denderen, B. J., Jorgensen, S. B., Honeyman, J. E., Steinberg, G. R., Oakhill, J. S., Iseli, T. J., Koay, A., Gooley, P. R., Stapleton, D., et al. (2008). Thienopyridone drugs are selective activators of amp-activated protein kinase β1-containing complexes. *Chemistry & biology*, *15*(11), 1220–1230.

Shaw, R. J., Lamia, K. A., Vasquez, D., Koo, S.-H., Bardeesy, N., DePinho, R. A., Montminy, M., & Cantley, L. C. (2005). The Kinase LKB1 Mediates Glucose Homeostasis in Liver and Therapeutic Effects of Metformin. *Science*, *310*(5754), 1642–1646. https://doi.org/10.1126/science.1120781

Skoufias, D. A., Burgess, T. L., & Wilson, L. (1990). Spatial and temporal colocalization of the golgi apparatus and microtubules rich in detyrosinated tubulin. *The Journal of cell biology*, *111*(5), 1929–1937.

Stahmann, N., Woods, A., Carling, D., & Heller, R. (2006). Thrombin Activates AMP-Activated Protein Kinase in Endothelial Cells via a Pathway Involving Ca $^{2+}$ /Calmodulin-Dependent Protein Kinase Kinase β. *Mol Cell Biol*, *26*(16), 5933–5945. https://doi.org/10.1128/MCB.00383-06

Steinberg, G. R., O'Neill, H. M., Dzamko, N. L., Galic, S., Naim, T., Koopman, R., Jørgensen, S. B., Honeyman, J., Hewitt, K., Chen, Z.-P., Schertzer, J. D., Scott, J. W., Koentgen, F., Lynch, G. S., Watt, M. J., van Denderen, B. J., Campbell, D. J., & Kemp, B. E. (2010). Whole Body Deletion of AMP-activated Protein Kinase β2 Reduces Muscle AMPK Activity and Exercise Capacity. *J. Biol. Chem.*, *285*(48), 37198–37209. https://doi.org/10.1074/jbc.M110.102434

Storey, M. K., Byers, D. M., Cook, H. W., & Ridgway, N. D. (1998). Cholesterol regulates oxysterol binding protein (OSBP) phosphorylation and Golgi localization in Chinese hamster ovary cells: correlation with stimulation of sphingomyelin synthesis by 25-hydroxycholesterol. *Biochem. J.*, *336*(1), 247–256. https://doi.org/10.1042/bj3360247

Tamás, P., Hawley, S. A., Clarke, R. G., Mustard, K. J., Green, K., Hardie, D. G., & Cantrell, D. A. (2006). Regulation of the energy sensor AMP-activated protein kinase by antigen receptor and Ca2+ in T lymphocytes. *J. Exp. Med.*, *203*(7), 1665–1670. https://doi.org/10.1084/jem.20052469

Tang, D., & Wang, Y. (2013). Cell cycle regulation of Golgi membrane dynamics. *Trends Cell Biol.*, *23*(6), 296–304. https://doi.org/10.1016/j.tcb.2013.01.008

Taylor, F. R., & Kandutsch, A. A. (1985). Oxysterol binding protein. *Chemistry and physics of lipids*, *38*(1-2), 187–194.

Terai, K., Hiramoto, Y., Masaki, M., Sugiyama, S., Kuroda, T., Hori, M., Kawase, I., & Hirota, H. (2005). AMP-Activated Protein Kinase Protects Cardiomyocytes against Hypoxic Injury through Attenuation of Endoplasmic Reticulum Stress [Number: 21]. *Molecular and Cellular Biology*, *25*(21), 9554–9575. https://doi.org/10.1128/MCB.25.21.9554-9575.2005

Thornton, C., Snowden, M. A., & Carling, D. (1998). Identification of a Novel AMP-activated Protein Kinase β Subunit Isoform That Is Highly Expressed in Skeletal Muscle. *J. Biol. Chem.*, *273*(20), 12443–12450. https://doi.org/10.1074/jbc.273.20.12443

Thyberg, J., & Moskalewski, S. (1999). Role of Microtubules in the Organization of the Golgi Complex. *Exp. Cell Res.*, *246*(2), 263–279. https://doi.org/10.1006/excr.1998.4326

Timms, R. T., Zhang, Z., Rhee, D. Y., Harper, J. W., Koren, I., & Elledge, S. J. (2019). A glycine-specific N-degron pathway mediates the quality control of protein *N* -myristoylation [Number: 6448]. *Science*, *365*(6448), eaaw4912. https://doi.org/10.1126/science.aaw4912

Treebak, J. T., Birk, J. B., Hansen, B. F., Olsen, G. S., & Wojtaszewski, J. F. P. (2009). A-769662 activates AMPK β_1 -containing complexes but induces glucose uptake through a PI3-

kinase-dependent pathway in mouse skeletal muscle. *American Journal of Physiology-Cell Physiology*, *297*(4), C1041–C1052. https://doi.org/10.1152/ajpcell.00051.2009

Tuerk, R. D., Auchli, Y., Thali, R. F., Scholz, R., Wallimann, T., Brunisholz, R. A., & Neumann, D. (2009). Tracking and quantification of 32P-labeled phosphopeptides in liquid chromatography matrix-assisted laser desorption/ionization mass spectrometry. *Anal. Biochem.*, *390*(2), 141–148. https://doi.org/10.1016/j.ab.2009.04.015

Vazquez-Martin, A., Oliveras-Ferraros, C., & Menendez, J. A. (2009). The active form of the metabolic sensor AMP-activated protein kinase α (AMPKα) directly binds the mitotic apparatus and travels from centrosomes to the spindle midzone during mitosis and cytokinesis. *Cell Cycle*, *8*(15), 2385–2398. https://doi.org/10.4161/cc.8.15.9082

Višnjić, D., Lalić, H., Dembitz, V., Tomić, B., & Smoljo, T. (2021). AICAr, a Widely Used AMPK Activator with Important AMPK-Independent Effects: A Systematic Review. *Cells*, *10*(5), 1095. https://doi.org/10.3390/cells10051095

Voss, M., Paterson, J., Kelsall, I. R., Martín-Granados, C., Hastie, C. J., Peggie, M. W., & Cohen, P. T. (2011). Ppm1E is an in cellulo AMP-activated protein kinase phosphatase. *Cell. Signal.*, *23*(1), 114–124. https://doi.org/10.1016/j.cellsig.2010.08.010

Vucicevic, L., Misirkic, M., Kristina, J., Vilimanovich, U., Sudar, E., Isenovic, E., Prica, M., Harhaji-Trajkovic, L., Kravic-Stevovic, T., Vladimir, B., & Trajkovic, V. (2011). Compound C induces protective autophagy in cancer cells through AMPK inhibition-independent blockade of Akt/mTOR pathway. *Autophagy*, *7*(1), 40–50. https://doi.org/10.4161/auto.7.1.13883

Walton, K., Leier, A., & Sztul, E. (2020). Regulating the regulators: role of phosphorylation in modulating the function of the GBF1/BIG family of Sec7 ARF-GEFs. *FEBS Lett*, *594*(14), 2213–2226. https://doi.org/10.1002/1873-3468.13798

Wang, B., Stanford, K. R., & Kundu, M. (2020). ER-to-Golgi Trafficking and Its Implication in Neurological Diseases [Number: 2]. *Cells*, *9*(2), 408. https://doi.org/10.3390/cells9020408

Warden, S. M., Richardson, C., Jr, J. O. O. N. N. E. L. L., Stapleton, D., Kemp, B. E., & Witters, L. A. (2001). Post-translational modifications of the β-1 subunit of AMP-activated protein kinase affect enzyme activity and cellular localization, 9.

Wen, Z., Jin, K., Shen, Y., Yang, Z., Li, Y., Wu, B., Tian, L., Shoor, S., Roche, N. E., Goronzy, J. J., & Weyand, C. M. (2019). N-myristoyltransferase deficiency impairs activation of kinase AMPK and promotes synovial tissue inflammation. *Nat. Immunol.*, *20*(3), 313–325. https://doi.org/10.1038/s41590-018-0296-7

Woods, A., Johnstone, S. R., Dickerson, K., Leiper, F. C., Fryer, L. G., Neumann, D., Schlattner, U., Wallimann, T., Carlson, M., & Carling, D. (2003). LKB1 Is the Upstream Kinase in the AMP-Activated Protein Kinase Cascade. *Curr. Biol.*, *13*(22), 2004–2008. https://doi.org/10.1016/j.cub.2003.10.031

Woods, A., Vertommen, D., Neumann, D., Türk, R., Bayliss, J., Schlattner, U., Wallimann, T., Carling, D., & Rider, M. H. (2003). Identification of Phosphorylation Sites in AMP-activated Protein Kinase (AMPK) for Upstream AMPK Kinases and Study of Their Roles

by Site-directed Mutagenesis. *J. Biol. Chem.*, *278*(31), 28434–28442. https://doi.org/10.1074/jbc.M303946200

Wu, J., Puppala, D., Feng, X., Monetti, M., Lapworth, A. L., & Geoghegan, K. F. (2013). Chemoproteomic Analysis of Intertissue and Interspecies Isoform Diversity of AMP-activated Protein Kinase (AMPK). *J. Biol. Chem.*, *288*(50), 35904–35912. https://doi.org/10.1074/jbc.M113.508747

Xiao, B., Sanders, M. J., Carmena, D., Bright, N. J., Haire, L. F., Underwood, E., Patel, B. R., Heath, R. B., Walker, P. A., Hallen, S., Giordanetto, F., Martin, S. R., Carling, D., & Gamblin, S. J. (2013). Structural basis of AMPK regulation by small molecule activators. *Nat Commun*, *4*(1), 3017. https://doi.org/10.1038/ncomms4017

Yamasaki, A., Menon, S., Yu, S., Barrowman, J., Meerloo, T., Oorschot, V., Klumperman, J., Satoh, A., & Ferro-Novick, S. (2009). mTrs130 Is a Component of a Mammalian TRAPPII Complex, a Rab1 GEF That Binds to COPI-coated Vesicles (A. Nakano, Ed.). *MBoC*, *20*(19), 4205–4215. https://doi.org/10.1091/mbc.e09-05-0387

Yamauchi, T., Iwabu, M., Okada-Iwabu, M., Ueki, K., & Kadowaki, T. (2010). Adiponectin and adipor1 regulate pgc-1α and mitochondria by ca2+ and ampk/sirt1. *Nature*, *464*(7293), 1313–1319.

Yavari, A., Bellahcene, M., Bucchi, A., Sirenko, S., Pinter, K., Herring, N., Jung, J. J., Tarasov, K. V., Sharpe, E. J., Wolfien, M., Czibik, G., Steeples, V., Ghaffari, S., Nguyen, C., Stockenhuber, A., Clair, J. R. S., Rimmbach, C., Okamoto, Y., Yang, D., … Ashrafian, H. (2017). Mammalian γ2 AMPK regulates intrinsic heart rate. *Nat Commun*, *8*(1), 1258. https://doi.org/10.1038/s41467-017-01342-5

Zagorska, A., Deak, M., Campbell, D. G., Banerjee, S., Hirano, M., Aizawa, S., Prescott, A. R., & Alessi, D. R. (2010). New roles for the lkb1-nuak pathway in controlling myosin phosphatase complexes and cell adhesion. *Science signaling*, *3*(115), ra25–ra25.

Zhang, C.-S., Hawley, S. A., Zong, Y., Li, M., Wang, Z., Gray, A., Ma, T., Cui, J., Feng, J.-W., Zhu, M., et al. (2017). Fructose-1, 6-bisphosphate and aldolase mediate glucose sensing by ampk. *Nature*, *548*(7665), 112–116.

Zhang, C.-S., Jiang, B., Li, M., Zhu, M., Peng, Y., Zhang, Y.-L., Wu, Y.-Q., Li, T. Y., Liang, Y., Lu, Z., Lian, G., Liu, Q., Guo, H., Yin, Z., Ye, Z., Han, J., Wu, J.-W., Yin, H., Lin, S.-Y., & Lin, S.-C. (2014). The Lysosomal v-ATPase-Ragulator Complex Is a Common Activator for AMPK and mTORC1, Acting as a Switch between Catabolism and Anabolism. *Cell Metab.*, *20*(3), 526–540. https://doi.org/10.1016/j.cmet.2014.06.014

Zhao, S., Li, C. M., Luo, X. M., Siu, G. K. Y., Gan, W. J., Zhang, L., Wu, W. K. K., Chan, H. C., & Yu, S. (2017). Mammalian TRAPPIII Complex positively modulates the recruitment of Sec13/31 onto COPII vesicles. *Sci Rep*, *7*(1), 43207. https://doi.org/10.1038/srep43207

Zheng, J., Knighton, D. R., Taylor, S. S., Xuong, N.-H., Sowadski, J. M., & Eyck, L. F. T. (1993). Crystal structures of the myristylated catalytic subunit of cAMP-dependent protein kinase reveal open and closed conformations [Number: 10]. *Protein Science*, *2*(10), 1559–1573. https://doi.org/10.1002/pro.5560021003

Zhou, G., Myers, R., Li, Y., Chen, Y., Shen, X., Fenyk-Melody, J., Wu, M., Ventre, J., Doebber, T., Fujii, N., Musi, N., Hirshman, M. F., Goodyear, L. J., & Moller, D. E. (2001). Role

of AMP-activated protein kinase in mechanism of metformin action. *The Journal of Clinical Investigation, 108*(8), 9.

Katyayanee Neopane

Life Science Researcher

Nepal

Swiss B-Permit

CONTACT

katyayanee.neopane@gmail.com

+41 (0) 78 206 1674

Vaud, Switzerland

/in/katyayanee/

PROFESSIONAL SKILLS

- Communication
- Teamwork and Adaptability
- Work Ethics
- Collaborative Mindset
- Attention to Detail

TECHNICAL SKILLS

- Experimental design and execution
- Microscopy *(Image processing and analysis)*

SOFTWARE & TOOLS

- Analysis & Visualization *(MS Office, GraphPad Prism, ImageJ)*
- Illustration *(Adobe Illustrator, Inkscape, BioRender)*
- Programming Language *(LateX, R, Python)*

AWARDS

- Merit-based scholarship, NCCR Chemical Biology, Switzerland (2016-2018)
- Best poster presentation, 4th European workshop on AMPK, Belgium (2019)

I am a highly motivated and passionate life science researcher, aspiring to apply my knowledge and interests in research and development to contribute to fundamental and translational science. With good coordination and communication skills, strong motivation, and ability to learn, I bring to any team an enthusiasm and a positive mindset to achieve goals on time and with excellence.

EXPERIENCE

DOCTORAL CANDIDATE Jun 2018 - Present

Société des Produits Nestlé S.A. (Lausanne, Switzerland)

- Developed sound knowledge of **metabolism and signaling pathways**
- Acquired ability to work in **cross-functional teams** to deliver high-quality results for publications and patents

RESEARCH INTERN Mar 2018 - May 2018

École Polytechnique Fédérale de Lausanne (EPFL) (Ecublens-VD, Switzerland)

- Contributed to the successful completion of a project and **publication in a well-recognized peer-reviewed journal**

PROJECT STUDENT Feb 2017 - Feb 2018

École Polytechnique Fédérale de Lausanne (EPFL) (Ecublens-VD, Switzerland)

- Developed solid knowledge of **cancer biology and protein therapeutics**

RESEARCH TRAINEE Jan 2016 - Sep 2016

École Polytechnique Fédérale de Lausanne (EPFL) (Ecublens-VD, Switzerland)

- Developed hands-on skills on **Molecular Biology and Biochemistry** tools and assays

EDUCATION

Ph.D. in Molecular Life Sciences 2018-2022 *(ongoing)*

NIHS/EPFL (Lausanne, Switzerland) EPFL

Thesis topic: AMP-activated protein Kinase: New molecular insights and novel downstream targets

M.Sc. in Chemical Biology 2016-2018

University of Geneva (Geneva, Switzerland) UNIVERSITÉ DE GENÈVE

Thesis topic: Cytosolic delivery of Monobodies using bacterial toxin subunits

B.Tech. in Biotechnology 2011-2015

Kathmandu University (Dhulikhel, Nepal)

Thesis topic: Selection and characterization of potential Baker's Yeast from indigenous resources of Nepal

SELECTED CONFERENCE PRESENTATIONS

"***AMPK activation phosphorylates Golgi-related proteins and induces Golgi fragmentation***", From Golgi organization to Glycan Function, The Old Ship Hotel, Brighton, UK, April 2022.

*"**Investigation of the mechanism by which β-subunit myristoylation regulates cellular AMPK activity**", The 11th International Meeting on AMPK, Palais Lumière, Evian-Les-Bains, France, September 2021.*

*"**Investigation of the regulation for the AMPK beta subunit isoforms**", 4th European Workshop on AMPK, Louvain-La-Neuve, Belgium, September 2019.*

Katyayanee Neopane

Life Science Researcher

Nepal

Swiss B-Permit

CONTACT

katyayanee.neopane@gmail.com

+41 (0) 78 206 1674

Vaud, Switzerland

/in/katyayanee/

WORKSHOPS PARTICIPATION

- "Make an impact, create strong social network!" by Dimitra Karatolou, 2017
- "Assertiveness: the key to open and efficient communication" by Dimitra Karatolou, 2017
- "Impactful Presenting" by Dramatic Resources (UK), Nestlé Research, 2022

LANGUAGES

Nepali

English

French

HOBBIES

Hiking

Biking

Badminton

Cooking

Travelling

COURSES/TRAININGS

- Responsible conduct in Biomedical research, EPFL
- The making of an innovative medicine, EPFL
- Scientific writing for Biomedical articles, EPFL
- Python Bootcamp, EPFL
- Introduction to Statistics with R, Nestlé Research
- Advanced microscopy for Life Science, EPFL
- Image processing for Life Science, EPFL

PUBLICATIONS & PATENTS

Neopane, K., Kozlov, N., Segal, L. M., Negoita, F., Brink, R., ... Sakamoto, K., Galic, S. "Blocking AMPK β1 myristoylation enhances AMPK activity and protects mice from high-fat diet-induced obesity and hepatic steatosis", *under revision (Cell Reports).*

Sanders, M. J., Ratinaud, Y., **Neopane, K.**, Bonhoure, N., Day, E. A., Ciclet, O., . . . Sakamoto, K. (2022). Natural (dihydro)phenanthrene plant compounds are direct activators of AMPK through its allosteric drug and metabolite binding site. Journal of Biological Chemistry, 101852.

Ahwazi, D., **Neopane, K.**, Markby, G. R., Kopietz, F., Ovens, A. J., Dall, M., . . . Sakamoto, K. (2021). Investigation of the specificity and mechanism of action of the ULK1/AMPK inhibitor SBI-0206965. Biochemical Journal, 478(15), 2977-2997.

Schmit, N. E., **Neopane, K.**, & Hantschel, O. (2019). Targeted protein degradation through cytosolic delivery of monobody binders using bacterial toxins. ACS Chemical Biology, 14(5), 916-924.

SUBSTITUTED RESORCYLIC ACID COMPOUNDS AS AMPK ACTIVATOR AND USES THEREOF. Barron, D., Ciclet, O., Naranjo, M. P., Neopane, K., Ratinaud, Y., Sanders, M. (2022). European Patent Office. Application date: 02.11.2021. Publication date: 12.05.2022. Patent number WO2022096423A1.

SUBSTITUTED RESORCINOL COMPOUNDS AS AMPK ACTIVATORS, COMPOSITIONS, METHODS AND USES THEREOF. Barron, D., Ciclet, O., Naranjo, M. P., Neopane, K., Ratinaud, Y., Sanders, M. (2020). European Patent Office. Application date: 18.11.2021. Publication date: 27.05.2022. Patent number WO2022106557A1.